

Synthesis and Application of Tagging Agents in Mass Spectrometry-based Targeted Metabolomics Studies

By

Aliyah Salem Alhawiti

201564288

Supervisor

Dr. David G. Watson

A Thesis Submitted in Partial Fulfilment of the Requirement for the Award of a Degree of Doctor of Philosophy in the Strathclyde Institute of Pharmacy and Biomedical Sciences at the University of Strathclyde.

July, 2019

Author's Declaration:

I declare that this thesis is the result of the author's original research. It has been composed by the author and has not been previously submitted for examination which has led to the award of a degree.

The copyright of this thesis belongs to the author under the terms of the United Kingdom Copyright Acts as qualified by University of Strathclyde Regulation 3.50. Due acknowledgement must always be made of the use of any material contained in, or derived from, this thesis.

Signed: -----

Date: -----

Acknowledgments

Firstly, I am grateful to Allah for giving me the strength, patience, and health to complete my PHD project. I am very thankful for my supervisor Dr Dave Watson who extensively supported me through this research project under his supervision, and for giving me the opportunity to be trained in his lab. He has always encouraged and supported me during my journey of this study with his patience and knowledge. You are such an inspiration to me, just seeing how hard you have worked, inspires me to do the same. I also want to thank my second supervisor Dr Colin Gibson, as well as Dr Abedawn Khalaf for their help, advice and words of encouragement. My sincere thanks also go to all of my colleagues for their cooperation, assistance and helpful discussions.

I am deeply thankful to my mother who supported me since my childhood to achieve all of my goals. I would also like to express the deepest appreciation to my husband Khalid for his support and encouragement during the difficult times of my life.

Thanks to my children Areej, Aram, Tariq and Ibrahim for carrying this journey with me.

Thanks to my brothers, sisters and my friends for their support.

Finally, I am so grateful to Tabuk University for the funding and support.

Dedication

I would like to dedicate this thesis to my family especially remembering
my late father Salem Alhawiti.

My late brother Ibrahim Alhawiti who always supported my dream.

My late brother brother Mohammed Alhawiti.

Finally, my late Eid Alhawiti for his continuous support and encouragement.

Table of Contents

ABBREVIATIONS AND ACRONYMS	23
1 GENERAL INTRODUCTION	27
1.1 METABOLOMICS OVERVIEW.....	27
1.2 SEPARATION METHODS UTILISED IN MASS SPECTROMETRY MEDIATED METABOLOMICS:.....	29
1.2.1 <i>Liquid Chromatography:</i>	29
1.2.2 <i>Gas Chromatography:</i>	29
1.2.3 <i>Capillary Electrophoresis (CE):</i>	30
1.3 ANALYTICAL METHODS USED FOR METABOLOMICS STUDIES:.....	31
1.3.1 <i>Nuclear Magnetic Resonance Spectroscopy (NMR):</i>	31
1.3.2 <i>Mass Spectrometry (MS):</i>	31
1.4 MASS SPECTROMETRY IONIZATION METHODS:	32
1.4.1 <i>Electrospray Ionization (ESI):</i>	32
1.4.2 <i>Electron ionisation (EI):</i>	34
1.4.3 <i>Chemical ionisation (CI):</i>	35
1.4.4 <i>Matrix Assisted Laser Desorption/ionisation (MALDI)</i>	35
1.5 ION SEPARATION AND DETECTION METHODS.....	36
1.5.1 <i>Quadrupole systems</i>	37
1.5.2 <i>Ion traps</i>	38
1.5.3 <i>Time-of-flight analysers (TOF analyser)</i>	38
1.5.4 <i>Fourier transform ion cyclotron resonance analyser (FT-ICR)</i>	38
1.5.5 <i>Orbitrap mass analyser</i>	39
1.6 LIMITATIONS OF METABOLOMICS PROFILING/STUDY:	40
1.7 FLUX ANALYSIS:	42
1.8 CHEMICALLY DERIVATIZED ISOTOPE-CODED MASS TAG METABOLITES STUDY:	42
1.9 THE AIM OF THE PROJECT:	44

2 APPLICATION OF ANILINE DERIVATISATION IN THE ANALYSIS OF SUGARS BY

LCMS	46
2.1 INTRODUCTION	46
2.2 AIM.....	48
2.3 MATERIALS AND METHODS.....	50
2.3.1 <i>Chemicals and reagents</i>	50
2.3.2 <i>Synthesis of (N-[4-(dimethylamino)phenyl]acetamide (1) [81].</i>	50
2.3.3 <i>Synthesis of methyl 4-methylbenzenesulfonate (2.)[82]</i>	51
2.3.4 <i>Synthesis of Trimethyl(p-acetamidophenyl)ammonium p-toluenesulfonate (3) [83].</i>	52
2.3.5 <i>Synthesis of trimethyl(p-aminophenyl)ammonium chloride hydrochloride (4) [83].</i>	53
2.4 DERIVATISATION OF THE SUGARS	54
2.4.1 <i>Derivatisation with trimethyl(p-aminophenyl)ammonium chloride hydrochloride (4).</i>	54
2.4.2 <i>Derivatisation with aniline and deuterated aniline- d₅</i>	55
2.5 RESULTS	55
2.5.1 <i>Synthesis of the tagging agent</i>	55
2.5.2 <i>Derivatization with trimethyl(p-aminophenyl)ammonium chloride</i>	62
2.5.3 <i>Derivatization with deuterated aniline- d₅</i>	66
2.5.4 <i>Derivatization of other sugars tagged with trimethyl(p-aminophenyl)ammonium chloride hydrochloride</i>	69
2.5.5 <i>Derivatization of other sugars with deuterated aniline</i>	71
2.5.6 <i>Profiling of sugar isomers in urine.</i>	72
2.6 DISCUSSION	73
2.7 CONCLUSION	74
3 ANALYSIS OF SHORT CHAIN FATTY ACIDS IN BIOLOGICAL FLUIDS.....	77
3.1 INTRODUCTION	77
3.2 MATERIALS AND METHODS.....	80
3.2.1 <i>Materials</i>	80
3.2.2 <i>Urine Samples</i>	81

3.2.3	<i>Preparation of reference and internal standards</i>	81
3.2.4	<i>Summary of Stock solutions and Calibration Ranges</i>	82
3.2.5	<i>Preparation of urine samples</i>	82
3.2.6	<i>Derivatisation with EDC and DPD</i>	83
3.2.7	<i>LCMS conditions</i>	83
3.3	RESULTS	84
3.3.1	<i>The derivatisation reaction</i>	84
3.3.2	<i>Fatty acids derivatisation</i>	90
3.3.3	<i>Calibration of the Method</i>	92
3.3.3.1	<i>Calibration curve for acetate standard</i>	92
3.3.3.2	<i>Calibration with butyrate standards</i>	93
3.3.4	<i>Determination of acetate, butyrate, and propionate in urine samples</i>	95
3.3.5	<i>Calculation of propionate and butyrate in urine samples</i>	99
3.3.6	<i>Effect of treatment on propionate and butyrate concentrations</i>	100
3.4	DISCUSSION	102
3.5	CONCLUSION	104
4	INVESTIGATION OF THE EFFECT OF ULTRAMARATHON EXERCISE ON SIX	
	OXIDIZED FATTY ACIDS	106
4.1	INTRODUCTION	106
4.2	MATERIALS AND METHODS	112
4.2.1	CHEMICALS AND SOLVENTS	112
4.2.2	PLASMA SAMPLES COLLECTION	113
4.2.3	PREPARATION OF PLASMA SOLUTION, REAGENTS AND STANDARD SOLUTIONS	114
4.2.4	NATIVE FATTY ACIDS AND INTERNAL STANDARDS	115
4.2.5	COUPLING OF THE FATTY ACIDS AND THEIR OXIDISED DERIVATIVES	115
4.2.5.1	LCMS ANALYSIS	116
4.3	RESULTS	118
4.3.1	PHYSIOLOGICAL RESPONSE TO THE MARATHON	118

4.3.2	DERIVATISATION OF FATTY ACIDS	118
4.3.3	DATA EXTRACTION AND ANALYSIS	127
4.3.4	CALIBRATION CURVES OF STANDARD OXIDISED FATTY ACIDS.....	127
4.4	DISCUSSION	131
4.4.1	COMPARISON OF OFAS IN PLASMA SAMPLES.....	131
4.5	CONCLUSION	151
5	VARIATION OF FOUR MONOSACCHARIDES IN CROHN'S DISEASE AND ULCERATIVE COLITIS IN COMPARISON WITH HEALTHY CONTROLS	154
5.1	INTRODUCTION	154
5.1.1	AIM OF STUDY.....	158
5.2	MATERIALS AND METHODS	159
5.2.1	CHEMICALS AND SOLVENTS	159
5.2.2	PARTICIPANTS	159
5.2.3	FAECAL SAMPLE PREPARATION	159
5.2.4	STANDARD SUGAR SAMPLE PREPARATION	159
5.2.5	DERIVATISATION OF SUGARS.....	160
5.2.5.4	LCMS CONDITIONS	161
5.3	RESULTS AND DISCUSSIONS.....	161
5.3.1	CALIBRATION CURVES	161
5.3.2	LEVELS OF SUGARS IN HEALTHY, CROHN'S DISEASE AND ULCERATIVE COLITIS PATIENTS.....	167
5.3.3	STATISTICAL COMPARISONS OF THE SUGARS	171
5.4	DISCUSSION	172
5.4.1	LEVELS OF MONOSACCHARIDE SUGARS.....	172
5.5	CONCLUSIONS	174
6	SYNTHESIS OF 2-HYDRAZINO-1-METHYL-1-METHYLPYRIDINE (HMP) AS TAGGING AGENTS IN THE ANALYSIS OF KETOSTEROIDS BY LCMS	177
6.1	GENERAL INTRODUCTION TO STEROIDS	177

6.1.1 NOMENCLATURE OF STEROIDS	179
6.1.2 USES OF STEROIDS	180
6.1.3 DETERMINATION OF STEROIDS BY LCMS.....	180
6.1.4 AIM	181
6.2 MATERIALS AND METHODS.....	183
6.2.1 CHEMICALS AND REAGENTS	184
6.2.2 SYNTHESIS OF TAGGING AGENTS	184
6.2.2.1 2-HYDRAZINYL-1-METHYLPYRIDIN-1-IUM-METHYLBENZENESULFONATE [203, 207].	186
6.2.2.2 2-FLUORO-1,3-DIMETHYLPYRIDIN-1-IUM 4-METHYLBENZENESULFONATE [204].	186
6.2.2.3 METHYL-D3 4-METHYLBENZENESULFONATE [205].	187
6.2.2.4 2-FLUORO-3-METHYL-1-(METHYL-D3)PYRIDIN-1-IUM 4-METHYLBENZENESULFONATE [204].	188
6.2.2.5 2-[2-(TERT-BUTOXYCARBONYL)HYDRAZINYL]-1,3-DIMETHYLPYRIDINIUM] BIS(TRIFLUOROACETATE) [206].	189
6.2.2.6 2-[2-(TERT-BUTOXYCARBONYL)HYDRAZINYL]-3-METHYL-1-(METHYL-D3)PYRIDINIUM] BIS(TRIFLUOROACETATE) [206].	189
6.2.2.7 2-HYDRAZINYL-1,3-DIMETHYLPYRIDINIUM BIS(TRIFLUOROACETATE).....	190
6.2.2.8 2-HYDRAZINYL-3-METHYL-1-(METHYL-D3)PYRIDINIUM BIS(TRIFLUOROACETATE).....	191
6.3 DERIVATISATION OF THE STEROIDS	191
6.3 RESULTS	192
6.3.1 CHARACTERIZATION OF SYNTHESISED COMPOUNDS.	192
6.3.1.1 2-HYDRAZINYL-1-METHYLPYRIDIN-1-IUM 4-METHYLBENZENESULFONATE.	192
6.3.1.2 2-FLUORO-1, 3-DIMETHYLPYRIDIN-1-IUM 4-METHYLBENZENESULFONATE.....	194
6.3.1.3 METHYL-D3 4-METHYLBENZENESULFONATE [205].	196
6.3.1.4 2-FLUORO-3-METHYL-1-(METHYL-D3)PYRIDIN-1-IUM 4-METHYLBENZENESULFONATE.	197
6.3.1.5 2-[2-(TERT-BUTOXYCARBONYL)HYDRAZINYL]-1,3-DIMETHYLPYRIDINIUM] (TRIFLUOROACETATE).....	199
6.3.1.6 2-[2-(TERT-BUTOXYCARBONYL)HYDRAZINYL]-3-METHYL-1-(METHYL-D3)PYRIDINIUM] (TRIFLUOROACETATE).	201
6.3.1.7 2-HYDRAZINYL-1,3-DIMETHYLPYRIDINIUM (TRIFLUOROACETATE).....	203
6.3.1.8 2-HYDRAZINYL-3-METHYL-1-(METHYL-D3)PYRIDINIUM (TRIFLUOROACETATE).....	205
6.4 FORMATION OF DERIVATIVES OF THE STEROIDS.....	206
7.0 GENERAL DICSCSSION AND FUTURE WORK.....	214

7.1	TAGGING METHODS IN THE ANALYSIS OF SUGARS.....	214
7.2	THE ANALYSIS OF SCFAs IN URINE IN RELATION TO DIET.....	215
7.3	ANALYSIS OF OXIDISED FATTY ACIDS IN MARATHON RUNNERS USING CHOLINE AS A TAGGING AGENT.	215
7.4	ANALYSIS OF SUGARS IN IBD.....	216
7.5	SYNTHESIS OF HMP FOR THE DERIVATISATION OF KETO STEROIDS.....	216
8	APPENDIX.....	218
9.0	REFERENCES.....	227

Table of Figures

Figure 1-1 Ionization process of ESI	34
Figure 1-2 Mass spectrometer operating process[2].	37
Figure 1-3 The parts of the LTQ-Orbitrap:(I) heated capillary, (II) multi-pole focusing devices, (III) a gating lens, multi-pole (IV) a, transfer octopole; b, curved RF-only quadrupole (c-trap); c, gate electrode; d, trap electrode; e; ion optics, f; inner spindlelike; g, outer barrel-like [68]	40
Figure 2-1 The α - and β - anomers of the pyranose and furanose forms of glucose.	46
Figure 2-2: A Fischer projection representation of the different sugars used in the experiment. They are all isomers with molecular formula $C_6H_{12}O_6$ and MW 180.16.	48
Figure 2-3: The reaction of glucose with the tagging agent, 4-Amino-N,N,N-trimethylanilinium, to produce the target stable derivative.	49
Figure 2-4: Synthesis of (N-[4-(dimethylamino)phenyl]acetamide from N,N-dimethyl-benzene-1,4-diamine.	51
Figure 2-5: Synthesis of methyl-p-toluenesulfonate from p-toluenesulfonyl chloride	52
Figure 2-6 Synthesis of trimethyl(p-acetamidophenyl)ammonium p-toluene sulfonate 3 from N-(4-(dimethylamino)phenyl)acetamide 1 and methyl-p-toluenesulfonate 2	53
Figure 2-7 Synthesis of trimethyl(p-aminophenyl)ammonium chloride 4 from trimethyl(p-acetamidophenyl)ammonium p-toluene sulfonate 3	54
Figure 2-8 1H NMR spectrum for N-(4-(dimethylamino)phenyl)acetamide	56
Figure 2-9 1H NMR spectrum for methyl 4-methylbenzenesulfonate	57
Figure 2-10 1H NMR spectrum of trimethyl(p-aminophenyl)-4-acetamido-N,N,N-trimethylbenzammonium-4-methylbenzenesulfonate.	58
Figure 2-11 1HNMR spectra for 4-amino-N,N,N-trimethylbenzenaminium.	60
Figure 2-12 $^{13}CNMR$ spectra for 4-amino-N,N,N-trimethylbenzenaminium	61
Figure 2-13 Mass spectra for 4-amino-N,N,N-trimethylbenzenaminium	62
Figure 2-14 Mass spectrum showing the mass-to-charge ratio of the derivatized hexose sugars showing the molecular ion at m/z 315.1909 and the correct elemental composition of $C_{15}H_{27}O_5N_2$	64

<i>Figure 2-15 The extracted ion chromatograms of the four derivatives of the hexoses glucose (A), galactose (B), mannose (C) and fructose (D) with trimethyl(p-aminophenyl) ammonium chloride hydrochloride (4).</i>	65
<i>Figure 2-16 ²H₅-aniline (A) and aniline (B) derivatives of 1 µg amounts of hexose standards run of a ZICHILIC column in acetonitrile/water containing 0.01% formic acid (90:10) at 0.6 ml/min.</i>	66
<i>Figure 2-17 Mass spectra representing the mass of the glucose (top) and galactose (bottom) derivatized with aniline-d₅ showing the molecular ion [M+H]⁺ at m/z 263.1641 which is correct for the calculated elemental composition of C₁₂H₁₅²H₅O₅N,</i>	68
<i>Figure 2-18 Chromatogram of the mix containing derivatives of the four hexose sugars derivatized with aniline-d₅ fructose (6.21 min), glucose (12.77 min), galactose (18.00 min) and mannose (18.83 min), run isocratically at 5% 0.01% (v/v) formic acid in water and 95% 0.01% formic acid in acetonitrile.</i>	69
<i>Figure 2-19 Structure of trehalose showing the C₁-C'₁ glycosidic linkage</i>	70
<i>Figure 2-20 The chromatograms of the four pentose sugars derivatized with trimethyl(p-aminophenyl) ammonium chloride hydrochloride 4; ribose (A), arabinose (B) and xylose (C) and the disaccharide lactose (D).</i>	71
<i>Figure 2-21 The chromatograms of four pentose sugars derivatized aniline-d₅; ribose (A), arabinose (B), xylose (C) and 2-deoxy-D-ribose (D).</i>	72
<i>Figure 2-22 The chromatograms showing sugars identified in urine sample derivatized aniline-d₅ acetonitrile/water (90:10) containing 0.01% formic acid.</i>	73
<i>Figure 3-1 Derivatisation of short chain fatty acids (SCFAs) with EDC and DPD. The EDC deprotonates and activates the SCFA leading to the formation of an O-acylisourea, an intermediate which then reacts with DPD to form the final stable amide derivative.</i>	85
<i>Figure 3-2 Mass spectrum of positively charged derivative of [²H₅] butyrate showing the expected accurate mass of 212.1806 with five deuterium atoms.</i>	87
<i>Figure 3-3 Mass spectrum of the positively charged derivative of butyrate showing the expected accurate mass of 207.1490.</i>	87
<i>Figure 3-4 Mass spectrum of the positively charged derivative of ¹³C₂-labelled acetate with the expected accurate mass of 181.1245.</i>	88
<i>Figure 3-5 Mass spectrum of the positively charged derivative of acetate showing a mass of 179.1177.</i>	88

Figure 3-6 Mass spectrum of the positively charged $^2\text{H}_2$ propionate showing the expected accurate mass of 195.1460.....	89
Figure 3-7 Mass spectrum of the positively charged derivative of propionate showing the expected mass of 193.1332.....	89
Figure 3-8 Extracted ion chromatograms for the three labelled and three unlabeled fatty acid standards at concentrations of $1\mu\text{g}/\text{ml}$ run on a ZICHILIC column using the gradient shown in table 3-3.....	90
Figure 3-9 Calibration curve for acetate using acetate- ^{13}C as internal standard.	92
Figure 3-10 Calibration curve for propionate using propionate- d_2 as internal standard.	93
Figure 3-11 Calibration curve of butyrate using butyrate- d_5 as internal standard with all points included.	94
Figure 3-12 Calibration curve of butyrate using butyrate- d_5 as internal standard.	95
Figure 3-13 Calibration curve of acetate using acetate- ^{13}C as internal standard.	97
Figure 3-14 Calibration curve of propionate using propionate- d_2 as internal standard.	97
Figure 3-15 Calibration curve of butyrate using butyrate- d_5 as internal standard. Note that all the curves in Figures 3-9 to 3-12 produced linearity of $R^2 > 0.99$ except butyrate which gave $R^2 = 0.98$	98
Figure 3-16 Derivatives of short chain organic acids in urine ($100\mu\text{l}$) spiked with labelled internal standards ^{13}C -acetic acid ($1\mu\text{g}$), $^2\text{H}_2$ -propionic acid and $^2\text{H}_5$ -butyric acid and ($0.5\mu\text{g}$).	100
Figure 3-17 Boxplot illustrating the difference in propionic acid levels between treatment and control urine samples. The magnitude of difference was $0.00189\mu\text{g}/\text{ml}$ (95% CI: $-0.00449, 0.00071$) with treatment samples having a slightly higher but insignificant level of propionate compared to the control samples.	101
Figure 3-18 Boxplot illustrating the difference in butyric acid levels between treatment and control urine samples. The magnitude of difference was $0.00194\mu\text{g}/\text{ml}$ (95% CI: $-0.00127, 0.00515$) with treatment samples having a slightly lower (but insignificant) level of butyrate compared to the control samples.	101
Figure 3-19 An interval plot illustrating the levels of propionate and butyrate in control and treatment samples of urine. Paired T-test analyses revealed that there were no significant differences between control and treatment samples when each SCFA was considered separately. However, the levels of butyrate were significantly higher than those of propionate in both controls and treatment samples.	102
Figure 4-1 Schematic depiction of the choline derivatisation of fatty acids reaction using FMP as coupling agent.	116

Figure 4-2 Depiction of coupling reaction with the fatty acids Dodecanoic acid, Myristic acid and Palmitic acid utilizing FMP as coupling agents with the accurate masses of the derivatized products.....	119
Figure 4-3 Total ion chromatogram of MIX-STD (1µg).....	120
Figure 4-4 Extracted ion chromatogram and mass spectrum for dodecanoic acid (1µg).....	120
Figure 4-5 Extracted ion chromatogram and mass spectrum for myristic acid (1µg).....	121
Figure 4-6 Extracted ion chromatogram and mass spectrum for palmitic acid (1µg).....	121
Figure 4-7 Total ion chromatogram for standard MIX-STD (1ng).....	122
Figure 4-8 Extracted ion chromatograms for standard MIX-STD (1ng/ml).....	123
Figure 4-9 Standard mixture of oxidized fatty acid derivatives from Linoleic Acid and Arachidonic Acid.	124
Figure 4-10 MIX-1 (Linoleic Acid Oxylipin's A = (±)12(13)-DiHOME ; B = (±)9(10)-DiHOME ;C = 13(S)-HODE ;D = 9(S)-HODE ;E = (±)12(13)-EpOME ;F = (±)9(10)-EpOME ;G = 13 OxoODE ;H = 9 OxoODE).	125
Figure 4-11 MIX-3 arachidonic acid oxylipins.	126
Figure 4-12 Calibration curve for 9(S)-HODE.	128
Figure 4-13 Calibration curve for 13(S)-HODE.	128
Figure 4-14 Calibration curve for (±)12(13)-EpOME.	129
Figure 4-15 Calibration curve for (±)9(10)-EpOME.	129
Figure 4-16 Calibration curve for 13-OxoODE.....	130
Figure 4-17 Calibration curve for 9-OxoODE.....	130
Figure 4-18 Representative Chromatograph for LAO derivatives extracted from plasma showing: A:-13-OxoODE, and 9-OxoODE; B:-9(S)-HODE 13(S)-HODE, (±)12(13)-EpOME, (±)9(10)-EpOME.	131
Figure 4-19 Plot of Mean concentrations against the three sample time points plus baseline for 9(S)-HODE...	134
Figure 4-20 Plot of Mean concentrations against the three sample time points plus baseline for 13(S)-HODE.	137
Figure 4-21 Plot of Mean concentrations against the three sample time points plus baseline for (±)12(13)-EpOME.	140
Figure 4-22 Plot of Mean concentrations against the three sample time points plus baseline for (±)9(10)-EpOME.....	143
Figure 4-23 Plot of Mean Peak area ratios against the three sample time points plus baseline for 13-OxoODE.	146
Figure 4-24 Plot of Mean concentrations against the three sample time points plus baseline for 9-OxoODE...	149

Figure 5-1 Depiction of the reaction between the sugars and the tagging agent, $^2\text{H}_5$ -aniline, to produce the target stable derivative utilizing Fructose as an example.	161
Figure 5-2 Calibration curve for glucose using $^{13}\text{C}_6$ -glucose as internal standard.	163
Figure 5-3 Calibration curve for galactose using $^{13}\text{C}_6$ -glucose as internal standard.	163
Figure 5-4 Calibration curve for xylose using $^{13}\text{C}_6$ -glucose as internal standard.	164
Figure 5-5 Calibration curve for arabinose $^{13}\text{C}_6$ -glucose as internal standard.	164
Figure 5-6 Extracted ion chromatograph of derivatized standard sugar mix (0.8 μg) with $^{13}\text{C}_6$ -glucose (1 μg) as internal standard; A = $^{13}\text{C}_6$ -glucose, B = xylose, C = Arabinose, D = Glucose, E = Galactose	165
Figure 5-7 Extracted ion peaks for a standard mixture of hexose and pentose sugars (0.8 μg) with $^{13}\text{C}_6$ -glucose (1 μg) as internal standard; A = $^{13}\text{C}_6$ -glucose, B = Xylose, C = Arabinose, D = Ribose, E = Fructose, F = Glucose, G = Altrose, H = Allose + Gulose, I = Galactose, J = Talose, K = Mannose	166
Figure 5-8 Extracted ion chromatographs of derivatised sugars found in samples from healthy participants with $^{13}\text{C}_6$ -glucose (1 μg) as internal standard; A = $^{13}\text{C}_6$ -glucose, B = xylose, C = Arabinose, D = Glucose, E = Galactose	169
Figure 5-9 Extracted ion chromatographs of derivatised sugars found in samples from participants with CD with $^{13}\text{C}_6$ -glucose (1 μg) as internal standard; A = $^{13}\text{C}_6$ -glucose, B = xylose, C = Arabinose, D = Glucose, E = Galactose	170
Figure 5-10 Extracted ion chromatographs of derivatised sugars found in samples from participants with UC with $^{13}\text{C}_6$ -glucose (1 μg) as internal standard; A = $^{13}\text{C}_6$ -glucose, B = xylose, C = Arabinose, D = Glucose, E = Galactose	170
Figure 6-1 General structure of and numbering of steroids	177
Figure 6-2 Some Classes of Steroids.....	179
Figure 6-3 The structures of HMP, 3MHMP and 3MHMP- d_3 and the steroid standards 5 α -Pregnane-21-ol-3,20,-dione, (DsTd1), 4-Pregnene-20 β ,21-diol-3-one, (DsTd2), 5 α -Pregnane-3 β -ol-20-one, (DsTd3), 3 β -Hydroxy-5 α -androstane-17-one, (DsTd4), used in the study.....	182
Figure 6-4 The reaction of DsT2 with HMP, to produce the target stable derivative.	183
Figure 6-5: Schematic depicting the reaction for the synthesis of HMP.	184
Figure 6-6 Schematic depicting the overall reaction scheme for the synthesis of HMP analogues 3MHMP and 3MHMP- d_3	185

Figure 6-7 ¹ H NMR Spectrum for 2-hydrazinyl-1-methylpyridin-1-ium 4-methylbenzenesulfonate	193
Figure 6-8 MS Spctrum for 2-hydrazinyl-1-methylpyridin-1-ium 4-methylbenzenesulfonate.....	194
Figure 6-9 ¹ H NMR Spectrum for 2-fluoro-1, 3-dimethylpyridin-1-ium 4-methylbenzenesulfonate.	195
Figure 6-10 MS Spectrum for 2-fluoro-1, 3-dimethylpyridin-1-ium 4-methylbenzenesulfonate.....	195
Figure 6-11 ¹ HNMR Spectrum for Methyl-d3 4-methylbenzenesulfonate	196
Figure 6-12 MS Spectrum for Methyl-d3 4-methylbenzenesulfonate.....	197
Figure 6-13 ¹ HNMR Spectrum for 2-fluoro-3-methyl-1-(methyl-d3)pyridin-1-ium 4-methylbenzenesulfonate..	198
Figure 6-14 MS Spectrum for 2-fluoro-3-methyl-1-(methyl-d3)pyridin-1-ium 4-methylbenzenesulfonate.	199
Figure 6-15 ¹ HNMR Spectra for 2-[2-(tert-butoxycarbonyl)hydrazinyl]-1,3-dimethylpyridinium] (trifluoroacetate)	200
Figure 6-16 MS Spectra for 2-[2-(tert-butoxycarbonyl)hydrazinyl]-1,3-dimethylpyridinium] (trifluoroacetate)	200
Figure 6-17 ¹HNMR Spectrum for 2-[2-(tert-butoxycarbonyl)hydrazinyl]-3-methyl-1-(methyl-d3)pyri	202
Figure 6-18 MS Spectrum for 2-[2-(tert-butoxycarbonyl)hydrazinyl]-3-methyl-1-(methyl-d3)pyridinium] (trifluoroacetate	203
Figure 6-19 ¹ H NMR Spectrum for 2-hydrazinyl-1,3-dimethylpyridinium (trifluoroacetate)	204
Figure 6-20 MS Spectrum for 2-hydrazinyl-1,3-dimethylpyridinium (trifluoroacetate).....	204
Figure 6-21 ¹ H NMR Spectrum for 2-hydrazinyl-3-methyl-1-(methyl-d3)pyridinium (trifluoroacetate)	206
Figure 6-22 MS Spectrum for 2-hydrazinyl-3-methyl-1-(methyl-d3)pyridinium (trifluoroacetate).....	206
Figure 6-23 Extracted ion Chromatograph for DsTD1 derivatisation with HMP.....	208
Figure 6-24 Extracted ion Chromatograph for DsTD2 derivatisation with HMP.....	209
Figure 6-25 Extracted ion Chromatograph for DsTD3 derivatisation with HMP.....	210
Figure 6-26 Extracted ion Chromatograph for DsTD4 derivatisation with HMP.....	211

List of Tables

<i>Table 2-1 Summary of the results obtained from the analysis of sugars tagged with trimethyl(p-aminophenyl)ammonium chloride hydrochloride (4).</i>	65
<i>Table 2-2 Changes in the retention times of the hexose sugars with mobile phase composition.</i>	67
<i>Table 2-3 Pentose and disaccharide sugars.</i>	69
<i>Table 2-4 Summary of the results obtained in the analysis of sugars tagged with trimethyl(p-aminophenyl) ammonium chloride hydrochloride (4).</i>	70
<i>Table 3-1 Structures of short chain fatty acids (SCFAs) showing their molecular formulae and weights. From the MWs, it can be seen that the m/z values of deprotonated species in negative mode LCMS are quite low.</i>	78
<i>Table 3-2 Structures of the derivatising reagents EDC and DPD used in the study.</i>	80
<i>Table 3-3 Illustration of mobile phase gradient program used in LCMS analysis.</i>	84
<i>Table 3-4 Formulae and MW of the predicted SCFA derivatives after reaction with EDC and DPD.</i>	86
<i>Table 3-5 RSDs were calculated from peak area ratios of the standards in the mixture after four injections per sample of standard.</i>	91
<i>Table 3-6 Values for the calibration curve of acetate using 1 µg of acetate-¹³C for internal standardization. after three injections per sample of standard.</i>	92
<i>Table 3-7 Values for the calibration curve of propionate using 0.5 µg of propionate-d₂ as internal standard .after three injections per sample of standard.</i>	93
<i>Table 3-8 Values for the calibration curve of butyrate using 0.5 µg of butyrate-d₅ as internal standard. after three injections per sample of standard.</i>	94
<i>Table 3-9 Values for the calibration curve of acetate using acetate-¹³C as internal standard. These values were used for the determination of acetate in urine samples from patients after three injections per sample of standard.</i>	96
<i>Table 3-10 Values for the calibration curve of propionate using propionate-d₂ as internal standard. These values were used for the determination of propionate in urine samples from patients after three injections per sample.</i>	97

<i>Table 3-11 Values for the calibration curve of butyrate using butyrate-d5 as internal. These values were used for the determination of butyrate in urine samples from patient samples after three injections per sample.</i>	<i>98</i>
<i>Table 3-12 Concentrations of butyrate and propionate detected in patients before and after treatment.</i>	<i>99</i>
<i>Table 4-1 Structures of the derivatizing reagent FMP and the fatty acids of interest used in the study.</i>	<i>111</i>
<i>Table 4-2 Biographic information and metadata of participants.</i>	<i>114</i>
<i>Table 4-3 Illustration of mobile phase gradient program used in LCMS analysis.</i>	<i>117</i>
<i>Table 4-4 Peak area ratios calculated for the six OFAs against 50 ng of HODE ²H₄.</i>	<i>127</i>
<i>Table 4-5 Mean concentrations (µg/mL) obtained for 9(S)-HODE.....</i>	<i>132</i>
<i>Table 4-6 ANOVA Test Data for the mean concentrations obtained for 9(S)-HODE.....</i>	<i>132</i>
<i>Table 4-7 Tukey HSD Dependent Variable Data: Mean concentrations obtained for 9(S)-HODE.....</i>	<i>133</i>
<i>Table 4-8 Mean concentrations (µg/mL) obtained for 13(S)-HODE.....</i>	<i>135</i>
<i>Table 4-9 ANOVA Test Data for the mean concentrations obtained for 13(S)-HODE.....</i>	<i>135</i>
<i>Table 4-10 Tukey HSD Dependent Variable: Mean concentrations obtained for 13(S)-HODE</i>	<i>136</i>
<i>Table 4-11 Mean concentrations (µg/mL) obtained for (±)12(13)-EpOME.....</i>	<i>137</i>
<i>Table 4-12 ANOVA test results for the Mean concentrations obtained for (±)12(13)-EpOME.</i>	<i>138</i>
<i>Table 4-13 Tukey HSD Dependent Variable: Mean concentrations obtained for (±)12(13)-EpOME</i>	<i>139</i>
<i>Table 4-14 Mean concentrations (µg/mL) obtained for (±)9(10)-EpOME.....</i>	<i>140</i>
<i>Table 4-15 ANOVA test results for the mean concentrations obtained for (±)9(10)-EpOME.....</i>	<i>140</i>
<i>Table 4-16 Tukey HSD Dependent Variable: Mean concentrations obtained for (±)9(10)-EpOME.</i>	<i>141</i>
<i>Table 4-17 Mean concentrations (µg/mL) obtained for 13-OxoODE.....</i>	<i>143</i>
<i>Table 4-18 ANOVA test results for the mean concentrations of 13-OxoODE.</i>	<i>144</i>
<i>Table 4-19 Tukey HSD Dependent Variable: Mean concentrations obtained for 13-OxoODE.....</i>	<i>145</i>
<i>Table 4-20 Mean concentrations (µg/mL) obtained for 9-OxoDE.....</i>	<i>147</i>
<i>Table 4-21 ANOVA test results for the mean concentrations of 9-OxoDE.</i>	<i>147</i>
<i>Table 4-22 Tukey HSD Dependent Variable: Mean concentrations obtained for 9-OxoDE.</i>	<i>148</i>
<i>Table 4-23 The levels of oxidized fatty acids (Means and SD's) in plasma of participant's pre, midway and immediately upon completion of an 80 km ultramarathon run.</i>	<i>150</i>
<i>Table 4-24 One-way ANOVA for the differences in levels of the six oxidized fatty acids between four times points (Baseline, Pre 80 km, 40 km, and Post 80 km).</i>	<i>150</i>

<i>Table 5-1 Summary of data from the calibration curves for Glucose, Galactose, Xylose and Arabinose</i>	<i>162</i>
<i>Table 5-2 Summary of sugar levels for each of the participants in the study following derivatization with ²H₅-aniline.</i>	<i>168</i>
<i>Table 5-3 Mean values of Sugars from the participant groups from the study.</i>	<i>171</i>
<i>Table 5-4 Means and SDs of the levels of sugars in the three groups of participants used in the study.</i>	<i>172</i>
<i>Table 5-5 One-way ANOVA for the differences in levels of the four monosaccharide sugars between healthy, Crohn's disease and ulcerative colitis patients.</i>	<i>172</i>

ABSTRACT

Metabolomics is a technique which provides comprehensive metabolite profiling as well as metabolic pathway elucidation and potentially has a wide range of applications for medical research including disease diagnosis and monitoring. In this thesis, some synthetically prepared and existing tagging agents were applied to targeted quantitative analysis of certain metabolites in biological samples. The thesis is divided into six chapters: Chapter one provides a general introduction to metabolomics and to the use of chemical tagging in targeted analysis and briefly looks at the type of instrumentation used in metabolomics profiling.

Chapter two, described the synthesis of the tagging agent trimethyl(*p*-aminophenyl) ammonium chloride (PMTA) and along with aniline and D5-aniline was assessed for suitability for the analysis of hexose sugars. The detection of the sugars by hydrophilic interaction chromatography (HILIC) in combination with mass spectrometry (MS) was greatly improved along with chromatographic resolution allowing for easy identification of sugar isomers.

In Chapter three, analysis of short chain fatty acids utilising *N*-(3-Dimethylaminopropyl)-*N*-ethylcarbodiimide hydrochloride (EDC) and *N,N*-Dimethyl-*p*-phenylenediamine (DPD) as derivatizing agents was carried out on urine samples from the. The aim of the study was to evaluate the novel CDTREAT diet in comparison to the standard enteral nutrition (EEN) diet. The study confirmed that the detection and quantification of SCFAs by LCMS was greatly enhanced by derivatisation and showed no difference in the levels of SCFAs between the treatment and control groups which implies that the diets had similar effects on the levels of SCFAs in urine and thus could be deemed equivalent.

In Chapter four, an investigation of the effect of ultramarathon exercise on oxylipin metabolites in plasma samples from the University of Kingston was carried out. In this study 2-fluoro-

3-methyl pyridine (FMP) was utilised as a catalyst to add choline as a tagging agent which facilitated the sensitive detection and quantification of the oxylipins. These compounds are thought to have biological effects on blood flow. Statistical analysis of the results showed no significant change in the amounts of any of the oxylipins in the study pre and post-exercise.

In Chapter five, a study to determine the variation in four monosaccharides from stool samples of a group of IBS sufferers plus controls was undertaken using D5-aniline as the tagging agent. The data generated in this study appears on analysis to indicate a clear difference in the levels of some sugars between each of the test groups (UC, CD and healthy controls) which might be a result of alteration in the microbiome in CD. This is significant because it implies that this could be developed as not only a diagnostic tool for IBS it can be used to differentiate between sufferers of CD and UC.

In Chapter 6, 2-Hydrazino-1-methylpyridine (HMP), as well as a novel analogue of HMP, MHMP, and its deuterated analogue MHMP-d₃ were synthesised. The HMP was passed on to a co-worker who utilised it in a separate study for the analysis of androgens in saliva. It was however not possible to detect any of the tagged steroids utilising MHMP-d₃ which may be due to difficulties in obtaining the reagent in high purity.

Publications

Papers

1 Sami Bawazeer, Ali Muhsen Ali, **Aliyah Alhawiti**, Abedawn Khalaf, Colin Gibson, Jonans Tusiimire, David G. Watson. *A method for the analysis of sugars in biological systems using reductive amination in combination with hydrophilic interaction chromatography and high resolution mass spectrometry*. *Talanta*, 2017. **166**: p. 75-80.

2. Mansour A. Alzahrani; Gareeb O. Alshuwaier; Khalid S. Aljaloud; Colin Gibson; Abedawn Khalaf; **Aliyah S. Alhawiti**; David G. Watson. *Development of a Derivatization Method for Investigating Testosterone and Dehydroepiandrosterone Using Tandem Mass Spectrometry in Saliva Samples from Young Professional Soccer Players Pre- and Post-Training*. *Scientia Pharmaceutica*, 2019. **87**(2): p. 11.

Posters

1. Synthesis of Stable Isotope Tagging Agents for Use in the Application of Analytical Chemistry to Metabolomics Studies.

Aliyah Alhawiti, Collin Gibson, Abedawn Khalaf, & David G. Watson

30th ESCPB Congress Barcelona 4th-7th September 2016.

New European Society for Comparative Physiology and Biochemistry in Barcelona, Spain.

2. Synthesis of Stable Isotope Tagging Agents for Use in the Application of Analytical Chemistry to Metabolomics Studies.

Aliyah Alhawiti, Collin Gibson, Abedawn Khalaf, & David G. Watson

City of Glasgow College, Glasgow, Scotland, UK. Scottish Metabolomics Network Symposium,

2nd and 3rd of November 2017.

Abbreviations and Acronyms

Å	Angstrom
δ	Delta
ACN	Acetonitrile
ANOVA	Analysis of Variance
APCI	Atmospheric Pressure Chemical Ionisation
BMI	Bodymass Index
CE	Capillary Electrophoresis
CD	Crohn's Disease
Da	Daltons
DAD	Diode Array Detector
DCM	Dichloromethane
DPD	N,N-Dimethyl-P-phenylenediamine
DMSO	Dimethyl Sulphoxide
EDC	N-(3-Dimethylaminopropyl)-N-ethylcarbodiimide hydrochloride
EI	Electron Ionisation
ESI	Electrospray Ionisation
ESI-MS	Electrospray Ionisation-Mass spectrometry
FMP	2-fluoro-3-methyl pyridine
FT	Fourier Transformation
FT-IR	Fourier Transformation Infrared

GC	Gas Chromatography
GC-CI-MS	Gas Chromatography-Chemical Ionisation-Mass Spectrometry
GC-MS	Gas Chromatography-Mass Spectrometry
GIT	Gastrointestinal Tract
HILIC	Hydrophilic Interaction Liquid Chromatography
¹ HNMR	Proton Nuclear Magnetic Resonance
HMP	2-Hydrazino-1-methylpyridine
HPLC	High Performance Liquid Chromatography
HRMS	High Resolution Mass Spectrometry
Hz	Hertz
IBD	Irritable Bowel Disease
IBS	Irritable Bowel Syndrome
ICD	Ileal Crohn's Disease
LC	Liquid Chromatography
LC-ESI-MS	Liquid Chromatography-Electrospray Ionisation-Mass Spectrometry
LCMS	Liquid Chromatography-Mass Spectrometry
LTQ	Linear Trap Quadrupole
m/z	Mass to Charge Ratio
MALDI	Matrix Assisted Laser Desorption/Ionisation
3MHMP	2-hydrazinyl-1,3-dimethylpyridinium bis(trifluoroacetate)
3MHMP-d ₃	2-hydrazinyl-3-methyl-1-(methyl-d ₃)pyridinium bis(trifluoroacetate).
MS	Mass Spectrometry

MS/MS	Tandem Mass Spectrometry
mw	Molecular Weight
NIESI	Negative ion electrospray ionisation
NMR	Nuclear Magnetic Resonance
NP	Normal Phase
PDA	Photodiode Array detector
PIES	Positive ion electrospray ionisation
PTMA	Trimethyl(p-aminophenyl) ammonium chloride hydrochloride
PPM	Parts Per Million
QToF	Quadrupole-Time of Flight
RP	Reversed phase
RT	Room Temperature
SCFAs	Short Chain Fatty Acids
TEA	Triethyl amine
TFA	Trifluoroacetic Acid
ToF	Time of Flight
Uv	Ultra Violet
VO ₂	Maximal Oxygen Uptake

Chapter One:

Introduction to Metabolomics

1 GENERAL INTRODUCTION

1.1 Metabolomics overview

Metabolomics is a newly emerging field of study which is concerned with the study, measurement and quantification, of the small molecule products and intermediates, (metabolites), which are the products of the metabolic processes which occur in biological systems, cell, tissues, organ, biological fluid or organism at a specific time point [1]. The small molecule, products and intermediates as well as their interactions within the biological systems are collectively referred to as the metabolome. The word metabolome is derived from the Greek word 'metabolome' which means change [2]. It is defined as the total list of metabolites present in a biological system as low molecular weight compounds, which are involved in the metabolic reactions necessary for normal function, growth, and maintenance [3]. For example, genomics identifies genes; transcriptomics is the study of transcriptome, highlighting gene conversion into RNA; proteomics indicates whether or not RNA translates to protein; and finally metabolomics informs about the variations that occur in the metabolite profile due to changes in protein expression [4]. According to Dunn, the definition of metabolomics is, "The non-biased quantification and identification of all metabolites present in a biological system"[3]. Metabolomics can also be referred to as the quantitative assessment of metabolic responses of multicellular systems that are multi-parametric and time-related to the genetic modification or pathological stimuli [2].

Metabolites are present in very large numbers in biological systems due to the various metabolic processes and pathways. Therefore, the identification and quantification of these metabolites can only be achieved with the application of a variety of analytical technologies. It is

very difficult task to achieve this goal utilising a single technique. Consequently, several analytical techniques and instruments, are required for the complete study of the metabolites in a metabolome [5]. There are still significant challenges faced by analysts currently while conducting detailed metabolic profiling of multiple samples. This is because of the difficulty in accomplishing high-throughput and comprehensive analysis simultaneously.

According to Fiehn, metabolomics approaches can be categorized as follows; metabolite target analysis, metabolite profiling, metabolite fingerprinting, metabolite foot-printing and flux analysis [6, 7]. Metabolite target analysis techniques examines the specific metabolites or sets of preselected metabolites, for example phenol groups, which are linked by a common reaction or pathway [3]. Metabolite profiling investigates groups of non-specific metabolites which can be analysed in parallel by a common analytical technique like mass spectrometry, (MS) [8]. Metabolic fingerprinting aims to quantify intracellular metabolite pools, [(including still unknown metabolites (the *endo*-metabolome)], while metabolic foot-printing is used for the analysis of metabolites excreted from cells, the *exo*-metabolome [9, 10]. Flux analysis is an approach that helps in the determination of the flow of metabolites through the pathway resulting in the metabolite, in an organism or cell, using stable isotopes such as ^{13}C , ^{15}N , ^{18}O or, classically, radioactive isotopes. Fluxomics is the term which describes high-throughput analyses of metabolite fluxes [11]. Metabolomics has a wide range of applications and has been used in a whole host of disciplines such as biomarker detection, drug discovery, drug efficacy, toxicity analysis, drug development, disease pathophysiology, and agriculture [12]. This wide range of applications is due to rapid advancements in analytical methods such as MS, which is considered as one of the most important platforms for metabolomics studies [13]. Despite the advantages of MS, profiling of unknown compounds is still a challenge [14].

1.2 Separation methods utilised in Mass Spectrometry mediated

Metabolomics:

1.2.1 Liquid Chromatography:

Liquid chromatography is a technique used for separating mixtures of different components into their component parts physically. Two phases are involved in this process, the mobile phase which is a liquid (solvent) in which the sample is dissolved which passes over a solid absorbent material packed in a column known as the stationary phases. This method of separation is utilised extensively for the quantitation of drugs. In the most common configuration, liquid chromatography is combined with high-resolution mass spectrometry systems for effective results. This analytical technique is one of the most useful tools used in drug research analysis, specifically for the classification and separation of drug metabolites. Several types of stationary phases can be used each with its own characteristics which separate the components of the mixture based on the affinities of the components for the stationary phase material. A detailed review of stationary phase columns utilised for the separation of different compounds in liquid chromatography/ liquid chromatography-mass spectrometry (LCMS) system's components, and different extraction procedures for the analysis of samples are contained in the report by Albratty *et al* [15].

1.2.2 Gas Chromatography:

Discovered in the 1950's, gas chromatography (GC) is used for separating compounds which can easily be vaporised without decomposition. The mobile phase is an inert carrier gas such as helium while the stationary phase is a thin layer of liquid or polymer on an inert solid support packed into a long metal or glass capillary several meters long therefore unlike LCMS,

the separation of the components here occurs between the gas phase and the liquid stationary phase. Gas chromatography can also be coupled to a high-resolution mass spectrometry system (GC-MS) to maximise the value of the results. GC-MS has greatly influenced the development of metabolomics in a positive manner. Through the capillary GC column, a high-resolution separation is achieved. GC also offers a significant improvement of peak resolution through its controlled temperature programme and has also facilitated the recognition of the unknowns by matching the libraries with electron impact ionisation mass spectra. In addition to this, as the GC-MS uses an inert gas as the mobile phase, no solvent background noise is obtained as is the case in LCMS. However, the use of GC-MS has a major drawback as the sample to be analysed has to be volatile, which may not be the case with most metabolites. A review of the recent advances in GC-MS approaches to metabolomics can be found in the report by Beale *et al* [16].

1.2.3 Capillary Electrophoresis (CE):

Capillary electrophoresis (CE) is a powerful analytical technique for separating liquid samples. The component ions in the sample are separated on the basis of the charge they carry as well as their electrophoretic mobility by utilising an applied voltage. The electrophoretic mobility is the observed rate of movement of a charged species in a medium divided by the applied electric field strength in a particular medium and is dependent the charge carried by the ion as well as its size and the viscosity of the medium. Neutral molecules therefore will not be separated by this technique as they are not affected by an electric field. For ions of the same size the ion which has the larger charge moves fastest. As a method of analysing the metabolomic samples CE is under used but has gained popularity in the recent times when used in

combination with mass spectrometry [17]. CE is mainly used to separate isomeric compounds [4].

1.3 Analytical methods used for Metabolomics Studies:

1.3.1 Nuclear Magnetic Resonance Spectroscopy (NMR):

Nuclear Magnetic Resonance (NMR) spectroscopy is a powerful analytical tool with diverse applications in research from structure elucidation to understanding reaction mechanisms and kinetics. In recent years NMR has been widely utilised as a technique for metabolomics studies especially in the agricultural, veterinary, medicinal and pharmacological disciplines where it is employed to identify biomarkers of diseases [18]. It provides complementary information to mass spectrometric-based metabolomics profiling, however, in comparison to mass spectrometry, NMR is a much less sensitive, but highly specific method [4, 19]. A summary of the recent advances in NMR approaches to metabolomics can be found in the reviews by Kerem, Bingol *et al* and Nagana *et al* [20-22].

1.3.2 Mass Spectrometry (MS):

The analysis of molecules on the basis of their relative molecular mass is achieved by the analytical tool technique called Mass spectrometry. Mass spectrometry provides both qualitative and quantitative information about an analyte and works by the formation, in the gas phase, of ions (either positively or negatively charged) which are accelerated in a detector and subjected to either an electric or magnetic field then separated by differences in mass to charge ratio (m/z) of the ions [23]. With the ability of the technique to monitor a huge number of metabolites simultaneously, mass spectrometry has been recognised as the most powerful metabolomics technique [19]. This technique has proved to be helpful for the development of the metabolomics field

because it is highly sensitive and specific when used in conjunction with different chromatography platforms like gas chromatography, liquid chromatography or capillary electrophoresis. Its use in combination with other platforms is due to the limitations of a single technique to detect all the metabolites present. Thus limitation can however be overcome with the use of multiple platforms and increasingly larger quantities of metabolites can be detected. Despite the time limitation of the technique, due to the long analysis times (30-60 min/run), it provides highly reliable methods for the detection, quantification and identification of metabolites to a great extent [2, 4, 24].

1.4 Mass Spectrometry Ionization Methods:

1.4.1 Electrospray Ionization (ESI):

In ESI, an electric charge is applied to a solution of the sample to aid the transfer of ions from the solution into the gaseous phase. This means that both charged species in solution as well as neutral molecules, which are converted into positive ions by protonation, can be analysed with great sensitivity [23]. Polar solvents with an organic modifier, to aid ionisation, are often used for dissolving the sample which facilitates its transportation through a channel with a high electric potential. A Taylor cone is formed between the mass spectrometer and the needle containing a charged aerosol. The charge on the aerosol is obtained from the high electric potential that is applied to the needle (1-4 kV). The charged droplets evaporate in a stream of warm nitrogen and become smaller, which increases the electrostatic repulsion between individual ions within the droplet. This electrostatic repulsion causes the droplets to break up eventually producing naked ions (Figure 1-1). The action of the electric field applied between the needle and ion transfer capillary causes the ions to move towards the latter. These ions

are then transferred to the high vacuum region of the mass analyser where their charge to mass ratios (m/z) are determined [25]. The advantages provided by this method make it the most used technique with liquid chromatography. ESI is based on two ion modes, namely negative ion electrospray ionisation (NIESI) and positive ion electrospray ionisation (PIESI). Amino acids, having both positive and negative charges, can be detected in either mode; however, PIESI provides more sensitivity in comparison to NIESI. Although PIESI enables detection of amine group-containing compounds below 1 ng/ml, polar acid groups cannot be ionised with it. Compounds which contain polar acid groups include Krebs cycle intermediates such as succinate and fumarate that can easily be detected by NIESI. In the ESI, there is a likelihood to form multiple ions with adducts from the species contained in the mobile phase. For instance, methanol, ammonia, calcium, acetonitrile and potassium adducts are formed in the positive mode and chloride, acetic acid and formic acid adducts are formed in negative mode. A high percentage of organic solvent in the mobile phase can enhance efficient ionisation of compounds during ESI because it facilitates aerosol formation and solvent evaporation leading to the formation of gas phase ions [24, 26].

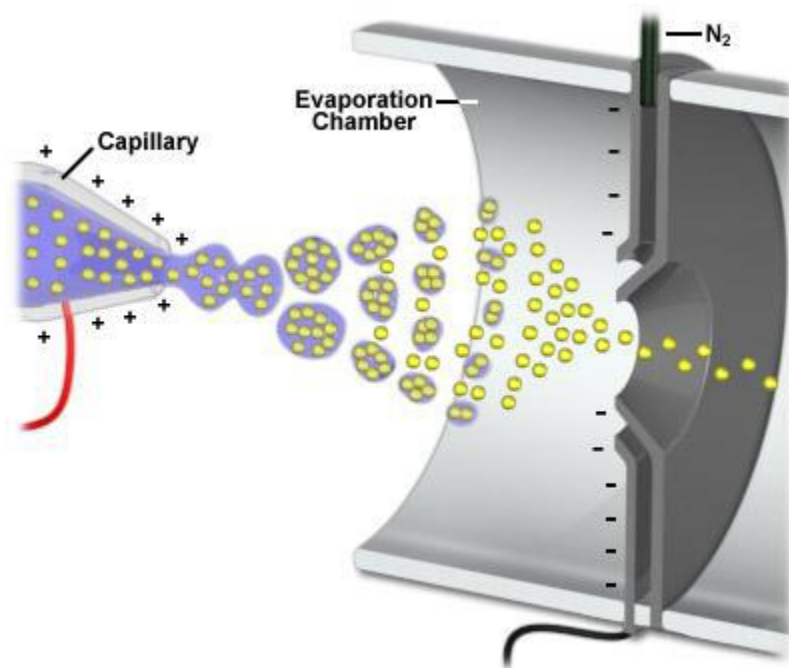


Figure 1-1 Ionization process of ESI

1.4.2 Electron ionisation (EI):

First described in 1918, EI, formerly known as Electron impact Ionisation and Electron bombardment ionisation is one of the oldest ionisation techniques used in mass spectrometry [27-29]. EI is a hard ionisation technique which works by the bombardment of solid or gas phase atoms with high energy electrons to form ions and leads to extensive fragmentation. It is compatible with several separation techniques and has found applications in GC-MS and LCMS [30]. Obtaining spectra with many fragments is one of the important advantages of EI-MS, because of its application to structure elucidation [31]. A diagnostic fingerprint can be produced by the use of fragments that comprise the spectra. This fingerprint is compared with spectral libraries *via* mass/intensity correlation. The spectral libraries are very broad and widespread having been built up over the years since the introduction of EI-MS. Due to the long history of EI and extension of the spectral libraries, there are more than 100,000 spectra

currently available [4]. EI-MS is a very popular ionisation technique which has found applications a diverse range of research areas such as in archaeology, environmental sciences, forensics, agriculture, pharmaceuticals, food and biological sciences among others [30, 32-35].

1.4.3 Chemical ionisation (CI):

First introduced in 1966 by Burnaby Munson and Frank H. Field, CI is a soft ionisation technique which operates by the reaction of ionized reagent gas molecules, ionised by EI, with molecules of the analyte in the gas phase to form ions of the analyte [36-38]. This ionization process leads to less ionization than the direct ionization seen in EI and the extent of ionization can be controlled by careful selection of reagent gas. As for EI, the fragments obtained in CI are useful for the elucidation of molecular structures of unknown molecules [31]. CI can also be coupled with separation techniques such as GC in GC-CI-MS, LC in LC-CI-MS and capillary electrophoresis. It is however restricted to volatile compounds. Popular variants of CI include atmospheric pressure chemical ionization (APCI), in which water is usually used as the reagent gas, charge exchange chemical ionisation which differs from CI by the production of a radical cation which has an odd number of electrons and negative chemical ionization (NCI or NICI), in which the analyte has to be able to produce a negative ions [39-41].

1.4.4 Matrix Assisted Laser Desorption/ionisation (MALDI)

Matrix Assisted Laser Desorption/ionisation, a term coined by Hillenkamp *et al*, is an ionisation technique discovered in the 80's which utilises lasers, (UV or IR), in conjunction with a crystalline compound referred to as a matrix which is capable of absorbing laser energy and transferring it in order to ionise large molecules with little fragmentation of the molecule [42-45]. MALDI can be coupled with chromatographic techniques such as LC and size exclusion

chromatography and has a wide range of applications in chemistry, biochemistry, materials, biological and medical sciences [46-52]. MALDI is a static technique in which the sample to be tested is co-crystallised on a plate together with the matrix. MALDI is one of the most effective techniques for the ionisation of molecules which are highly phosphorylated. In many instances, molecules are suppressed rather than ionised during ESI-MS however, this can however be overcome by utilising MALDI. It has been observed that the process of ionisation of highly phosphorylated compounds such as ATP, NADP and acetyl-CoA are suppressed during ESI-MS while ionisation occurs readily utilising MALDI [53, 54]. This is because compounds that are highly phosphorylated tend to form tight pairs with other ions contained in the biological matrix. These ion pairs are so strongly bound that the individual compounds cannot be ionised by ESI-MS. Without interfacing with chromatography, automated systems exist that help in the application of MALDI in combination with separation. These systems help to collect LC fractions and spot them on the sample plate for analysis by MALDI. The process of spatial mapping of tissues benefits greatly by the use of the MALDI technique[4].

1.5 Ion Separation and Detection Methods

Mass spectrometry is used for the determination of the mass of analytes and this process is accomplished in four major steps (Figure 2). First, the sample is introduced either in the liquid or gaseous form. In the second step, the ionisation process produces ions from the sample after the introduction of the sample. Thirdly, a mass analyser is used to separate the ions produced from the sample on the basis of their mass to charge ratio (m/z). In the last step, the ions are physically detected. This process of detection is based on the ion current. The whole process of sample analysis is depicted in the image reproduced below (Figure 1-2) [2].

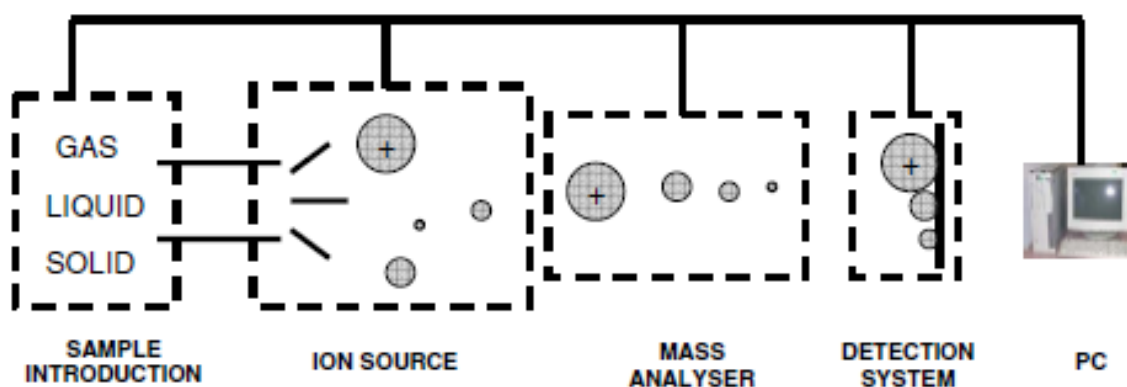


Figure 1-2 Mass spectrometer operating process[2].

Metabolite identification utilising molecular mass measurement can be accomplished by two different protocols using the mass spectrometer. The first approach is to obtain the molecular mass to a high degree of accuracy in order to determine the precise elemental composition (molecular formula). The second approach involves obtaining a collection of the mass spectra of fragments from the analyte, which can be used to elucidate the molecular structure of the analyte. The process of metabolomics can be carried out with the aid of different types of mass analysis techniques also known as ion separation techniques.

1.5.1 Quadrupole systems

In combination with a high-quality chromatographic system, a single quadrupole instrument is capable of providing data regarding highly complex systems. Moreover, the reasonable cost of these LCMS systems provides an additional advantage. It however fails to deliver accurate mass measurement or fragmentation patterns. Triple quadrupole (Tandem MS) instruments are used mainly to produce fragments in the analysis of drugs and their metabolites. These instruments deliver high sensitivity. The resolution of these instruments is limited to about 0.5 amu which is considered as the one of its major disadvantages.

1.5.2 Ion traps

Another type of mass analyser is an ion trap mass analyser or quadrupole ion trap. They operate by storing the ions generated from the analytes in an ion trap prior to detection [55]. They however have a lower mass resolution when compared to other types of instruments [56]. They are cheap to manufacture and have the added advantage of that multiple fragmentation, MS/MS experiments, can be performed on the stored ions which provides useful additional structural information as well as the molecular ion.

1.5.3 Time-of-flight analysers (TOF analyser)

In time-of-flight analysers, measurements of the time taken by the ions to arrive at the detector is used to determine the charge to mass ratio (m/z) with the aid of an electric field of known strength. TOF instruments initially faced the problem of poor resolution due to the variations in the kinetic energies exhibited by the ion population [57]. This problem was solved by the introduction of the reflectron which greatly improved the focusing of these ions [58]. The use of quadrupole time of flight (QTOF) instruments is recommended for the routine analysis of metabolomics samples as this hybrid instrument is able to obtain accurate mass data and provide fragmentation information. The resolution of this instrument is dependent on the length of the flight tubes, which is a drawback that affects its resolving power. Very sensitive methods for the detection of proteins has been developed by combining TOF and MALDI [59-61].

1.5.4 Fourier transform ion cyclotron resonance analyser (FT-ICR)

Developed about 30 years ago by Comisarow and Marshall, FT-ICR has a high sensitivity and gives the highest mass resolution of all ion detection systems [62]. It also has a mass accuracy

less than 1 ppm but only when internal standardisation is used [63]. FT-ICR functions similarly to an ion trap however here the ion trap is embedded in a magnetic field which causes the trapped ions to resonate at their cyclotron frequency. A secondary electric field at or near the cyclotron frequency of the trapped ions then excites the ions into a larger orbit which is measured as they pass by detectors situated on opposite sides of the trap [62]. The major drawback with the instrument is that FT-ICR's ion-to-ion interaction limits the range of measurements, which depends on the frequency of the oscillating ions. In addition, the cost of this mass analyser is very high [64].

1.5.5 Orbitrap mass analyser

The Orbitrap mass analyser was invented by Makarov and was later introduced to the market by Thermo Fisher Scientific in the year 2005 [65-67]. In this system, ions are trapped on the basis of electrostatic trapping. During analysis, ions are injected into the trap (Orbitrap) with the aid of the C-trap which acts as a temporary storage trap of ions separated from the linear trap component of the system. The Orbitrap consists of an outer barrel-like electrode and an inner spindle like electrode. Injected ions undergo both circular motion about the inner electrode as well as axial harmonic oscillations, and it is the latter that are dependent on the mass-to-charge (m/z) ratios of the ions. Ion detection occurs *via* an image current generated by the ions undergoing lateral oscillations along the axis of the inner electrode. Fourier transformation of the image current gives rise to the m/z ratios of the ions in the trap. Even low concentrations of ions (<1 ng/ml) can be easily measured as the Orbitrap can detect very small variations in the current image. The orbital trapping is based on axial rotations of the ions which has no connection with m/z ratios. It has a large space charge capacity at higher masses and large trapping volume and high mass resolution.

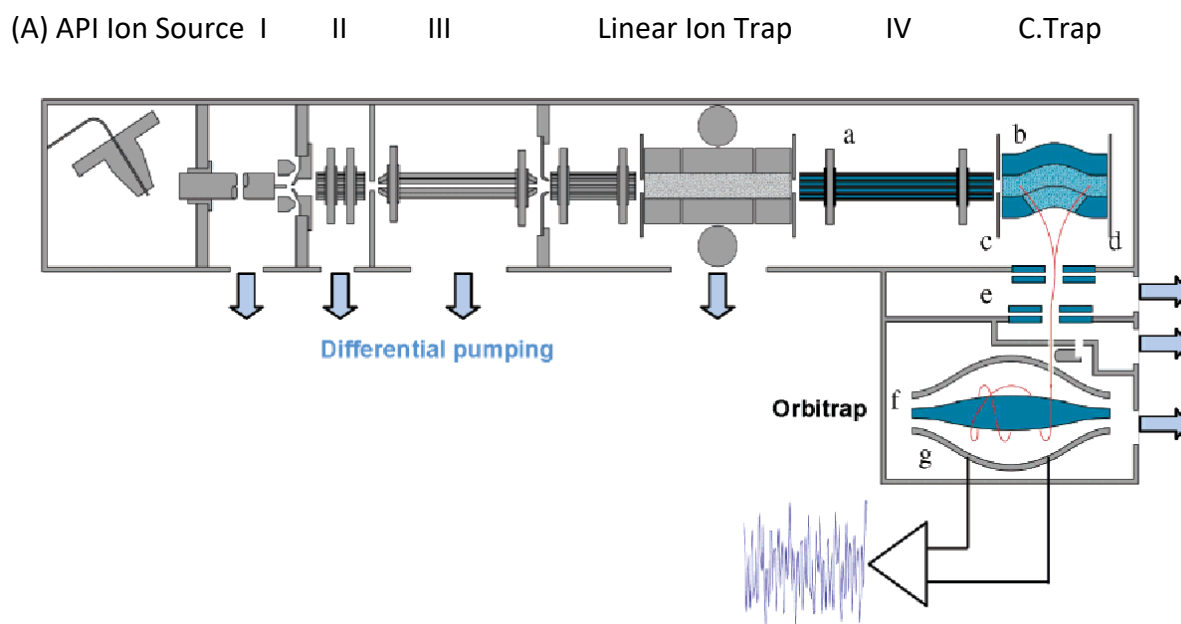


Figure 1-3 The parts of the LTQ-Orbitrap: (I) heated capillary, (II) multi-pole focusing devices, (III) a gating lens, multi-pole (IV) a, transfer octopole; b, curved RF-only quadrupole (c-trap); c, gate electrode; d, trap electrode; e; ion optics, f; inner spindlelike; g, outer barrel-like [68]

These features are missing in FT-ICR instruments and the Paul trap. The Exactive, Discovery and Orbitrap XL are the three Orbitrap instrument that are available on the market. Exactive instruments measures masses accurately without fragmentation, although the Q-Exactive can now provide fragmentation information, while Discovery instruments provides both the benefits of accurate mass measurements and fragmentation. Orbitrap XL instruments provide additional advantages of high/low energy fragmentations [4, 24, 65, 69].

1.6 Limitations of metabolomics profiling/study:

Many compounds are inherently difficult to analyse and may thus escape detection *via* liquid chromatography–electrospray ionization mass spectrometry (LC–ESI–MS). Some compounds may be too hydrophilic to be sufficiently retained in the reverse phase LC column or have low ionization yields due to the absence of ionisable functional groups. Similarly, MS responses

might vary, even under the same LC conditions, due to metabolite fluctuations and variations in ionization efficiencies, making the quantitative profiling of metabolites by MS an ongoing challenge [70].

One major solution to these problems comes *via* the application of chemical tagging a strategy that has been industrialised for MS-based platforms. Both qualitative and quantitative profiling of metabolites is possible *via* this technique. Chromatographic behaviours of poorly retained polar and ionic metabolites are altered by the addition of ionizable functional groups tagging. Moreover, the isotope-labelled versions of the tags can be used to prepare internal standards to overcome matrix and ion suppression effects [70]. This technique introduces a light isotope tag to the analytes in one sample and a heavy isotope tag to another comparative sample [71]. Common functional group metabolites are recognised easily by “determination of a chromatographically co-eluted pair of isotope-labelled analytes (MS doublet peaks) with characteristic mass difference” which enables their identification and quantification [72]. For example, use of ^{13}C and ^{12}C -dansyl chloride has been shown by Guo *et al.* to derivatise amine and phenolic hydroxyl groups [72, 73]. Their experiment highlighted the improved separation of labelled metabolites on a reversed phase liquid chromatography (RPLC) column.

This technique also allows for the analysis of polar and even ionic metabolites using RPLC since the derivatising ligand can alter the overall polarity of the resulting molecule. This increases the likelihood of successful analysis of amine and phenol groups in the sub-metabolome, with diverse physiochemical properties, using only one LCMS condition. When compared to an untagged metabolite, the detection sensitivity of the instrument increases up to 1000-fold with the use of dansyl-labelled metabolites. A variety of biomarkers of diseases and

cellular metabolomics have been discovered *via* this dansyl-labelling LCMS protocol. The only issues that exist arise from multiplexed sample preparation including isotope labelling [74].

1.7 Flux Analysis:

Using metabolic fingerprinting, it is possible to study changes in steady state levels of metabolites, while flux analysis allows for direct recognition of synthesis or breakdown of specific intermediates. An excellent example of usage of glucose (carbon or nitrogen flux analysis) is given in the report by Yang *et al.* which postulated about the functioning of a C4 pathway in cyanobacteria using stable isotopes [75]. A ^{13}C labelled glucose analogue was used for the investigation of the metabolic reorganization in *Synechocystis* 6803 (freshwater cyanobacteria) under heterotrophic and mixotrophic growth conditions.

In 2011, reports by both Huege *et al.* and Young *et al.*, used ^{13}C -bicarbonate pulse-labelling to define the major Ci fixation pathways in the cyanobacterium *Synechocystis* 6803 [76-78]. ^{13}C enrichment was seen for up to 60 minutes after addition of the ^{13}C -label. The use of high level, state of the art modelling approaches are required for the evaluation of such labelling experiments and fluxomics, using labelled precursors, have been shown to provide the best insight into cyanobacterial metabolism and its regulation [76]. At present, most of these models provide a rather descriptive analysis and can be used for searching for gaps in pathways or in synthetic biology experiments or for the production of biofuels [79].

1.8 Chemically derivatized isotope-coded mass tag metabolites study:

As the numbers of isotopic analogues of metabolites are limited, the approach of LCMS is not very feasible for metabolomics profiling. *In vivo* stable isotope labelling requires cell culturing which cannot be applied for the analysis of non-culturable samples like human bio-fluids. As

an alternative approach, the use of chemical derivatisation is now possible to introduce an isotope-coded mass tag, produced by chemical synthesis, to metabolites that possess a common functional group (amine, acid, phenol, ketone, etc). A number of reported labelling tags are available commercially [71]. This method leads to an improvement in the separation of compounds by LC and better detection by MS based on improved ionisation. Subsequently, this leads to the generation of better and more comprehensive profiles of the sub-metabolome of a biological system compared to older LCMS methods [80].

1.9 Limitations and Challenges:

As a result of their speed, high throughput, sensitivity and selectivity, mass spectrometry (MS) techniques, play an important role in metabolite profiling. However, many unsolved problems still hamper the progress of continuous exploration of this field such as the concentration of metabolites which can vary greatly between samples and the detection of trace-level metabolites still presents a challenge for MS-based metabolomics. Therefore, the need for well-established, standardized methods and procedures is imperative. Currently, many MS based metabolomic studies rely on relative quantification of the metabolites, which has been referred to as the “Achilles heel” of metabolomics [81]. The chemo-selective formation of adducts, CS-tagging, of specific metabolite functional groups and subsequent detection by high resolution MS has been used to facilitate detection and identification of challenging metabolites. Isotopically enriched tagging reagents have been designed to specifically react with particular functional groups contained by metabolites, such as carboxylate, carbonyl, amino, and sulfhydryl [82-86].

1.10 The aim of the project:

There are many compounds that remain difficult to analyse and detect by liquid chromatography-mass spectrometry due to either poor retention on reversed phase chromatographic systems or limited ionisation due to the absence of ionisable functional groups. Such analytes include sugars and acids. The overall aim of this project is to synthesise appropriate tagging agents labelled with and without stable isotope labelling which will be used in metabolomics profiling of these types of analytes from biological samples. It is envisaged that these tagging agents will:

1. Increase the ionization efficiency in the mass spectrometry system and thus aid detection of analytes.
2. Improve the selectivity and separation of the target analytes.

Chapter Two:

Application of Deuterated Aniline and *p*-(Trimethylammonium) Aniline as Tagging Agents in the Analysis of Sugars by LCMS

2 APPLICATION OF ANILINE DERIVATISATION IN THE ANALYSIS OF SUGARS BY LCMS

2.1 Introduction

Sugars are inherently difficult to analyse because they ionise poorly during liquid chromatography–electrospray ionization mass spectrometry (LC–ESI–MS). Their lack of readily ionisable functional groups leads to low ionization yields. Their strong hydrophilicity also means that they are not sufficiently retained on reverse phase columns giving them poor chromatographic profiles. Sugars can exist as several isoforms in solutions with each of these isoforms interacting differently with the stationary phase of the column which leads to poor resolution of the peaks. Their peaks are typically broad and unresolved from each other which hinders their detection, separation and identification during metabolic profiling studies by LCMS. The broad peaks result from the fact that most sugars can exist as α - and β - anomers of their pyranose and furanose forms which are in equilibrium e.g. glucose shown in figure 2-1.

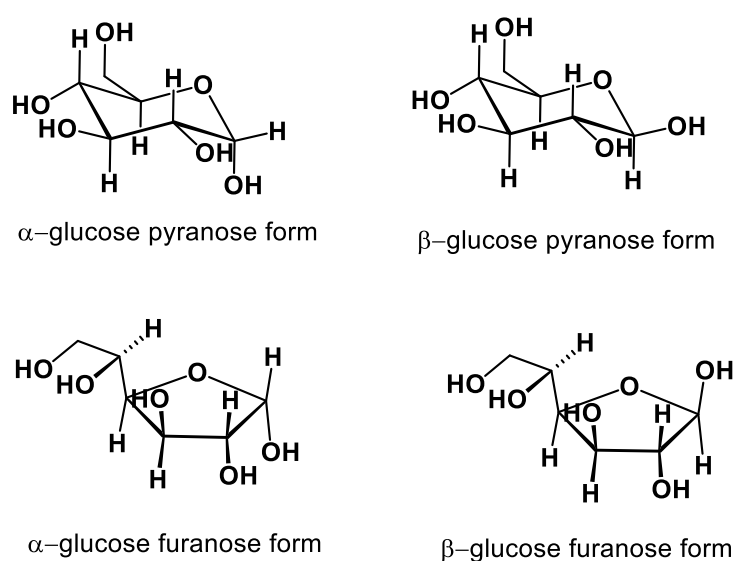


Figure 2-1 The α - and β - anomers of the pyranose and furanose forms of glucose.

The use of tagging agents could greatly improve the detection of sugars and thus significantly increase coverage of the entire metabolome. Chemically synthesised tagging agents could therefore be very important tools for use in the metabolomic profiling of acids and sugars in biological samples. The tag can improve the detection of the ordinarily poorly ionising sugars and also generally alters the overall polarity of the resultant molecule thus modifying their chromatographic profiles leading to better separation on an appropriate column during the chromatographic process [70]. Tagging can aid the analysis of polar and ionic metabolites by reversed phase LC by increasing the lipophilicity of the tagged molecule which leads to an increase in their retention on the column. Tagging also increases the likelihood of successful analysis of both positively and negatively charged compounds within the same sample. For example, derivatizing all the acids in a sample with a positively charged tagging agent before analysing the samples enables their detection in ion positive mode. By this protocol, a more comprehensive analysis of a given sub-metabolome can be achieved.

One of the commonly used tagging procedures involves the use of isotope-labelled analogues which also act as internal standards to overcome the effects of matrix and ion suppression [70]. In this technique, a light isotope tag is introduced to the analytes in one sample and a heavy isotope tag is introduced to a second comparative sample [71]. Common functional group metabolites are easily recognised by “determination of a chromatographically co-eluted pairs of isotope-labelled analytes (MS doublet peaks) with a characteristic mass difference” which enables their identification and quantification [72]. For example, the use of ^{13}C and ^{12}C -dansyl chloride was reported by Guo *et al*, to be of use in the derivatisation of amine and phenolic hydroxyl groups [72, 73]. When compared to unlabelled metabolites, detection

sensitivity of the instrument increased by up to 1000-fold with the use of dansyl-labelled metabolites [73]. A variety of biomarkers of diseases and cellular metabolomics have been discovered *via* this dansyl-labelling LCMS method. The only negative issues that exist with this method come from the complex sample preparation required including isotopic labelling [74].

2.2 Aim

The aim of this study was to investigate the suitability of three tagging agents, trimethyl(*p*-aminophenyl)ammonium chloride hydrochloride, aniline and D₅-aniline, for the analysis of hexose sugars to evaluate their suitability for application to metabolomics samples. The PTMA tagging agent was first synthesised and purified before its use in the derivatisation reactions. The tagging agents were used in the first instance to derivatize the four hexose sugars: glucose, galactose, mannose, and fructose before analysis of the resulting derivatives by ESI-LCMS on an Orbitrap mass spectrometer.

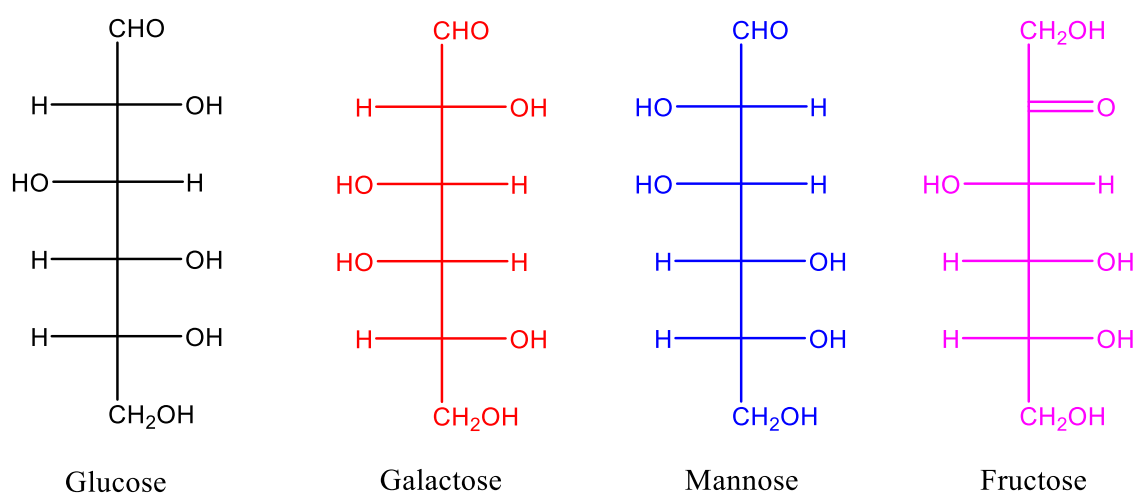


Figure 2-2: A Fischer projection representation of the different sugars used in the experiment. They are all isomers with molecular formula C₆H₁₂O₆ and MW 180.16.

The general scheme for the derivatisation reactions is as represented in the schematic diagram, (Figure 2-3), which shows the reaction for glucose. The tagging reaction involves a 2 stage reductive amination of the aldehydic form of the sugar firstly forming a Schiff's base intermediate which is then reduced by a suitable reducing agent to afford a stable amine derivative which is envisaged to simplify the chromatography of the sugar because it forms a single amine product with all the isoforms of the sugar which is also stable against hydrolysis. The open aldehydic form of glucose is favoured at low pH. This is achieved by the use of 10% acetic acid in the solvent. The amine from the tagging group will only react with the aldehydic form of the sugar if it is unprotonated therefore the selection of the amine is very important because sufficient amounts of the amine must remain unprotonated at the pH at which the reaction is run in order to favour the sugar adopting the open aldehydic conformation in the reaction solution. Glucose reacts with the free amino group of the tagging agent in a reductive amination reaction which is accompanied by the loss of water. The resulting intermediate Schiff's base (both *Z*- and *E*- forms) is then reduced in the presence of picoline borane to form the target stable derivative. Picoline borane is favoured as the reducing agent in this experiment because it is stable at the low pH in which the reaction is run at.

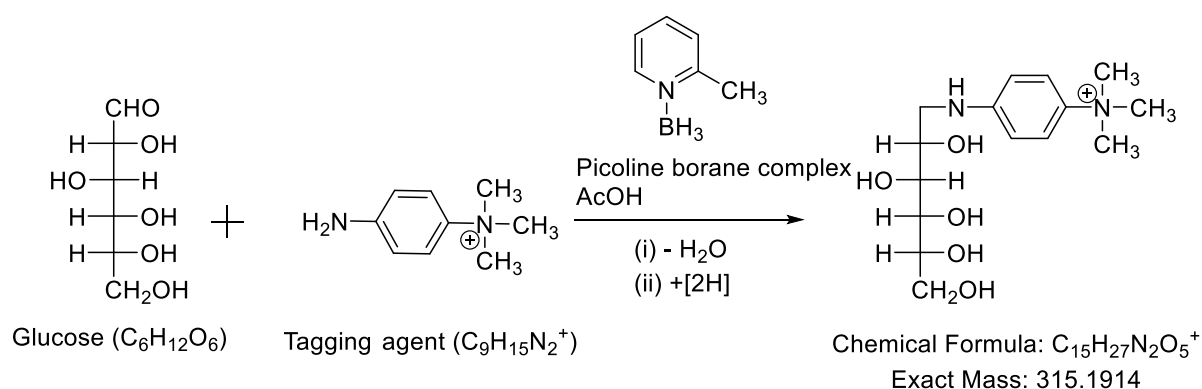


Figure 2-3: The reaction of glucose with the tagging agent, 4-Amino-N,N,N-trimethylanilinium, to produce the target stable derivative.

2.3 Materials and methods

^1H and ^{13}C NMR spectra were measured on a Bruker DPX-400 MHz spectrometer with chemical shifts given in ppm (δ values), relative to proton and carbon traces in solvent. Coupling constants are reported in Hz. Mass spectra were obtained on an Orbitrap Mass Spectrometer. Anhydrous solvents were obtained from a Puresolv purification system, from Innovative Technologies, or purchased as such from Aldrich. Rotary evaporators were used to produce dry samples in preparation for analysis by removing water or organic solvents. Melting points were recorded on a Reichert hot stage microscope, and are uncorrected. Chromatography was carried out using 200Å, 400 mesh silica gel.

2.3.1 Chemicals and reagents

All commercially available solvents and reagents including the hexose and pentose sugars, aniline, $^2\text{H}_5$ -aniline and 2-Picoline-borane complex were obtained commercially from Sigma-Aldrich, UK, except those synthesized in the laboratory as described in the experimental section, and were used as supplied without further purification

2.3.2 Synthesis of (N-[4-(dimethylamino)phenyl]acetamide (1) [87].

This first reaction of the series for the synthesis of the target tagging agent was performed according to the method reported by Maier et al [87]. A solution of *N,N*-dimethylbenzene-1,4-diamine (1.0 g, 7.34 mmol) was made in dichloromethane (15 mL). To this solution, (1.634 g, 2.25 mL, 16.15 mmol) of triethylamine was added at 0 °C. The mixture was then stirred for 15 minutes before adding (0.69 ml, 0.75 g, 7.3 mmol) of acetic anhydride solution in dichloromethane (10 mL) at 0 °C. The reaction was then allowed to proceed at room temperature for

an extra 5 hours before quenching by the addition of water. The organic layer, which contained the desired product **1** (Figure 2-4), was extracted and dried over anhydrous Na_2SO_4 before being concentrated under vacuum to give the crude product. Following further purification *via* column chromatography eluting with ethyl acetate/hexane (1:1) as the mobile phase, the desired final product was isolated in a 63% yield (0.83 g, 4.65 mmol) as a brown solid.

mp 132-133 °C.

^1H NMR (500 MHz, $\text{DMSO}-d_6$) δ 1.98 (s, 3H), 2.83 (s, 6H), 6.67 (d, $J = 9.1$ Hz, 2H), 7.37 (d, $J = 9.1$ Hz, 2H), 9.59 (s, 1H).

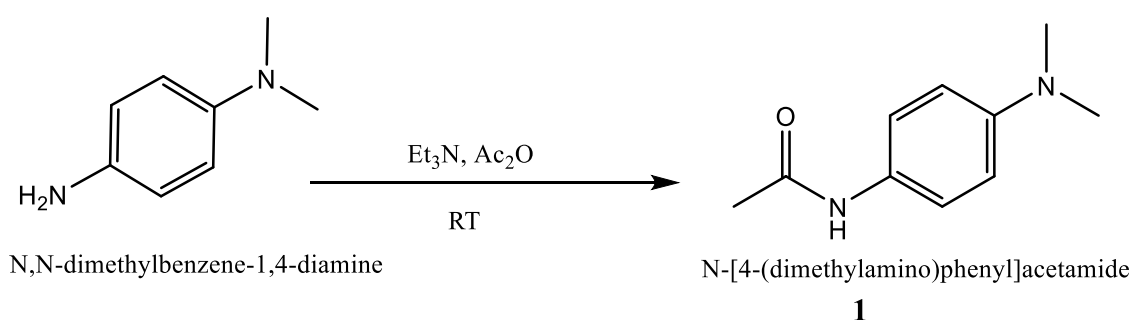


Figure 2-4: Synthesis of (N-[4-(dimethylamino)phenyl]acetamide from N,N-dimethyl-benzene-1,4-diamine.

2.3.3 Synthesis of methyl 4-methylbenzenesulfonate (2.)[88]

A volume of 20 mL of methanol was first dried by heating it under reflux in the presence of magnesium and iodine for 30 min. The dry methanol was then distilled from this mixture. Triethylamine (1.9 mL, 13.6 mmol) was added to the dried methanol (0.5 mL, 1.23 mmol). *p*-Toluenesulfonyl chloride (2.50 g, 13.5 mmol) dissolved in 9 mL of dry toluene was then added to the cooled reaction mixture in 3 ml portions over 10 min. The mixture was stirred for 1 hour at 0 °C before being filtered over Celite®. The filter cake was washed with 20 mL of

ice-cold toluene. The solvent was then removed under reduced pressure to give the crude desired compound **2** as an amber liquid (Figure 2-5). Further purification by column chromatography eluting with ethyl acetate/hexane (1:4) gave the title compound (1.78 g, 9.57 mmol, 73%) as a colorless oil.

$^1\text{H NMR}$ (500 MHz, $\text{DMSO-}d_6$) δ 2.44 (s, 3H), 3.71 (s, 3H), 7.50 ((d, $J = 8.3$ Hz, 2H), 7.79 (d, $J = 8.3$ Hz, 2H).

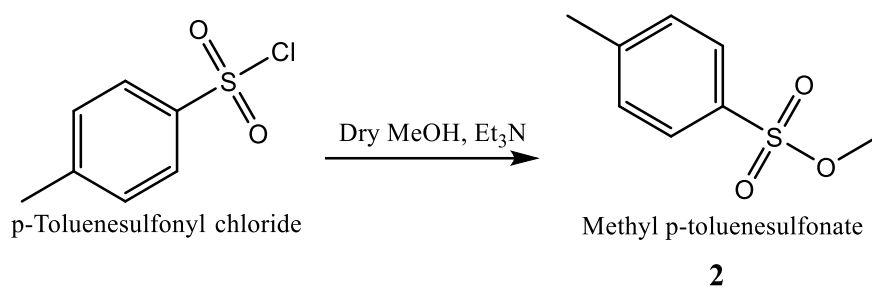


Figure 2-5: Synthesis of methyl-*p*-toluenesulfonate from *p*-toluenesulfonyl chloride

2.3.4 Synthesis of Trimethyl(*p*-acetamidophenyl)ammonium *p*-toluenesulfonate (**3**) [89].

This synthesis was carried out according to the method reported by Taylor *et al* [89]. A solution containing *p*-dimethylaminoacetamide (**1**) (0.5 g, 2.80 mmol) and methyl *p*-toluenesulfonate (**2**) (0.5 g, 2.68 mmol) in 100 ml of acetone was refluxed, with stirring, for a period of 3 hours. The intended final product **3** crystallized out of the solution (Figure 2-6) to give the target product (0.35 g, 9.60 mmol) in 73% yield.

mp 217-218 °C.

$^1\text{H NMR}$ (500 MHz, $\text{DMSO-}d_6$) δ 2.08 (s, 3H), 2.29 (s, 3H), 3.57 (s, 9H), 7.11 (d, $J = 8.1$ Hz, 2H), 7.48 (d, $J = 8.1$ Hz, 2H), 7.76 (d, $J = 9.5$ Hz, 2H), 7.88 (d, $J = 9.5$ Hz, 2H), 10.27 (s, 1H).

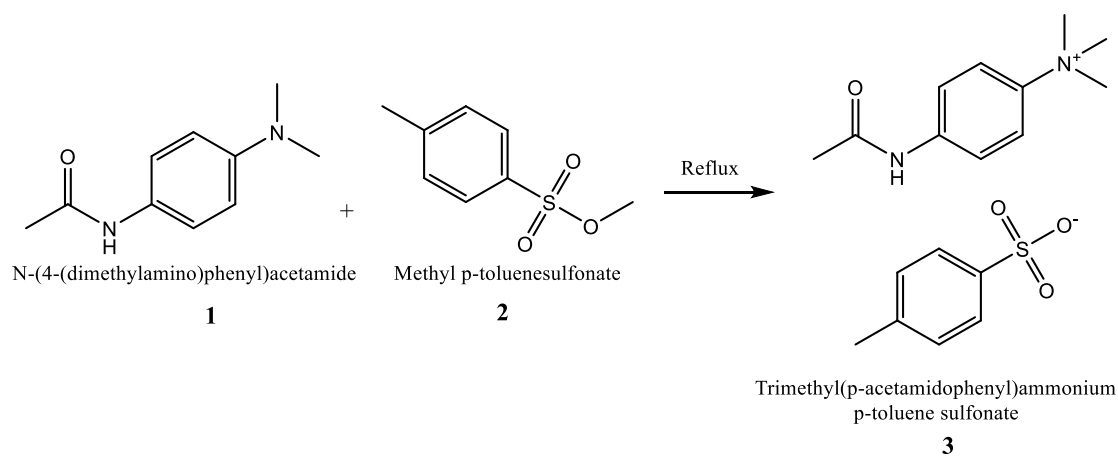


Figure 2-6 Synthesis of trimethyl(p-acetamidophenyl)ammonium p-toluene sulfonate **3** from N-(4-(dimethylamino)phenyl)acetamide **1** and methyl-p-toluenesulfonate **2**

2.3.5 Synthesis of trimethyl(p-aminophenyl)ammonium chloride hydrochloride (**4**) [89].

This final product **4** was synthesised according to the method by Taylor *et al* [89].

A solution containing (0.3 g, 8.23mmol) of trimethyl(*p*-acetamidophenyl) ammonium *p*-toluenesulfonate **3** in 20 mL of 50% (v/v) concentrated hydrochloric acid-ethanol was refluxed for 2-3 hours (Figure 2-7). Acetone was then added to the hot solution drop wise until it became cloudy. The resulting mixture was then allowed to cool which led to the formation of the target compound as clear white crystals (0.135 g, 6.05 mmol) in a 74% yield.

mp at 223 °C

^1H NMR (500 MHz, DMSO- d_6) δ 3.58 (s, 9H), 7.16 (d, $J = 8.6$ Hz, 2H), 7.85 (d, $J = 9.2$ Hz, 2H).

^{13}C NMR (126 MHz, DMSO- d_6) δ 57.0, 119.6, 122.0.

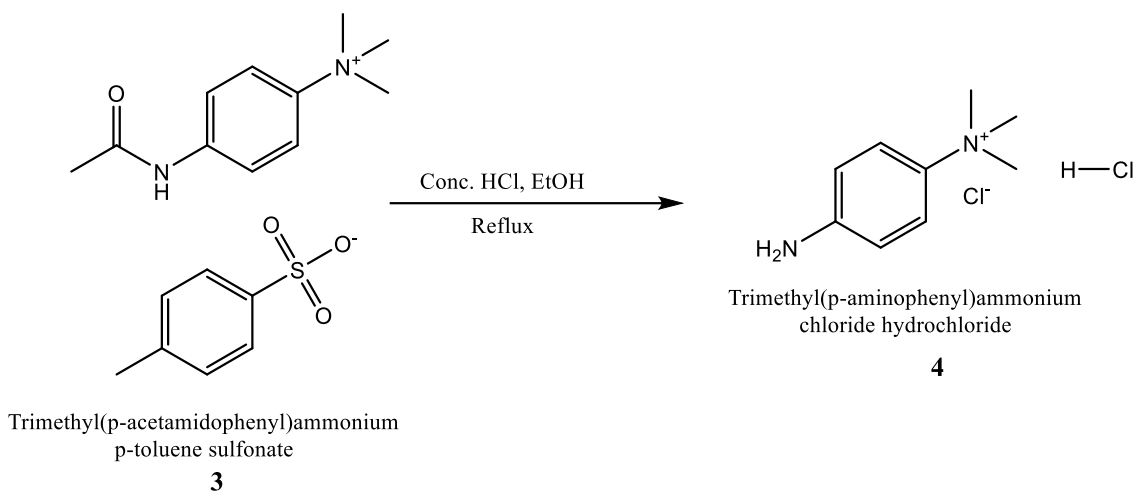


Figure 2-7 Synthesis of trimethyl(*p*-aminophenyl)ammonium chloride 4 from trimethyl(*p*-acetamidophenyl)ammonium *p*-toluene sulfonate 3

2.4 Derivatisation of the sugars

2.4.1 Derivatisation with trimethyl(*p*-aminophenyl)ammonium chloride hydrochloride (4).

A solution of each of the sugars was prepared at a concentration of 1 mg/mL in methanol/water (1:1). The tagging compound, trimethyl(*p*-aminophenyl)ammonium chloride hydrochloride (**4**), was prepared at a concentration of 10 mg/mL in methanol/water containing 10% v/v acetic acid (50:50) (solution A). A solution containing 10 mg/mL of picoline borane was also prepared in methanol/water (1:1) (solution B). 50 µg of the sugar was then mixed with 40 µL of solution A and heated in a heating block at 40 °C for 30 minutes before adding 20 µL of solution B. The resulting mixture was again heated at 40 °C for 45 minutes. After the heating, the sample was blown to dryness with nitrogen, re-dissolved in 0.2 mL of water containing 0.1 % formic acid, and then 1 mL of acetonitrile was added. The resulting final solution was analysed by LCMS on the Orbitrap Exactive using a ZIC-HILIC column eluting with 0.01% formic

acid buffer, at a flow rate of 0.6 ml/min with mobile phase A (0.01% v/v formic acid in water) and B (0.01% formic acid in acetonitrile) under the following gradient conditions: 0 min (80% B), 30 min (40% B), 31 min (80% B) and 35 min (80% B).

2.4.2 Derivatisation with aniline and deuterated aniline- d₅

The same procedure described above was repeated using aniline and deuterated aniline as tagging agents. In addition, the derivatized sugars were run under isocratic conditions using the same mobile phase with (A/B) of 20/80, 10/90 and 5/95 respectively. The data was analysed with XCalibur to obtain extracted ion chromatograms to compare the retention times of the derivatives.

2.5 Results

Reductive amination at low pH offers the best approach for chromatographic separation since it causes all the four structural forms of each sugar to form only one final product [90-93]. This approach uses weak bases which should have sufficient amounts of the unprotonated form of the amine available for the reaction with the sugar under the reaction conditions and a reducing agent, which is stable at the low pH required to keep the sugars in their ring open aldehydic/ketonic forms, to convert the sugars into amines [94].

2.5.1 Synthesis of the tagging agent

2.5.1.1 Characterisation of *N*-(4-(dimethylamino)phenyl)acetamide 1

The synthesis began with *N,N*-dimethylbenzene-1,4-diamine therefore as expected the proton NMR spectrum of the isolated compound displayed the characteristic AA'BB' coupling

pattern for a 1,4-disubstituted aromatic moiety at δ_{H} (ppm) δ 6.67 (d, $J = 9.1$ Hz, 2H), 7.37 (d, $J = 9.1$ Hz, 2H) for two sets of two protons each with identical coupling constants. A six proton singlet at δ 2.83 (s, 6H), attributed to the $\text{N}(\text{CH}_3)_2$ group. Another 3 proton singlet at δ 1.98 (s, 3H), attributed to the $\text{CH}_3\text{C}(\text{O})$ - group which was introduced during the reaction and the NH proton at δ 9.59 (s, 1H) confirms the identity of the target compound.

δ_{H} (ppm) 1.98 (s, 3H), 2.83 (s, 6H), 6.67 (d, $J = 9.1$ Hz, 2H), 7.37 (d, $J = 9.1$ Hz, 2H), 9.59 (s, 1H).

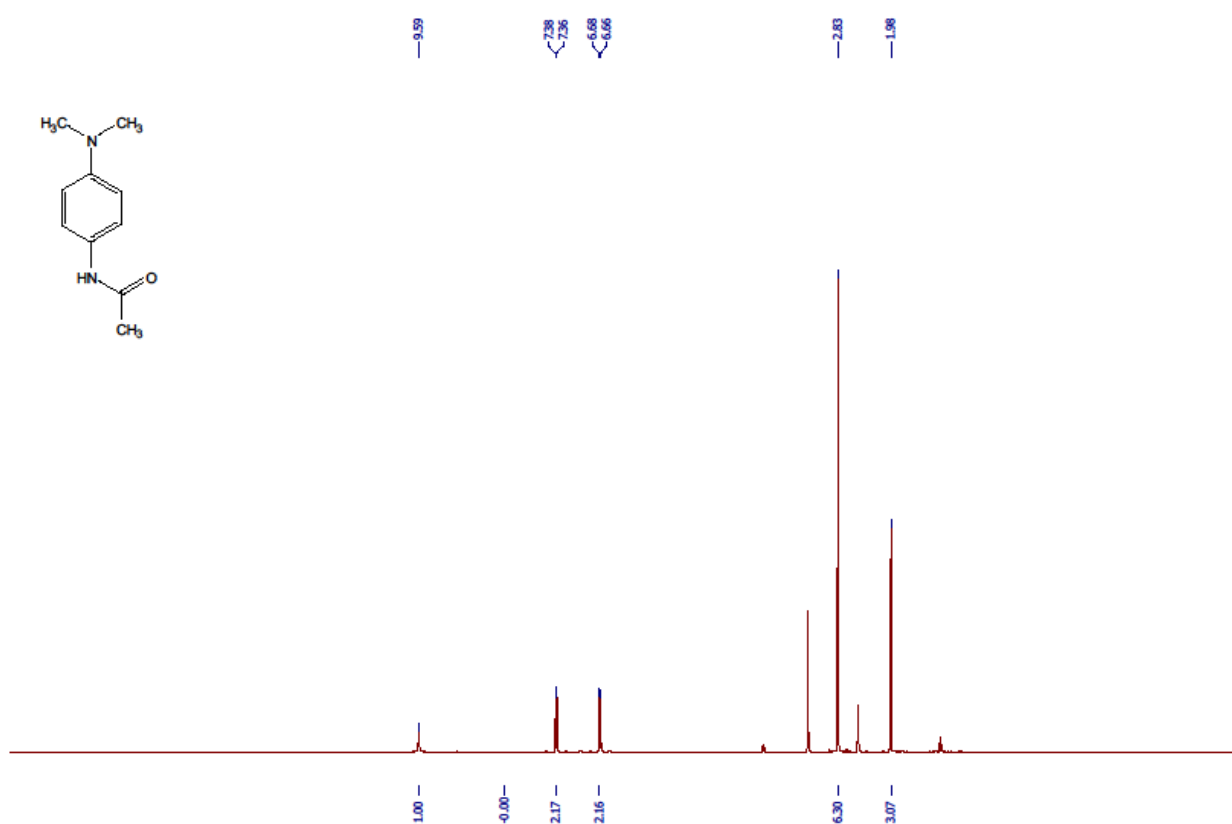


Figure 2-8 ^1H NMR spectrum for N-(4-(dimethylamino)phenyl)acetamide

2.5.1.2 Characterisation of methyl-4-methylbenzenesulfonate 2

As expected the proton NMR of this compound also displayed the characteristic AA'BB' coupling for 1,4-disubstituted aromatic moieties at δ_{H} (ppm) δ 7.50 ((d, $J = 8.3$ Hz, 2H), 7.79 (d, $J = 8.3$ Hz, 2H) for two sets of two protons each with identical coupling constants since the

synthesis was started with p-Toluenesulfonyl chloride. Two 3 proton singlets the first at δ 2.44 (s, 3H), attributed to the aromatic -CH₃ group and another 3 proton singlet at δ 3.71 (s, 3H), attributed to the CH₃O-group complete the identification of the target compound.

δ_{H} (ppm) δ 2.44 (s, 3H), 3.71 (s, 3H), 7.50 ((d, J = 8.3 Hz, 2H), 7.79 (d, J = 8.3 Hz, 2H)

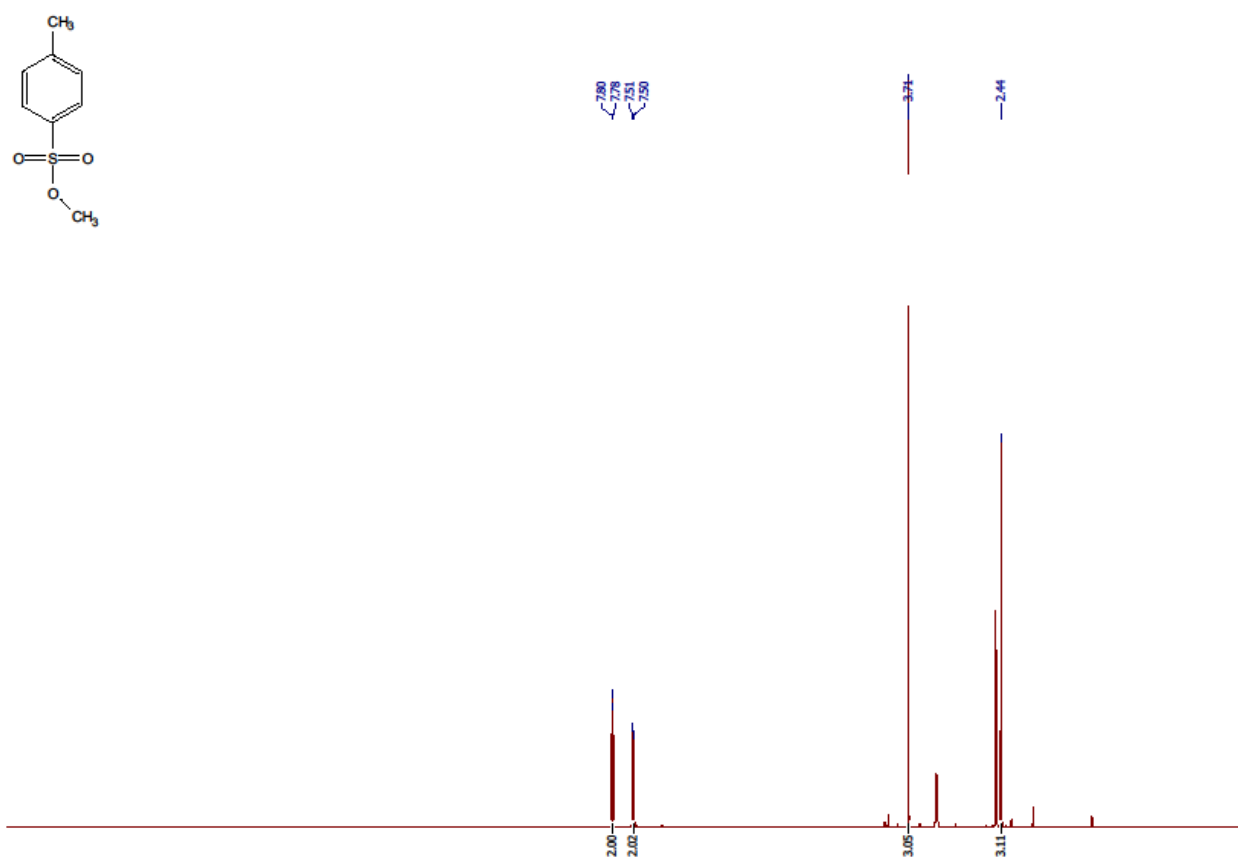


Figure 2-9 ¹H NMR spectrum for methyl 4-methylbenzenesulfonate

2.5.1.3 Characterisation of trimethyl(p-aminophenyl)-4-acetamido-N,N,N-trimethylbenzammonium-4-methylbenzenesulfonate.

The proton spectrum displayed 2 sets of characteristic AA'BB' couplings for 1,4-disubstituted aromatic moieties at δ_{H} (ppm) 7.88 (d, J = 9.5 Hz, 2H) and 7.76 (d, J = 9.5 Hz, 2H) for two sets

of 2 protons each with identical coupling constants for the benzaminium moiety and another two sets of 2 protons each with identical coupling constants for the sulphonamide moiety at δ_{H} (ppm) 7.48 (d, $J = 8.1$ Hz, 2H) and 7.11 (d, $J = 8.1$ Hz, 2H). The three methyl groups on the ammonium ion were observed at δ 3.57 (s, 9H) while the methyl group on the sulphonic acid was observed at δ 2.29 (s, 3H). The proton attributed to the $-\text{NH}$ group was observed at δ 10.27 (s, 1H) while the acetamide methyl (s, 3H) was observed at δ 2.08 ppm.

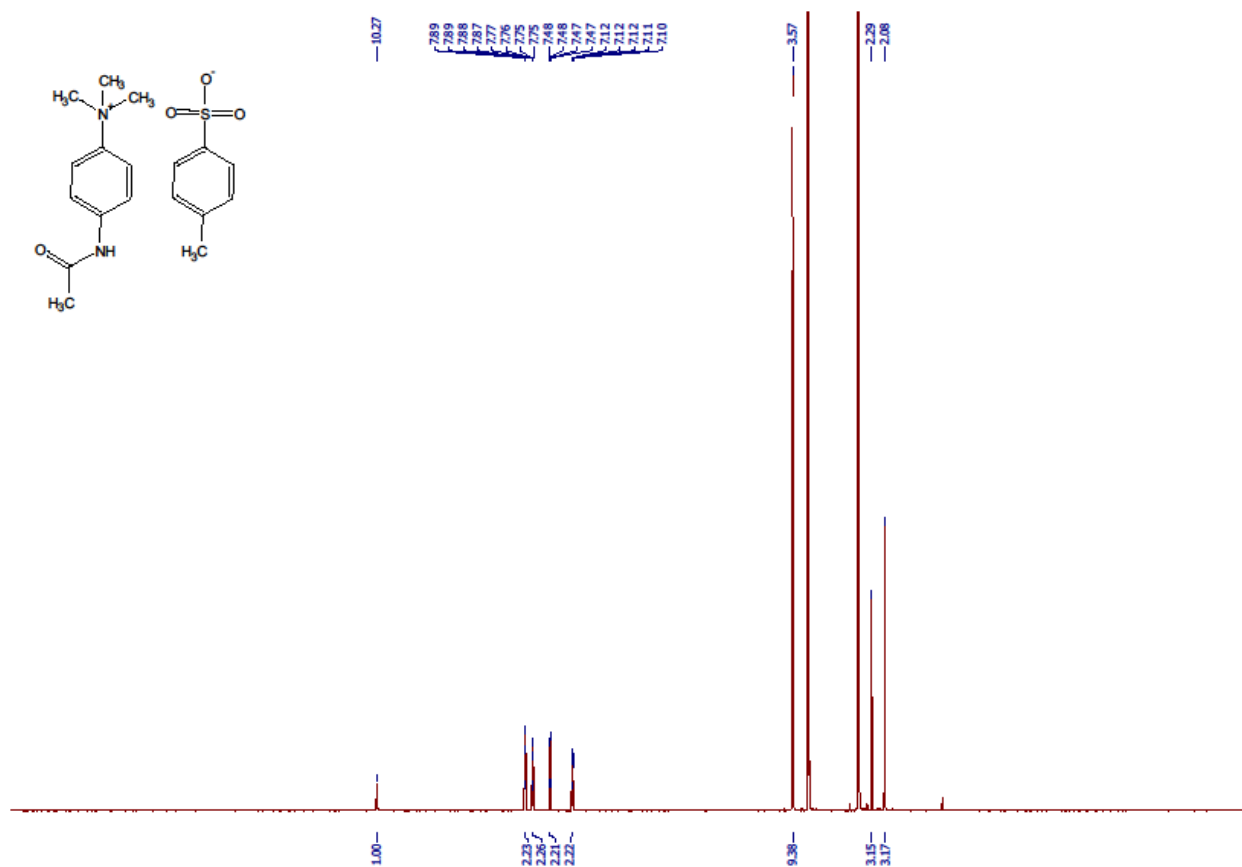


Figure 2-10 ^1H NMR spectrum of trimethyl(p-aminophenyl)-4-acetamido-N,N,N-trimethylbenzaminium-4-methylbenzenesulfonate.

2.5.1.4 Characterisation of 4-amino-N,N,N-trimethylbenzenaminium

Interestingly, the proton spectrum showed complex AA'BB' coupling at δ_{H} 7.16 (d, $J = 9.2$ Hz, 2H) for one set of 2 protons with coupling constants of 9.2 Hz and another at 7.85 (m, 2H)

which appears as a multiplet. This is probably due to long range coupling with the protons from the CH₃ groups on the adjacent trimethylammonium ion (N⁽⁺⁾CH₃)₃ moiety. The three methyl groups on the trimethylammonium ion were observed at as a singlet at δ 3.58 (s, 9H). The –NH₂ protons from the ammonium group were not observed probably due to their being exchangeable however the absence of the acyl group protons indicates that the desired compound was formed. The identity of the final product was confirmed by accurate mass LCMS on the LTQ-Orbitrap in positive ionization mode giving (m/z 151.23 calculated for C₉H₁₅N₂⁺; found 151.12) which taken together with the NMR data confirms that the desired target compound was successfully synthesised.

¹H NMR (500 MHz, DMSO-*d*₆) δ 7.87 – 7.83 (m, 2H), 7.16 (d, *J* = 8.6 Hz, 2H), 3.58 (s, 9H).

¹³C NMR (126 MHz, DMSO-*d*₆) δ 122.0, 119.6, 57.0.

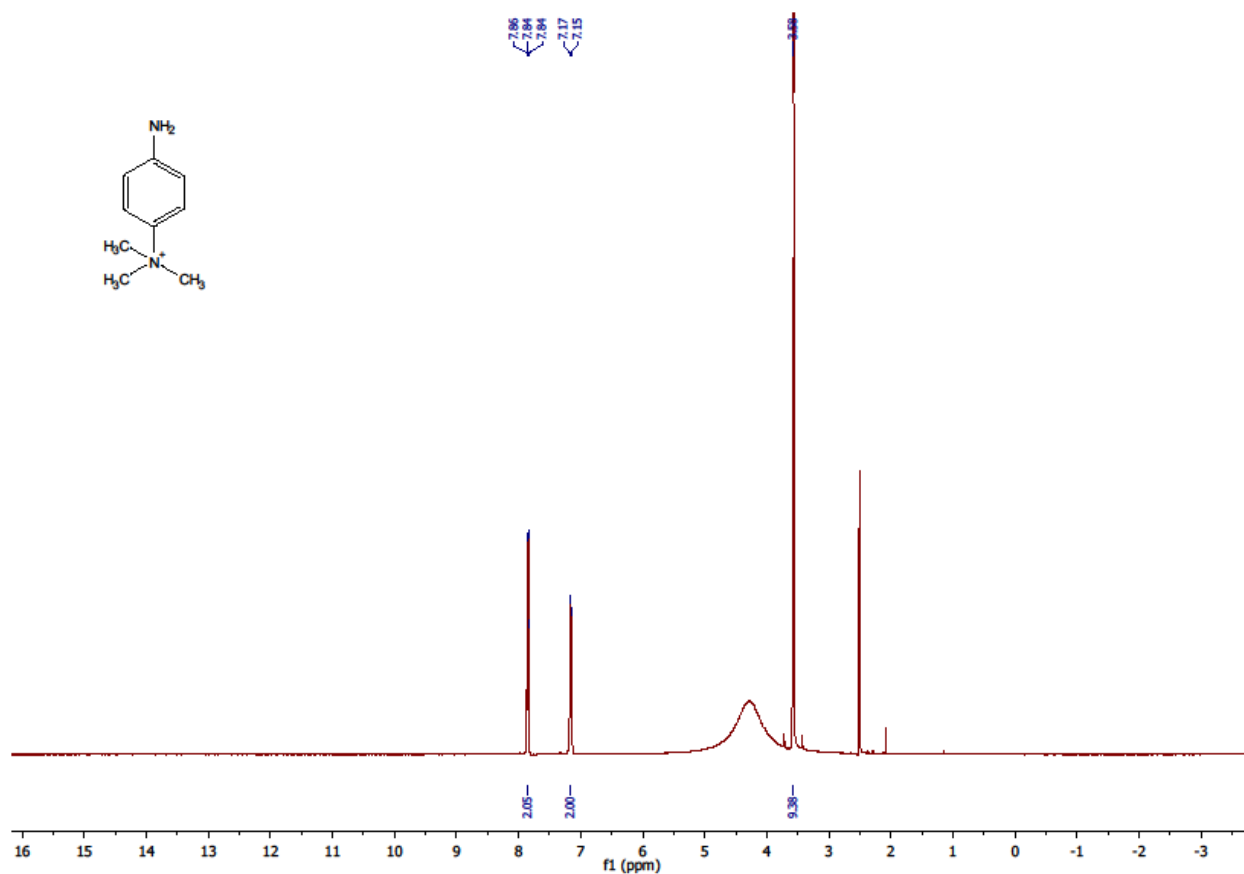


Figure 2-11 ¹H NMR spectra for 4-amino-*N,N,N*-trimethylbenzenaminium.

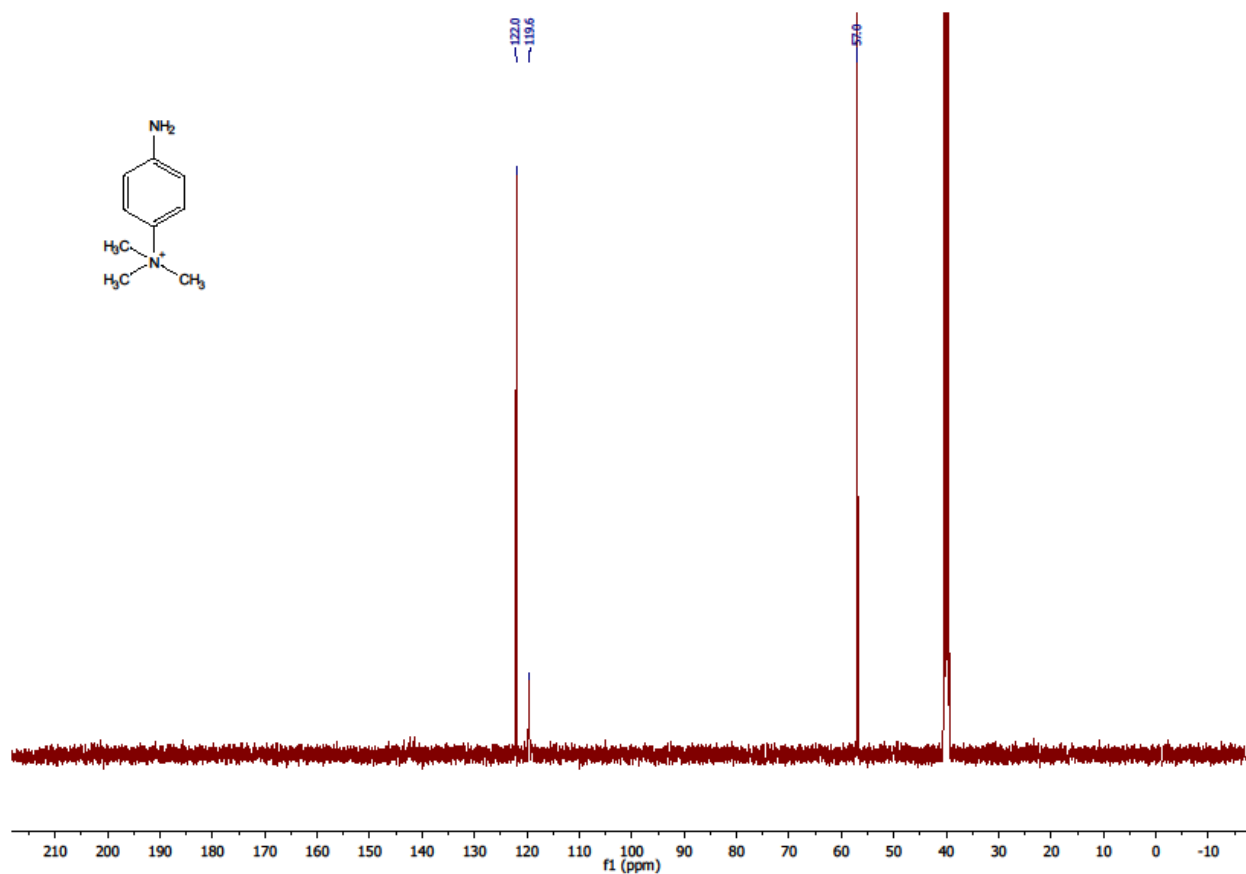


Figure 2-12 ¹³C NMR spectra for 4-amino-*N,N,N*-trimethylbenzenaminium

A008 - mix#1012 RT: 8.44 AV: 1 NL: 7.15E7
F: FTMS + c ESI Full ms [75.00-1200.00]

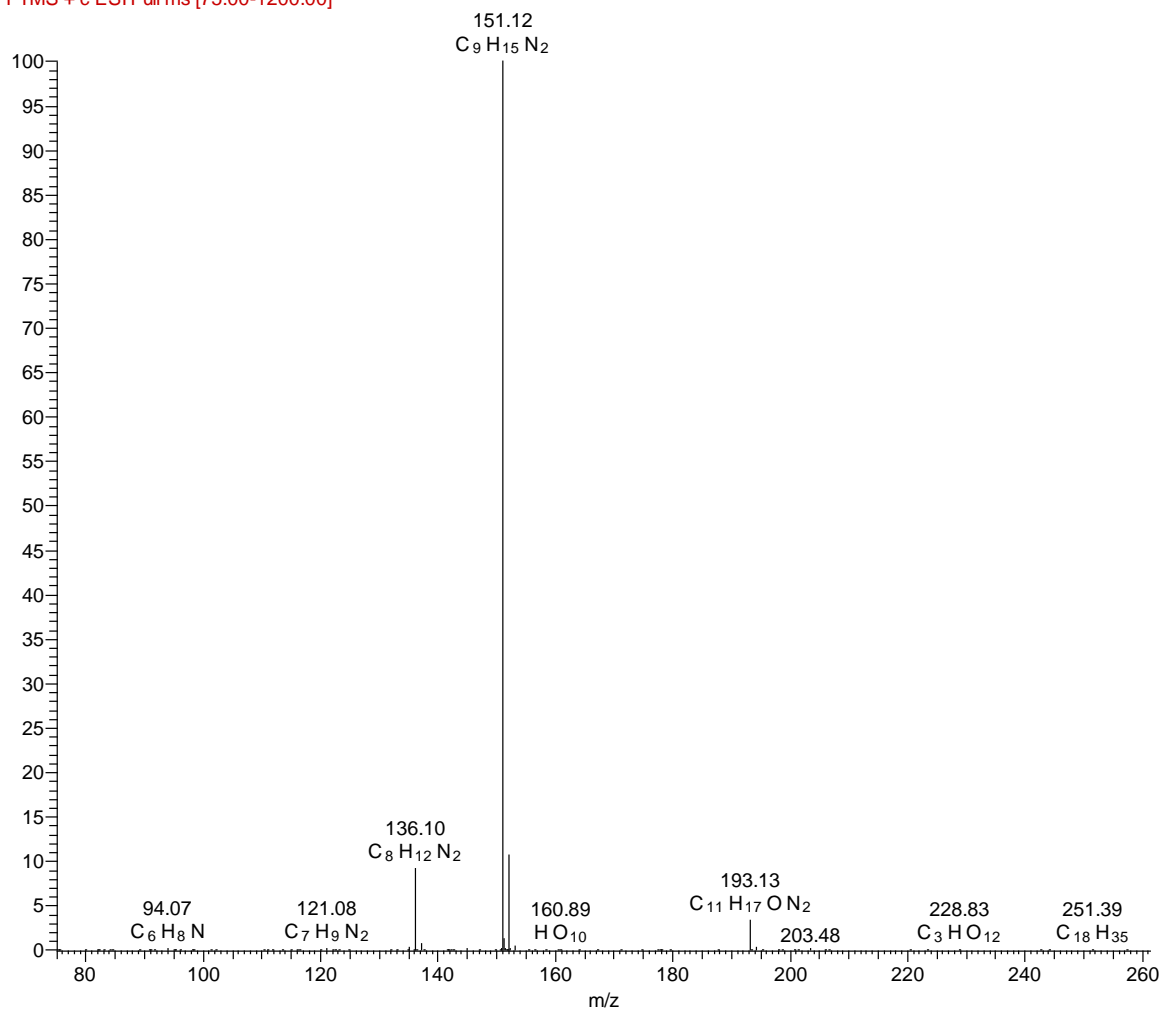


Figure 2-13 Mass spectra for 4-amino-*N,N,N*-trimethylbenzenaminium

2.5.2 Derivatisation with trimethyl(*p*-aminophenyl)ammonium chloride

The charge to mass ratio (m/z) of the derivatives of the tagged sugars expected to be found on the mass spectra can be predicted by the formula:

$$m/z \text{ of derivative} = MW \text{ of sugar} + MW \text{ of tagging compound} - 16$$

Where 16 is the mass of the oxygen atom which is lost during the course of the reaction. In other words, the molecular formula of the derivative is the sum of the molecular formulae of the two reactants minus the weight of one oxygen atom.

For example, for all the hexoses:

- MW ($C_6H_{12}O_6$) = 180.16
- MW of tagging compound ($C_9H_{15}N_2^+$) = 151.23
- Therefore, calculated m/z of the hexose derivative is $180.16 + 151.23 - 16 = 315.39$.
- The elemental composition would then be $C_{15}H_{27}O_5N_2$ in the positive mode.

The mass spectra of the derivatized hexose sugars showed the expected molecular ion at m/z 315.1909 which is correct for the elemental composition of $C_{15}H_{27}O_5N_2$. (Figure 2-14). The retention times of the sugars showed that the derivative of galactose was the least retained (RT 15.91 minutes), while the derivative of fructose was the most retained (RT 16.83 minutes), of all the sugars (Table 2-1). The tagged sugars were strongly retained on the ZICHILIC column, but there was not much separation between the four sugar derivatives all coming between 15.91 and 16.83 minutes (Figure 2-15). Their peak shapes were however approximately symmetrical, which is indicative of good chromatography. Adjustment of the mobile phase to isocratic conditions gave long elution times for the derivatives without offering any improvement in the resolution between the tagged sugars.

AA002-mannose #1820 RT: 16.23 AV: 1 SB: 2 12.26, 13.41 NL: 9.60E7
F: FTMS + c ESI Full ms [75.00-1200.00]

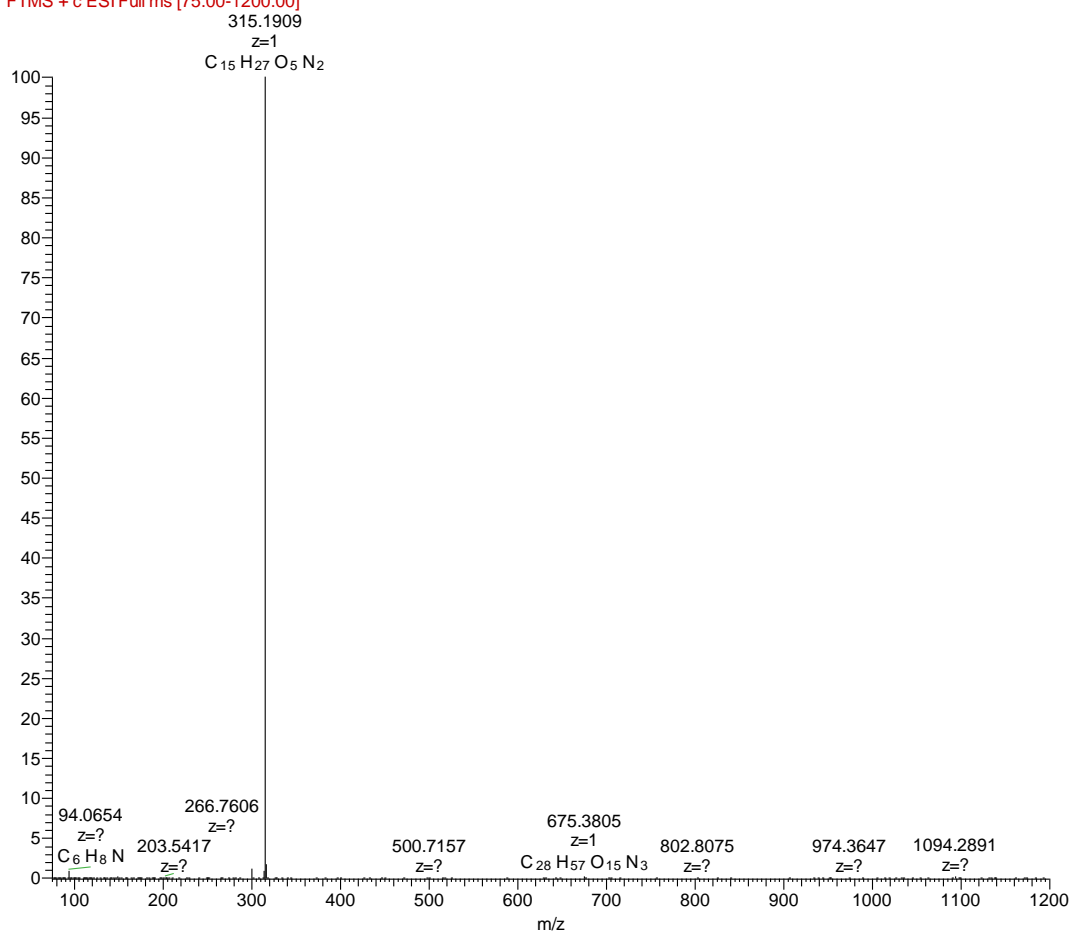


Figure 2-14 Mass spectrum showing the mass-to-charge ratio of the derivatized hexose sugars showing the molecular ion at m/z 315.1909 and the correct elemental composition of $C_{15}H_{27}O_5N_2$.

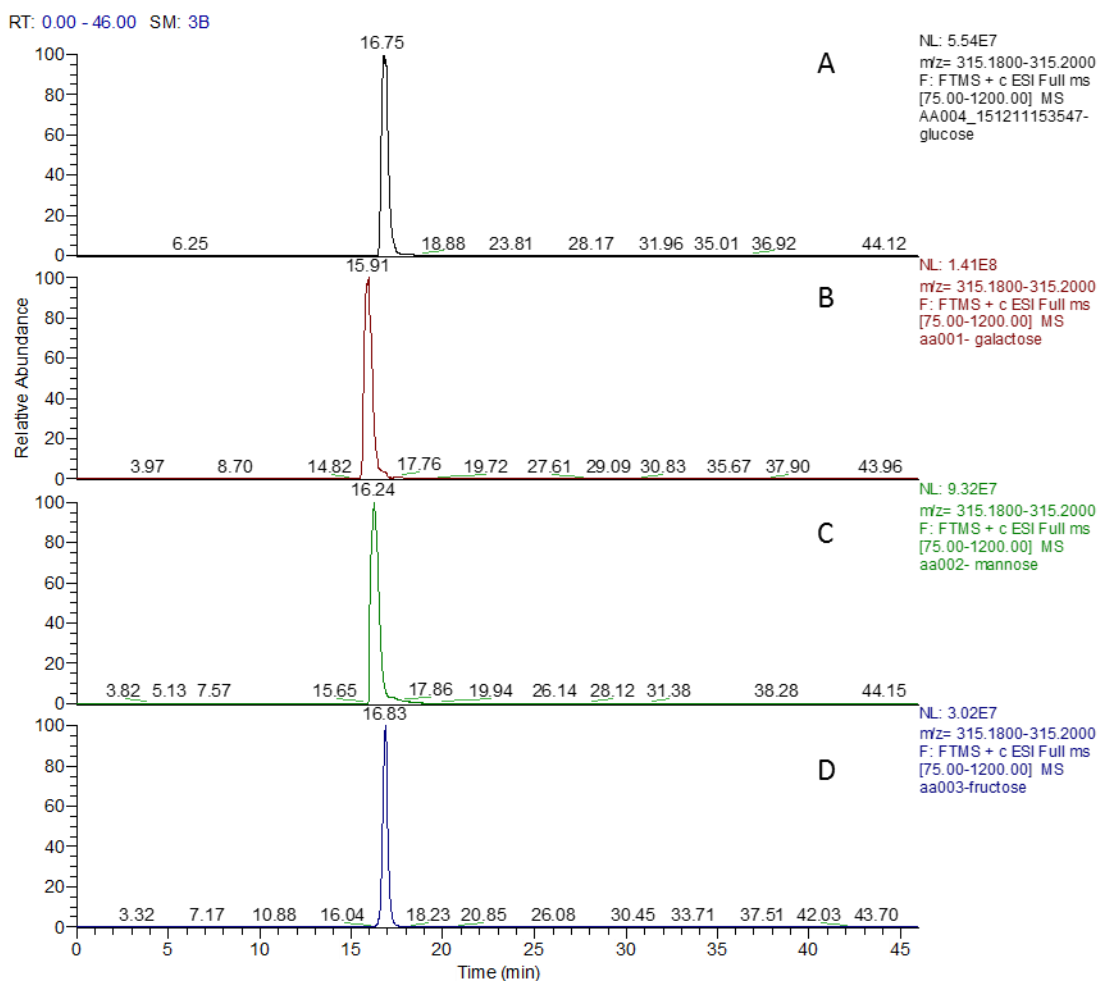


Figure 2-15 The extracted ion chromatograms of the four derivatives of the hexoses glucose (A), galactose (B), mannose (C) and fructose (D) with trimethyl(p-aminophenyl) ammonium chloride hydrochloride (4).

Table 2-1 Summary of the results obtained from the analysis of sugars tagged with trimethyl(p-aminophenyl)ammonium chloride hydrochloride (4).

Sugar	Elemental composition	m/z	RT (min)	Peak shape
Glucose	C ₁₅ H ₂₇ N ₂ O ₅	315.19	16.75	Good
Galactose	C ₁₅ H ₂₇ N ₂ O ₅	315.19	15.91	Good
Mannose	C ₁₅ H ₂₇ N ₂ O ₅	315.19	16.24	Good
Fructose	C ₁₅ H ₂₇ N ₂ O ₅	315.19	16.83	Good

2.5.3 Derivatisation with deuterated aniline- d₅

Initial derivatisation with aniline and indicated that derivatives formed with deuterated aniline gave superior peak shape and retention in comparison to aniline (Figure 2-16). It had originally been the intention that the deuterated aniline would be used for preparation of internal standards for quantitative studies. However, since the separation of galactose and mannose was critical and deuterated aniline was not expensive this was used as the preferred tagging agent. Under HILIC conditions the retention times of the deuterated aniline derivative is slightly longer than those of the aniline derivatives.

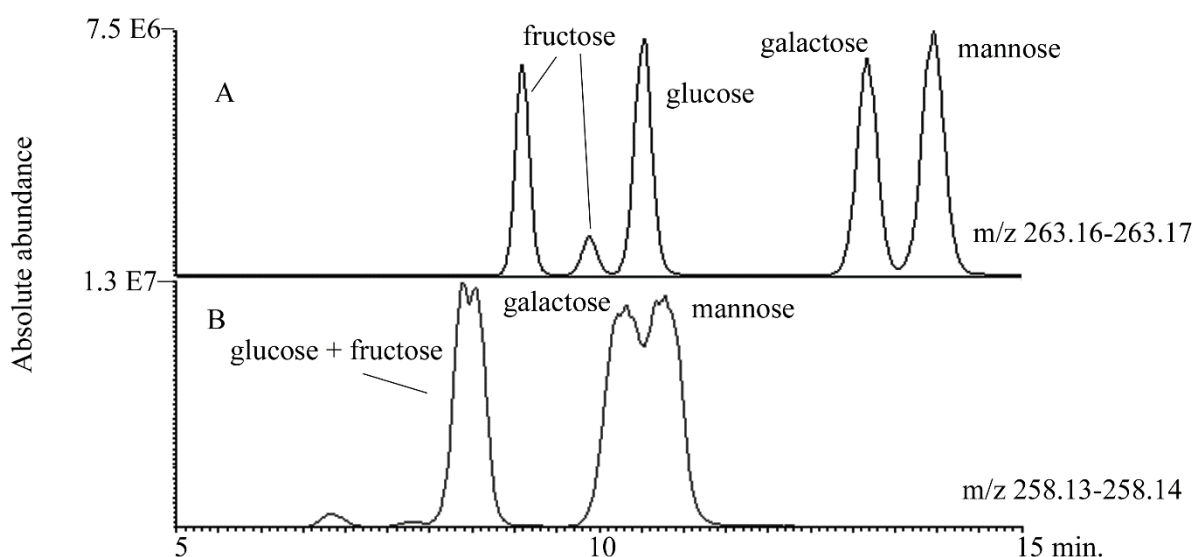


Figure 2-16 ²H₅-aniline (A) and aniline (B) derivatives of 1 µg amounts of hexose standards run on a ZICHILIC column in acetonitrile/water containing 0.01% formic acid (90:10) at 0.6 ml/min.

The mass spectra of the d₅-aniline derivatized hexose sugars showed an expected molecular ion [M+H]⁺ at m/z 263.1641 which is correct for the calculated elemental composition of C₁₂H₁₅²H₅O₅N, with the 5 deuterium atoms present in the molecule (Table 2-2). The retention times of the sugars showed that fructose was the least retained while mannose was the most retained of the sugars (Figure 2-16). Glucose and fructose were well separated from galactose

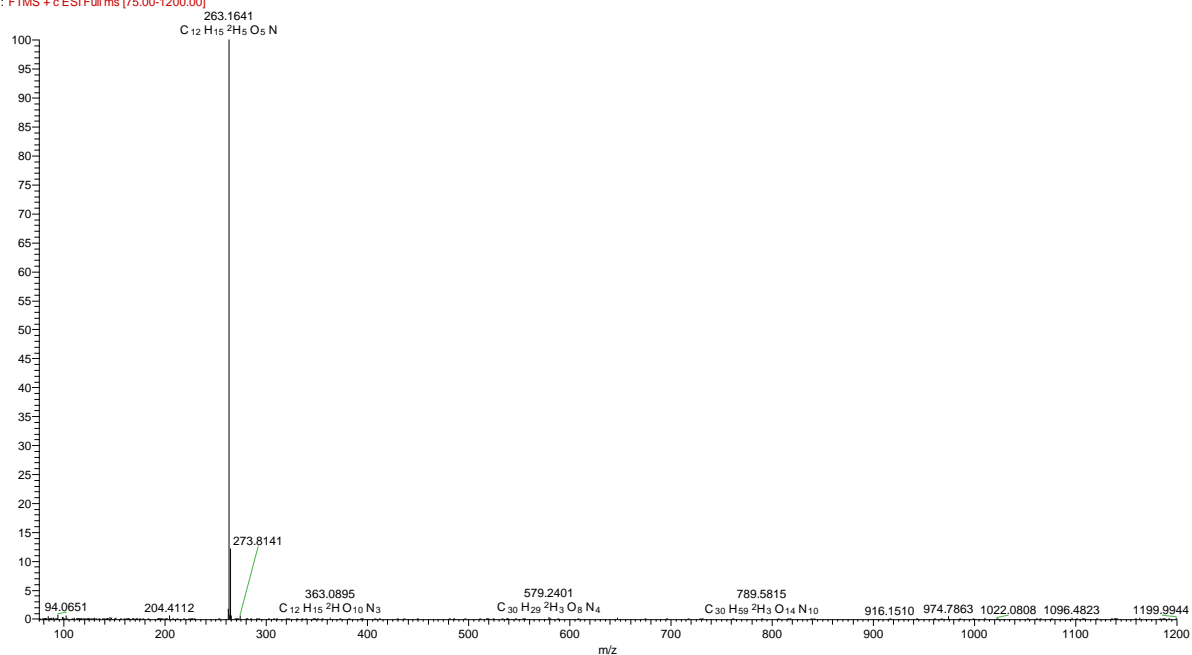
and mannose which had very close retention times. The peak shapes for the sugar derivatives were approximately symmetrical, characteristic of good chromatography. On increasing the percentage of eluent B from 80 to 90 and then 95%, there was gradual increase in the retention times of the sugar derivatives, similar to what would be expected in hydrophilic interaction liquid chromatography (HILIC) [95]. In addition, the resolution between galactose and mannose improved slightly although it did not get anywhere close to the desired baseline separation, required for good separation, even at 95% of eluent B. However, it was clear that the use of deuterated aniline provided better separation of the isomers compared to derivatisation with trimethyl(p-aminophenyl) ammonium chloride hydrochloride (**4**).

Table 2-2 Changes in the retention times of the hexose sugars with mobile phase composition.

Sugar	Elemental composition	m/z	RT (min) at different %B for 20 min			
			80	90	90 (mix)	95 (mix) [‡]
Glucose	C ₁₂ H ₁₅ ² H ₅ O ₅ N	263.16	6.62	8.95	9.90	12.77
Galactose	C ₁₂ H ₁₅ ² H ₅ O ₅ N	263.16	7.64	11.42	12.62	18.00
Mannose	C ₁₂ H ₁₅ ² H ₅ O ₅ N	263.16	7.70	11.84	12.75	18.83
Fructose	C ₁₂ H ₁₅ ² H ₅ O ₅ N	263.16	4.15	5.09	5.21	6.21

*Flow rate used was 0.6 ml/min.

Glucose #843 RT: 6.60 AV: 1 NL: 1.66E8
F: FTMS + c ESI Full ms [75.00-1200.00]



Galactose #977 RT: 7.65 AV: 1 NL: 1.48E8
F: FTMS + c ESI Full ms [75.00-1200.00]

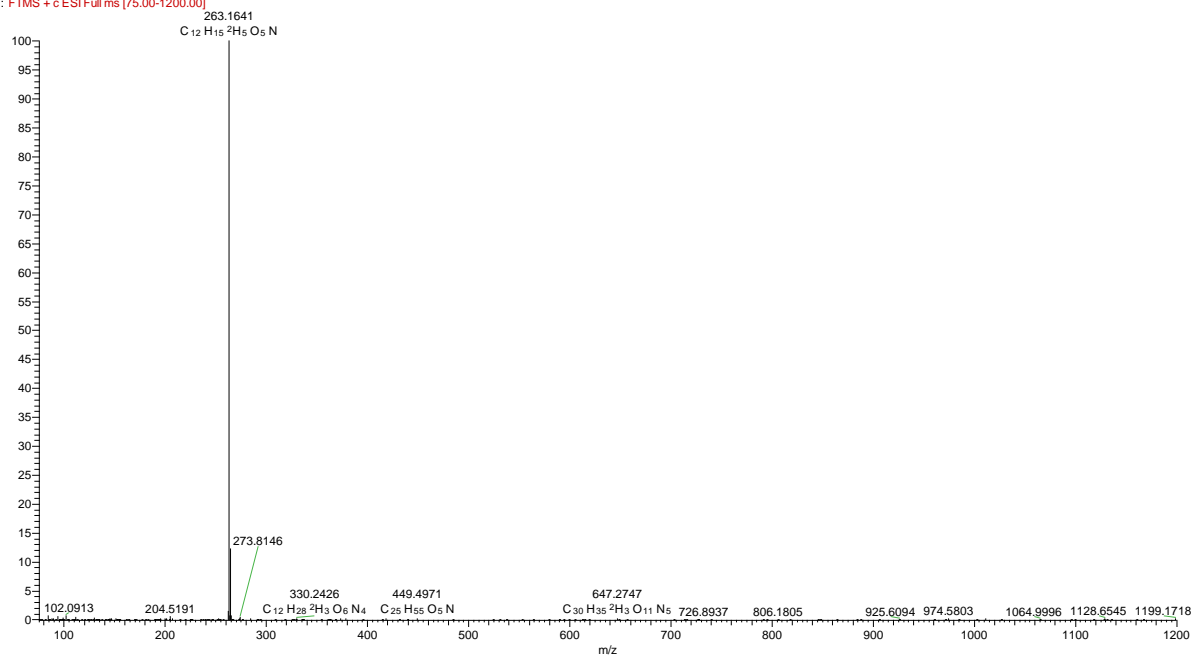


Figure 2-17 Mass spectra representing the mass of the glucose (top) and galactose (bottom) derivatized with aniline-d₅ showing the molecular ion [M+H]⁺ at m/z 263.1641 which is correct for the calculated elemental composition of C₁₂H₁₅²H₅O₅N,

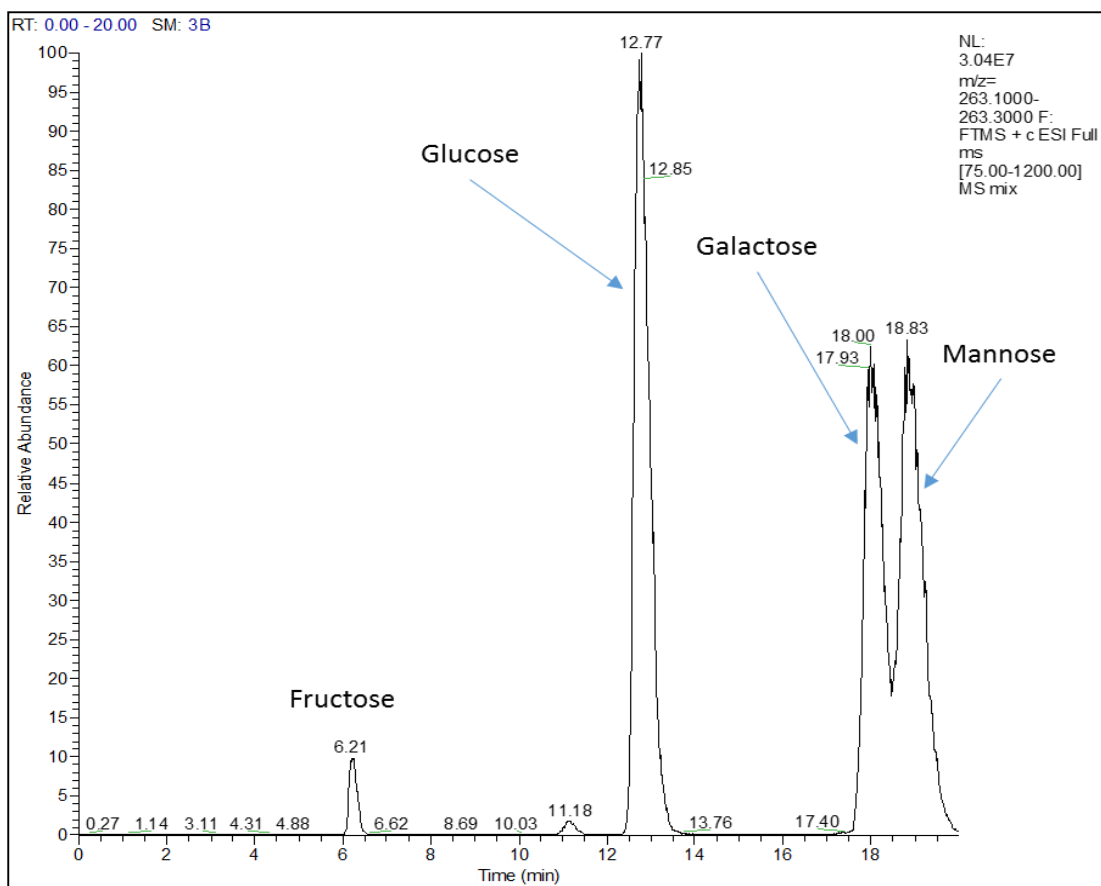


Figure 2-18 Chromatogram of the mix containing derivatives of the four hexose sugars derivatized with aniline- d_5 fructose (6.21 min), glucose (12.77 min), galactose (18.00 min) and mannose (18.83 min), run isocratically at 5% 0.01% (v/v) formic acid in water and 95% 0.01% formic acid in acetonitrile.

2.5.4 Derivatisation of other sugars tagged with trimethyl(p-aminophenyl)ammonium chloride hydrochloride

Table 2-3 Pentose and disaccharide sugars.

Ribose	$C_5H_{10}O_5$	Pentose	150.13
Arabinose	$C_5H_{10}O_5$	Pentose	150.13
Xylose	$C_5H_{10}O_5$	Pentose	150.13
Lactose	$C_{12}H_{22}O_{11}$	Disaccharide (glc-gal: 1 \rightarrow 6')	342.30
Trehalose	$C_{12}H_{22}O_{11}$	Disaccharide (glc-glc: 1 \rightarrow 1')	342.30

The retention times of the derivatized pentose sugars ribose, arabinose and xylose varied significantly from those of the other sugar types.

Table 2-4 Summary of the results obtained in the analysis of sugars tagged with trimethyl(p-aminophenyl) ammonium chloride hydrochloride (4).

Sugar	Elemental composition	m/z	RT (min)	Peak shape
Ribose	C ₁₄ H ₂₅ N ₂ O ₄	285.18	14.13	Fair
Arabinose	C ₁₄ H ₂₅ N ₂ O ₄	285.18	14.21	Fair
Xylose	C ₁₄ H ₂₅ N ₂ O ₄	285.18	14.20	Fair
Lactose	C ₁₈ H ₃₉ NO ₁₃	477.24	29.53	Good

The derivatized disaccharide lactose was the most retained, followed by the derivatized hexoses and finally the derivatized pentoses. Thus the sugar classes were separated on the basis of molecular weight, and retention times increased with size of the molecule. Overall the peak shapes for the sugar derivatives were good especially for hexoses and lactose but the pentoses showed some tendency for peak broadening (Table 2-4). It was also noted that trehalose (Figure 2-19) could not form a derivative with the tagging agent because the C₁-C₁ glycosidic linkage between the two glucose residues forming the disaccharide leaves no free aldehyde/ketone to react with the amino group of the tagging agent.

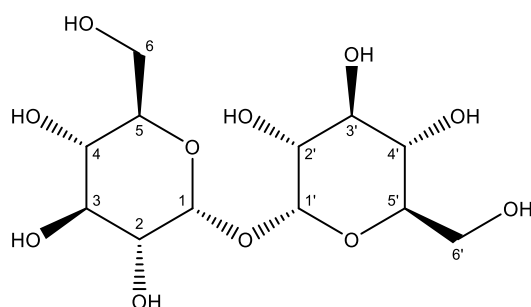


Figure 2-19 Structure of trehalose showing the C₁-C₁' glycosidic linkage

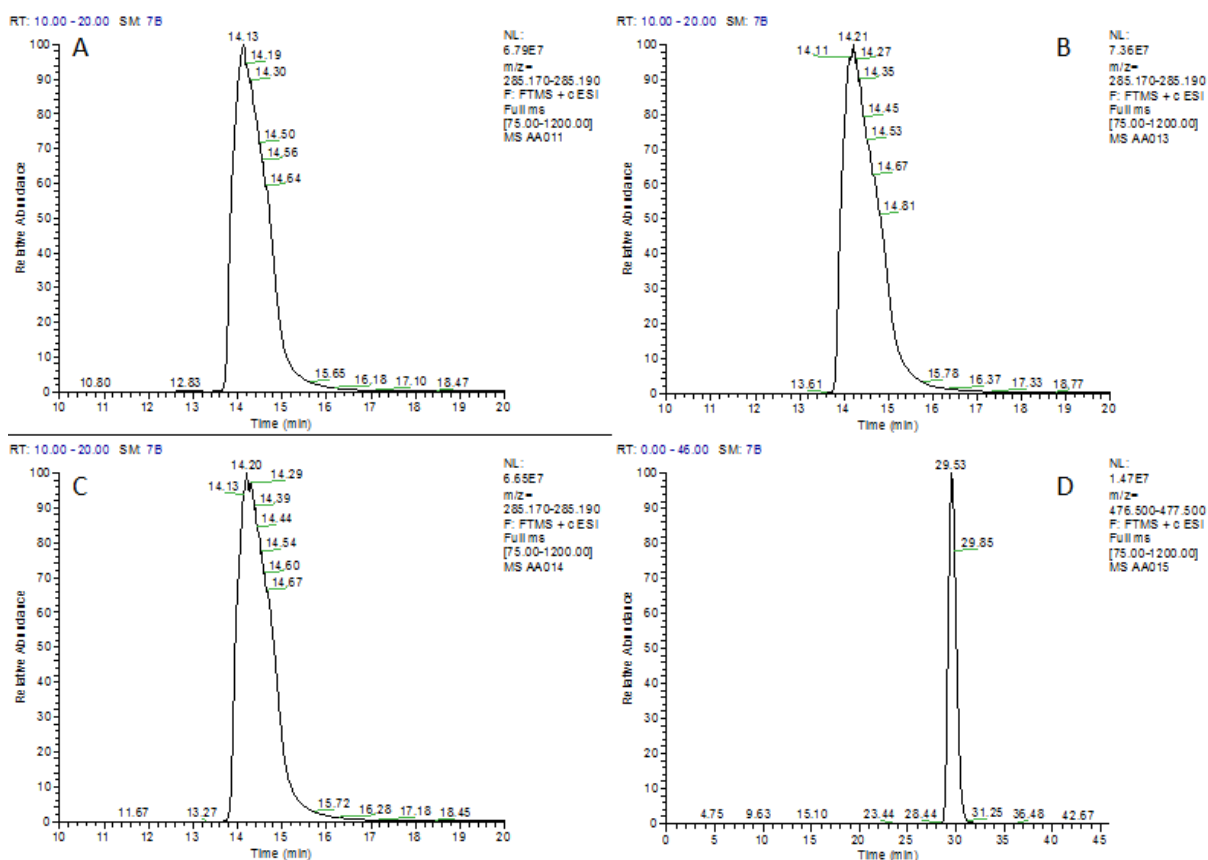


Figure 2-20 The chromatograms of the four pentose sugars derivatized with trimethyl(p-aminophenyl) ammonium chloride hydrochloride 4; ribose (A), arabinose (B) and xylose (C) and the disaccharide lactose (D).

2.5.5 Derivatisation of other sugars with deuterated aniline

Figure 2.21 shows the chromatograms obtained from reaction of deuterated aniline with three pentose sugars and a deoxypentose. It can be seen that there is some separation between the isomers.

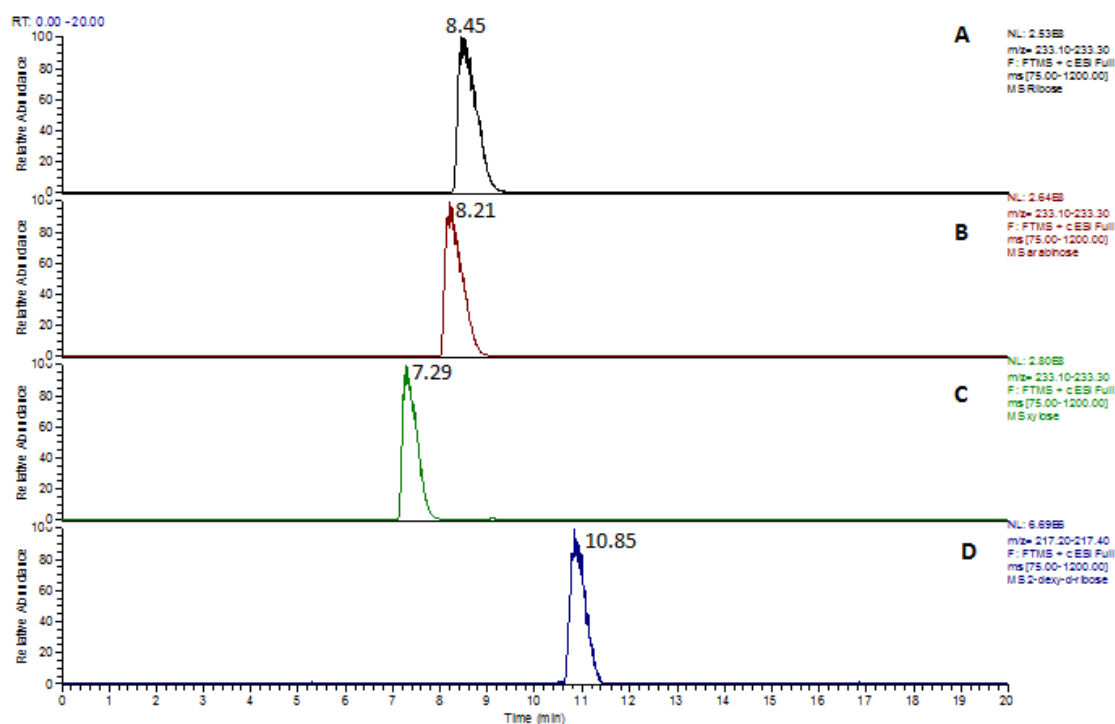


Figure 2-21 The chromatograms of four pentose sugars derivatized aniline-d₅; ribose (A), arabinose (B), xylose (C) and 2-deoxy-D-ribose (D).

2.5.6 Profiling of sugar isomers in urine.

In order to evaluate the efficacy of this method to identify unique patterns, the derivatisation procedure was used in the analysis of samples of human urine. The extracted ion traces for the sugar derivatives found is shown in (Figure 2-22). Glucose was found to be the most abundant hexose in urine is with small amounts of mannose and galactose also present. There was also an unknown hexose whose abundance was similar to galactose which ran close to glucose between glucose, mannose and galactose. Since mannose is derived from microbial breakdown of complex polysaccharides in the diet, it is therefore likely that the other hexoses, pentoses and deoxy sugars observed in the profile of urine samples may be similarly derived [96].

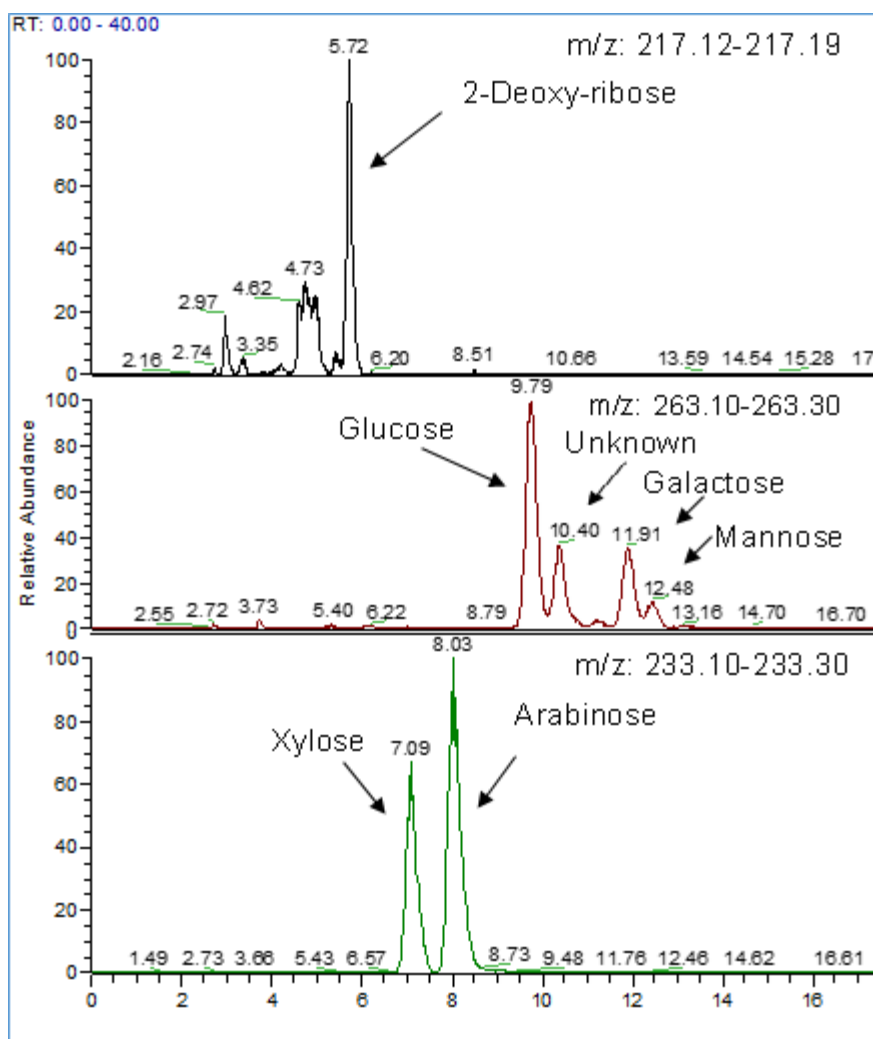


Figure 2-22 The chromatograms showing sugars identified in urine sample derivatized aniline- d_5 acetonitrile/water (90:10) containing 0.01% formic acid.

2.6 Discussion

Sugars, are difficult to analyse and detect by LCMS due to their poor retention during reversed phase chromatography and their limited ionisation because of an absence of ionisable functional groups [90-93]. Tagging such analytes has been demonstrated to be of great value in overcoming these challenges [90-93].

This work was therefore focused on the investigation of the application of *p*-trimethylammonium aniline (PMTA) and deuterated (d_5)-aniline (D_5A) as tagging agents in order to evaluate

their ability to aid the analysis of hexose sugars. The use of both PMTA and D₅A tags significantly increased the degree of ionization which aided their detection in positive mode by LCMS (Figure 2-15). However, the resolution obtained with PMTA was not satisfactory because although the peak shapes were improved following derivatisation for each sugar, very little separation was achieved between the individual derivatized sugars in mixtures of sugars (Figure 2-15). With D₅A, however, the resolution was greatly improved especially for glucose and fructose. On the other hand, galactose and mannose almost co-eluted forming a critical. Although their separation improved with an increase in the percentage of eluent acetonitrile used, it never achieved baseline separation even at the highest concentration (95% of eluent B) used in the study. In order to achieve complete separation, it may be necessary to increase the length of the column to 25 cm from the 15 cm used. It is anticipated that this would improve the efficiency of the separation, resulting in better resolution of the peaks. Once complete resolution can be obtained for all the hexoses in the mixture, it is envisioned that this fairly quick and inexpensive method would be suitable for use in the analysis of hexose sugars in metabolomics samples such as urine, plasma and tissue extracts.

2.7 Conclusion

The results of the studies confirm that derivatisation of sugars can greatly improve their detection identification and quantification by HILIC LCMS. The ionisation efficiency for all the sugars in our experiments was improved and the masses expected for the derivatized sugars was observed in all cases. The retention times were greatly improved also however decent separation of the various sugar was only achieved using only one of our tagging agents, deuterated aniline. There is probably room for optimisation of the derivatisation of fructose which gave smaller peaks than were obtained for the aldolases. This is probably because the

ketone group in fructose reacts more slowly than the aldehyde group in the other sugars. This however demonstrates that the concept works and that better tagging agents can be developed which will meet the initial aims of the study. PMTA remains potentially a useful tagging agent and some preliminary work was carried out in examining it as a tagging agent for glycan chains released from proteins although the results prove inconclusive.

Chapter Three:
Analysis of Short Chain Fatty Acids in Biological
Fluids

3 ANALYSIS OF SHORT CHAIN FATTY ACIDS IN BIOLOGICAL FLUIDS

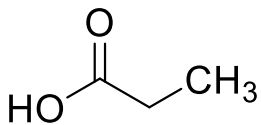
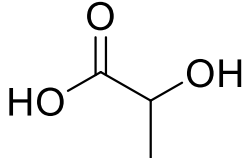
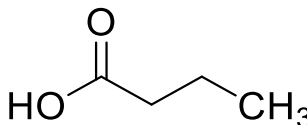
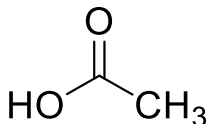
3.1 Introduction

Short chain fatty acids (SCFAs) constitute some of the most important endogenous metabolites in the human body [97]. SCFAs, especially acetate, propionate and butyrate, are produced as the final products from the fermentation of dietary fibres and non-digestible carbohydrates by bacteria in the large intestine [98, 99]. They typically are made up of short hydrocarbon chains (2-5 carbon atoms) and contain a carboxylic acid functionality. Commonly occurring SCFAs include propionic acid, lactic acid, butyric acid, and acetic acid, some of which are products of bacterial fermentation of non-digestible carbohydrates within the large intestines (Table 3-1). These SCFAs have been shown to have beneficial physiological and metabolic effects in the human gut, and play a significant role in the outcomes of metabolic diseases such as Crohn's disease (CD), irritable bowel syndrome (IBS), among others [99]. This implies that SCFAs can be used as important biomarkers for diagnosis and monitoring of disease progression for inflammatory bowel disease's (IBDs).

As they contain a carboxylic acid functional group, SCFAs are easily ionised for detection in negative mode LCMS. However, they are also polar due to their low molecular weight and presence of the ionisable carboxyl group and are thus poorly retained on reversed phase chromatography or are not sufficiently polar to be retained by hydrophilic interaction chromatography (HILIC) Their negatively ionised species which have m/z values which are often

too close to the lower boundary of the routinely used detection ranges of most LCMS instruments and they are also very volatile which might mean they might not form stable ions in electrospray ionisation mode. All these factors contribute to making the analysis of free SCFA by LCMS extremely challenging [100, 101].

Table 3-1 Structures of short chain fatty acids (SCFAs) showing their molecular formulae and weights. From the MWs, it can be seen that the m/z values of deprotonated species in negative mode LCMS are quite low.

Name	Structure	Formula	MW
Propionic acid		C ₃ H ₆ O ₂	74.08
Lactic acid		C ₃ H ₆ O ₃	90.09
Butyric acid		C ₄ H ₈ O ₂	88.11
Acetic acid		C ₂ H ₄ O ₂	60.05

Therefore, for practical purposes, as well as to overcome the challenges associated with the analysis of SCFAs by LCMS, derivatisation of these metabolites is essential. In addition to improving the chromatographic properties of the acids, such as their retention times and peak efficiency, derivatisation also enhances the selectivity and sensitivity of LCMS for their analysis [94]. This improvement in the sensitivity and selectivity enables the detection of subtle

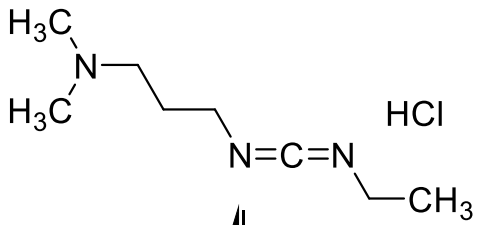
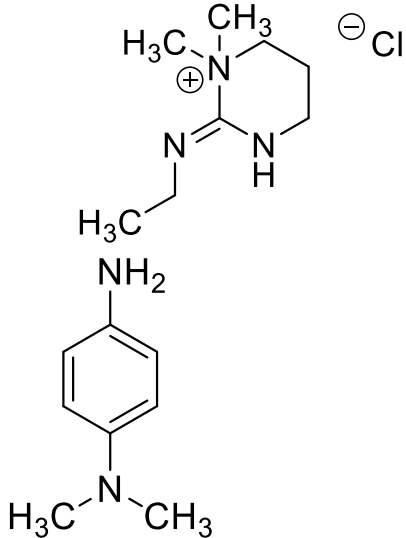
changes in SCFAs allowing for a more accurate interpretation of the metabolic processes occurring in a given metabolome [102].

Several derivatising agents have been previously reported, including the use of 1-(*tert*-butyldimethylsilyl) imidazole followed by GC-MS with chemical ionization and ammonia as the reagent gas [103]. However, this method requires the use of non-aqueous conditions which are not suitable for the processing of biological samples. This is because, it would require that the samples are first extracted then evaporated to dryness and then reconstituted in a suitable solvent. This risks the loss of analytes, introduction of contamination and is very time consuming.

Techniques which require little or no sample preparation are therefore best suited for the analysis of biological samples. LCMS is ideally suited to the analysis of SCFAs because of the relative ease of identification of molecular weights and retention time. The versatility of this technique comes partly from the fact that it can be used for both polar and nonpolar analytes by merely changing the column stationary phase. The drawbacks with this technique arise from potential sensitivity due to interference by sample matrix which might lead to quantitative inaccuracies during experiments. However, these errors can be minimised by the use of isotope labelled internal standards.

The SCFAs which were focused on in this study were acetic acid, propionic acid, butyric acid. They were derivatized by using *N,N*-Dimethyl-*p*-phenylenediamine (DPD) **6** and *N*-(3-Dimethylaminopropyl)-*N'*-ethylcarbodiimide hydrochloride (EDC) **5** as reagents prior to analysis by LC-ESI-MS on an Orbitrap mass spectrometer (Table 3-2). In the current study the effect of an experimental diet for promoting gut health on the levels of SCFAs in urine.

Table 3-2 Structures of the derivatising reagents EDC and DPD used in the study.

Structure	Name	Formula	MW	Str. No.
	EDC [§]	C ₈ H ₁₇ N ₃ ·HCl	191.70	5
	DPD [¥]	C ₈ H ₁₂ N ₂	136.19	6

[§]N-(3-Dimethylaminopropyl)-N'-ethylcarbodiimide hydrochloride; [¥]N, N-Dimethyl-p-phenylenediamine

3.2 Materials and methods

3.2.1 Materials

Labelled Fatty acid internal standards, acetic acid-¹³C₂, propionic acid-²H₂, and butyric acid-²H₅ and their corresponding unlabelled standards acetic acid, propionic acid, and butyric acid, as well as HPLC grade acetonitrile, tetrahydrofuran (THF), formic acid, and methanol were obtained from Sigma-Aldrich (Dorset, U.K.).

3.2.2 Urine Samples

Urine samples were provided by the Human Nutrition Department in Glasgow Royal Infirmary. Healthy adults (>18 years old) were recruited from the community. Participants had stable weight (± 2 kg) in the past month, no history of gut surgery, and had not used antibiotics or steroids during the previous 3 months. Participants were randomly allocated to the enteral nutrition diets (EEN) and the experimental diet (CDTREAT) for 7 days each, with a 14-day washout period in between to restore the gut microbiome to its baseline state and avoid intervention contamination bias. Modulen IBD was used for the EEN trial, as described previously [104]. During CD-TREAT, participants were provided with a food list from which to choose their preferred items. An individualized dietary plan was developed by the research dietitians providing their daily energy requirements. Urine samples were collected from the participants at the end of each experimental diet.

3.2.3 Preparation of reference and internal standards

The THF was purified by filtration through a short column containing 50 g of base activated alumina (aluminium oxide) in order to remove any traces of organic acids prior to use. Solutions of 10 $\mu\text{g}/\text{ml}$ of sodium acetate- $^{13}\text{C}_2$, propionate- $^2\text{H}_2$, and butyrate- $^2\text{H}_5$ were respectively prepared by dissolving 10 mg of each of the isotope-labelled salts in 1 ml of THF:water (1:1) and then diluting the resulting 10 mg/ml solution 1000-fold. Stock solutions of unlabelled standards of acetate (10 $\mu\text{g}/\text{ml}$), butyrate (1 $\mu\text{g}/\text{ml}$), and propionate (1 $\mu\text{g}/\text{ml}$) were also prepared. Finally, calibration standards containing acetate- $^{13}\text{C}_2$ (1 μg), propionate- d_2 (0.5 μg), and butyrate- d_5 (0.5 μg) were prepared as internal standards for acetate (range: 0, 0.1, 0.2, 0.4, 0.8 and 1.6 μg), propionate (range: 0, 0.04, 0.08, 0.16, 0.32, and 0.64 μg) and butyrate (range:

0, 0.04, 0.08, 0.16, 0.32, and 0.64 µg). The resulting solutions were mixed thoroughly by centrifugation (MyFuge™ mini, Benchmark Scientific, Edison, NJ, USA) for 5 min. Following centrifugation, the supernatants were then respectively transferred into separate clean vials for derivatisation.

3.2.4 Summary of Stock solutions and Calibration Ranges

All labelled acids = 10 µg/ml

Unlabelled acetate = 10 µg/ml

Unlabelled butyrate = 1 µg/ml

Unlabelled propionate = 1 µg/ml

Pipetted volumes Used to Prepare Calibration Series

Labelled acetate = 100 µl (1 µg)

Labelled propionate = 50 µl (0.5 µg)

Labelled butyrate = 50 µl (0.5 µg)

Unlabelled acetate = 0, 10, 20, 40, 80, 160 (µl) = 0, 0.1, 0.2, 0.4, 0.8, 1.6 (µg)

Unlabelled propionate = 0, 40, 80, 160, 320, 640 (µl) = 0, 0.04, 0.08, 0.16, 0.32, 0.64 (µg)

Unlabelled butyrate = 0, 40, 80, 160, 320, 640 (µl) = 0, 0.04, 0.08, 0.16, 0.32, 0.64 (µg)

3.2.5 Preparation of urine samples

A sample of urine (100 µl) was mixed with 300 µl of THF in an Eppendorf vial and then centrifuged for 15 min. The resultant supernatant was then transferred carefully, in small aliquots, and pooled in a clean vial for derivatisation.

3.2.6 Derivatisation with EDC and DPD

First, standard stock solutions of both EDC and DPD were respectively prepared as described below. A 1 M solution of EDC was prepared by weighing 1.92 g of EDC into a vial and dissolving it in a mixture of THF:water (1:1) to make 10 ml of solution. Similarly, 10 ml of a 10 mM solution of DPD was prepared by weighing out 20.9 mg of DPD and dissolving it in THF:water (1:1). Finally, 25 μ l of 1M EDC and 50 μ l of 10 mM DPD were added to each sample vial and the mixture was heated in a heating block at 60 degrees for 45 min. 600 μ l of water was then added and solution transferred into HPLC vials for LCMS analysis.

3.2.7 LCMS conditions

The ESI interface was operated in dual positive/negative switching mode, with a spray voltage was 4.5 kV for positive mode and 4.0 kV for negative mode. The temperature of the ion transfer capillary was 275 °C and sheath and auxiliary gas were set at 50 and 17 arbitrary units respectively. The full scan range was 50 to 1200 m/z for both positive and negative modes with the settings for the Automatic Gain Control (AGC) target and resolution set as Balanced and High (1e6 and 50,000) respectively. The data was recorded using the Xcalibur 2.1.2 software package (ThermoFisher Scientific, Bremen, Germany). Mass calibration was performed for both ESI polarities prior to the analysis using the standard ThermoCalmix solution with additional compounds to cover the low mass range and the signals of 83.0604 m/z (2 x ACN + H) and 91.0037 m/z (2 x formate - H) were selected as lock masses for positive and negative mode respectively during each analytical run. A SeQuant® ZIC®-HILIC column, (SeQuant® ZIC®-HILIC – 150 x 4.6 mm, 3.5 μ m, 200 Å.), was used with 0. 1% formic acid in water (as mobile phase A) and 0. 1% Formic acid in acetonitrile (as mobile phase B). The gradient used is illustrated in in the table below (Table 3.3)

Table 3-3 Illustration of mobile phase gradient program used in LCMS analysis.

Time	A%	B%	Flow Rate ($\mu\text{L}/\text{min}$)
0	20	80	300
20	50	50	300
21	20	80	300
25	20	80	300

3.3 Results

3.3.1 The derivatisation reaction

The derivatisation of SCFA occurs *via* deprotonation and activation of the acid which is achieved when the acid reacts with the carbodiimide, EDC, resulting in the formation of an *O*-acylisourea as key intermediate [105, 106]. This intermediate then reacts with the amine, DPD, to form a final stable amide and a urea by-product (Figure 3-1).

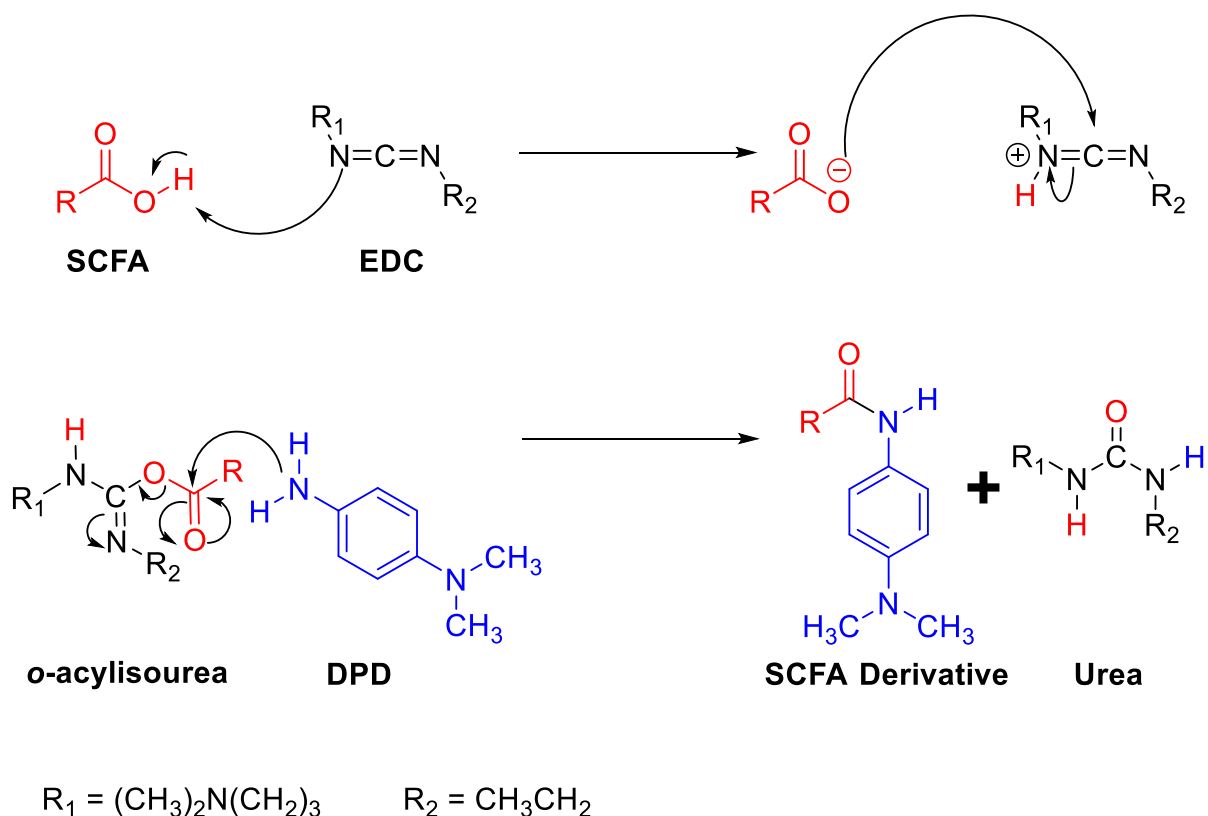


Figure 3-1 Derivatisation of short chain fatty acids (SCFAs) with EDC and DPD. The EDC deprotonates and activates the SCFA leading to the formation of an O-acylisourea, an intermediate which then reacts with DPD to form the final stable amide derivative.

Based on the reaction outline above, (Figure 3-1), it is apparent that the net effect of the derivatisation is that the SCFA loses a hydroxyl group (OH 17 Da) while DPD loses a proton (1 Da), both of which are transferred to EDC to form the urea by-product. Thus the mass of the amide derivative can be calculated from by the following formula:

$$\text{Mass of amide derivative} = (\text{mass of SCFA}) + (\text{mass of DPD}) - 18$$

Therefore the masses of the derivatives for the three SCFAs of interest can be determined, following the reaction, as shown in the table below (for DPD, Formula = $\text{C}_8\text{H}_{12}\text{N}_2$, MW = 136.19) (Table 3-4).

Table 3-4 Formulae and MW of the predicted SCFA derivatives after reaction with EDC and DPD.

SN	Name	Underivatised		Derivatised	
		Formula	MW	Formula*	MW*
1	Propionic acid	C ₃ H ₆ O ₂	74.08	C ₁₁ H ₁₆ ON ₂	192.27
2	Butyric acid	C ₄ H ₈ O ₂	88.11	C ₁₂ H ₁₈ ON ₂	206.30
3	Acetic acid	C ₂ H ₄ O ₂	60.05	C ₁₀ H ₁₄ ON ₂	178.24

*These are the expected values following derivatisation. The expected MW of derivatives of the isotope labelled standards could also be derived from the unlabelled standards by accounting for the number and type of the isotope labels in the molecules as follows: acetic acid-¹³C₂ (180.24), propionic acid-²H₂ (194.27) and butyric acid-²H₅ (211.30).

It should be noted that following the reaction illustrated above (Figure 3-1), the SCFA derivatives formed no longer ionise in the negative ESI mode since the carboxylate group has been converted into an amide. The ionisation is now determined by the tertiary amino group on the DPD reagent *para* to the site of derivatisation with the SCFA. This implies that the derivatives will ionise in the positive mode, thereby gaining a proton to form *m/z* values one atomic mass unit higher than the calculated MW of the individual derivatives.

The figures below (Figures 3-2 to 3-7) show the mass spectra and elemental compositions of the derivatives of acetic acid, propionic acid and butyric acid and their corresponding stable-isotope labelled standards as obtained after derivatisation with DPD in presence of EDC.

F-MIX0-1 #649 RT: 7.64 AV: 1 NL: 2.44E6
T: FTMS (1,1) + p ESI Full lock ms [75.00-1200.00]

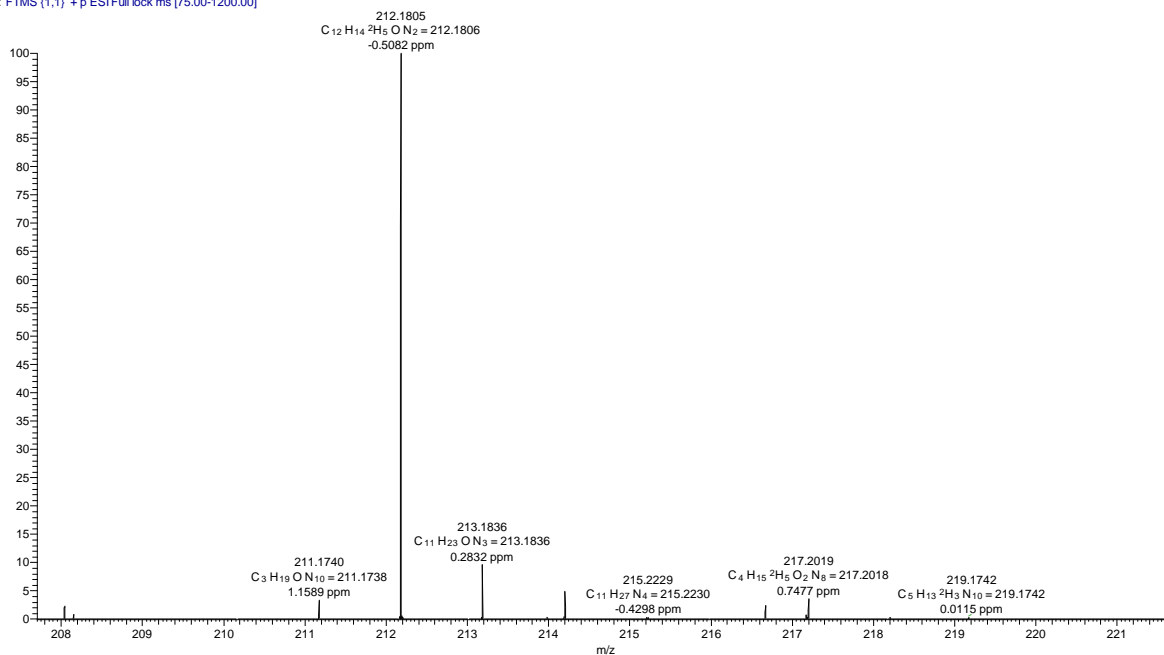


Figure 3-2 Mass spectrum of positively charged derivative of [²H₅] butyrate showing the expected accurate mass of 212.1806 with five deuterium atoms.

F-MIX10-3 #643 RT: 7.51 AV: 1 NL: 8.98E5
T: FTMS (1,1) + p ESI Full lock ms [75.00-1200.00]

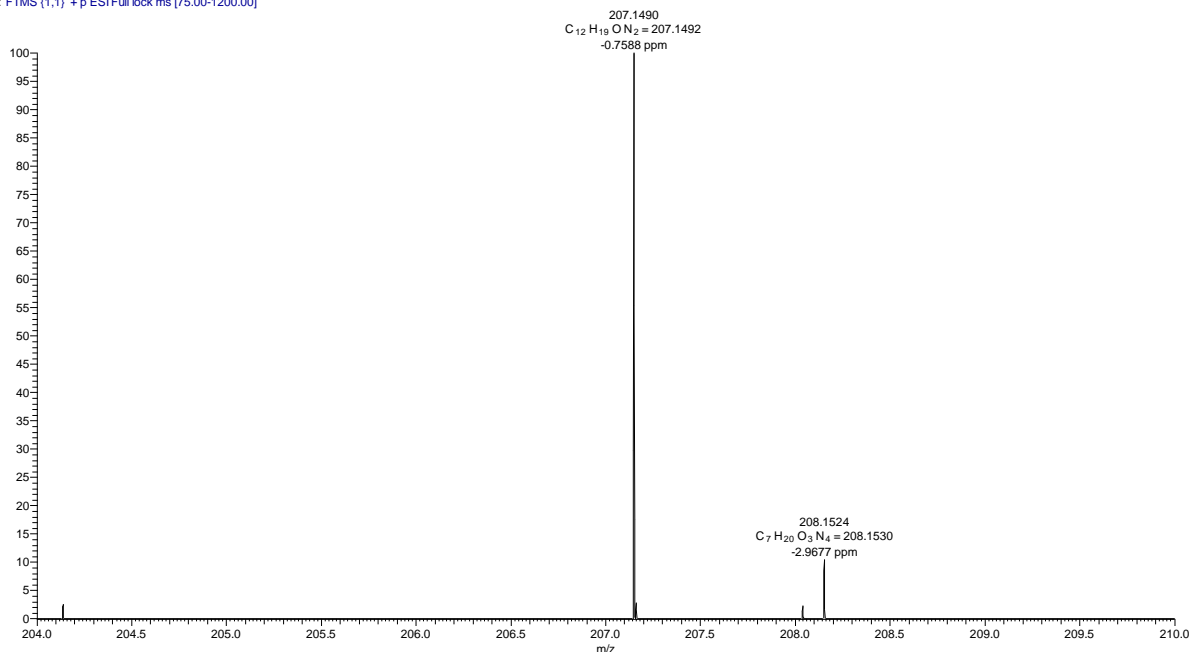


Figure 3-3 Mass spectrum of the positively charged derivative of butyrate showing the expected accurate mass of 207.1490.

F-MIX10-3 #747 RT: 8.72 AV: 1 NL: 3.41E6
T: FTMS (1,1) + p ESI Full lock ms [75.00-1200.00]

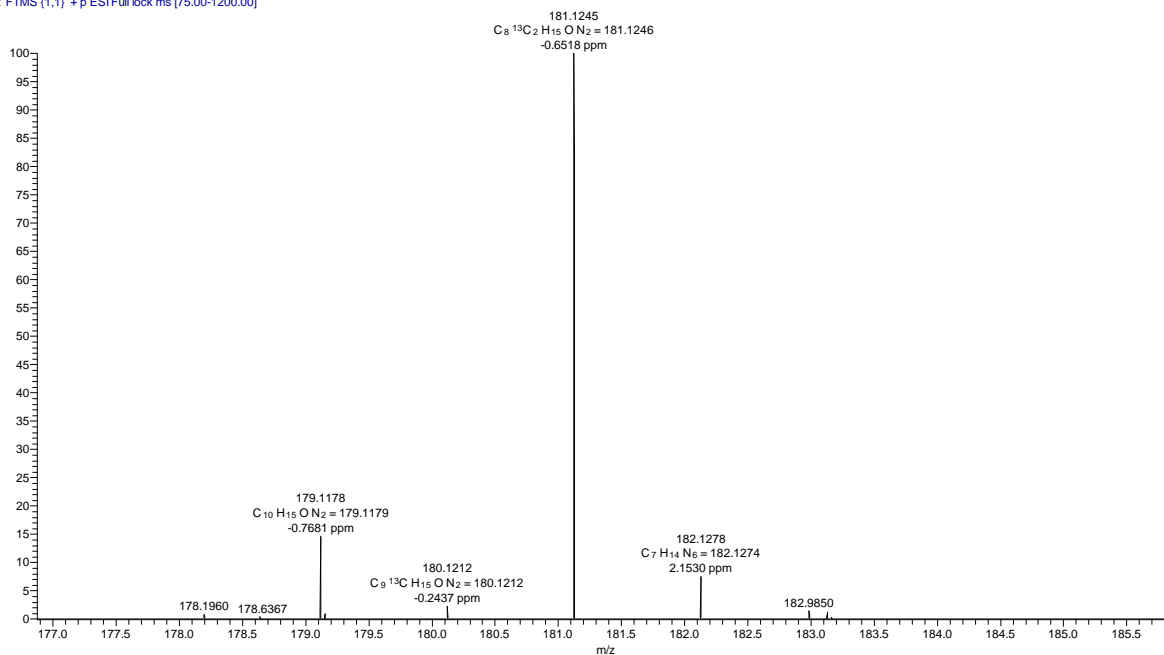


Figure 3-4 Mass spectrum of the positively charged derivative of ¹³C₂-labelled acetate with the expected accurate mass of 181.1245.

F-MIX10-3 #743 RT: 8.67 AV: 1 NL: 4.44E5
T: FTMS (1,1) + p ESI Full lock ms [75.00-1200.00]

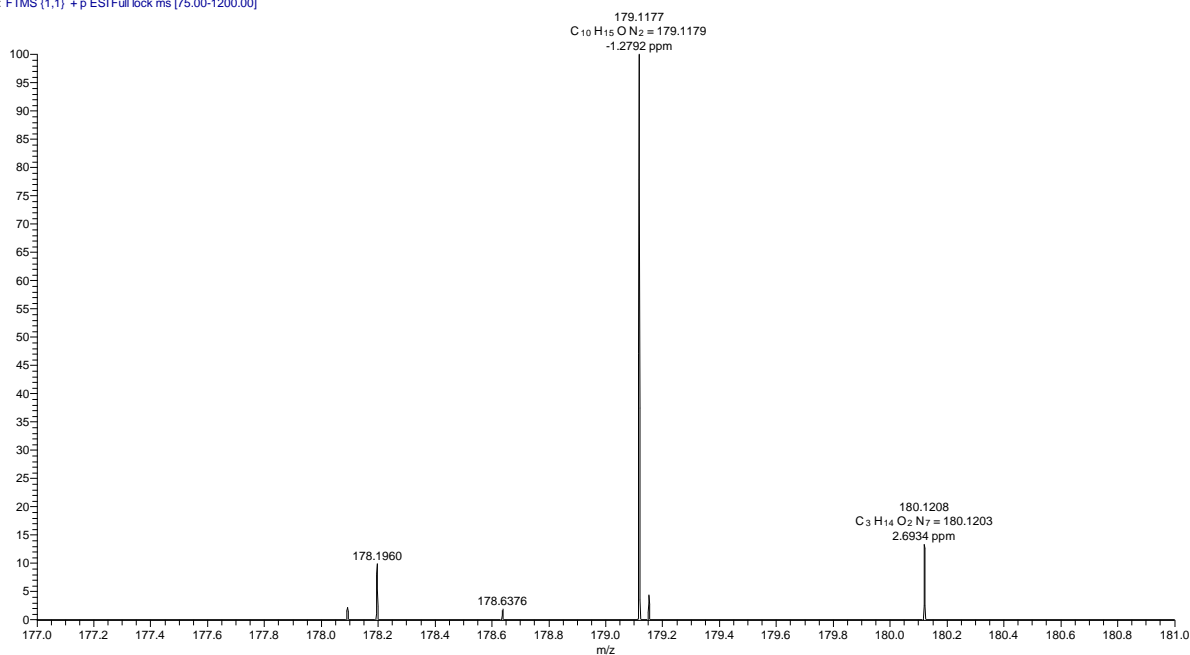


Figure 3-5 Mass spectrum of the positively charged derivative of acetate showing a mass of 179.1177.

F-MIX10-3 #687 RT: 8.02 AV: 1 NL: 2.87E6
T: FTMS (1,1) + p ESI Full lock ms [75.00-1200.00]

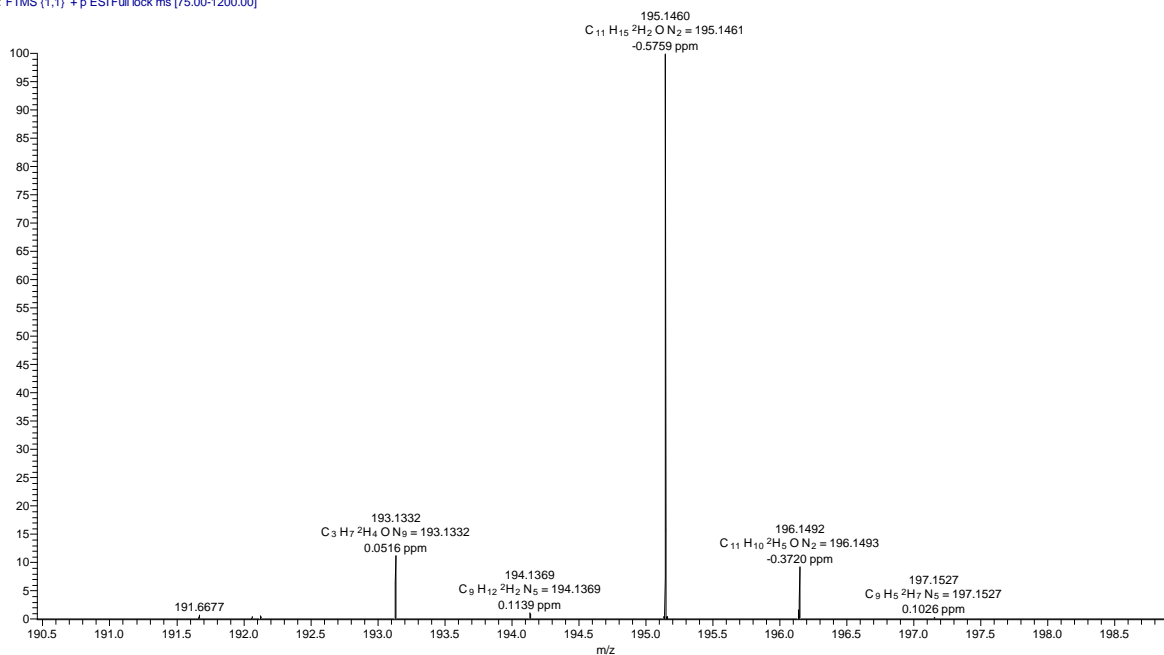


Figure 3-6 Mass spectrum of the positively charged 2H_2 propionate showing the expected accurate mass of 195.1460.

F-MIX10-3 #687 RT: 8.02 AV: 1 NL: 3.24E5
T: FTMS (1,1) + p ESI Full lock ms [75.00-1200.00]

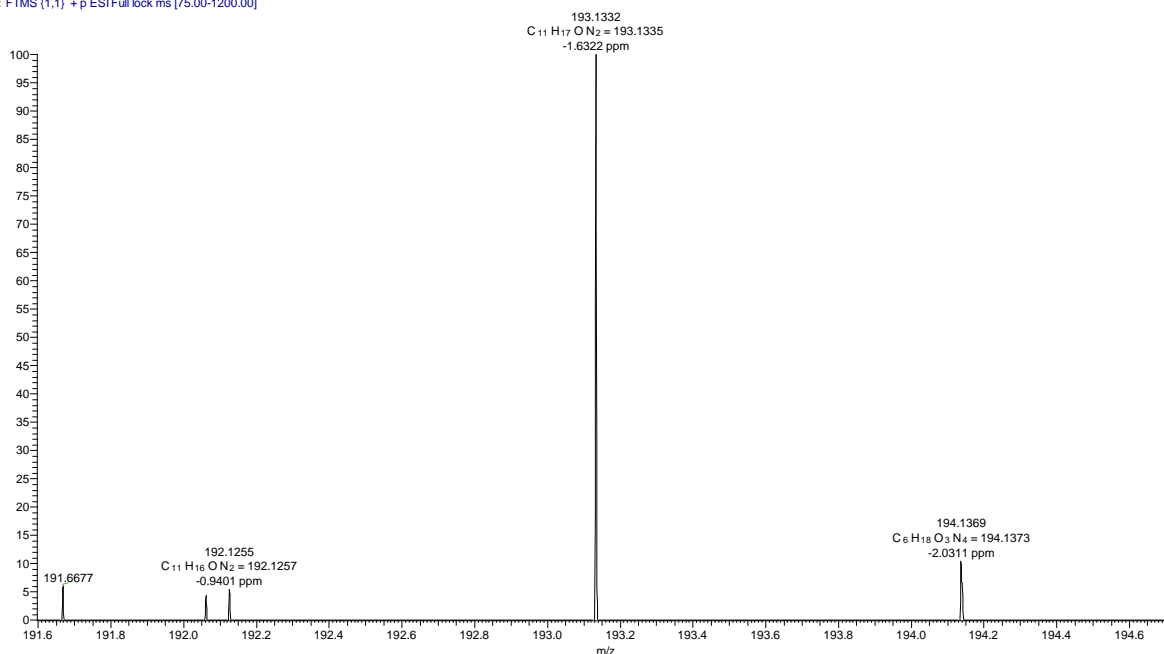


Figure 3-7 Mass spectrum of the positively charged derivative of propionate showing the expected mass of 193.1332.

3.3.2 Fatty acids derivatisation

A mixture containing all the six fatty acids of interest were labelled with internal standards $^{13}\text{C}_2$ acetic acid, $^2\text{H}_2$ propionic acid and $^2\text{H}_5$ butyric acid and their corresponding unlabelled standards. Repeat injections ($n=4$) were run for the same mixture and the analysis was performed on the Orbitrap.

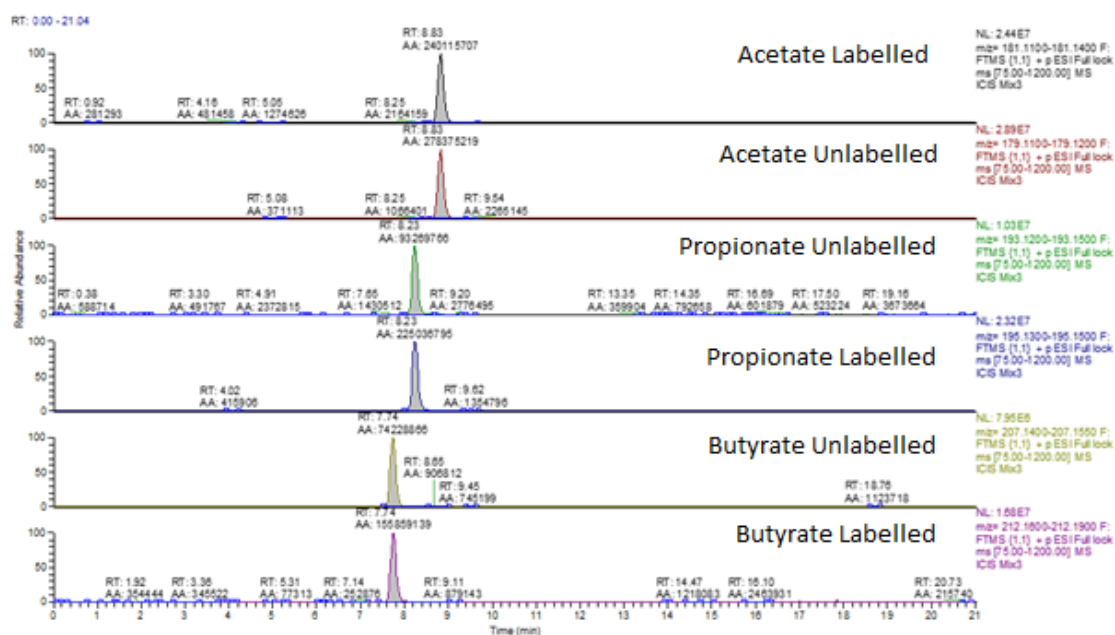


Figure 3-8 Extracted ion chromatograms for the three labelled and three unlabelled fatty acid standards at concentrations of $1\mu\text{g}/\text{ml}$ run on a ZICHILIC column using the gradient shown in table 3-3.

All peaks extracted from Mix 1 had good peak shapes (Figure 3-8). The retention times were in the order 7.74 min (butyrate), 8.23 min (propionate) and 8.83 min (acetate) which is in order of decreasing lipophilicity. The labelled and unlabelled derivatives co-eluted as expected. The derivatives of the different acids however did not show any appreciable separation between them. This implies that although all the short chain fatty acids analysed can all be successfully tagged with the derivatising reagent; the tag did not make them sufficiently different to result in appreciable separation between the SCFAs under the conditions of the

method. This is however not a problem when using the Orbitrap as the derivatives have different masses and can therefore be accurately integrated even in a mixture as seen in Table 3-5.

Table 3-5 RSDs were calculated from peak area ratios of the standards in the mixture after four injections per sample of standard.

Experiment No.	Acetate			Butyrate			Propionate		
	<i>m/z 179</i>	<i>m/z 181</i>	<i>Ratio</i>	<i>m/z 207</i>	<i>m/z 212</i>	<i>Ratio</i>	<i>m/z 193</i>	<i>m/z 195</i>	<i>Ratio</i>
1	20741556	18387482	1.128	4872189	43674413	0.112	94538702	57172811	1.654
2	17077616	14706435	1.161	3187368	30358787	0.105	73326336	47743337	1.536
3	12887110	11771998	1.095	2334110	23249404	0.100	56241121	40743802	1.380
4	18171283	17890295	1.016	4480401	37557511	0.119	101233347	59367583	1.705
Mean			1.098			0.109			1.5636
STD DEV			0.062			0.076			0.092
RSD %			5.65			7.6			9.2

From Table 3.5, the repeatability from repeat injections of the same mixture is good because the %RSD of the peak area ratios between each acid and its corresponding labelled internal standard is low (<9.2%). The highest precision was obtained with acetate (RSD=5.65%) while the least precision was obtained for propionate (RSD=9.2%).

3.3.3 Calibration of the Method

3.3.3.1 Calibration curve for acetate standard

The calibration curve for acetate is shown in figure 3-9 and the data in table 3-6.

Table 3-6 Values for the calibration curve of acetate using 1 µg of acetate-¹³C for internal standardization. after three injections per sample of standard.

Conc (µg/ml)	Mean ratio	STD	%RSD
0	0.0590	0.00203	3.44
0.1	0.1366	0.00619	4.53
0.2	0.2241	0.00187	0.83
0.4	0.4405	0.00613	1.39
0.8	0.8691	0.02690	3.10
1.6	1.7987	0.05937	3.30

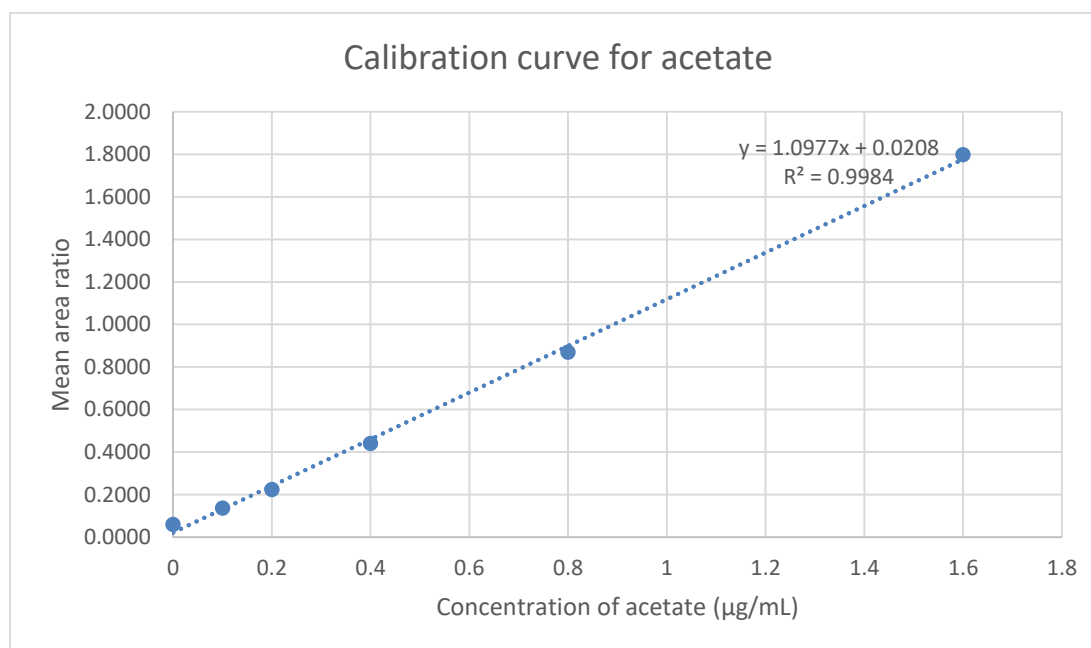


Figure 3-9 Calibration curve for acetate using acetate-¹³C as internal standard.

The calibration curve obtained for propionate is shown in figure 3-10 and the associated data in table 3-7.

Table 3-7 Values for the calibration curve of propionate using 0.5 µg of propionate-d₂ as internal standard .after three injections per sample of standard.

Conc (µg/ml)	Mean ratio	STD	%RSD
0	0.0061	0.000581	9.52
0.04	0.1059	0.00285	2.69
0.08	0.2479	0.012872	5.19
0.16	0.5162	0.0099	1.92
0.32	1.0466	0.030195	2.89
0.64	2.2723	0.1601	7.05

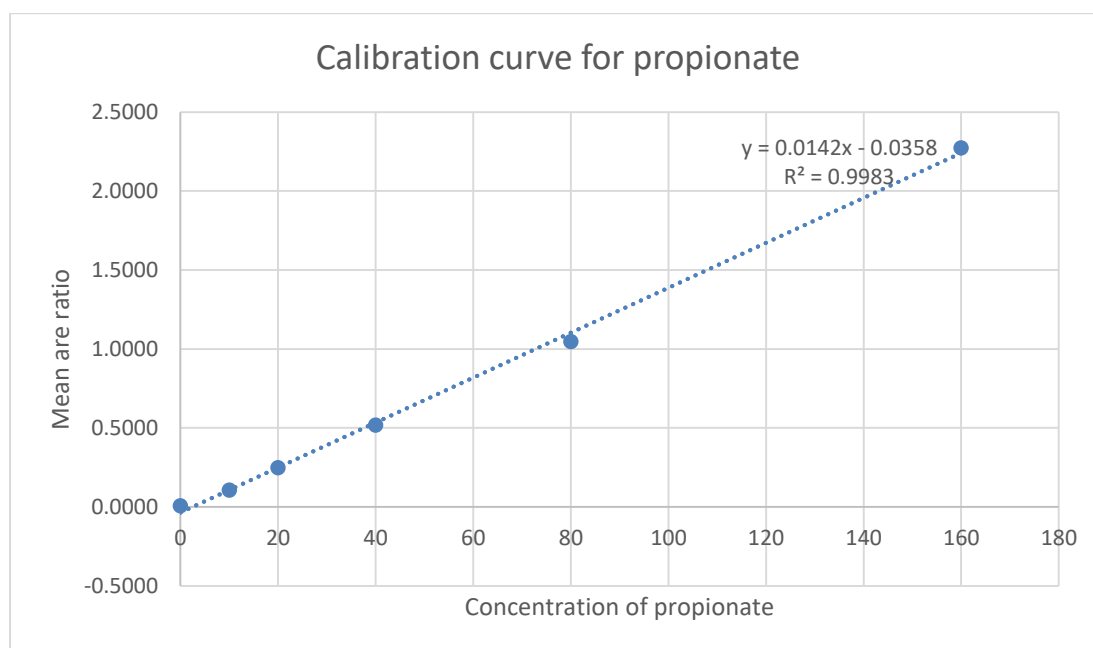


Figure 3-10 Calibration curve for propionate using propionate-d₂ as internal standard.

3.3.3.2 Calibration with butyrate standards

The calibrations for butyrate are shown in figures 3-11 and 3-12 and the associated data in table 3-8.

Table 3-8 Values for the calibration curve of butyrate using 0.5 µg of butyrate-d₅ as internal standard. after three injections per sample of standard.

Conc (µg/ml)	Mean ratio	STD	%RSD
0	0.1091	0.0044	4.03
0.04	0.6785	0.013	1.90
0.08	1.0611	0.078	7.31
0.16	2.2337	0.040	1.80
0.32	4.5671	0.23	5.11
0.64	5.5431	0.86	15.5

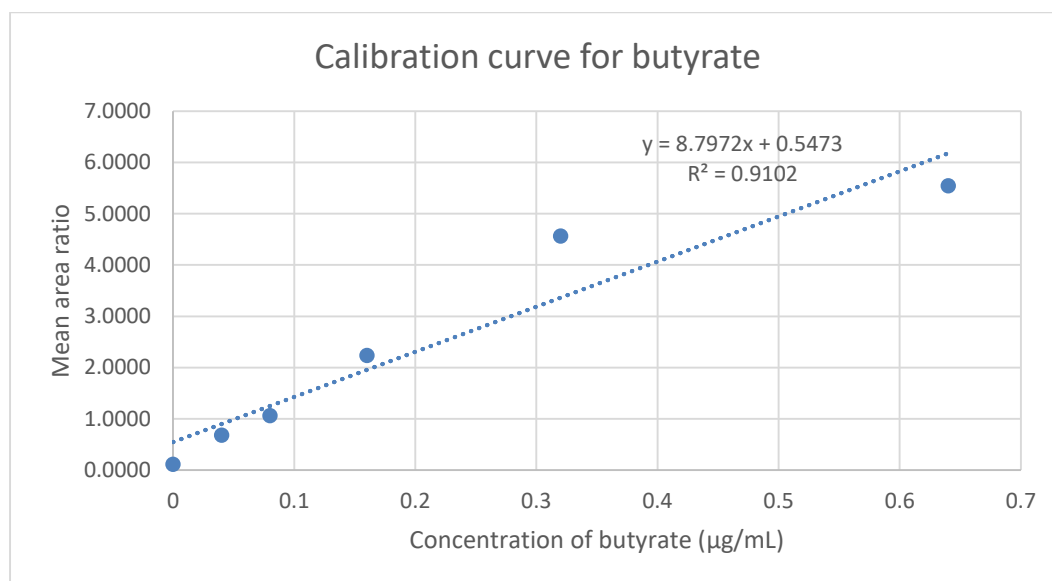


Figure 3-11 Calibration curve of butyrate using butyrate-d₅ as internal standard with all points included.

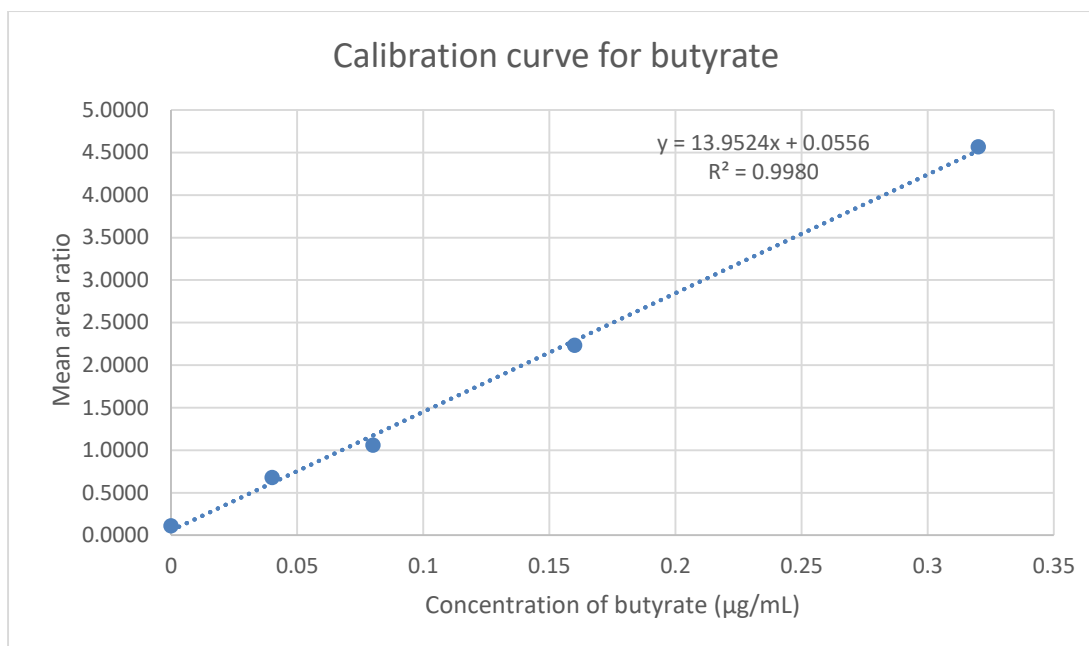


Figure 3-12 Calibration curve of butyrate using butyrate-d₅ as internal standard.

Calibration curves for acetate, (Figure 3-9), and propionate, (Figure 3-10), have $R^2 > 0.998$, implying that there is good linearity within the entire range. For butyrate, (Figure 3-11), the linearity was not as good ($R^2 = 0.9102$) for the 0 to 0.64 µg/mL range due to the lack of precision especially at the 0.64 µg/mL concentration (RSD = 15.5%). Without this point, linearity is improved to $R^2 = 0.998$ (Figure 3-12).

3.3.4 Determination of acetate, butyrate, and propionate in urine samples

Samples from 25 healthy people treated with enteral nutrition versus a novel food based diet were collected pre and post treatment, 50 samples in total. The “treatment” consisted of a special diet rich in fibre, Treatment-with-Eating/CD-TREAT diet. Current evidence suggests that the gut and dietary influences are as important as genetics in the aetiology of Crohn's disease (CD). Studies have recently shown that disease improvement, following treatment

with EEN, produces changes in the gut microbiota [107, 108]. This study was therefore intended to explore whether or not the experimental CD treat diet, which is more acceptable than the EEN, would produce an altered profile of SCFAs in urine. The samples were prepared as described above in the materials and methods (section 3.2.3) and derivatised as described in materials and methods (section 3.2.6). A method which utilised internal standardisation was employed, where each of the SCFAs had its own internal standard containing stable isotope labels either with deuterium or carbon-13. The final derivatised SCFAs were analysed by LCMS and detected using extracted ion chromatograms. The levels of the SCFAs were quantified in the urine samples based on freshly prepared calibration curves (Appendix 1) using the respective standards plotted as peak area ratios against concentrations of the standards. Peak area ratios were obtained by dividing the peak areas of each SCFA by the corresponding peak area of the internal standard used in each case. The results were further analysed by paired T-tests to determine if there were any significant differences between the test samples and controls, based on p-values and 95% confidence intervals (CI).

Table 3-9 Values for the calibration curve of acetate using acetate-¹³C as internal standard. These values were used for the determination of acetate in urine samples from patients after three injections per sample of standard.

Conc (µg/ml)	Mean Ratio	SD	%RSD
0	0.360	0.0017	0.47
0.1	0.664	0.0052	0.78
0.2	1.161	0.0030	0.26
0.4	1.937	0.0165	0.85
0.8	3.578	0.0389	1.09
1.6	5.899	0.0619	1.05

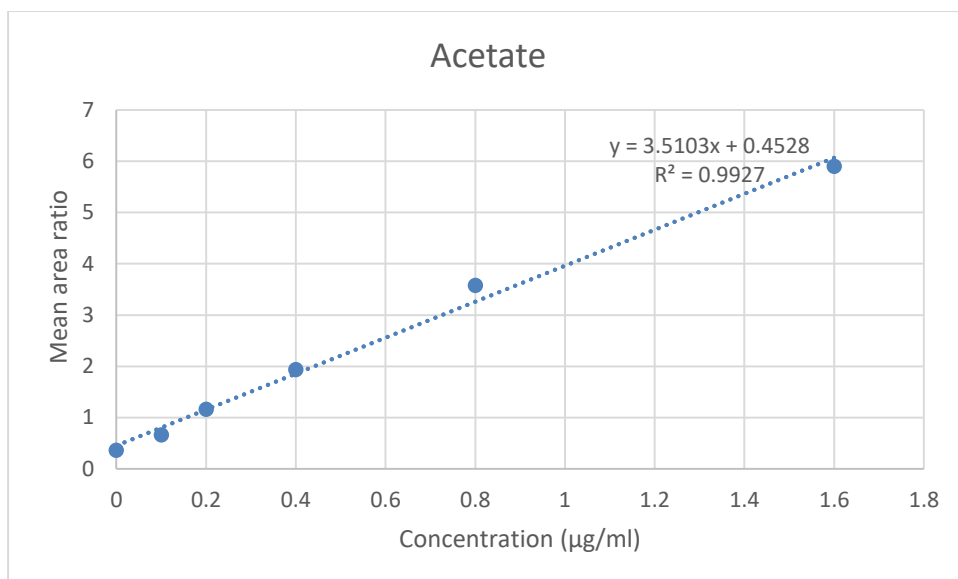


Figure 3-13 Calibration curve of acetate using acetate-¹³C as internal standard.

Table 3-10 Values for the calibration curve of propionate using propionate-d₂ as internal standard. These values were used for the determination of propionate in urine samples from patients after three injections per sample.

Conc (µg/ml)	Mean Ratio	SD	%RSD
0	0.121	0.0035	2.86
0.04	0.316	0.0047	1.48
0.08	0.420	0.0084	2.00
0.16	0.827	0.0112	1.36
0.32	1.531	0.0013	0.08
0.64	2.734	0.1199	4.39

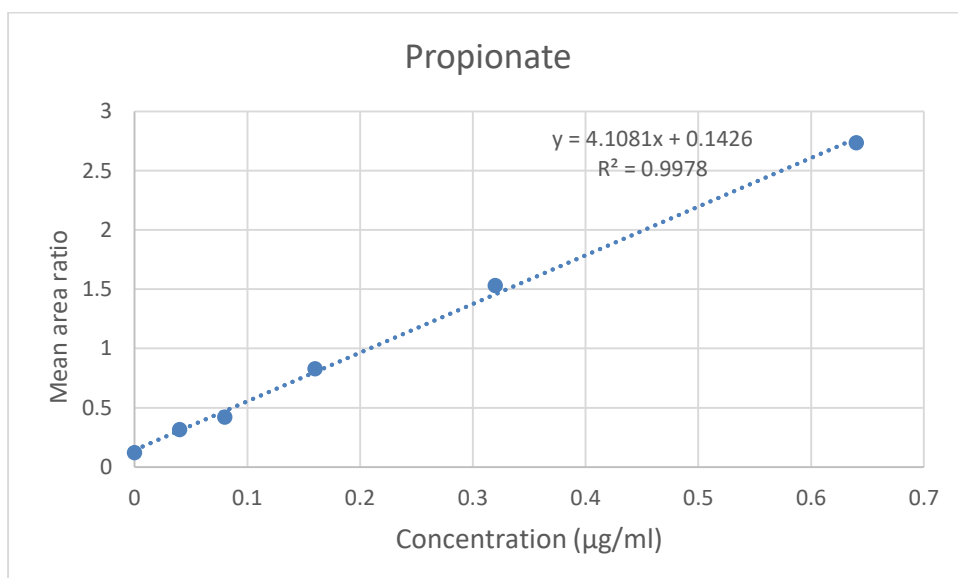


Figure 3-14 Calibration curve of propionate using propionate-d₂ as internal standard.

Table 3-11 Values for the calibration curve of butyrate using butyrate-d5 as internal. These values were used for the determination of butyrate in urine samples from patient samples after three injections per sample.

Conc (µg/ml)	Mean Ratio	SD	%RSD
0	0.026	0.0005	1.80
0.04	0.250	0.0012	0.50
0.08	0.481	0.0066	1.37
0.16	0.982	0.0161	1.64
0.32	1.642	0.0057	0.35
0.64	4.511	0.1723	3.82

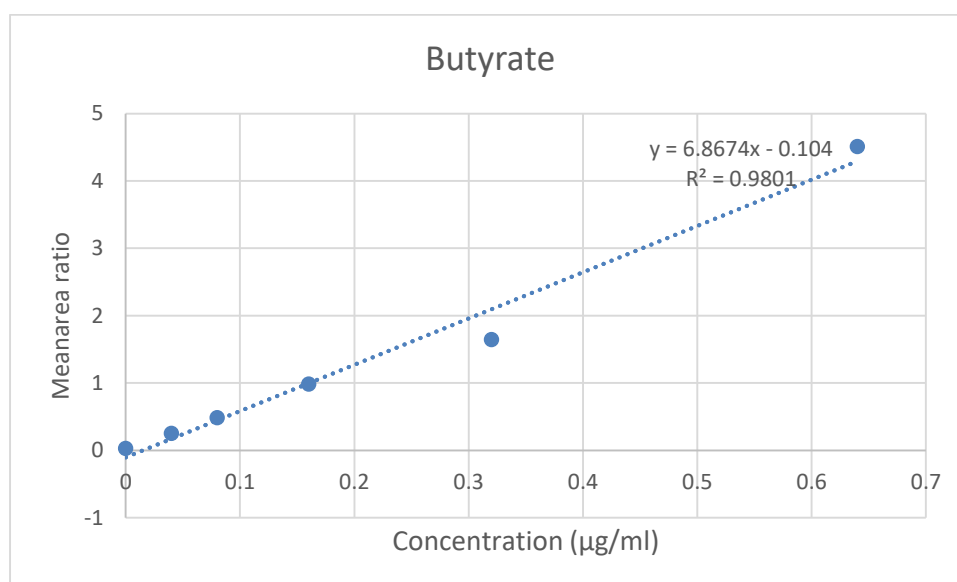


Figure 3-15 Calibration curve of butyrate using butyrate-d5 as internal standard. Note that all the curves in Figures 3-9 to 3-12 produced linearity of $R^2 > 0.99$ except butyrate which gave $R^2 = 0.98$.

3.3.5 Calculation of propionate and butyrate in urine samples

Table 3-12 Concentrations of butyrate and propionate detected in patients before and after treatment.

Sample No.	Calculated concentration of the SCFA [§] in µg/mL			
	Butyrate		Propionate	
	<i>EEN</i>	<i>CDTreat</i>	<i>EEN</i>	<i>CD Treat</i>
001	0.040	0.019	0.019	0.0098
002	0.021	*	0.008	0.0092
003	0.019	0.022	0.010	0.0112
004	0.028	0.024	0.009	0.0097
005	0.022	0.022	0.009	0.0091
006	0.022	0.021	0.012	0.0141
007	0.024	0.025	0.013	0.0122
008	0.034	0.020	0.012	0.0113
009	0.022	0.025	0.014	0.0164
010	*	0.026	0.012	0.0222
011	0.026	0.021	0.014	0.0116
012	0.030	0.027	0.012	0.0130
013	0.030	0.031	0.016	0.0131
014	0.023	0.022	0.040	0.0559
015	0.037	0.022	0.011	0.0131
016	0.024	0.027	0.012	0.0125
017	0.022	0.023	0.016	0.0205
018	0.024	0.020	0.015	0.0116
019	0.022	0.021	0.011	0.0113
020	0.020	0.031	0.014	0.0153
021	0.018	0.026	0.010	0.0304
022	0.029	0.030	0.009	0.0161
023	*	0.027	0.013	0.0082
024	0.028	0.028	0.015	0.0217
025	0.033	0.027	0.016	0.0115

[§]SCFA means short chain fatty acid; *Undetectable

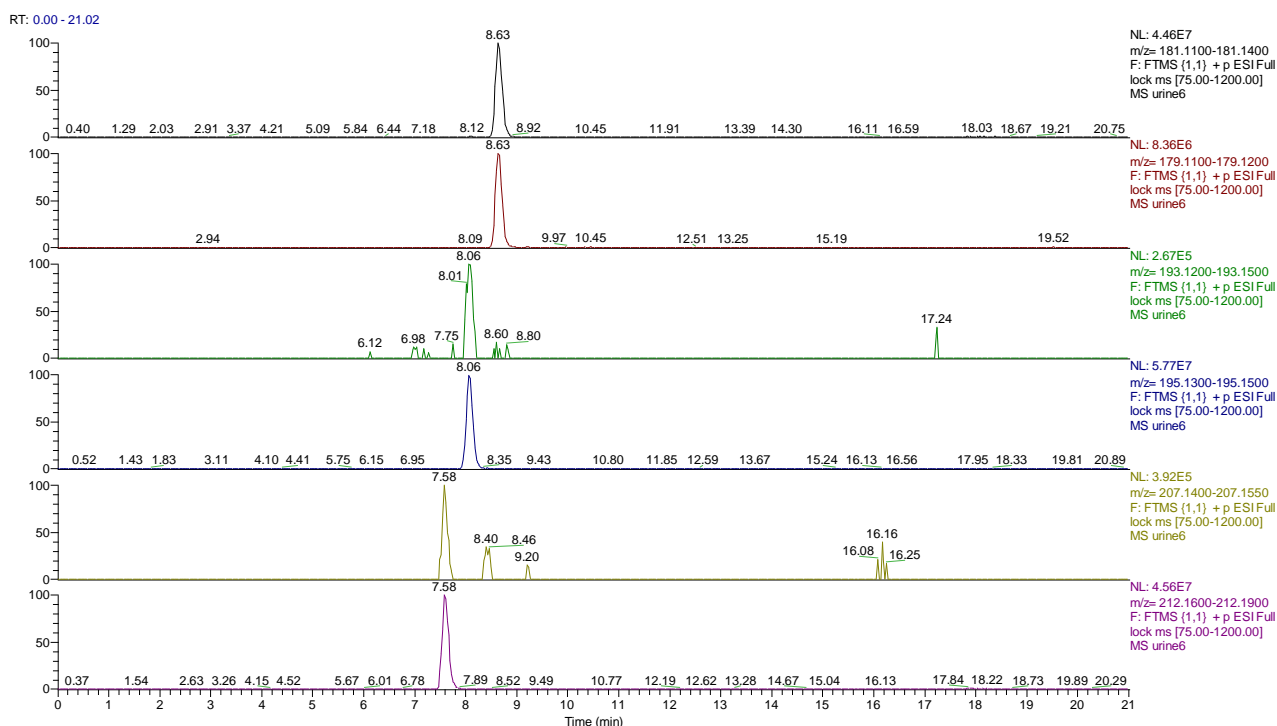


Figure 3-16 Derivatives of short chain organic acids in urine (100 µl) spiked with labelled internal standards ¹³C-acetic acid (1µg), ²H₂-propionic acid and ²H₅-butyric acid and (0.5µg).

3.3.6 Effect of treatment on propionate and butyrate concentrations

Comparison of the control and treatment samples showed that the mean (\pm SD) concentrations of propionate in the urine samples were 0.01375 ± 0.00614 µg/ml and 0.01564 ± 0.00979 µg/ml respectively, while those of butyrate were 0.02623 ± 0.00596 µg/ml and 0.02429 ± 0.00368 µg/ml respectively. In both cases, the paired T-test showed that the difference in the concentrations of the SCFAs between controls and treatment samples were insignificant with *p*-values of 0.146 and 0.222 for propionate and butyrate respectively. Although the analysis revealed that there was not a significant difference between the control and treatment samples when each SCFA was considered separately. However, the levels of butyrate were significantly higher than those of propionate in both controls and treatment samples.

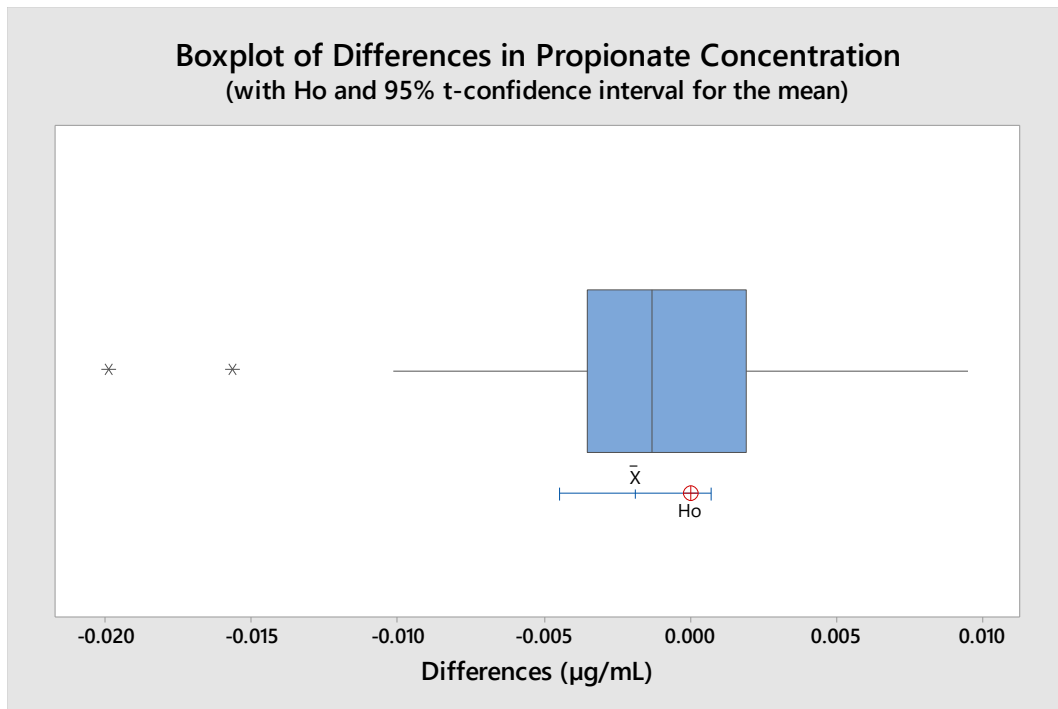


Figure 3-17 Boxplot illustrating the difference in propionic acid levels between treatment and control urine samples. The magnitude of difference was 0.00189 µg/ml (95% CI: -0.00449, 0.00071) with treatment samples having a slightly higher but insignificant level of propionate compared to the control samples.

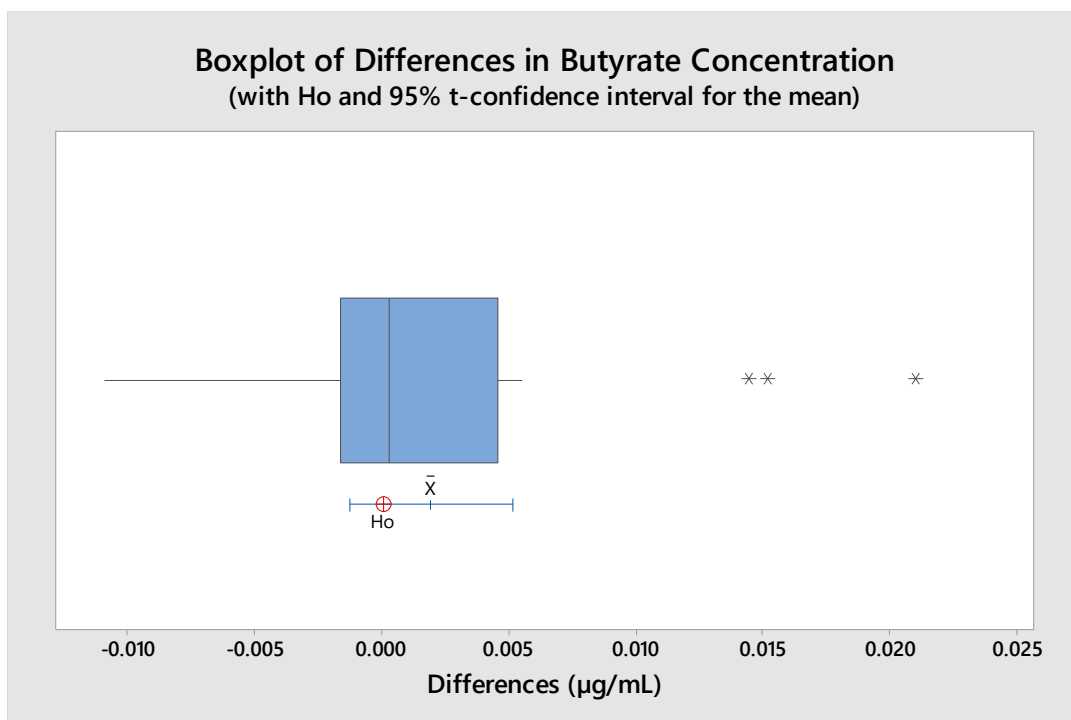


Figure 3-18 Boxplot illustrating the difference in butyric acid levels between treatment and control urine samples. The magnitude of difference was 0.00194 µg/ml (95% CI: -0.00127, 0.00515) with treatment samples having a slightly lower (but insignificant) level of butyrate compared to the control samples.

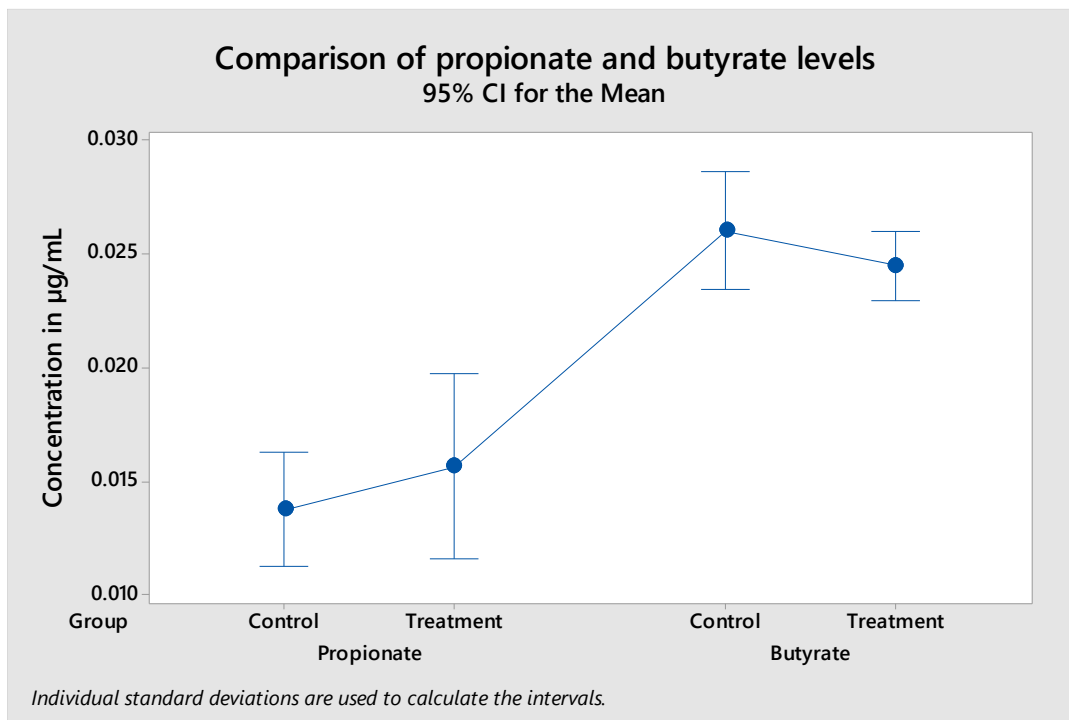


Figure 3-19 An interval plot illustrating the levels of propionate and butyrate in control and treatment samples of urine. Paired T-test analyses revealed that there were no significant differences between control and treatment samples when each SCFA was considered separately. However, the levels of butyrate were significantly higher than those of propionate in both controls and treatment samples.

3.4 Discussion

It was hoped that the study would produce evidence of the efficacy of the CD-TREAT diet which is intended to support the movement of the CD-TREAT treatment diet towards a preliminary clinical trial in patients with CD which is currently inappropriate and unethical to carry out in people with active CD undertaking contemporary medical treatment. The study was intended to investigate if the change in diet would have a measurable effect on the composition of the SCFAs in urine in both groups. The fact that there was no difference in the levels of SCFAs between the treatment and control group suggests that the diets are interchangeable and thus the CD treat diet provided no evidence for an adverse effect on the microbiome. There is an increasing interest in the role of butyrate as an anti-inflammatory agent which

enhances the defensive mechanisms of the gut preventing bacteria from crossing the epithelial barrier [109-113]. Butyrate is produced by bacteria in the gut and is the major energy source for the colonocytes which line the gastrointestinal tract [111]. Despite the extensive utilisation of butyrate by the colonocytes some of it is absorbed from the GI tract and it has been shown in pigs that the concentration of butyrate in the portal vein reflects the production in the gut [114, 115]. Thus it follows that urinary output could reflect the levels of butyrate produced in the gut. The current results demonstrate that a switch to the CD treat diet did not have an adverse effect on the levels of butyrate in urine. The successful derivatisation of SCFA to form the amine derivatives with DPD and EDC has been successfully demonstrated. The reaction can be very easily reproduced and the resulting derivative compound is more readily detectable. Using butyrate, propionate, and acetate compounds as a test system, the method has been shown to be reproducible and quantitative. It was also applied to the determination of the levels of the acids propionate and butyrate in urine samples collected from patients before and after treatment with a diet. The results of the dietary study showed no significant differences in the levels of butyrate and propionate after statistical comparisons using a paired T-test. Attempts were made to run the method with the quaternary ammonium tag which was synthesised in chapter 2 in order to further enhance the limits of detection for the SCFAs. However, no product was formed indicating that the presence of the strongly electron withdrawing quaternary amine group para to the primary aromatic amine reduces its basicity to such an extent that it will no longer react. The limits of detection (LODs) of the method developed above are quite low but ultimately the LODs are compromised by environmental contamination by SCFAs. These compounds are volatile and particularly in the case of acetate are abundant in a chemistry lab. Thus the only solution to an improved LOD

would be to have a clean lab isolated from contamination by other chemicals to improve the LODs.

3.5 Conclusion

The results of the study confirm that derivatisation of SCFAs can greatly improve their detection identification and quantification by LCMS. The ionisation SCFAs in positive mode in our experiments was improved following derivatisation with DPD in the presence of EDC and the masses expected for the derivatized SCFAs were observed in all cases. The retention times were greatly improved however there wasn't much separation between the various SCFAs under the conditions of the study analysis however this did not hinder the analysis because the derivatives all have different masses and so could be accurately integrated. The derivatisation with alternative tagging agents, such as the quaternary ammonium tag synthesised in chapter 2, can be optimised in an effort to improve the resolution between various SCFAs. The results of the dietary study showed no statistically significant differences in the levels of butyrate and propionate however environmental contamination is believed to have influenced the evaluation of acetate and this might only be overcome by repeating the experiment in a laboratory which is free from contamination and having dedicated automatic pipettes which have not been used to measure the unlabelled acids. The method is potentially high sensitive and thus very useful but more work is required to eliminate background contamination.

Chapter Four:

Investigation of the effect of Ultramarathon Exercise on Six Oxidized Fatty Acids in Human Plasma by using a derivatization method based on coupling to Choline

4 INVESTIGATION OF THE EFFECT OF ULTRA-MARATHON EXERCISE ON SIX OXIDIZED FATTY ACIDS

4.1 Introduction

In spite of the upward trend in life expectancy in the developed world over the last few decades, individual lifestyle choices are still a major challenge to longevity. A sedentary lifestyle, an unhealthy diet, excessive alcohol consumption, obesity and the smoking of cigarettes amongst others comprise some of the most common risk factors [97, 116]. The impact of these risk factors on the general health and wellbeing of the individual can be significantly reduced by simple interventions such as participating in regular physical activities, coupled with the choice of healthier foods and a reduction in the quantity of alcohol consumed, have all been shown to result in an improvement in health and wellbeing and can contribute to an increase in life expectancy [117]. This is evidenced by numerous reports in the literature that regular exercise can help to promote overall health and wellbeing such as the reports that regular exercise can help reduce the effects of sarcopenia and in the prevention and management of cardiovascular disease (CVD) in general [118-120]. Exercise is also prescribed for the treatment and control of type 2 diabetes [121-123], obesity [124], and has even been found to be of use in the management and treatment of moderate depression [120]. The number of cases of hypertension, hypercholesterolemia, and diabetes among others have also been reported to be lower among people who frequently participate in marathons. However, this reduction is not linked to the total distance which is run annually [125]. This is probably as a

result of the number of longer training runs undertaken by the marathoner in preparation for the marathons or may be due to other genetic or other innate differences between marathon runners and non-marathoners [125]. However, in spite of the clear health and general well-being benefits derived from regular exercise, sedentary behaviors/lifestyles are still very widespread. For instance, the indirect cost of physical inactivity is estimated to be 1.5%–3% of the total direct healthcare costs in developed countries, including the U.K. where this cost has been estimated to be about £7.4 billion per annum in England and is responsible for one in six UK deaths which is equal to the number of deaths attributed to smoking [126, 127]. An in depth understanding of how physical exercise affects health and wellbeing, as well as the correlation between physical performance and wellness are likely to provide good insights into how personalized comprehensive healthcare plans for promotion of wellbeing can be developed. The data currently available on the changes which occur to the metabolism during exercise are insubstantial and in need of significant improvement. In a recent study, it was reported that there were appreciable increases in the levels of the purine metabolites such as hypoxanthine, guanine, deoxyinosine, inosine, and xanthosine as well as several acyl carnitines and steroids in healthy adults who were subjected to submaximal exercise [128]. This could be beneficial for the management of purine metabolism disorders [129]. It is anticipated that a better indication of the metabolic changes which occur in the body and their correlations with other physical performance indicators can be obtained during high intensity and prolonged exercises such as marathons, which have fortuitously increasingly grown in popularity in recent years as social and fitness events globally and as a result of social media and charity campaigns. Understanding these metabolic changes would help provide an explanation of the ability of individuals to achieve and sustain peak physical performance and physiological function [130].

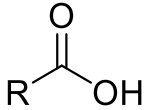
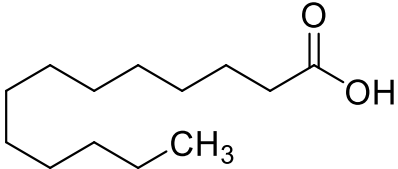
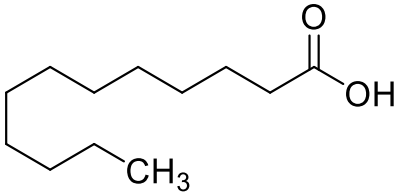
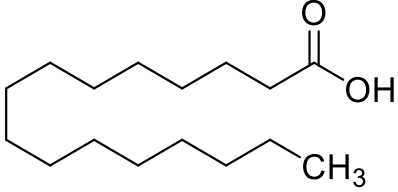
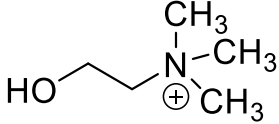
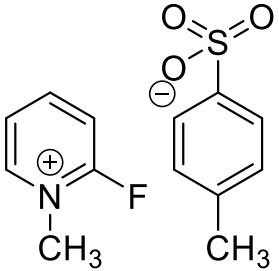
The physical performance of people who participate in marathons can be influenced by several factors such as their gender, [131-133] age [134], lifestyle, and body mass index (BMI) [135], environmental factors [136], and also due to physiological differences such as muscle strength and oxygen carrying capacity, morphological differences such as the percentage of body fat or muscle mass, as well as characteristics unique to the individual [137]. However, how much exercise is optimal for a particular individual cannot be accurately determined due to the lack of conclusive data relating to the molecular mechanisms which are the basics of exercise and how they are linked to health.

Therefore, investigations into the effects of exercise on the metabolism of people could provide useful information about phenotypic responses to exercise which can be utilized to facilitate the development of personalised training regimes for individuals which will be based upon the initial metabolic status of the individual [138], which in turn will provide very important diagnostic and prognostic biomarkers which will be invaluable to health care providers for the management of cardiovascular and other related diseases [139]. The most effective indicator of cardiovascular fitness is the maximal rate of oxygen consumption, known as VO_2 max. It can be determined by measuring respiratory variables during an incremental exercise test to exhaustion [128]. Carboxylic (Fatty) acids constitute some of the most common organic compounds present in living organisms. Fatty acids (FAs) perform a wide variety of essential functions in many biochemical processes within living organisms and are mainly characterised as metabolites which possess at least a single carboxyl group (-COOH) within their chemical formula. They are of particular interest because of the roles they play in metabolic pathways. The mechanisms by which fatty acid production is controlled has been shown to be of increasing importance in understanding the causes of many diseases and thus

the prevention of chronic diseases such as insulin resistance induced by obesity and atherosclerosis as well as the general promotion of cardiovascular health [140-142]. A lot of metabolites are synthesised within the body from simple precursors, however, some essential fatty acids (EFAs) cannot be produced in the body and as such are derived from the diet. Oxylipins or oxidised fatty acids are a class of lipophilic signalling metabolites derived from the oxidation of polyunsaturated fatty acids (PUFA), such as arachidonic acid (ArA) and linoleic acid (LA). Understanding the effect of subtle shifts in fatty acids or bioactive lipids, especially the oxylipins is a major challenge in nutrition studies because they are unstable or are rapidly expended by metabolism. They exist in low concentrations and often exist as isomers due to the similarities in their molecular formula further complicating their analysis [143]. However due to the important role they play, the investigation of the effects of changes to fatty acids on human health is essential in both the healthy and pathological condition. This investigation was a controlled laboratory study involving 12 healthy participants of both sexes in an 80 km marathon run simulated on a treadmill. Plasma samples collected at three different points before, midway and immediately after the marathon were analyzed for their metabolomic profiles using reversed phase (RP) liquid chromatography-mass spectrometry (LCMS) methods. Like SFCAs, fatty acids contain the carboxylic acid functional group. They are therefore also similarly ionised readily for detection in negative mode LCMS. Fatty acids and their oxidised metabolites are of particular interest because they are widely distributed, play vital roles in several biochemical processes and are also only present in relatively small quantities therefore methods which can improve the accuracy and precision of their analysis are of great importance. Chemical derivatisation has been demonstrated to be a versatile and extremely powerful technique for improving the chromatographic properties of fatty acids, such as their retention time and peak efficiency as well as the selectivity and sensitivity of their analysis by

LCMS enabling more accurate metabolomic analysis and interpretation of biological samples. Derivatisation reactions are designed to generate products with enhanced ionization and/or introduce an easily identifiable specific mass shift which allows for easy identification from the mass spectrum. Several reports can be found in the literature regarding the use of derivatisation reactions in MS analysis [23, 144-147]. The introduction of a permanent positive charge by use of derivatisation tags which contain quaternary ammonium groups which ensures the derivatized acid can be analysed in both acidic and basic mobile phase, due to the permanent charge, has been shown to be very useful for the analysis of peptides and amino acids by LCMS [148, 149]. Choline, 2-hydroxyethyl (trimethyl) azanium, which also contains a quaternary ammonium group, has been reported to have been successfully applied to the derivatisation of fatty acids [150, 151]. In this study, choline was also used as derivatisation agent for the development of a protocol for the analysis of fatty acid and oxylipin metabolites from biological samples. The Fatty acids focused on in this study were Dodecanoic Acid (**1**), Myristic Acid (**2**) and Palmitic Acid (**3**). They were derivatized by using Choline, 2-hydroxyethyl (trimethyl) azanium **5** and 2-Fluoro-1-methylpyridinium p-toluenesulfonate (FMP) (**4**) as reagents prior to analyses by LC-ESI-MS on an Exactive Orbitrap mass spectrometer (Table 4-1).

Table 4-1 Structures of the derivatizing reagent FMP and the fatty acids of interest used in the study.

Structure	Name	Formula	MW	Str. No.
	Fatty Acid	$C_nH_{12n+1}COOH$		
	Dodecanoic Acid	$C_{11}H_{23}COOH$	200.1 8	1
	Myristic Acid	$C_{13}H_{27}COOH$	228.2 1	2
	Palmitic Acid	$C_{15}H_{31}COOH$	256.2 4	3
	Choline	$C_5H_{14}NO^+$		4
	2-Fluoro-1-methylpyridinium p-toluenesulfonate (FMP)	$C_{13}H_{14}FNO_3S$	104.1 1	5
			283.0 7	

Oxylipins form a group of metabolites of interest which are biologically active fatty acids. Linoleic acid is the most common polyunsaturated fatty acid the diets and mammalian. Dietary

linoleic acid is converted to longer and more unsaturated fatty acids through enzymatic desaturation and elongation in cells. Linoleic acid can be converted to 13- and 9-hydroxy-octadecadienoic acid (13-HODE & 9-HODE). 13-HODE & 9-HODE are stable oxidation products and have been linked to pathological conditions such as atherosclerosis, diabetes, Alzheimer's disease, non-alcoholic steatohepatitis, psoriasis, chronic inflammation, obesity, and cancer [152]. Plasma levels of 13-HODE & 9-HODE are responsive to lifestyle changes and decrease when subjects adopt healthy diets and lose weight [153]. 13-HODE & 9-HODE are generated through the 15-lipoxygenase pathway in a variety of cell types [154] and are ligands of peroxisome proliferator-activated receptors (PPARs) [155] and can exert pro-inflammatory effects [156]. There is increasing evidence that exercise influences 13-HODE & 9-HODE levels with increases in these metabolites occurring post-exercise.

The aim of this study is to develop a protocol for the metabolomic analysis of fatty acids and their oxylipin metabolites from plasma samples from marathoners by LCMS utilizing the choline derivatisation reaction to enhance the sensitivity and selectivity of the protocol to detect the minute quantities of metabolites which may be present in the samples, to investigate the differences which extreme exercise has on the fatty acids and their metabolites which are produced in the body. By enhancing the ionisability of the oxidized fatty acids it was hoped that an untargeted rather than a targeted method could be developed for this class of metabolites.

4.2 Materials and Methods

4.2.1 Chemicals and Solvents

HPLC grade Acetonitrile (ACN), Tetrahydrofuran (THF) and formic acid were purchased from Sigma-Aldrich, (Dorset, U.K.). All reagents including dodecanoic acid, myristic acid, palmitic

acid, 2-fluoro-1-methyl-pyridinium p-toluene sulfonate (FMP), triethyl amine (TEA), and choline chloride were obtained from Sigma-Aldrich, (Dorset, U.K.). The standard mixtures of oxidized fatty acids including Linoleic Acid Oxylipin mixture (LAO), containing the oxylipin metabolites derived from linoleic acid ((±)12(13)-DiHOME, (±)9(10)-DiHOME, 9(s)-HODE, 13(s)-HODE, 13-OxoODE, 9-OxoODE, (±)12(13)-EpOME, and (±)9(10)-EpOME)), and an Arachidonic Acid Oxylipin (ArAO) mixture containing oxylipin metabolites derived from arachidonic acid (5-OxoETE, 12-OxoETE, 15-OxoETE, 15(S)-HETE, 12(S)-HETE, 11(S)-HETE, 9(R)-HETE, 8(S)-HETE, and 5(S)-HETE)). Internal standard mixtures, Deuterated Linoleic Acid oxylipins (DLAO), containing deuterated (²H) analogues of oxylipin metabolites derived from linoleic acid ((±)12(13)-DiHOME-d₄, 13(s)-HODE-d₄, 13-OxoODE-d₄, and (±)12(13)-EpOME-d₄). LAO, ArAO and DLAO compounds were purchased from Cayman Chemical Company. The relevant product information for them can be found on the company website [<https://www.caymanchem.com>] in products Item No 20794, Item No 20666 and Item No 20795, respectively. HPLC grade water was produced by Direct-Q 3 Ultrapure Water System from Millipore, UK.

4.2.2 Plasma samples collection

Plasma samples were collected from 12 participants of both sexes, male and female by collaborators at the University of Kingston. The subjects had a mean age of 38 ±12 years. The blood samples were collected at 3 time points for each participant during a simulated indoor ultramarathon run on a treadmill over a distance 80 km, namely: Pre-marathon, Halfway (40 km) and Post marathon (80 km). The 'Pre-marathon' samples were obtained immediately before commencement of the ultramarathon run while each participant was at rest. The 'halfway' samples were taken after each participant had completed 40 km of the ultramarathon run while the 'Post marathon' samples were collected immediately upon completion of the

80 km run for each participant except one who failed to complete the run and only completed 70 km of the ultramarathon. Baseline samples were also obtained from each of the participants ahead of the test day when each participant came in for the familiarization visit. All blood samples were then centrifuged to separate out the plasma which were stored in a -25 °C freezer until they were analyzed. Baseline testing (VO₂ max test) were conducted within a two-day window prior to each participants 80 km run.

Table 4-2 Biographic information and metadata of participants.

Participant ID	Gender	Age (years)	Body Mass (kg)	BMI (kg/m²)	VO₂ max (ml.min.kg)	Total Elapsed Time for 80.5 km (hr:min:sec)
P00	Male	27	65.55	20.5	62.2	08:12:00
P01	Male	32	77.3	23.9	62.5	07:40:48
P03	Male	33	83.55	25.2	55.6	10:37:37
P04	Male	33	61.95	20.5	66.9	07:04:19
P05	Male	34	69.45	22.8	59.5	09:20:37
P07	Male	50	67.47	21.7	57.8	10:02:38
P09	Female	33	75.55	27.0	44.3	10:20:25*
P10	Female	26	60.69	23.5	61.2	08:23:06
P13	Female	43	61.0	22.8	54.7	07:45:33
P14	Male	33	72.76	22.7	58.5	10:20:25
P15	Male	29	68.15	20.7	62.4	10:17:14
P16	Male	31	67.5	21.2	68.7	10:00:00

* Did not complete full marathon distance (~ 70 Km completed)

4.2.3 Preparation of plasma solution, reagents and standard solutions

The plasma samples obtained were first prepared for use in the analysis by transferring 50 µL of the separated plasma from the sample vials into an Eppendorf tube and diluting it with 100 µL of acetonitrile (ACN). The resultant mixture was then vortexed for two minutes prior to its being centrifuged for 10 minutes at 9000 rpm to facilitate the process of precipitation (PPT) of the proteins and any other solids materials in the sample. The supernatant was then carefully pipetted off and stored for use in the coupling reactions [36].

A stock solution of choline chloride was prepared using ACN as solvent to a final concentration of 1 mg/mL. A stock solution of the FMP coupling reagent was also prepared using ACN as solvent to a final concentration of 1 mg/mL.

4.2.4 Native Fatty Acids and Internal Standards

Standard solutions of the fatty acids focused on in this study, dodecanoic acid, myristic acid and palmitic acid, were prepared at final concentrations of 10 µg/mL using THF as solvent and then stored at room temperature until used.

In an attempt to increase the number of oxidized fatty acids which could be measured in each analytical run, seventeen oxylipins, from two different standard mixtures of oxidized fatty acid compounds, LAO and ArAO, which were received ready for use from Cayman Chemical Company at a concentration of 10 µg/mL in ethanol, were combined and used as a native standard. An internal standard (DLAO) consisting of the deuterated (²H) analogues of the four oxylipin metabolites derived from linoleic acid was added in order to help distinguish between the various isomers of oxidized linoleic acid was also received ready for use from Cayman Chemical Company at a concentration of 10 µg/mL.

4.2.5 Coupling of the fatty acids and their oxidised derivatives

The derivatisation of the fatty acids by esterification of the fatty acids using choline was performed using FMP as the coupling agent. A general illustration of the scheme of the reaction between choline and the fatty acids or their oxidized metabolites is depicted below (Figure 4-1).

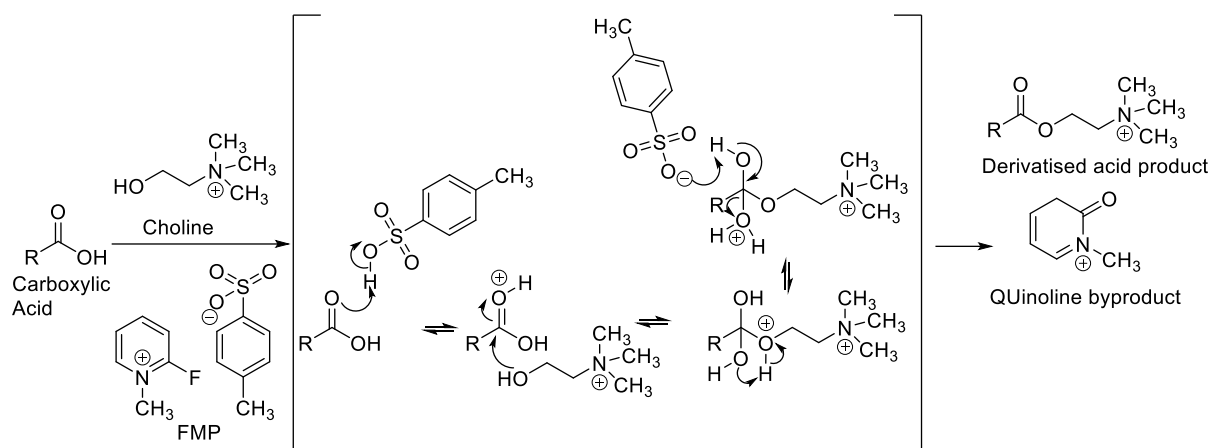


Figure 4-1 Schematic depiction of the choline derivatisation of fatty acids reaction using FMP as coupling agent.

An aliquot of the plasma sample (50 μ L), previously prepared as described above, was transferred to an Eppendorf tube containing 100 μ L of ACN and vortexed prior to centrifuging for 10 minutes at 9000 RPM. 100 μ L of the supernatant was then carefully transferred to a vial and 100 μ L of the oxidized fatty acid internal standards (50 ng), was then added. 100 μ L of the pre prepared choline chloride solution, (1 mg/mL in ACN), as well as 100 μ L of the FMP coupling agent stock solution previously prepared (1 mg/mL in ACN) were then added simultaneously. This was followed by the addition of 6 μ L of triethylamine (TEA) and the resulting mixture shaken for two minutes and then transferred to a vortex water bath set at 50 $^{\circ}$ C for a further 30 minutes. The reaction mixture was then blown to dryness under a stream of nitrogen gas and subsequently resolved in ACN (1 mL) in preparation for injection on the LCMS.

4.2.5.1 LCMS analysis

Measurements of samples and standards was carried out on Surveyor HPLC system combined with an Exactive Orbitrap mass spectrometer (Thermo Fisher Scientific, Hemel Hempstead, UK). The ESI interface was operated in dual positive/negative switching mode, with a spray

voltage was 4.5 kV for positive mode and 4.0 kV for negative mode. The temperature of the ion transfer capillary was 275 °C and sheath and auxiliary gas were set at 50 and 17 arbitrary units respectively. The full scan range was 50 to 1200 m/z for both positive and negative modes with the settings for the Automatic Gain Control (AGC) target and resolution set as Balanced and High (1e6 and 50,000) respectively. The data was recorded using the Xcalibur 2.1.2 software package (Thermo Fisher Scientific, Bremen, Germany). Mass calibration was performed for both ESI polarities prior to the analysis using the standard ThermoCalmix solution with additional compounds to cover the low mass range and the signals of 83.0604 m/z (2 x ACN + H) and 91.0037 m/z (2 x formate - H) were selected as lock masses for positive and negative mode respectively during each analytical run. An aliquot of each sample solution, (10 µl), was injected onto an ACE 3 C18 column (150 x 3.0mm, 5µm Hichrom, Reading, UK) with a flow rate was 300µl/min. Mobile phase A consisted of 0.1%v/v formic acid buffer in water and mobile phase B consisted of 0.1% v/v formic acid buffer in ACN. The gradient used is illustrated in in the table below (Table 4-3)

Table 4-3 Illustration of mobile phase gradient program used in LCMS analysis.

Time	A%	B%	Flow Rate
0	90	10	300
10	10	90	300
15	10	90	300
16	90	10	300
21	90	10	300

The last five minutes (16-21 minutes) are important to enable the column re-equilibrate before the next injection.

4.3 Results

4.3.1 Physiological response to the marathon

The mean (\pm SD) values of VO_2 max was 59.5 ± 6.3 ml.min.kg while that for the marathon completion time and $9.03 \text{ h} \pm 1.3$ hours respectively. The fastest finishing time was 07:04:19 while the longest time taken to complete the run was 10:37:37 however one runner did not complete the run completing only approximately 40 km in 10:20:25.

4.3.2 Derivatisation of Fatty Acids

It is generally accepted that derivatisation of fatty acids is the best technique for enhancing the detection of fatty acids in general. The sensitivity of mass spectrometers in negative ion mode is generally not as good as in positive ion mode and for a general metabolomics screen as opposed to a targeted analysis it would be better to convert low level compounds such as oxylipins into positively tagged derivatives. Therefore, a derivatisation strategy was deployed in a bid to maximise the potential of detection if any fatty acids as well as their oxidised fatty acid metabolites in the test samples. Dodecanoic acid, Myristic acid and Palmitic acid were coupled with choline utilising FMP as the coupling agent as model compounds in order to optimise the method before applying it to the analysis of oxidised fatty acids. FMP was chosen because it had been demonstrated in a prior study to be the most efficient coupling agent for this reaction [149, 151]. The reaction of the fatty acids is illustrated in the figure below (Figure 4-2)

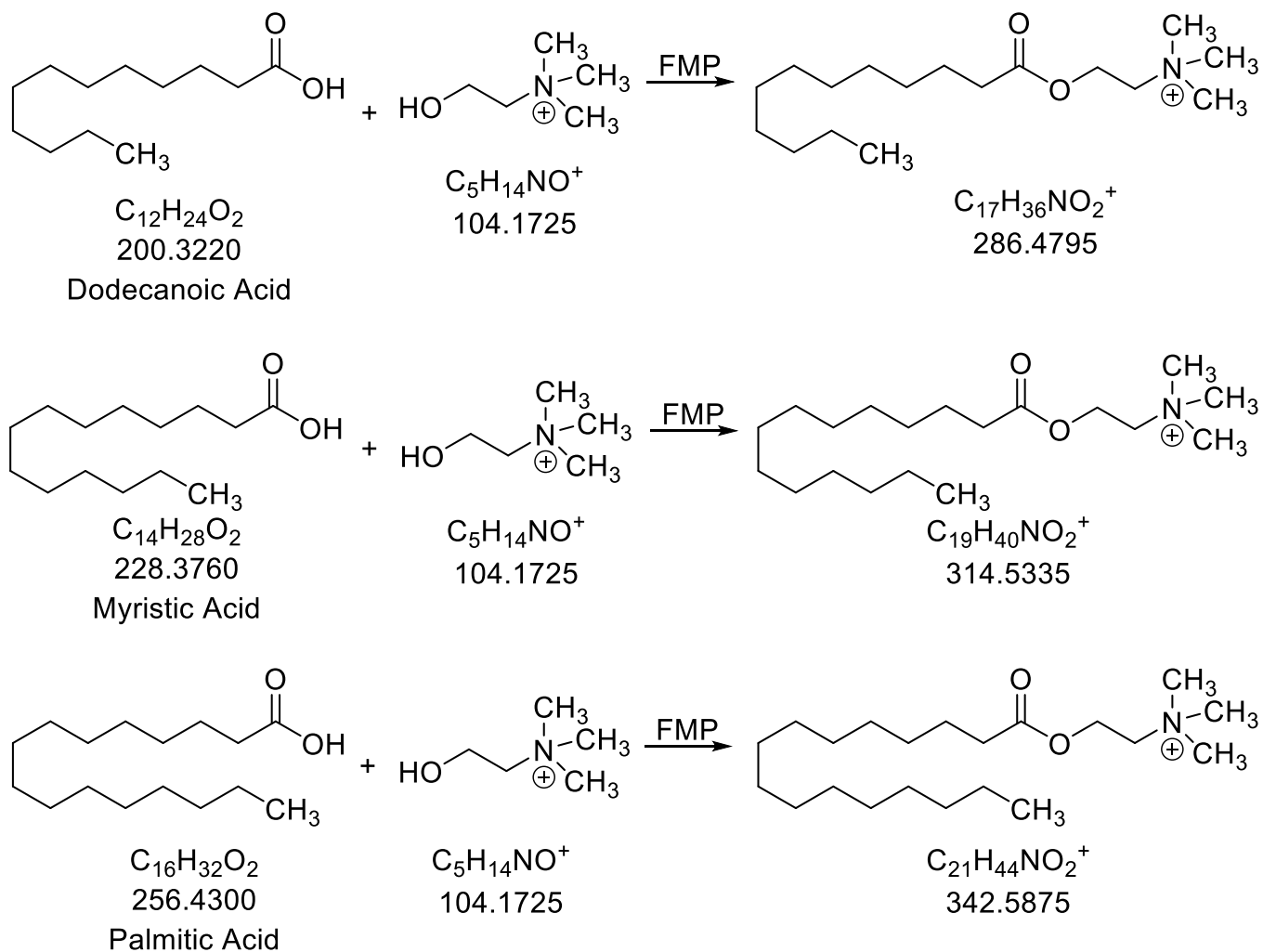


Figure 4-2 Depiction of coupling reaction with the fatty acids Dodecanoic acid, Myristic acid and Palmitic acid utilizing FMP as coupling agents with the accurate masses of the derivatized products.

The raw and extracted ion chromatographs as well as the mass spectrographs for each derivatized fatty acid is shown in the figures below (Figures 4-3 to 4-6).

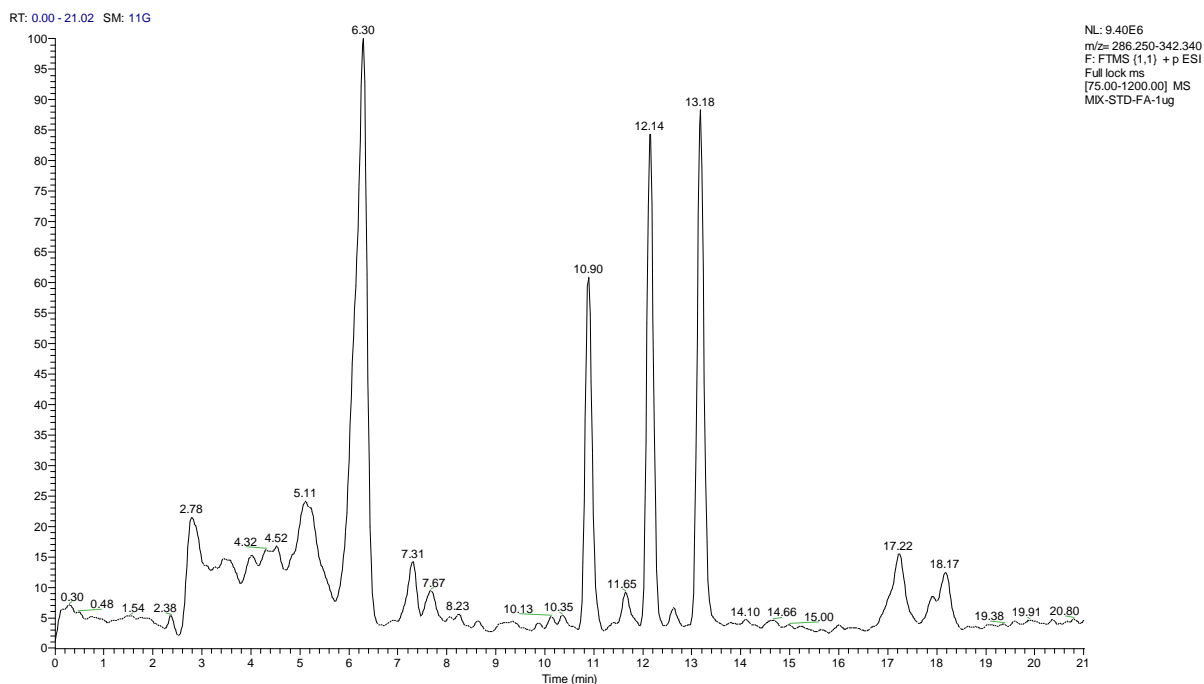


Figure 4-3 Total ion chromatogram of MIX-STD (1µg).

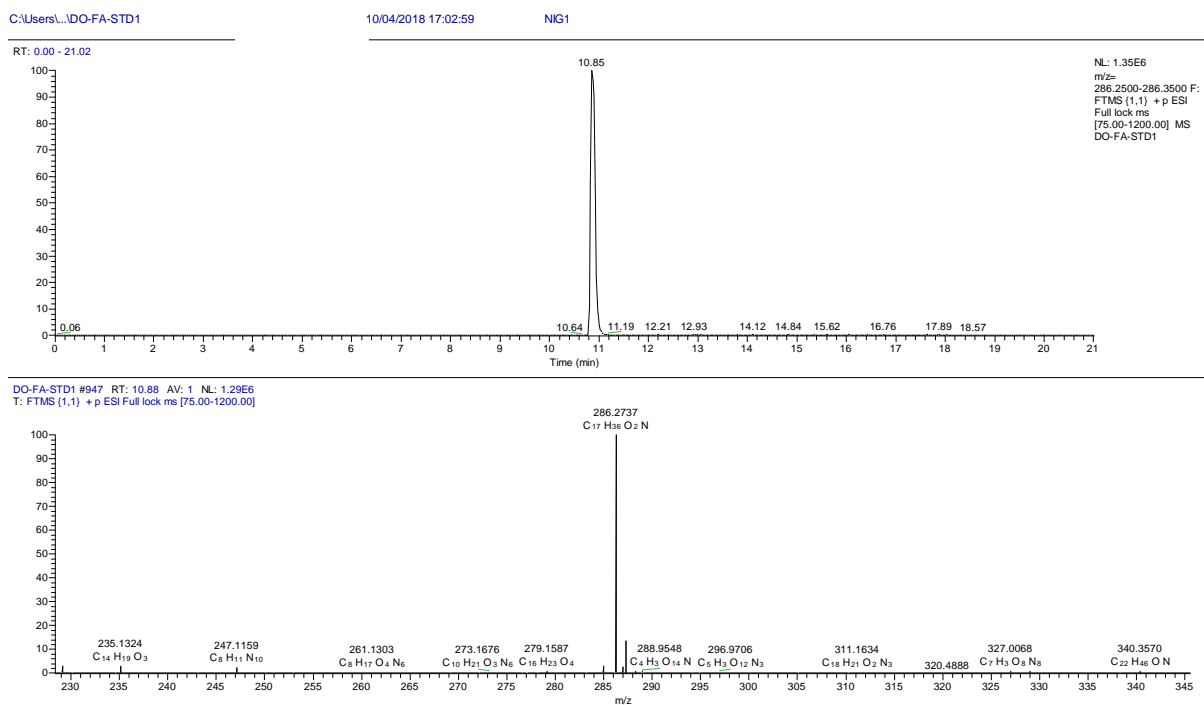


Figure 4-4 Extracted ion chromatogram and mass spectrum for dodecanoic acid (1µg).

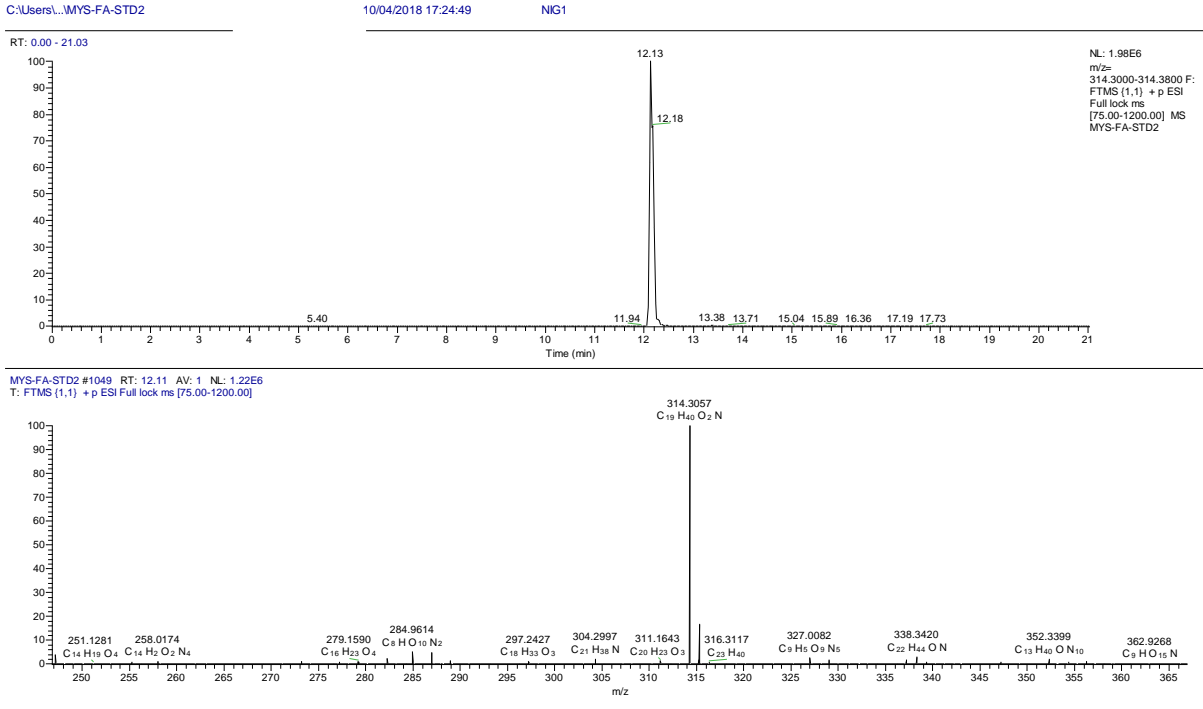


Figure 4-5 Extracted ion chromatogram and mass spectrum for myristic acid (1 μ g).

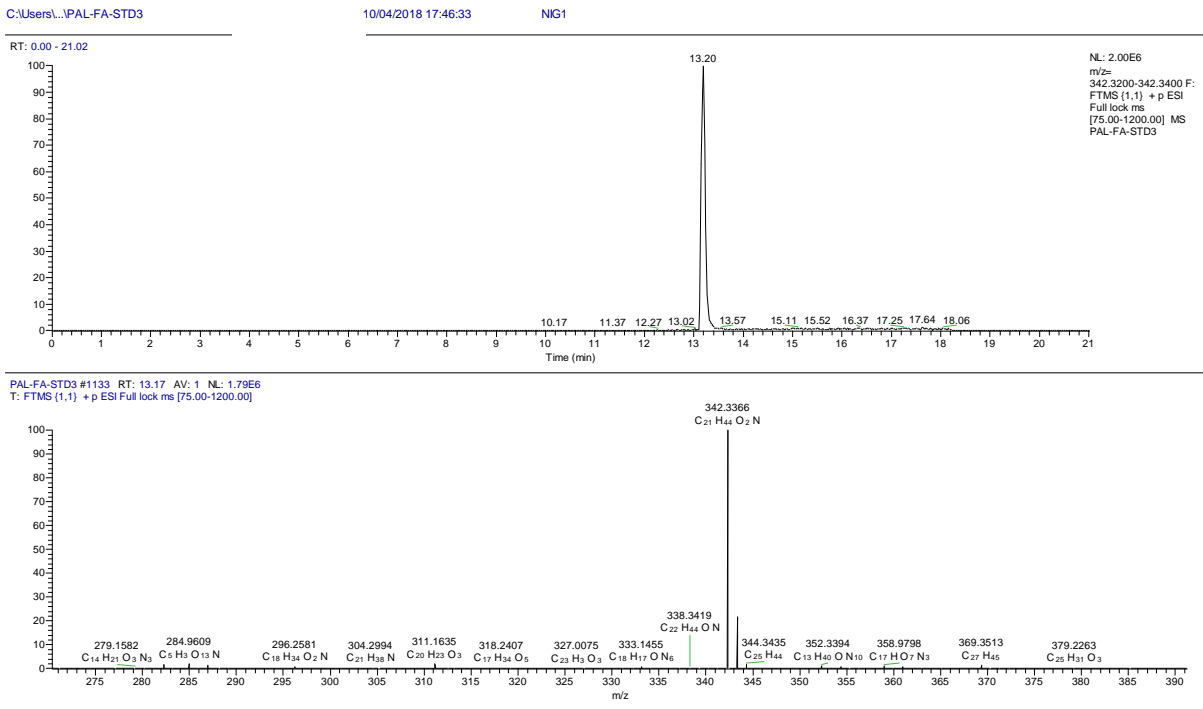


Figure 4-6 Extracted ion chromatogram and mass spectrum for palmitic acid (1 μ g).

To explore the limit of detection of the LCMS setup in a bid to determine if it would be sensitive enough to detect the minute quantities of metabolites in the samples a series of samples of increasingly lower amounts, (1.0 μ g, 0.1 μ g, 0.01 μ g, 0.001 μ g), of the mix of standard fatty acids were run. The spectra from the lowest quantity run, (0.001 μ g which is a sample concentration of 1ng/ml after preparation, as well as the extracted ion chromatographs for this run are shown in figures 4-7 & 4-8.

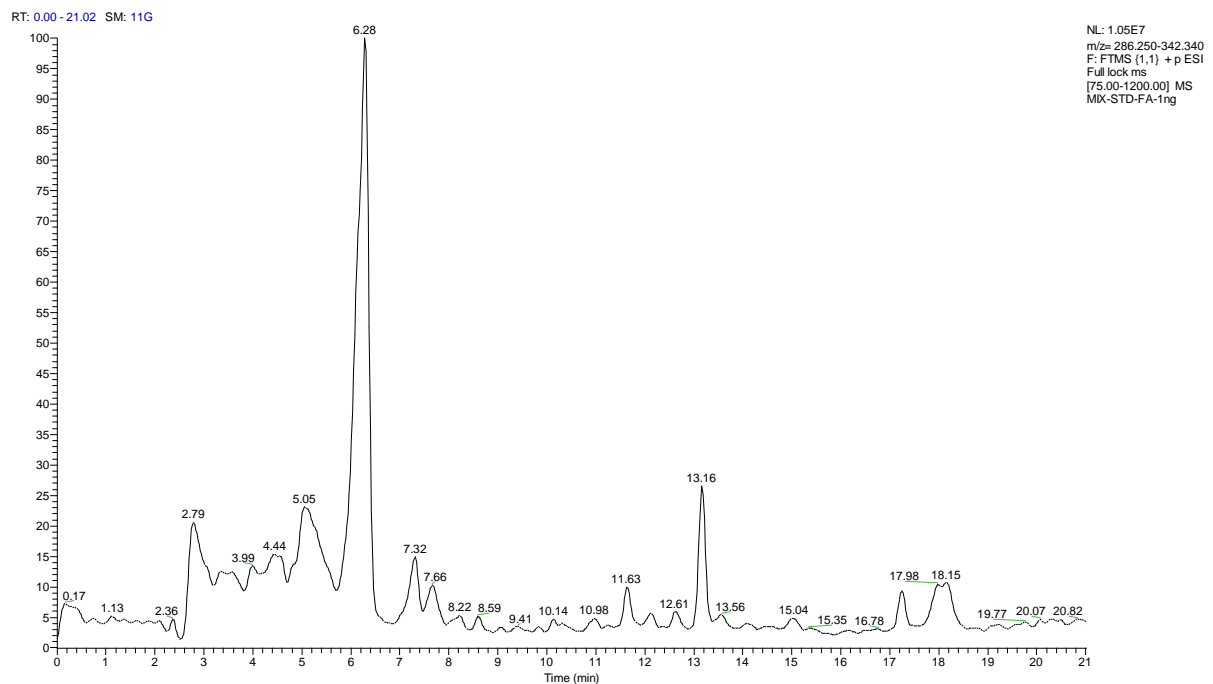


Figure 4-7 Total ion chromatogram for standard MIX-STD (1ng).

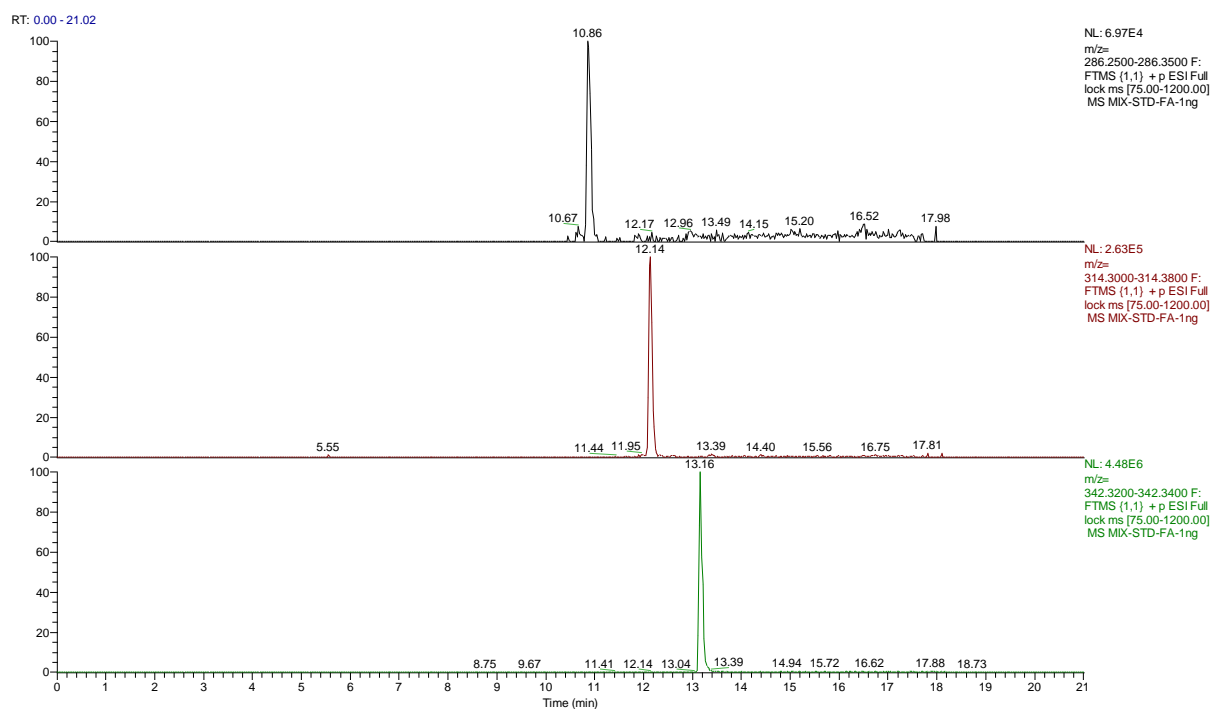


Figure 4-8 Extracted ion chromatograms for standard MIX-STD (1ng/ml).

These results clearly demonstrate that the LCMS system used in this study is capable of detecting extremely low concentrations of compounds similar to those which are of interest in this study.

The mixture containing all the six oxidised fatty acids of interest from the standard mix 1 (the Linoleic Acid derived oxylipins mixture (LAO), ((±)12(13)-DiHOME, (±)9(10)-DiHOME, 9(s)-HODE, 13(s)-HODE, 13-OxoODE, 9-OxoODE, (±)12(13)-EpOME, and (±)9(10)-EpOME))) as well as the mixture containing the nine oxidized fatty acids in mix 3 (the Arachidonic Acid derived oxylipins mixture(ArAO), (5-OxoETE, 12-OxoETE, 15-OxoETE, 15(S)-HETE, 12(S)-HETE, 11(S)-HETE, 9(R)-HETE, 8(S)-HETE, and 5(S)-HETE)) were derivatised similarly as for the fatty acids above (Section 3.2.6).

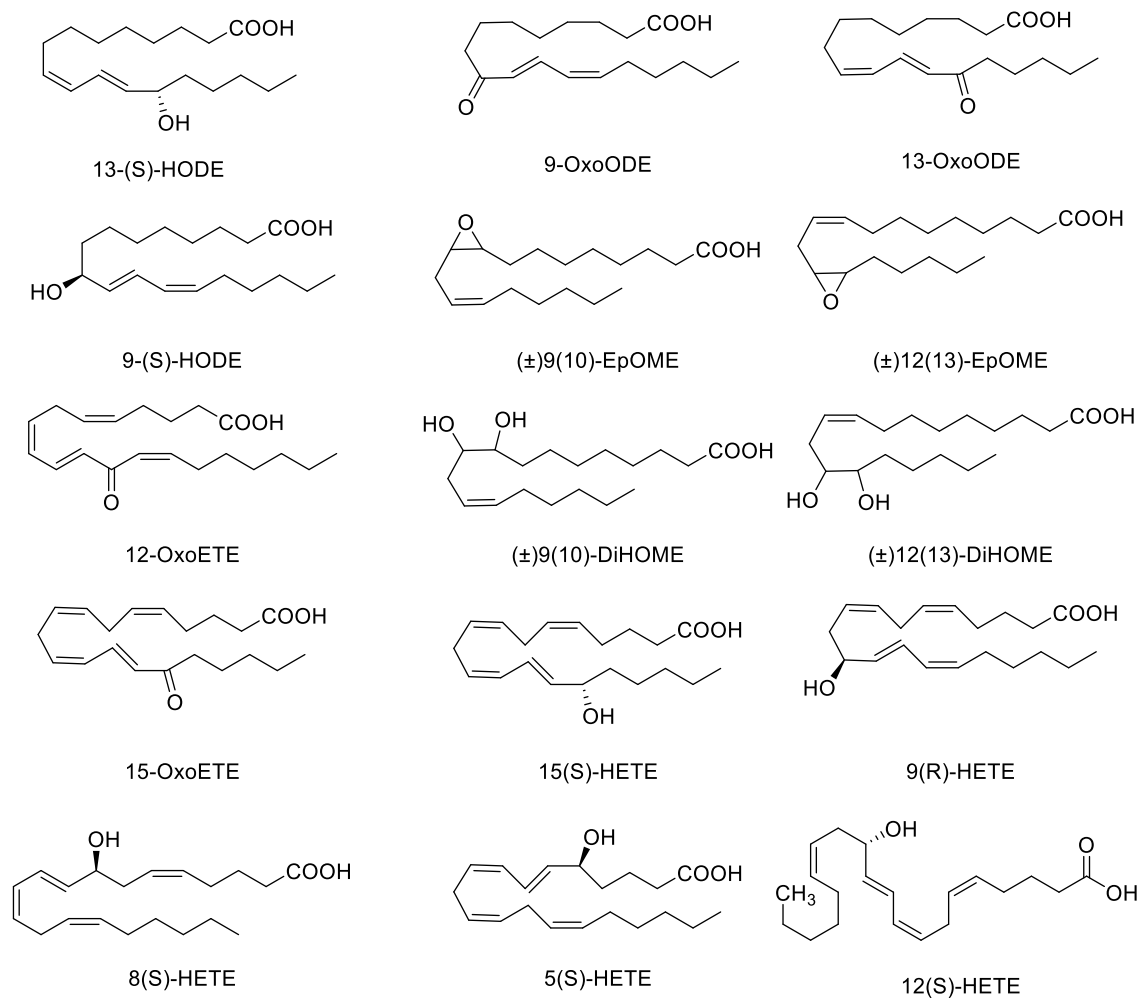


Figure 4-9 Standard mixture of oxidized fatty acid derivatives from Linoleic Acid and Arachidonic Acid.

However, prior to the derivatisation, 50ng/100µl of HODE-d₄ was added as internal standard to each concentration to help with quantification. The resulting mixtures were then analyzed by LCMS. Representative extracted ion chromatograms for the mixture as well extracted ion chromatograms for the oxylipin isomers are shown in Figures 4-10 & 4-11.

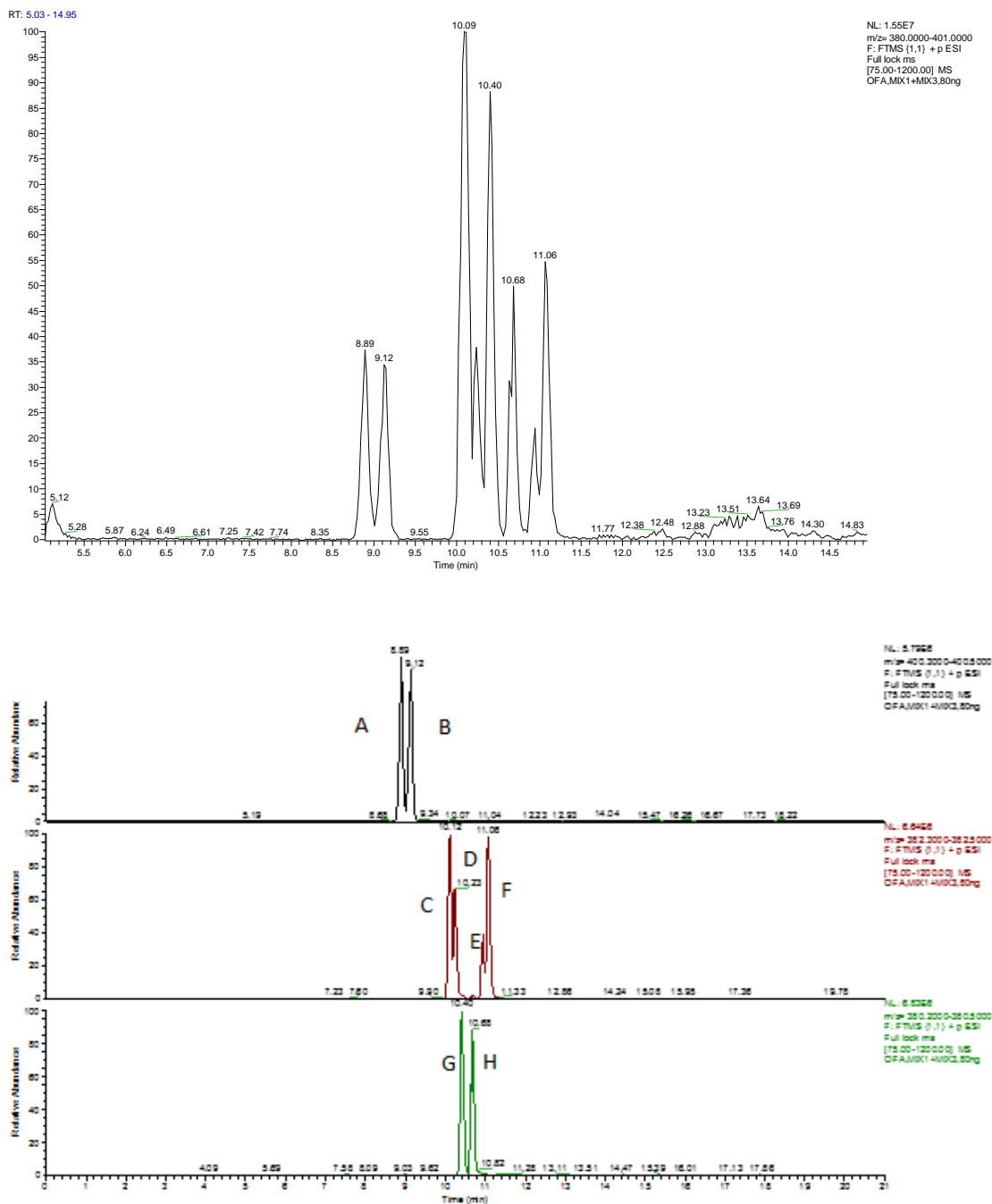


Figure 4-10 MIX-1 (Linoleic Acid Oxylipin's A = (\pm)12(13)-DiHOME ; B = (\pm)9(10)-DiHOME ; C = 13(S)-HODE ; D = 9(S)-HODE ; E = (\pm)12(13)-EpOME ; F = (\pm)9(10)-EpOME ; G = 13 OxoODE ; H = 9 OxoODE).

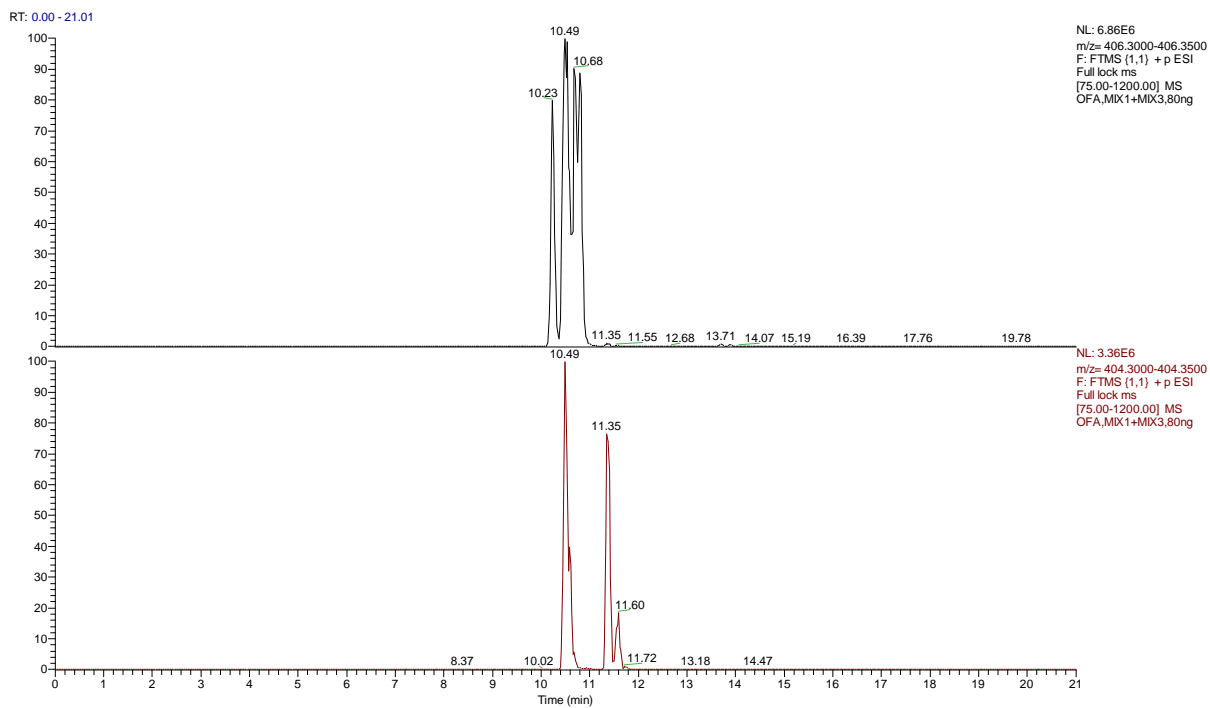
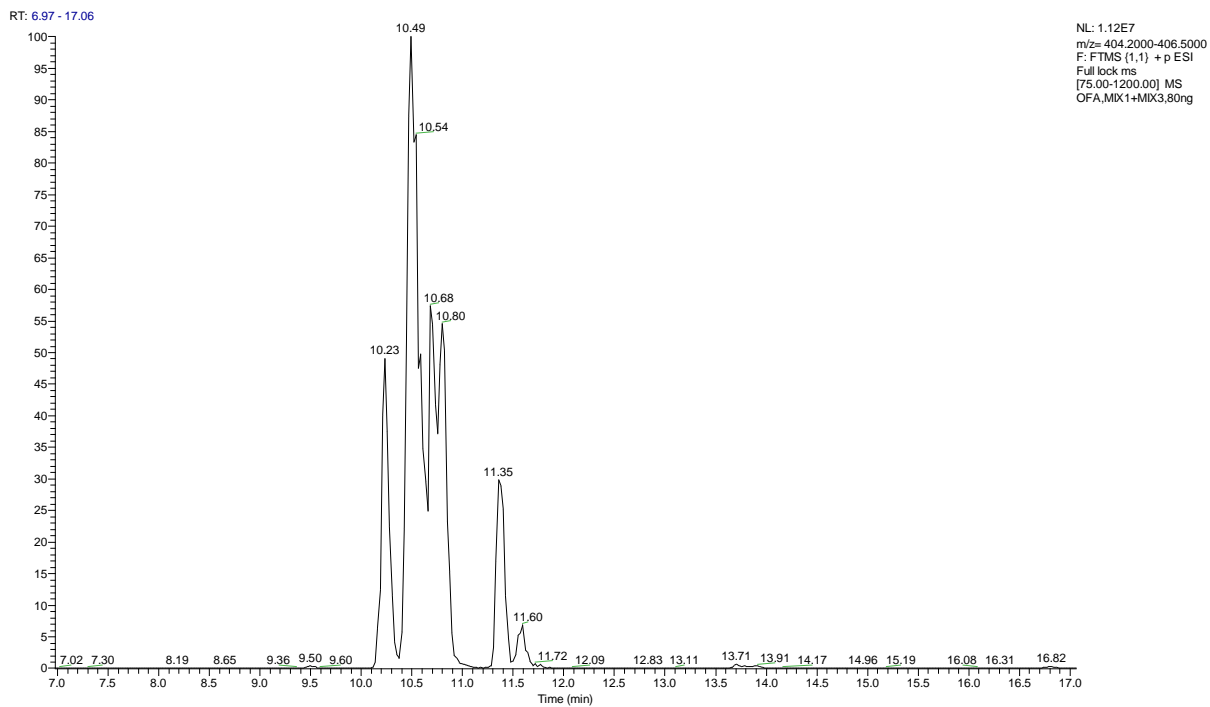


Figure 4-11 MIX-3 arachidonic acid oxylipins.

4.3.3 Data extraction and analysis

The peak area ratios were calculated for each of the six oxidized fatty acids [9(S)-HODE, 13(S)-HODE, (\pm)12(13)-EpOME, (\pm)9(10)-EpOME, 13-OxoODE, and 9-OxoODE] by dividing their peak areas with the peak areas of the internal standards which were added to each sample. For each of the fatty acids, the peak area ratios which were obtained, were analysed statistically (using between the four time points (baseline, pre 80 km, 40 km and post 80 km)). Statistical analysis was performed using IBM® SPSS® Statistics version 20.

4.3.4 Calibration curves of standard oxidised fatty acids

Calibration curves were prepared for mix 1 and the peak area ratios were computed for each of the six standard oxidized fatty acids [9(S)-HODE, 13(S)-HODE, (\pm)12(13)-EpOME, (\pm)9(10)-EpOME, 13-OxoODE, and 9-OxoODE] by dividing their peak areas with that of the internal standard added to the sample.

Table 4-4 Peak area ratios calculated for the six OFAs against 50 ng of HODE ²H₄.

Peak Area Ratios						
Conc	9(S)-	13(S)-HODE	(\pm)12(13)-	(\pm)9(10)-	13-OxoODE	9-OxoODE
0	0	0	0	0	0	0
0.005	0.19	0.083	0.037	0.150	0.034	0.021
0.010	0.41	0.121	0.068	0.310	0.073	0.026
0.020	1.02	0.395	0.221	0.776	0.125	0.089
0.040	2.92	1.065	0.512	2.140	0.208	0.153
0.080	4.77	1.863	0.986	3.797	0.416	0.298

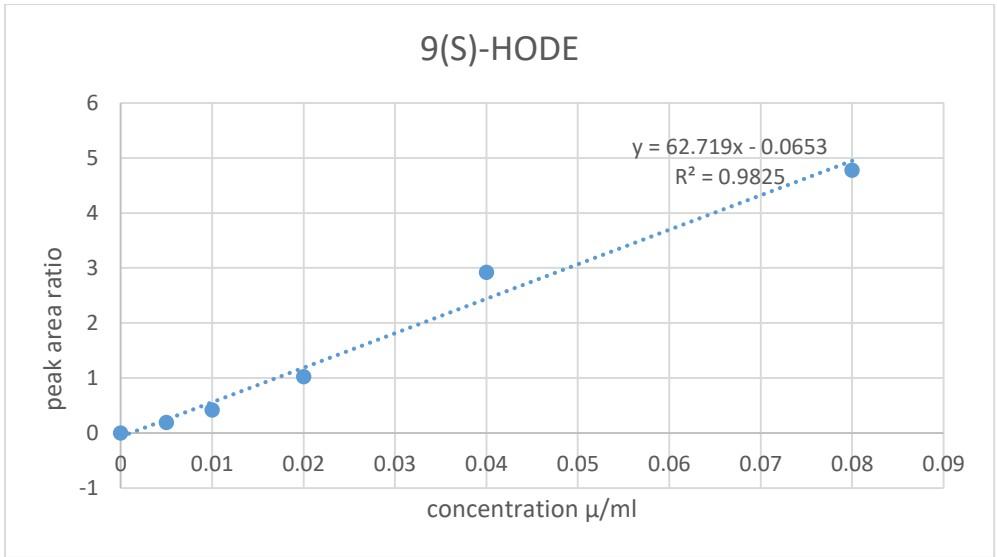


Figure 4-12 Calibration curve for 9(S)-HODE.

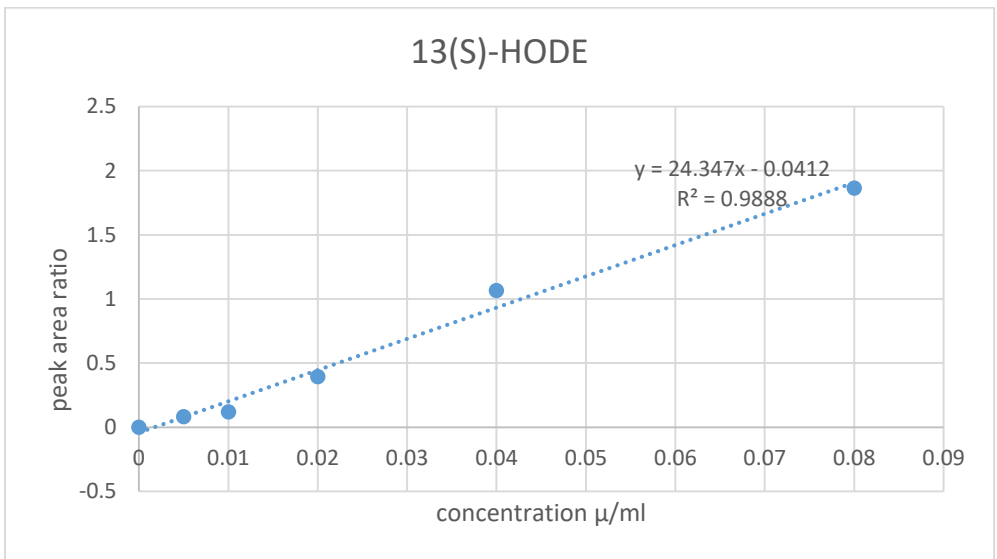


Figure 4-13 Calibration curve for 13(S)-HODE.

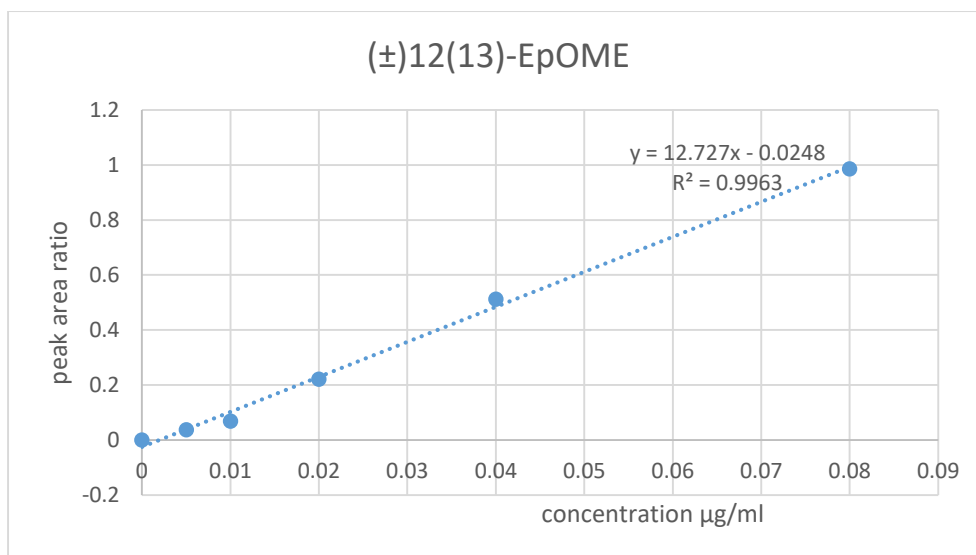


Figure 4-14 Calibration curve for (±)12(13)-EpOME.

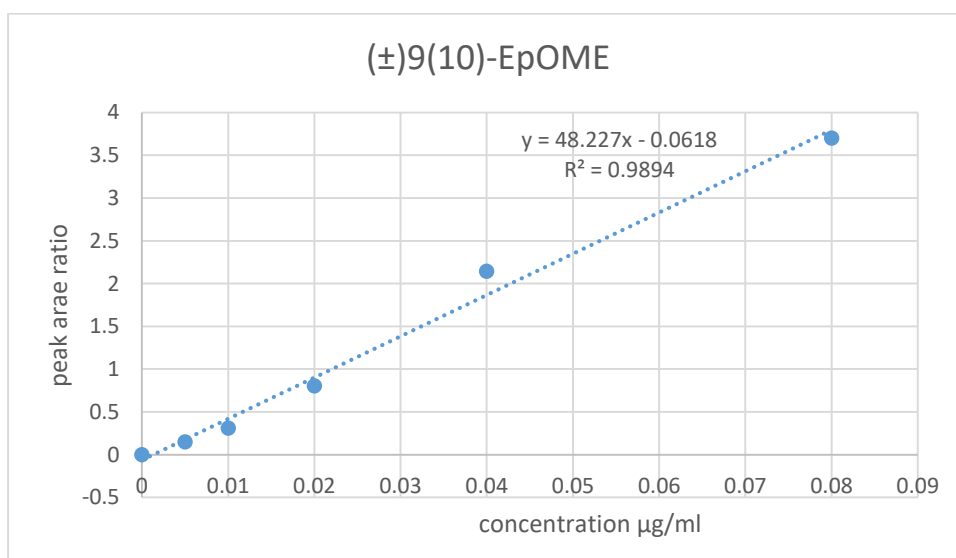


Figure 4-15 Calibration curve for (±)9(10)-EpOME.

Figures 4.12-4.17 show the calibration curves obtained. The linearity (based on R^2) for the first 4 standard OFA samples was very good. The poorest linearity was obtained with 9(S)-HODE ($R^2 = 0.9825$). There were no traces of the derivatized Oxylipin's present in the blanks offering good potential for the determination of low levels of these compounds.

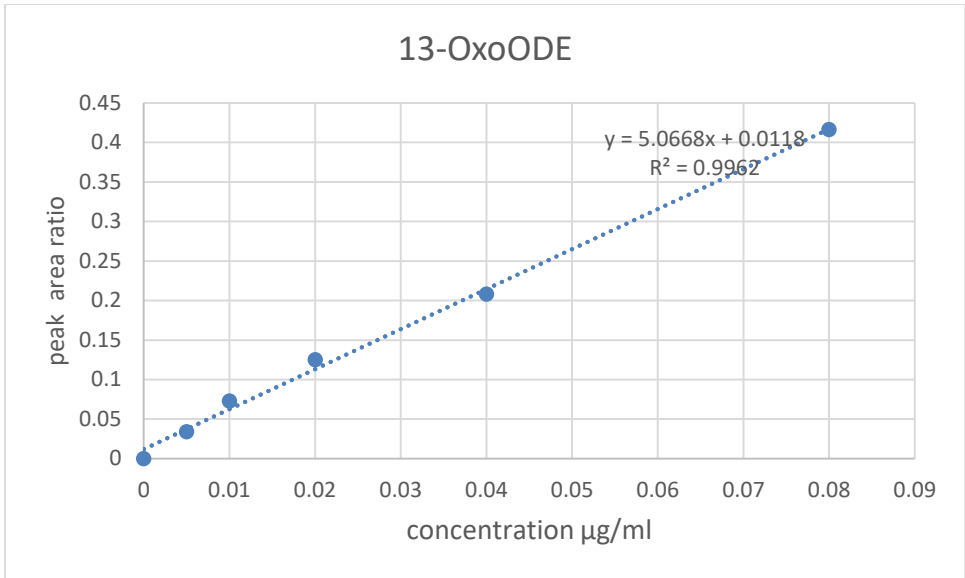


Figure 4-16 Calibration curve for 13-OxoODE.

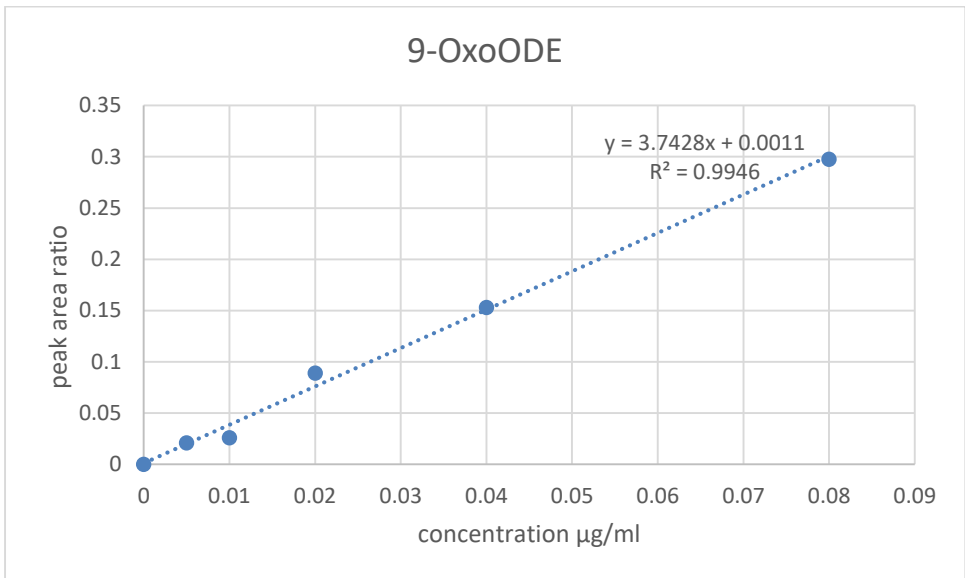


Figure 4-17 Calibration curve for 9-OxoODE.

The linearity of the regression line of peak area ratio versus concentration for all the fatty acids is generally very good ($R^2 > 0.98$).

4.4 Discussion

4.4.1 Comparison of OFAs in Plasma Samples

Statistical analysis of the plasma samples taken at the 3 data points during the marathon, (pre 80 km, 40 km and post 80 km), as well as the resting baseline samples was carried out to compare the levels of OFAs found in plasma samples at each of these time points. The peak area ratios for each of the six oxidized fatty acids, which were focused on in this study, were calculated for each sample by dividing their peak areas with the peak areas of the internal standard which was added to each of the samples. The six oxidized fatty acids which were the focused of this analysis are: 9(S)-HODE 13(S)-HODE, (\pm)12(13)-EpOME, (\pm)9(10)-EpOME, 13-OxoODE, and 9-OxoDE.

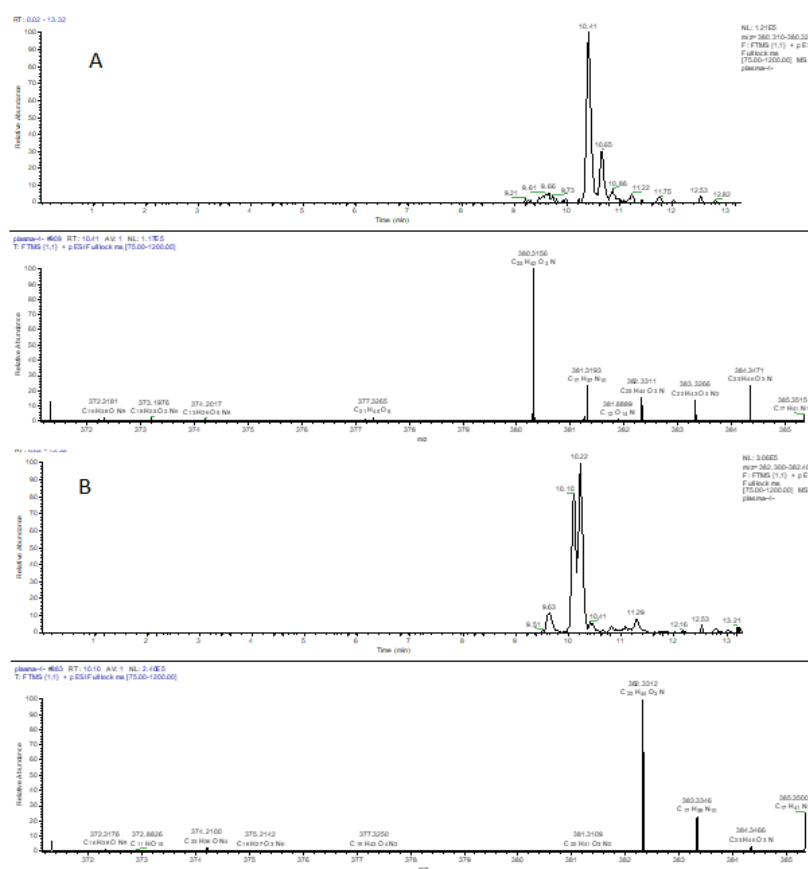


Figure 4-18 Representative Chromatograph for LAO derivatives extracted from plasma showing: A:-13-OxoODE, and 9-OxoDE; B:-9(S)-HODE 13(S)-HODE, (\pm)12(13)-EpOME, (\pm)9(10)-EpOME.

The mean concentrations which were obtained for each of the oxylipin metabolites, were compared statistically for the four time points at which plasma samples were obtained for each participant (baseline, pre 80 km, 40 km and post 80 km). The statistical analysis was performed using IBM® SPSS® Statistics version 20 and is presented below in the following tables and figures.

Data for the analysis of 9(S)-HODE

Table 4-5 Mean concentrations (µg/mL) obtained for 9(S)-HODE.

Descriptives						
	N	Mean (µg/mL)	Std. Deviation	Std. Error	Minimum	Maximum
Baseline	10	.2433	.07545	.02386	.14	.33
Pre 80 km	12	.2122	.07447	.02150	.10	.39
40 km	11	.2005	.07967	.02402	.08	.38
Post 80 km	12	.1660	.07054	.02036	.08	.29
Total	45	.2039	.07749	.01155	.08	.39

Table 4-6 ANOVA Test Data for the mean concentrations obtained for 9(S)-HODE.

	Sum of Squares	Mean Square	F	Sig.
Between Groups	.034	.011	2.001	.129
Within Groups	.230	.006		
Total	.264			

Table 4-7 Tukey HSD Dependent Variable Data: Mean concentrations obtained for 9(S)-HODE.

Multiple Comparisons

(I) Time Points	(J) Time Points	Mean Difference (I-J)	Std. Error	Sig.
Baseline	Pre 80 km	.03111	.03210	.768
	40 km	.04279	.03276	.564
	Post 80 km	.07734	.03210	.091
Pre 80 km	Baseline	-.03111	.03210	.768
	40 km	.01167	.03129	.982
	Post 80 km	.04622	.03061	.441
40 km	Baseline	-.04279	.03276	.564
	Pre 80 km	-.01167	.03129	.982
	Post 80 km	.03455	.03129	.689
Post 80 km	Baseline	-.07734	.03210	.091
	Pre 80 km	-.04622	.03061	.441
	40 km	-.03455	.03129	.689

The results of the ANOVA test indicate that there is no statistically significant difference in the levels of 9(S)-HODE found for each of the three time points at which plasma samples were obtained during the simulated ultra-marathon run as well as the baseline plasma sample ($p = 0.129$). Tukey multiple comparisons reproduced above (Table 4.7) agree with the results from the ANOVA tests in which none of the pairwise comparisons give a statistically significant difference.

However, a plot of the mean concentrations for each of the three time points at which plasma samples were obtained during the simulated ultra-marathon run as well as the baseline

plasma sample appears to show that the concentration decreased smoothly as the exercise progressed from baseline samples to post 80 km samples (Figure 4.19). This would imply that the ultra-marathon exercise had a negative impact on the levels of this oxidized fatty acid even if the change is too small to be of statistical significance.

Means Plots

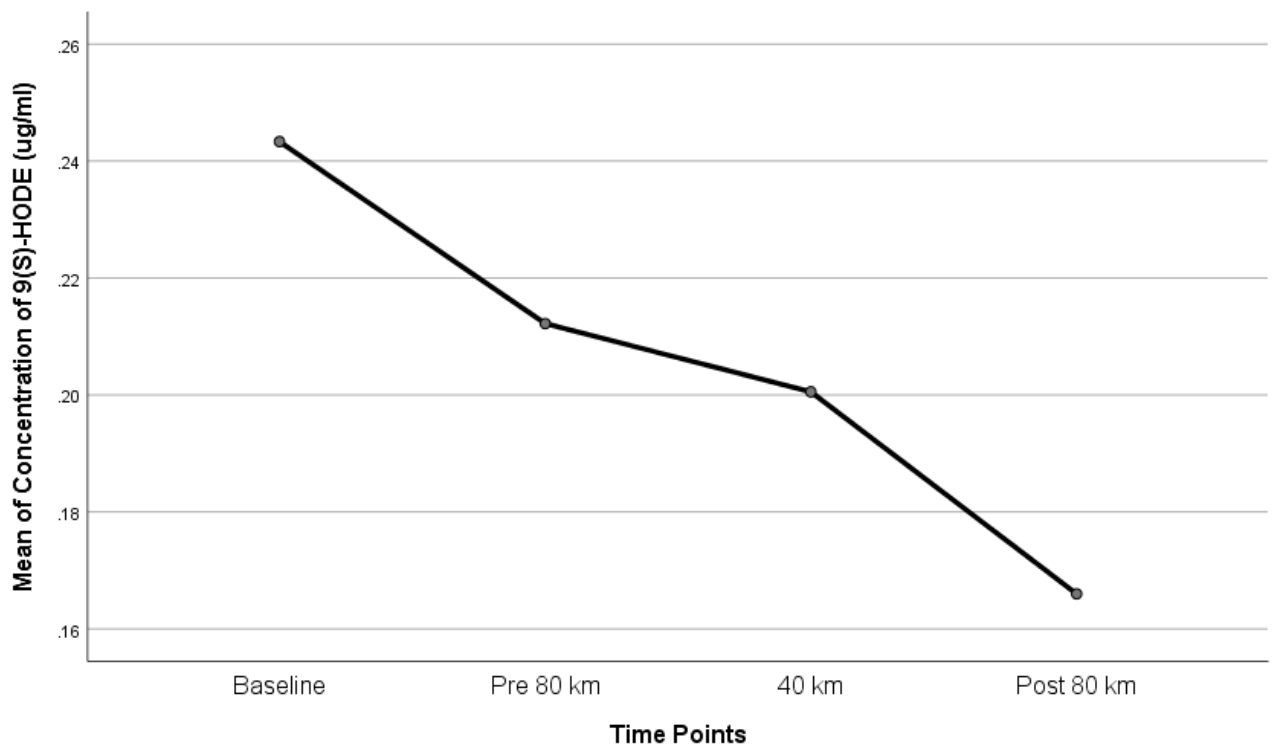


Figure 4-19 Plot of Mean concentrations against the three sample time points plus baseline for 9(S)-HODE.

This result however differs from existing reports which found up to 5 fold increases in the levels of 9 (S)-HODE following exercise [156].

Data for the analysis of 13(S)-HODE

Table 4-8 Mean concentrations (µg/mL) obtained for 13(S)-HODE.

Descriptives						
	N	Mean (µg/mL)	Std. Deviation	Std. Error	Minimum	Maximum
Baseline	10	.5362	.14053	.04444	.31	.74
Pre 80 km	12	.5009	.16820	.04856	.24	.79
40 km	11	.4256	.21129	.06371	.18	.89
Post 80 km	12	.3897	.23708	.06844	.16	1.00
Total	45	.4607	.19680	.02934	.16	1.00

Table 4-9 ANOVA Test Data for the mean concentrations obtained for 13(S)-HODE.

	Sum of Squares	Mean Square	F	Sig.
Between Groups	.150	.050	1.323	.280
Within Groups	1.554	.038		
Total	1.704			

The results of the ANOVA test show that there is no statistically significant difference in the levels of 13(S)-HODE found for each of the three time points at which plasma samples were obtained during the simulated ultra-marathon run as well as the baseline plasma sample ($p = 0.280$). Tukey multiple comparisons reproduced below (Table 4.10) is in agreement with the results from the ANOVA tests in which none of the pairwise comparisons gives a statistically significant difference.

Table 4-10 Tukey HSD Dependent Variable: Mean concentrations obtained for 13(S)-HODE

		Multiple Comparisons		
(I) Time Points	(J) Time Points	Mean Differ- ence (I-J)	Std. Error	Sig.
Baseline	Pre 80 km	.03530	.08335	.974
	40 km	.11056	.08505	.568
	Post 80 km	.14651	.08335	.308
Pre 80 km	Baseline	-.03530	.08335	.974
	40 km	.07526	.08126	.791
	Post 80 km	.11120	.07947	.507
40 km	Baseline	-.11056	.08505	.568
	Pre 80 km	-.07526	.08126	.791
	Post 80 km	.03594	.08126	.971
Post 80 km	Baseline	-.14651	.08335	.308
	Pre 80 km	-.11120	.07947	.507
	40 km	-.03594	.08126	.971

However, a plot of the mean concentrations for the for each of the three time points at which plasma samples were obtained during the simulated ultra-marathon run as well as the base-line plasma sample appears to show that the concentration decreased almost linearly as the exercise progressed from baseline samples to post 80 km samples (Figure 4.20). This would imply that the ultra-marathon exercise had a clear negative impact on the levels of this oxidized fatty acid even if the change is too small to be of statistical significance. This also differs from existing reports which found up to 5 fold increases in the levels of 9 (S)-HODE and 13 (S)-HODE following exercise [156].

Means Plots

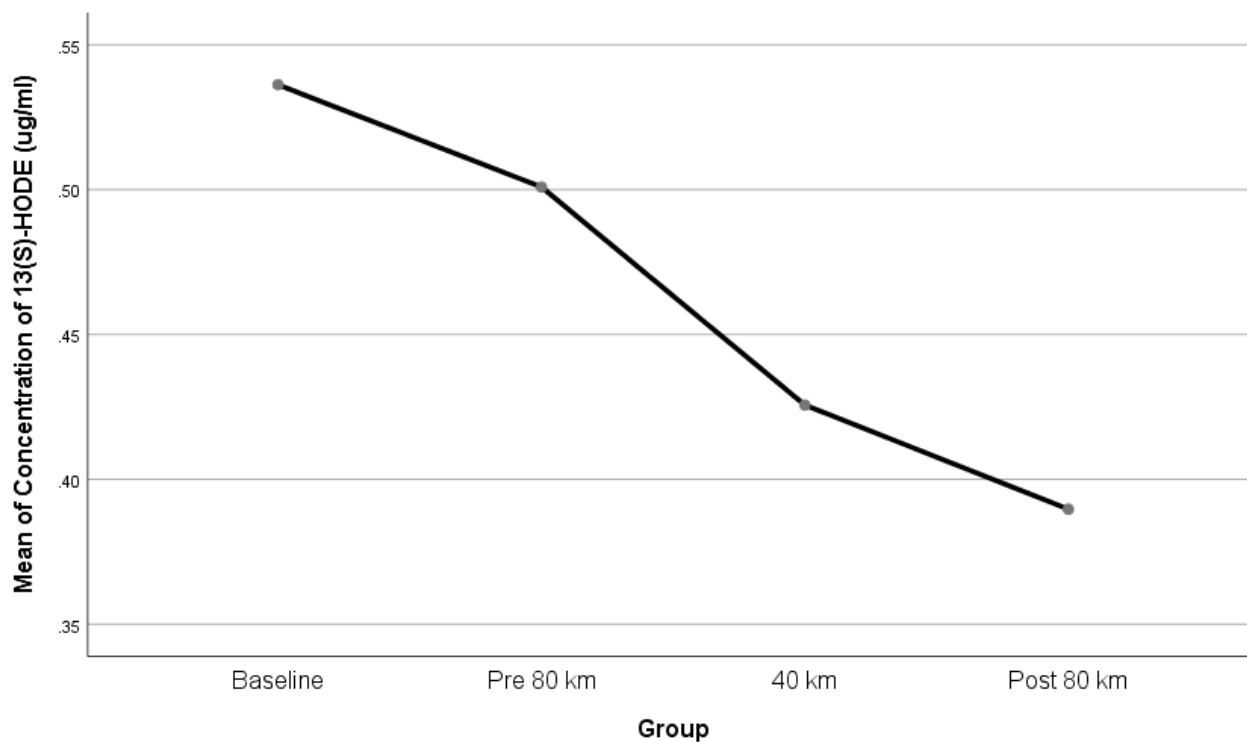


Figure 4-20 Plot of Mean concentrations against the three sample time points plus baseline for 13(S)-HODE.

Data for the analysis of (±)12(13)-EpOME

Table 4-11 Mean concentrations (µg/mL) obtained for (±)12(13)-EpOME.

	Descriptives					
	N	Mean (µg/mL)	Std. Deviation	Std. Error	Minimum	Maximum
Baseline	10	.0514	.01483	.00469	.04	.08
Pre 80 km	12	.0741	.02774	.00801	.04	.14
40 km	11	.0671	.02157	.00650	.04	.11
Post 80 km	12	.0549	.01231	.00355	.04	.08
Total	45	.0622	.02160	.00322	.04	.14

Table 4-12 ANOVA test results for the Mean concentrations obtained for (±)12(13)-EpOME.

	Sum of Squares	Mean Square	F	Sig.
Between Groups	.004	.001	3.070	.038
Within Groups	.017	.000		
Total	.021			

In this instance the ANOVA test shows a statistically significant difference in the levels of (±)12(13)-EpOME found between each of the three time points at which plasma samples were obtained during the simulated ultra-marathon run as well as the baseline plasma sample ($p = 0.038$). This is probably due to the large difference between the baseline and pre 80 km samples where the difference is greatest. The Tukey multiple comparisons unlike the ANOVA result indicates that none of the pairwise comparisons gave a statistically significant difference.

Multiple Comparisons

Table 4-13 Tukey HSD Dependent Variable: Mean concentrations obtained for (±)12(13)-EpOME

(I) Time Points	(J) Time Points	Mean Difference (I-J)	Std. Error	Sig.
Baseline	Pre 80 km	-.02272	.00866	.057
	40 km	-.01570	.00883	.299
	Post 80 km	-.00356	.00866	.976
Pre 80 km	Baseline	.02272	.00866	.057
	40 km	.00702	.00844	.839
	Post 80 km	.01916	.00825	.110
40 km	Baseline	.01570	.00883	.299
	Pre 80 km	-.00702	.00844	.839
	Post 80 km	.01214	.00844	.484
Post 80 km	Baseline	.00356	.00866	.976
	Pre 80 km	-.01916	.00825	.110
	40 km	-.01214	.00844	.484

A plot of the mean concentrations for the for each of the three time points at which plasma samples were obtained during the simulated ultra-marathon run as well as the baseline plasma sample appears to show that the concentration decreased almost linearly as the exercise progressed from the pre sample 80 km to the post 80 km samples (Figure 4-21). However, the baseline sample showed a much lower concentration for (±)12(13)-EpOME which means there was a significant rise in its concentration between the baseline and the pre sample. The results here also tend to imply that the ultra-marathon exercise in itself had an overall

negative impact on the levels of this oxidized fatty acid, as its levels appear to fall over the duration of the exercise, even though the change is too small to be of statistical significance.

Means Plots

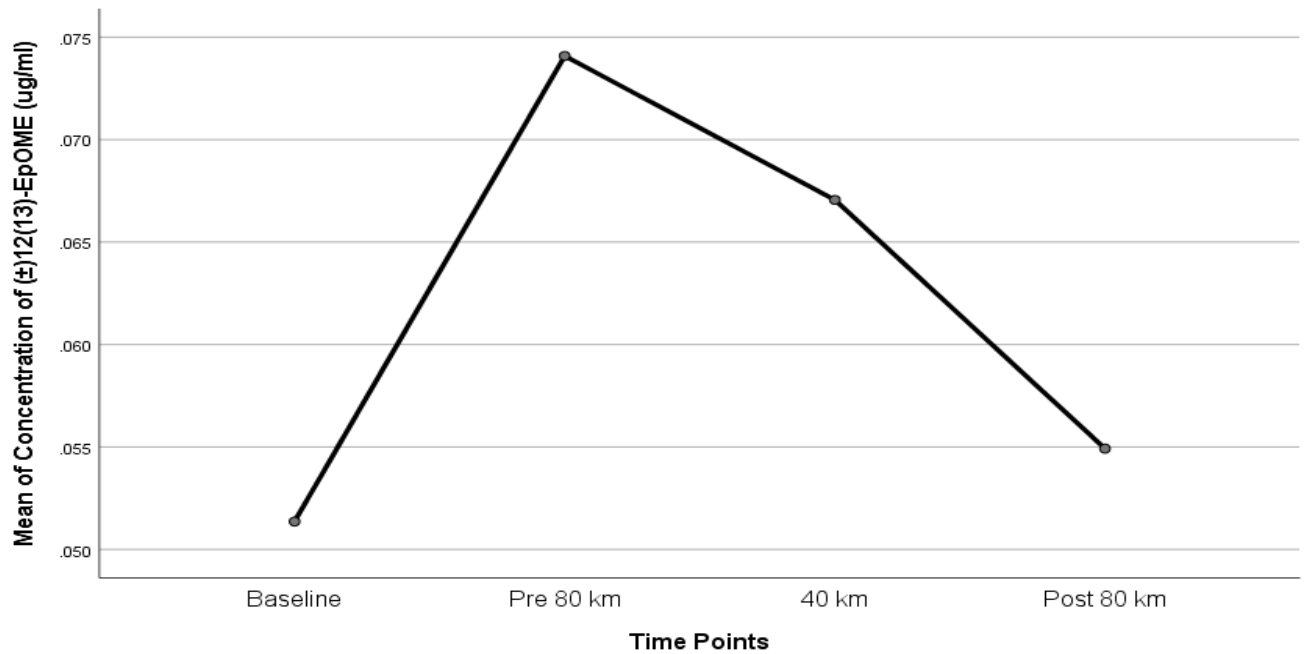


Figure 4-21 Plot of Mean concentrations against the three sample time points plus baseline for (±)12(13)-EpOME.

Data for the analysis of (±)9(10)-EpOM

Table 4-14 Mean concentrations (µg/mL) obtained for (±)9(10)-EpOME.

	Descriptives					
	N	Mean (µg/mL)	Std. Deviation	Std. Error	Minimum	Maximum
Baseline	10	.0385	.00537	.00170	.03	.05
Pre 80 km	12	.0420	.00683	.00197	.03	.05
40 km	11	.0450	.00655	.00197	.03	.05
Post 80 km	12	.0422	.00443	.00128	.04	.05
Total	45	.0420	.00610	.00091	.03	.05

Table 4-15 ANOVA test results for the mean concentrations obtained for (±)9(10)-EpOME.

	Sum of Squares	Mean Square	F	Sig.
Between Groups	.000	.000	2.123	.112
Within Groups	.001	.000		
Total	.002			

Multiple Comparisons

Table 4-16 Tukey HSD Dependent Variable: Mean concentrations obtained for (±)9(10)-EpOME.

(I) Time Points	(J) Time Points	Mean Difference (I-J)	Std. Error	Sig.
Baseline	Pre 80 km	-.00346	.00252	.522
	40 km	-.00647	.00257	.072
	Post 80 km	-.00366	.00252	.475
Pre 80 km	Baseline	.00346	.00252	.522
	40 km	-.00301	.00245	.613
	Post 80 km	-.00020	.00240	1.000
40 km	Baseline	.00647	.00257	.072
	Pre 80 km	.00301	.00245	.613
	Post 80 km	.00282	.00245	.663
Post 80 km	Baseline	.00366	.00252	.475
	Pre 80 km	.00020	.00240	1.000
	40 km	-.00282	.00245	.663

In this instance also the ANOVA test results show an absence of a statistically significant difference in the levels of (±)9(10)-EpOME found for each of the three time points at which

plasma samples were obtained during the simulated ultra-marathon run as well as the baseline plasma sample ($p = 0.112$). The Tukey multiple comparisons, (Table 4-16), also confirm the ANOVA result as none of the pairwise comparisons gave a statistically significant difference.

A plot of the mean concentrations for the for each of the three time points at which plasma samples were obtained during the simulated ultra-marathon run as well as the baseline plasma sample appears to show that the concentration increased almost linearly in this instance as the exercise progressed from the pre sample 80 km to the 40 km samples (Figure 4-22). However, the baseline sample showed a much lower concentration for (\pm)9(10)-EpOME which means there was also a rise in its levels between the baseline and the pre sample. The levels of (\pm)9(10)-EpOME then fell between the 40 km samples and the end of the run. In spite of this fall the overall trend from the plot tends to indicate that the ultra-marathon exercise had an overall positive impact on the levels of this oxidized fatty acid, as its levels appear to rise over the course of the exercise when compared with both the Pre samples and the baselines despite the dip after the 40 km samples. This change in concentration is however too small to be statistically significant.

Means Plots

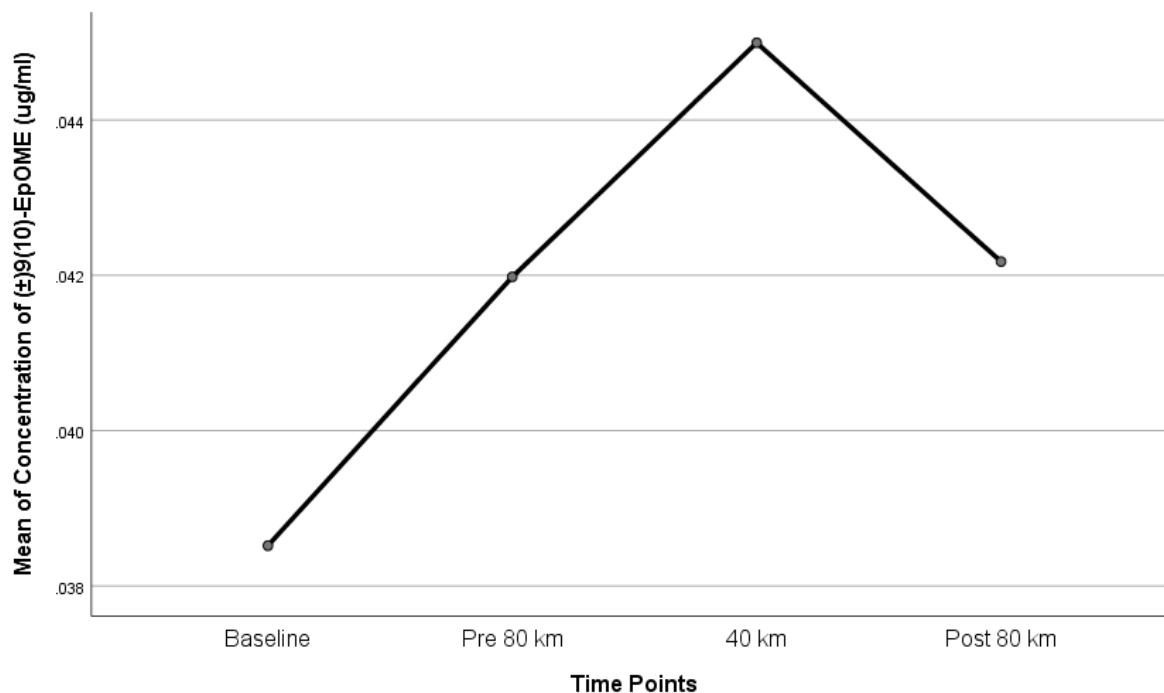


Figure 4-22 Plot of Mean concentrations against the three sample time points plus baseline for (±)9(10)-EpOME.

Data for the analysis of 13-OxoODE

Table 4-17 Mean concentrations (µg/mL) obtained for 13-OxoODE.

Descriptives						
	N	Mean (µg/mL)	Std. Deviation	Std. Error	Minimum	Maximum
Baseline	10	.3594	.21033	.06651	.08	.70
Pre 80 km	12	.2526	.12719	.03672	.07	.48
40 km	11	.2742	.26712	.08054	.03	.99
Post 80 km	12	.2626	.51569	.14887	-.01	1.88
Total	45	.2843	.31226	.04655	-.01	1.88

Table 4-18 ANOVA test results for the mean concentrations of 13-OxoODE.

	Sum of Squares	Mean Square	F	Sig.
Between Groups	.075	.025	.244	.865
Within Groups	4.215	.103		
Total	4.290			

The ANOVA test shows that there is no statistically significant difference in the levels of 13-OxoODE found for each of the three time points at which plasma samples were obtained during the simulated ultra-marathon run as well as the baseline plasma sample ($p = 0.865$). The Tukey multiple comparisons also confirm the ANOVA result as none of the pairwise comparisons gave a statistically significant difference.

Multiple Comparisons

Table 4-19 Tukey HSD Dependent Variable: Mean concentrations obtained for 13-OxoODE

(I) Time Points	(J) Time Points	Mean Difference (I-J)	Std. Error	Sig.
Baseline	Pre 80 km	.10686	.13729	.864
	40 km	.08518	.14009	.929
	Post 80 km	.09684	.13729	.894
Pre 80 km	Baseline	-.10686	.13729	.864
	40 km	-.02168	.13384	.998
	Post 80 km	-.01002	.13090	1.000
40 km	Baseline	-.08518	.14009	.929
	Pre 80 km	.02168	.13384	.998
	Post 80 km	.01166	.13384	1.000
Post 80 km	Baseline	-.09684	.13729	.894
	Pre 80 km	.01002	.13090	1.000
	40 km	-.01166	.13384	1.000

A plot of the mean concentrations for each of the three time points at which plasma samples were obtained during the simulated ultra-marathon run as well as the baseline plasma sample appears to show that the concentration increased from the pre sample 80 km to the 40 km samples (Figure 4-23). However, the baseline sample showed a much higher concentration for 13-OxoODE which meant there was a sharp fall in its levels between the baseline and the pre sample. The levels of 13-OxoODE initially rose from the start of the run then fell between the 40 km samples and the end of the run. In spite of this fall the overall trend from the plot tends to indicate that the ultra-marathon exercise had an overall positive impact on the levels

of this oxidized fatty acid, as its levels appear to rise over the course of the exercise when compared with the Pre samples despite the dip after the 40 km samples. This change is however too small to be statistically significant.

Means Plots

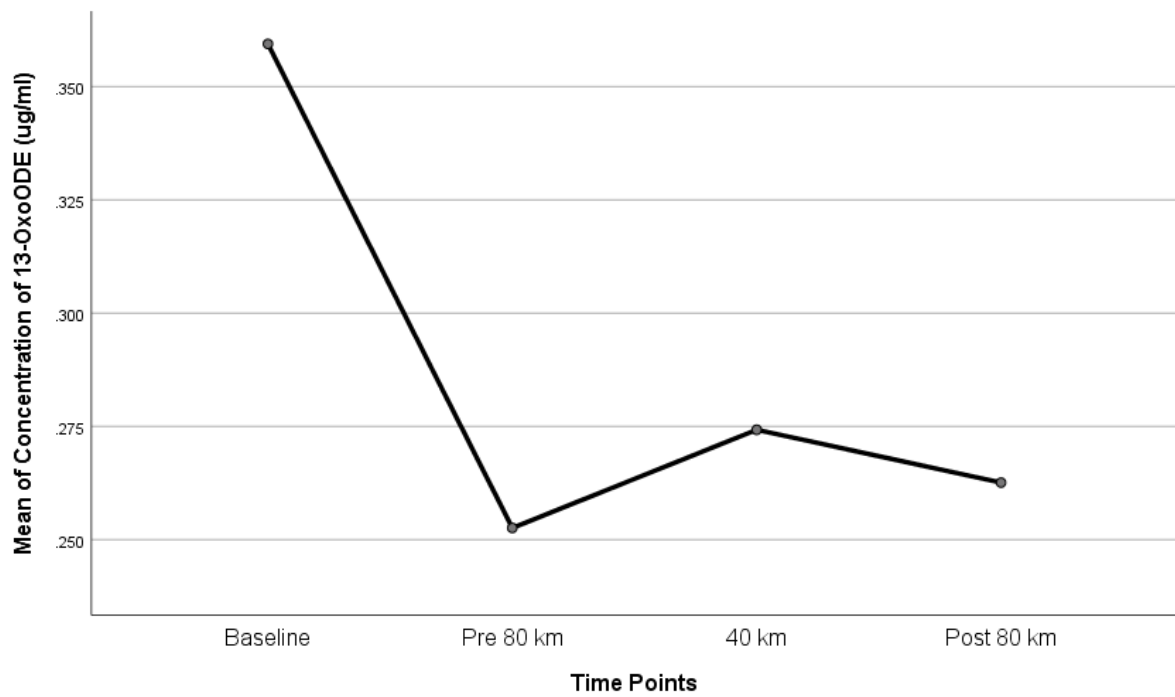


Figure 4-23 Plot of Mean Peak area ratios against the three sample time points plus baseline for 13-OxoODE.

Data for the analysis of 9-OxoODE

Table 4-20 Mean concentrations ($\mu\text{g/mL}$) obtained for 9-OxoDE

Descriptives						
	N	Mean ($\mu\text{g/mL}$)	Std. Deviation	Std. Error	Minimum	Maximum
Baseline	10	.1353	.08663	.02739	.03	.28
Pre 80 km	12	.1278	.10285	.02969	.05	.43
40 km	11	.1353	.08889	.02680	.04	.37
Post 80 km	12	.1146	.20197	.05830	.01	.75
Total	45	.1278	.12747	.01900	.01	.75

Table 4-21 ANOVA test results for the mean concentrations of 9-OxoDE.

	Sum of Squares	Mean Square	F	Sig.
Between Groups	.003	.001	.063	.979
Within Groups	.712	.017		
Total	.715			

The ANOVA test results show an absence of statistically significant differences in the levels of 9-OxoODE found for each of the three time points at which plasma samples were obtained during the simulated ultra-marathon run as well as the baseline plasma sample ($p = 0.946$). The Tukey multiple comparisons confirm the ANOVA result as none of the pairwise comparisons showed any difference which could be said to be statistically significant.

Multiple Comparisons

Table 4-22 Tukey HSD Dependent Variable: Mean concentrations obtained for 9-OxoDE.

(I) Time Points	(J) Time Points	Mean Difference (I-J)	Std. Error	Sig.
Baseline	Pre 80 km	.00752	.05641	.999
	40 km	-.00003	.05756	1.000
	Post 80 km	.02068	.05641	.983
Pre 80 km	Baseline	-.00752	.05641	.999
	40 km	-.00755	.05499	.999
	Post 80 km	.01316	.05378	.995
40 km	Baseline	.00003	.05756	1.000
	Pre 80 km	.00755	.05499	.999
	Post 80 km	.02071	.05499	.982
Post 80 km	Baseline	-.02068	.05641	.983
	Pre 80 km	-.01316	.05378	.995
	40 km	-.02071	.05499	.982

A plot of the mean concentrations for the for each of the three time points at which plasma samples were obtained during the simulated ultra-marathon run as well as the baseline plasma sample appears to show that the concentrations increased from the pre 80 km samples to the 40 km samples. The levels of 9-OxoODE then fell again between the 40 km samples and the end of the run returning to approximately the same levels as the pre 80 km samples implying no overall change was observed over the course of the marathon run. However, the baseline sample showed a much higher concentration for 9-OxoODE which led to a sharp fall

in its levels between the baseline and the pre sample (Figure 4-24). Taking the baseline into consideration, there was a fall in the levels of 9-OxoODE over the duration of the study with the biggest change occurring before the commencement of the run. The fluctuations in the levels 9-OxoODE during the course of the run however resulted in no change in its levels over the duration of the exercise run. These changes were however too small to be of any significance statistically.

Means Plots

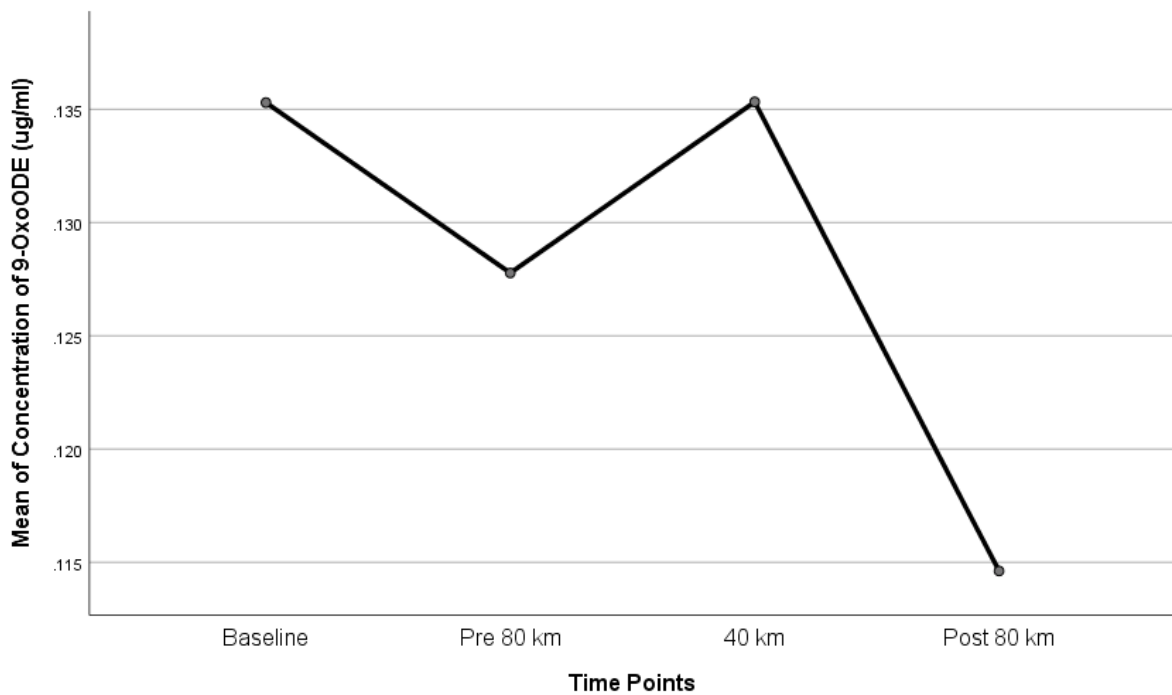


Figure 4-24 Plot of Mean concentrations against the three sample time points plus baseline for 9-OxoODE.

The summary of the statistical analysis showing the levels for the six oxidised fatty acids of interest in this study which were found in the various plasma samples is presented in the table below (Table 4-23).

Table 4-23 The levels of oxidized fatty acids (Means and SD's) in plasma of participant's pre, midway and immediately upon completion of an 80 km ultramarathon run.

Sample	Levels of oxidized fatty acids (Mean and SD) in µg/mL											
	9(S)-HODE		13(S)-HODE		(±)12(13)-EpOME		(±)9(10)-EpOME		13-OxoODE		9-OxoODE	
	Mean	SD	Mean	SD	Mean	SD	Mean	SD	Mean	SD	Mean	SD
Baseline	.2433	.07545	.5362	.14053	.0514	.01483	.0385	.00537	.3594	.21033	0.1353	.8663
Pre 80 km	.2122	.07447	.5009	.16820	.0741	.02774	.0420	.00683	.2526	.12719	.1278	.10285
40 km	.2005	.07967	.4256	.21129	.0671	.02157	.0450	.00655	.2742	.26712	.1353	.8889
Post 80 km	.1660	.07054	.3897	.23708	.0549	.01231	.0422	.00443	.2626	.51569	.1146	.20197

The results from the ANOVA test appear to indicate that there are no appreciable statistical differences in the levels for each of the six oxidised fatty acids, focused on in this study, during the course of the simulated ultra-marathon. The ANOVA results were also confirmed by Tukey multiple comparisons. These results indicate that none of the pairwise comparisons of the samples showed any significant difference statistically ($p > 0.05$). The results of the ANOVA tests are presented in the table below (Table 4-24).

Table 4-24 One-way ANOVA for the differences in levels of the six oxidized fatty acids between four times points (Baseline, Pre 80 km, 40 km, and Post 80 km).

Oxidized fatty acid	F	Sig.
9(S)-HODE	2.001	.129
13(S)-HODE	1.323	.280
(±)12(13)-EpOME	3.070	.038
(±)9(10)-EpOME	2.123	.112
13-OxoODE	.244	.865
9-OxoODE	.063	.979

The plots of the Mean concentrations against the three sample time points at which plasma samples were taken during the course of the run plus the baselines show that the levels for both 9(S)-HODE and 13(S)-HODE decreased gradually during the course of the run when a

comparison was made between the baseline samples and those taken during the run especially with the post 80 km samples. This appears to suggest a negative impact on the levels of these two oxidised fatty acids as a result of the marathon run. This trend was however not repeated for the rest of the OFAs as their levels tended to fluctuate over the course of the study period. This can be partly attributed to the differences between the pre 80km samples and the baseline samples which would have been expected to have a closer correlation as both are resting samples. These variations might however be due to other factors such as diet or warmup exercises performed in anticipation of the exercise run.

4.5 Conclusion

A Choline tagging strategy which used FMP as the coupling agent was successfully applied to the analysis of 46 plasma samples from a simulated ultra-marathon run in an attempt to investigate the effect of exercise on the amounts of oxidized fatty acids in the plasma over the duration of the exercise. The choline derivatisation was successful because stable derivatives of all the oxylipins of interest in the study were successfully detected to < 5 ng/ml and could potentially be quantified by reverse phase ESI LCMS since calibration curves were successfully constructed in the range of 5 ng-80 ng/ml. The statistical analysis of the samples appears to indicate that there is no statistically significant variation in the quantities of any of the oxidized fatty acids of interest over the course of the ultra-marathon run. However, plots of mean concentrations against the three sample time points plus baseline for tend to indicate that for two of the oxylipins, 9(S)-HODE and 13(S)-HODE, there was a clear almost linear reduction in their concentrations over the duration of the exercise. This relationship was not

apparent for the other four oxidised fatty acid metabolites. However, the analysis of the oxylipins in plasma gave values which were much higher than the existing literature, with the values obtained by Neimann *et al* post-exercise were around 16.8 ng/ml for 9-HODE and 28.3 ng/ml for 13-HODE and were also reported to increase as a result of rigorous exercise [156]. This might be because the current plasma samples had been stored for a long time resulting in further oxidation producing an increase in oxylipins from linoleic acid present in the plasma. The other oxylipins that we measured in the current study had not been measured in plasma before so it is difficult to judge whether or not the values obtained are sensible. Thus more investigation is required to establish whether this method is viable as a method for the analysis of these low level compounds in plasma. The sensitivity is excellent but there is the uncertainty with regard to whether or not the derivatization treatment might promote oxidation of linoleic acid. Deuterated choline is available should a strategy be used where labelled plasma fatty acids be used as an internal standard.

Chapter Five:

VARIATION OF FOUR MONOSACCHARIDES IN CROHN'S DISEASE AND ULCERATIVE COLITIS IN COMPARISON WITH HEALTHY CONTROLS

5 VARIATION OF FOUR MONOSACCHARIDES IN CROHN'S DISEASE AND ULCERATIVE COLI- TIS IN COMPARISON WITH HEALTHY CON- TROLS

5.1 Introduction

A variety of compounds are synthesised within the gastrointestinal tract (GIT) by the process of fermentation of nutrients and xenobiotics by the normal gut bacterial flora. These refer to compounds which are normally produced by the host but enter the gastrointestinal tract either *via* the diet or are produced or excreted within the host by the gut microbiota. These metabolites are either excreted or may alternatively be reabsorbed through the colonic mucosa thereby re-entering the systemic circulation where they may be subjected to further modification by metabolism [157].

It has been reported that *p*-cresol which is produced from the aromatic amino acid tyrosine in the colon by the process of bacterial fermentation is almost entirely reabsorbed by the host. First pass metabolism which involves the conjugation of *p*-cresol leading to the formation of *p*-cresol sulphate or *p*-cresol glucuronide within either the colon mucosa or the liver which makes *p*-cresol highly water soluble enabling its excretion through the kidney in the urine [158].

Some metabolites derived from the host's metabolism can analogously be returned to the gut by the process of biliary excretion and are then subject to further metabolism by the gut microbiota leading to new metabolites which may themselves be re-absorbed into the circulatory system of the host. This process occurs for bile acid metabolites which are not absorbed in the terminal ileum and are initially converted to secondary bile acids by microbial metabolism within the colon [159].

With regard to sugar metabolism. Plants in the form of fruits, vegetables and cereals are major components of the human diet. They provide carbohydrates that are readily digested by human intestinal enzymes, as well as dietary fibres, which are resistant to digestion and absorption in the human small intestine [160]. Dietary fibres undergo complete or partial microbial fermentation in the large intestine. Dietary fibres are composed of plant cell wall polysaccharides and this includes so called resistant starches which are resistant to breakdown by human enzymes. The human genome only codes for 17 enzymes which are able to digest carbohydrates [161]. Dietary fibres contain a wide range of sugars including glucose, galactose, rhamnose, xylose and fructose [160]. The fermentation of dietary fibres in the gut is related to the bacterial populations within the gut. For instance *Bacteroides thetaiotaomicron* bacteria contain over 260 carbohydrate digesting enzymes whereas *Firmicutes* bacteria have a more limited range of enzymes [162].

These metabolic interactions between the host and gut microbiome tend to complicate the interpretation of metabolite profiles. Additionally, the type of bio matrix selected for analysis plays an important role in the determination of the outcomes of metabolomic analyses which involve the gut microbiota. Microbial metabolism is therefore more accurately represented

by analysis of the faecal metabolome rather than either the urinary, serum or breath metabolomes [157]. Although the urinary profiles depict both human and human-microbial co-metabolites, it has been suggested that normally, serum profiles contain fewer products derived from microbial metabolism. The most commonly used bio matrices for the assessment of the gut microbial metabolomes are faeces, urine and serum.

In diseases of the GIT such as inflammatory bowel disease (IBD) and inflammatory bowel syndrome (IBS), the initiation and progression of the disease have been suggested to be associated with a dysbiosis of the microbiota [157]. In reports of studies of these disease states, it has been highlighted that there is significant disproportion of the amounts of the predominant bacteria in faecal samples when compared with the healthy state [163-165]. This is evidenced by the observation that for both IBD and IBS there is often a reduction in the diversity and abundance of Firmicutes bacteria in the samples from patients who present with symptoms of these conditions. Therefore, to understand disease pathogenesis for both of these conditions, IBD and IBS, it is important to understand the unique differences which result from the metabolic activities of the microbiota in these disease states in relation to healthy controls [166, 167]. This understanding could also be used to develop diagnostic tools for these conditions [157, 168].

Inflammatory bowel disease is a relapsing inflammatory condition of the GI tract consisting mainly of two diseases, Crohn's disease (CD) and ulcerative colitis (UC). Both diseases share similar characteristics in their physiopathology and patients often present with similar symptoms although the treatment, management and prognosis for the conditions are very different. In UC, which is the more common of the two, the disease is generally limited to the colon, while in CD the disease is more widespread and can occur throughout the gastrointestinal

tract. The manifestation of both diseases are influenced by both genetic, environmental as well as microbial factors. The current diagnosis for IBD relies heavily on techniques such as endoscopy and both radiological and histological examinations all of which are only effective when the disease is in an advanced stage. A diagnostic tool which utilises metabolomic techniques would not only be less invasive as the samples required for metabolomic analysis can be obtained from relatively conveniently sourced biological samples such as urine, serum, or faeces. A metabolomics based protocol would also offer the additional advantage that it has the potential to be used for, primary diagnosis of the condition at a much earlier stage in the disease cycle, monitoring the progress of treatment as well as early detection of relapses [157]. In addition to the discovery of novel biomarkers, metabolomics has a huge potential for improving the diagnosis of IBD patients especially in distinguishing between the different subtypes [169].

Biomarkers which have previously been reported from studies into IBD and IBS studies and which have also been evaluated *via* clinical trials include faecal markers (such as lactoferrin, calprotectin, and PMN-elastase), acute phase proteins such as C-reactive protein, and serological markers (antibodies against luminal antigens and anti-glycan antibodies) [170]. Metabolomic techniques have successfully been utilised to distinguish between patients with IBD and healthy controls, CD patients from UC patients, as well as patients with active disease from those in remission [171, 172]. The increasing number of reports like this in recent years tend to suggest that the role played by metabolomics in the understanding of the gut microbiota and the influence it has on the host's urinary, faecal and serum metabolomes *via* studies involving metabolite profiling are rapidly increasing in importance and are gaining widespread acceptance. Previous studies of host-microbiome metabolomes in IBD have mainly employed

techniques such as $^1\text{H-NMR}$ and GC-MS as analytical platforms. The use of other techniques such as ICR-FT/MS [173] and AA analyser [174] have also been reported. The first reports of the differentiation between patients suffering from IBD and healthy controls based on the analysis of aqueous extracts of faecal samples by $^1\text{H-NMR}$ and the differentiation of CD patients from patients with UC appeared in 2007 [175]. In that report, dysbacteriosis, which results in changes to or an imbalance in the normal gut microbial ecology was analysed by the successive depletion of bacterial metabolites such as short chain fatty acids (SCFA), dimethylamine and trimethylamine, resulting in the suggestion that the alteration in the gut microbial community was either a causative or consequential factor in IBD. Several other studies have revealed that it is possible to distinguish between CD patients and healthy controls based on the profiles of the metabolites found in faecal or urine samples. It was also possible to distinguish between patients in which the disease mostly affected the ileum from those in whom the colon is predominantly involved [157, 173, 175-187].

From the above it is clear that in spite of the previous successes reported for metabolomic analysis of samples from patients with IBD using other analytical platforms, the use of LCMS is yet to be significantly explored for analysis of samples from the gut microbiota. This might be because most of the metabolites associated with gut microbial fermentation have low molecular weights and are also not easily ionised which is essential for detection by mass spectroscopy. These shortcomings have however, been shown to be overcome in related studies by means of derivatisation of the metabolites prior to analysis [94].

5.1.1 Aim of study

The overall aim of this study is to separate, detect, identify and quantify the common hexoses: mannose, glucose, fructose and galactose, pentoses: arabinose, ribose and xylose and the

deoxy hexoses: rhamnose and fucose which occur in the faecal samples of participants in a study of IBD by application of a reductive amination derivatisation strategy utilising LCMS as the analysis platform.

5.2 Materials and Methods

5.2.1 Chemicals and Solvents

HPLC grade Acetonitrile (ACN) was purchased from Fisher Scientific (Loughborough, UK) and HPLC grade water was produced by a Direct-Q3 Ultrapure Water System (Millipore, Watford, UK). AnalaR-grade formic acid (98%) 2-picoline-borane, acetic acid, aniline, $^2\text{H}_5$ -aniline, galactose, glucose fructose, mannose, ribose, ribose, xylose, arabinose, allose, altrose, gulose, talose, 2-deoxyribose, rhamnose, $^{13}\text{C}_6$ -glucose were obtained from BDH-Merck (Poole, UK).

5.2.2 Participants

Pre-prepared faecal samples from 3 groups of participants were used in this study, 15 patients with Crohn's disease, 12 patients with ulcerative colitis (UC) and 15 normal controls.

5.2.3 Faecal Sample preparation

To exactly 100 μL of each faecal sample was added 100 μL of $^{13}\text{C}_6$ -glucose (10 mg/mL in MeOH: H_2O). The mixture was blown to dryness under a stream of nitrogen and then re-dissolved in 200 μL of methanol before being used in the $^2\text{H}_5$ -aniline derivatisation reactions.

5.2.4 Standard Sugar Sample preparation

Calibration curves using 6 concentration points (0.0, 0.05, 0.1, 0.2, 0.4, 0.8, 1.6 μg) were prepared for each of the sugar focused on in the study utilizing standard sugar samples prepared

to a final concentration of 1 mg/mL in methanol before being used in the $^2\text{H}_5$ -aniline derivatisation reactions.

5.2.5 Derivatisation of Sugars

Solutions of the reagents used in the tagging reaction were prepared as follows:

5.2.5.1 Preparation of $^2\text{H}_5$ -aniline solution (Solution A, 10 mg/mL)

Deuterated aniline, ($^2\text{H}_5$ -aniline, 5g), was dissolved in methanol, 5 mL. 100 μL of this solution was further dissolved in 900 μL of methanol. 100 μL of this solution was mixed with 100 μL of acetic acid, 400 μL of methanol and 400 μL of water to give a final concentration of 10 mg/mL.

5.2.5.2 Preparation of picoline-borane solution (Solution P, 10 mg/mL)

10 mg of picoline-borane powder was carefully weighed out and dissolved in 1 mL of methanol/water (1:1).

5.2.5.3 Protocol for the derivatisation of sugars.

To an aliquot of sample (sugar or sample solution, 100 μL), was added 40 μL of solution A. The resulting mixture was then heated for 30 minutes at 40 °C. 20 μL of solution P was then added and the resulting mixture was once again heated for 45-120 minutes at 30 °C. The length of this incubation is determined by the sugars of interest as fructose has been demonstrated to require the longer reaction time to complete the reaction process. The reaction mixture is then blown to dryness under a stream of nitrogen and re-dissolved in 200 μL of water containing 0.1 % formic acid and finally diluted with 1000 μL of acetonitrile.

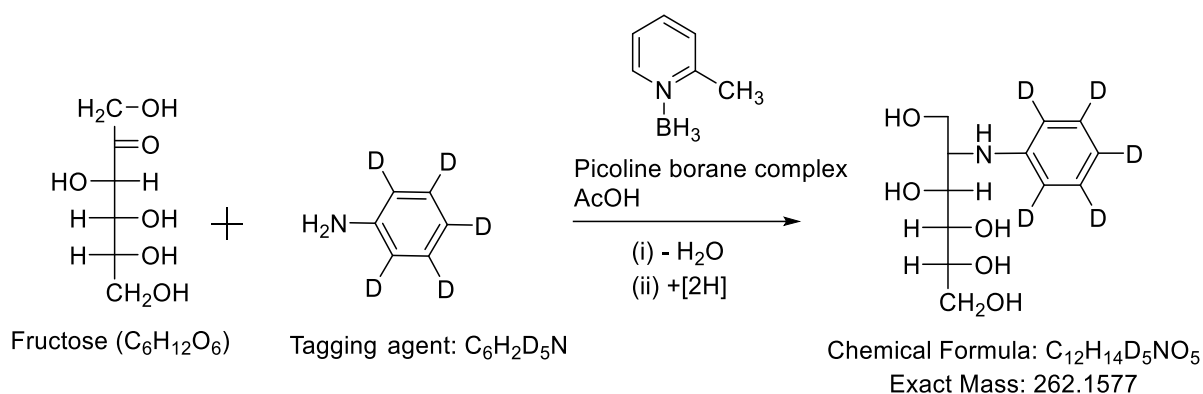


Figure 5-1 Depiction of the reaction between the sugars and the tagging agent, 2H_5 -aniline, to produce the target stable derivative utilizing Fructose as an example.

5.2.5.4 LCMS conditions

Liquid chromatographic separation was carried out on an Accela HPLC system interfaced to an Exactive Orbitrap mass spectrometer (Thermo Fisher Scientific, Bremen, Germany), utilizing the same column, conditions and settings described above (section 3.2.7) run isocratic with an acetonitrile/water (90:10) mobile phase with 0.01 % formic acid modifier at a flow rate of 0.6 mL/minute. Full scan data was obtained in the mass-to-charge ratio (m/z) range of 75 to 1200 for both ionization modes on the LCMS system which was fully calibrated prior to use according to the manufacturer's guidelines. The data was acquired using the XCalibur 2.1.0 software package (Thermo Fisher Scientific, Bremen, Germany).

5.3 Results and discussions

5.3.1 Calibration curves

Aniline is frequently used as a tagging agent for sugars. The deuterated aniline analogue 2H_5 -aniline was however used because it had been shown in previous studies to have produced a better peak shapes as well as separation between galactose and mannose than aniline [94].

Calibration curves were produced for the four sugars, glucose, galactose, xylose and arabinose, which were focussed on in this study at concentration points of 0.05, 0.1, 0.2, 0.4, 0.8, 1.6 µg/mL, using the derivatisation protocol outlined above, (section 5.2.5 Derivatisation of Sugars), and were analysed using ¹³C₆-glucose, 1 µg/mL, as internal standard on a ZIC-pHILIC column, run isocratic with an acetonitrile/water (90:10) mobile phase with 0.01 % formic acid modifier at a flow rate of 0.6 mL/minute. A summary of the data from these calibration curves is presented below (Table 5-1) while the calibration curves are depicted in figures 5-2 to 5-5.

Table 5-1 Summary of data from the calibration curves for Glucose, Galactose, Xylose and Arabinose

CONC (µg/mL)	Peak Area Ratio (Mean RT ± SD in Minutes)			
	<i>GLUCOSE</i> (11.04±0.07)	<i>GALACTOSE</i> (14.87±0.11)	<i>XYLOSE</i> (7.52±0.04)	<i>ARABINOSE</i> (8.68±0.05)
0	0.0000	0.0000	0.0000	0.0000
0.05	0.0491	0.0405	0.0481	0.0477
0.1	0.1010	0.0990	0.1074	0.1141
0.2	0.2172	0.2119	0.2208	0.2406
0.4	0.4378	0.3905	0.4247	0.4719
0.8	0.8801	0.6944	0.7888	0.8723
1.6	1.7956	1.3518	1.5598	1.7984

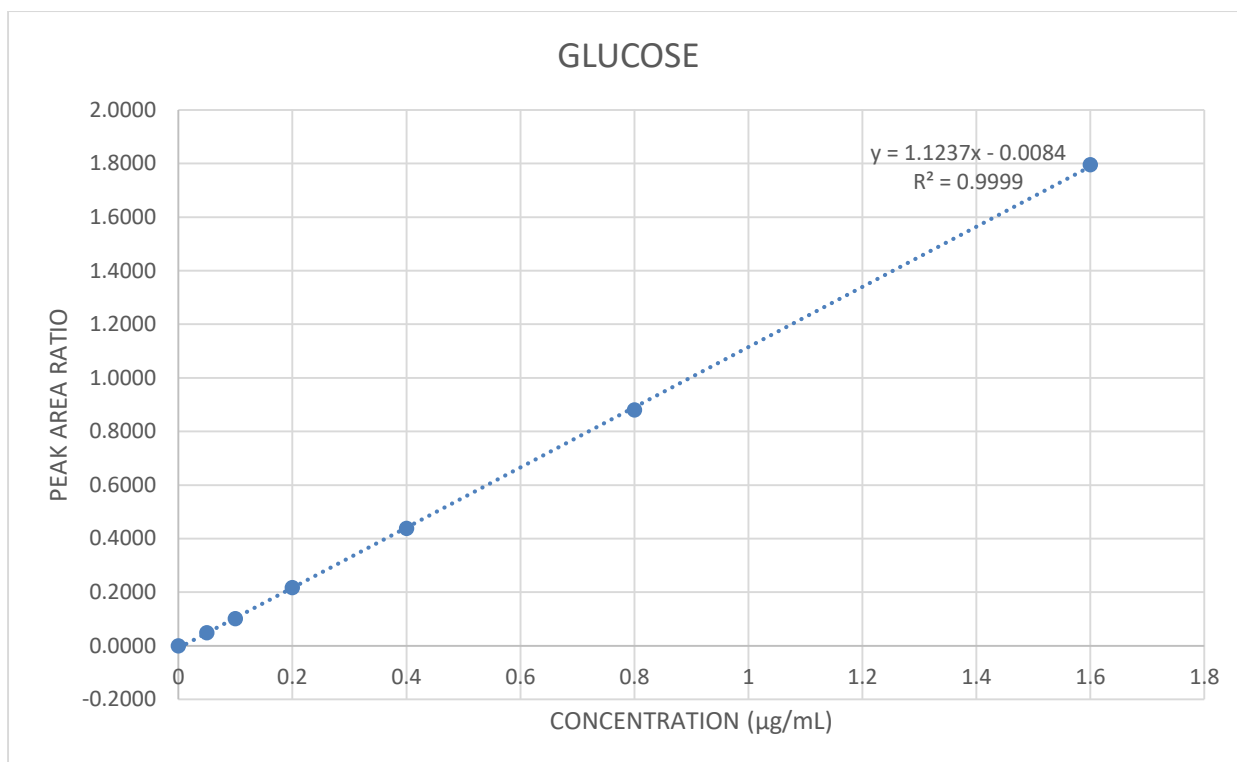


Figure 5-2 Calibration curve for glucose using $^{13}\text{C}_6$ -glucose as internal standard.

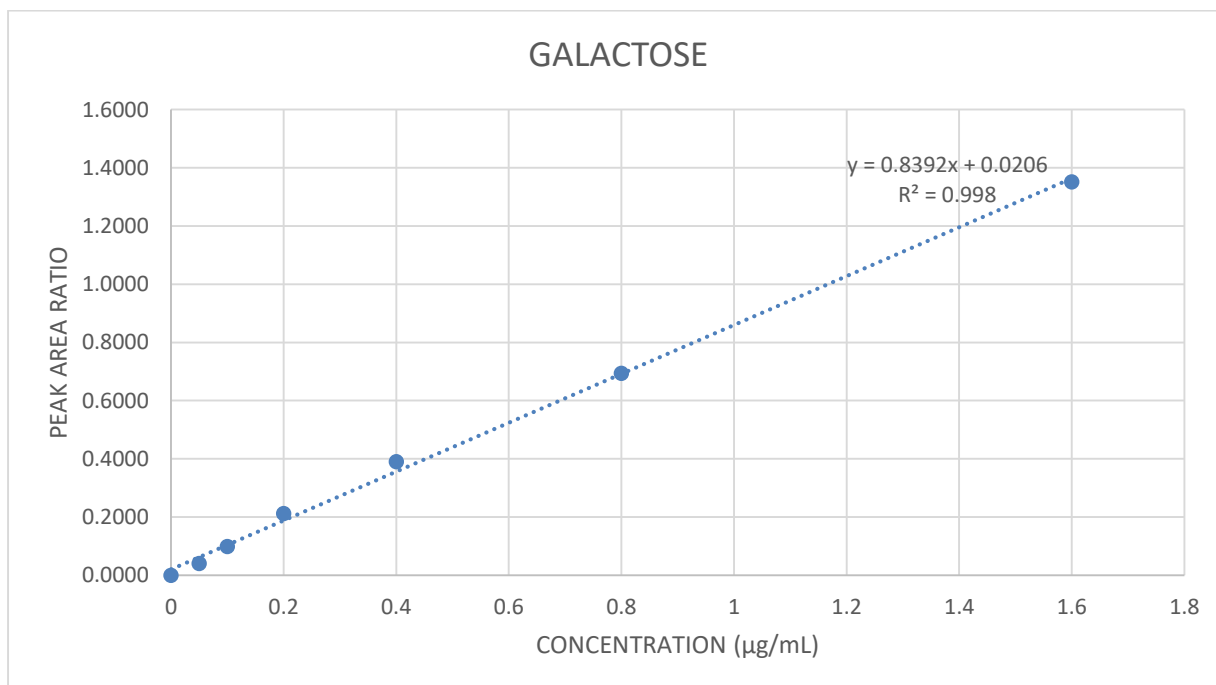


Figure 5-3 Calibration curve for galactose using $^{13}\text{C}_6$ -glucose as internal standard.

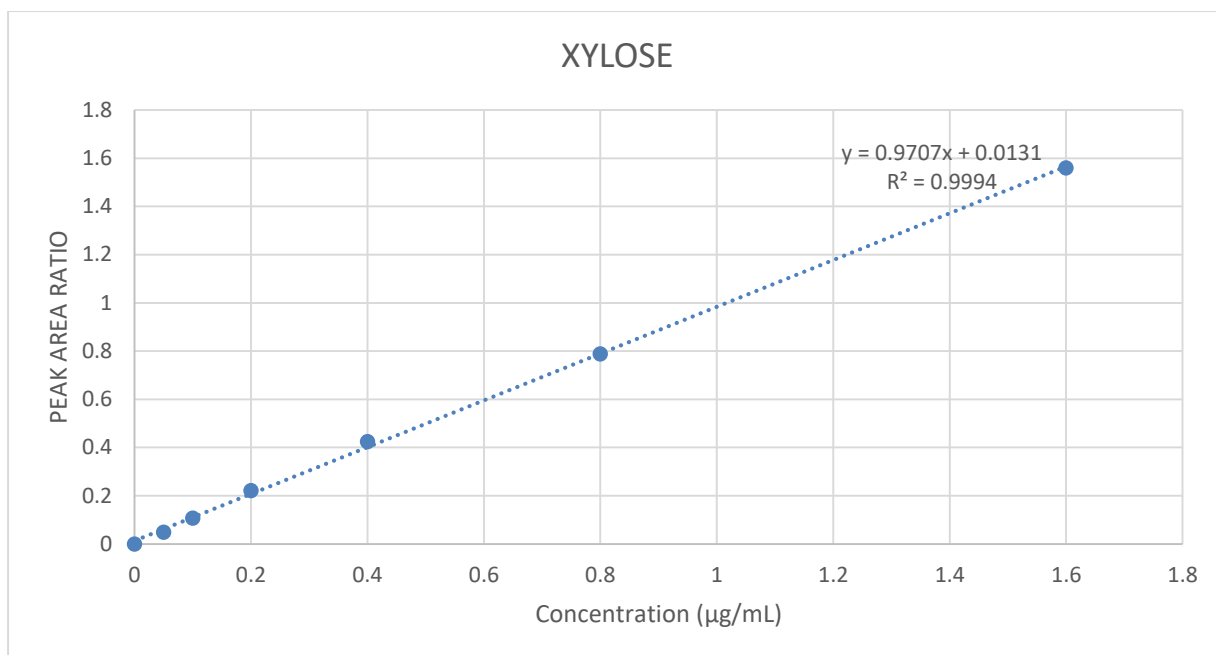


Figure 5-4 Calibration curve for xylose using $^{13}\text{C}_6$ -glucose as internal standard.

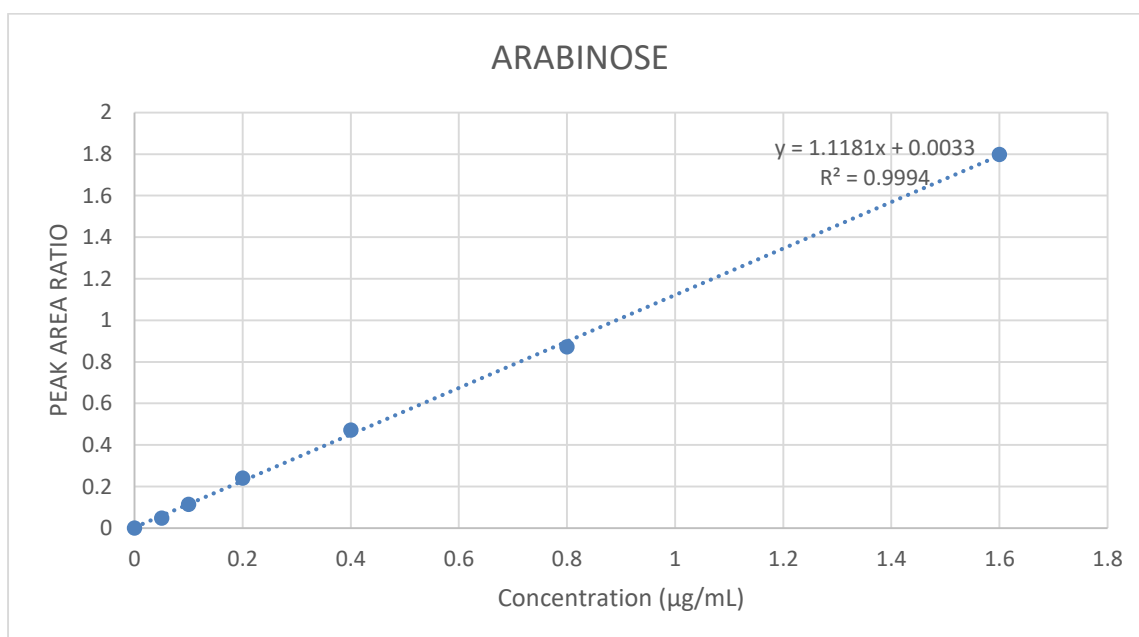


Figure 5-5 Calibration curve for arabinose $^{13}\text{C}_6$ -glucose as internal standard.

The calibration curves for all the four sugars gave very good linearity with $R^2 > 0.99$ in all cases.

The derivatisation reaction was carried out on samples of a test mix of standard sugars focused on in the study as well as the internal standard ($^{13}\text{C}_6$ -glucose-internal standard, xylose, arabinose, glucose, galactose) and as anticipated the obtained retention times from the derivatized sugar allowed for the positive identification and quantification of a number of sugars especially arabinose, galactose, glucose and xylose which were the sugars of interest in this study. Extracted ion chromatographs from a representative concentration from these experiments are shown in Figure 5-6.

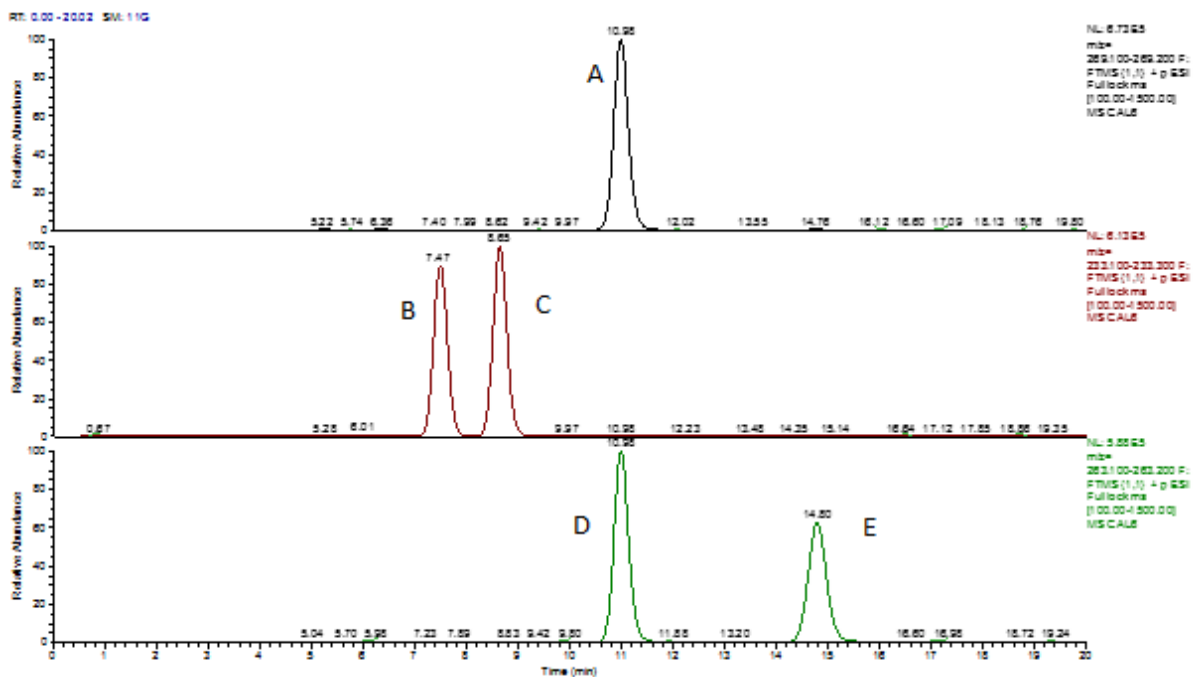


Figure 5-6 Extracted ion chromatograph of derivatized standard sugar mix (0.8 μg) with $^{13}\text{C}_6$ -glucose (1 μg) as internal standard; A = $^{13}\text{C}_6$ -glucose, B = xylose, C = Arabinose, D = Glucose, E = Galactose

The efficiency of the tagging was very good as all the four sugars in the test mix were successfully tagged and could be easily distinguished from each other due to the differences in the retention times of the derivatized sugars. The extracted ion chromatographs from a further

derivatisation experiment involving a second test mix containing 13 sugars, hexoses and pentose's as well as glucose internal standard ($^{13}\text{C}_6$ -glucose -Internal Standard), (Pentoses: Xylose, Arabinose, Ribose, Rhamanose), (Hexoses: Fructose, Glucose, Altrose, Allose, Gulose, Galactose, Talose, Mannose), is presented below (Figure 5-7). This was carried out in order to determine that there was no chance of confusing the isomers of interest with all of the possible isomers. Hexoses have four chiral centres resulting in eight diastereoisomers (each of which has in theory a corresponding enantiomer). Seven of the eight hexose isomers could be obtained commercially.

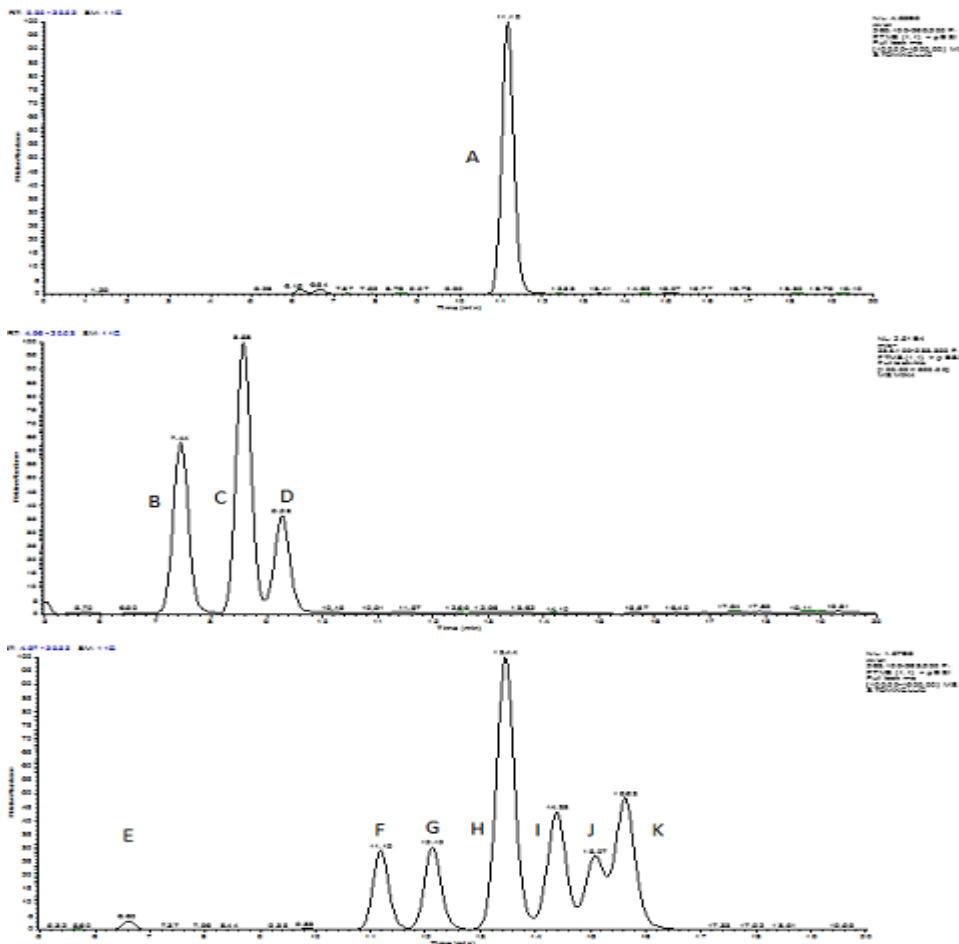


Figure 5-7 Extracted ion peaks for a standard mixture of hexose and pentose sugars (0.8 μg) with $^{13}\text{C}_6$ -glucose (1 μg) as internal standard; A = $^{13}\text{C}_6$ -glucose, B = Xylose, C = Arabinose, D = Ribose, E = Fructose, F = Glucose, G = Altrose, H = Allose + Gulose, I = Galactose, J = Talose, K = Mannose

The efficiency of the tagging reaction was generally good with the exception of fructose which only reacted sparingly (E - Figure 5-7). The poor reactivity of fructose can be attributed to its being a ketone which would generally react slower than the aldehyde sugars. Improvements in the tagging efficiency can be achieved by extending the reaction time to 2 hours to allow for better conversion. The pentose sugars could all be easily distinguished based on their retention times; this was the same with most of the hexoses. They all appear to have good tagging efficiencies as expected based on the peak areas but the separation of the derivatized sugars was poor in some cases such as for talose (J) and mannose (K) which overlap and for the peak (H) which contains both allose and gulose which co-elute based on the retention times obtained for the individual sugars (Figure 5-7).

5.3.2 Levels of sugars in healthy, Crohn's disease and ulcerative colitis patients

The test samples from the participants in the study were also subjected to the derivatisation reaction prior to analysis by LCMS using $^{13}\text{C}_6$ -glucose as internal standard and the results of this experiment are summarised below (Table 5-2).

Table 5-2 Summary of sugar levels for each of the participants in the study following derivatization with ²H₅-aniline.

Sample ID	Group	Concentration of sugar (µg/mL)			
		Glucose	Xylose	Galactose	Arabinose
286H	Healthy	8.7426	1.5928	1.0288	2.6908
287H		2.9458	1.4111	1.9484	5.5169
288H		4.3212	1.4441	1.3008	2.6982
289H		3.0191	1.5495	3.8011	4.9921
290H		8.9842	1.5141	2.3963	5.7262
291H		0.3992	0.0529	0.3354	0.9165
292H		1.3128	0.4205	0.3438	1.1658
293H		15.451	2.9922	7.7045	5.3901
294H		6.9373	1.668	2.3113	5.2338
295H		1.3863	0.092	0.875	2.8267
296H		0.6596	0.2129	0.4751	1.3948
297H		0.3682	0.084	0.2001	0.9086
298H		1.4038	0.09	0.3021	1.151
299H		5.0505	0.9193	2.9146	8.2951
300H		1.0665	0.0691	1.4084	2.499
CD2		Crohn's disease	8.7766	2.6009	3.5277
CD4	11.887		3.2878	7.8076	7.5158
CD5	12.137		0.6218	3.8955	2.9994
CD12	2.7891		0.3238	1.1126	3.8411
CD18	15.15		4.474	15.182	8.221
CD23	15.159		7.5363	6.8459	6.5655
CD56	6.0811		1.4468	2.8565	1.7232
CD66	10.319		0.3605	1.0754	1.263
CD29	9.2177		0.3492	4.0925	2.0568
CD34	4.4975		1.6388	5.6801	7.5202
CD40	0.4907		0.0417	0.2152	0.8898
CD45	15.115		1.0439	16.808	11.916
CD46	0.1726		1.288	2.8225	2.0146
CD53	24.545		18.322	22.158	12.327
CD62	1.128		0.0726	1.1105	1.5055
1UC	Ulcerative colitis		4.3839	0.4195	3.2152
28UC		2.1774	0.1519	8.7117	4.0271
52UC		1.9008	0.1904	1.8628	1.2119
64UC		1.2392	0.0755	1.3807	1.6175
89UC		0.4765	0.012	0.9767	0.2742
111UC		1.8385	1.1085	4.3319	5.2056
135UC		2.9202	0.3492	3.4295	4.0026
153UC		1.02	0.0321	0.1762	0.2596
169UC		1.6667	0.025	0.638	1.0741
186UC		1.5775	0.0169	0.918	0.807
193UC		9.255	3.6174	6.3641	1.6289
194UC		2.4374	0.3094	0.6739	1.0108

Representative extracted ion chromatographs from each class of participants in the study, healthy controls, CD and UC, are presented in the figures below (Figures 5-8 to 5-10). From the chromatograms it can be seen that there is no evidence for the presence of uncommon hexoses or pentoses in the samples. The main sugars observed are glucose, galactose, xylose and arabinose.

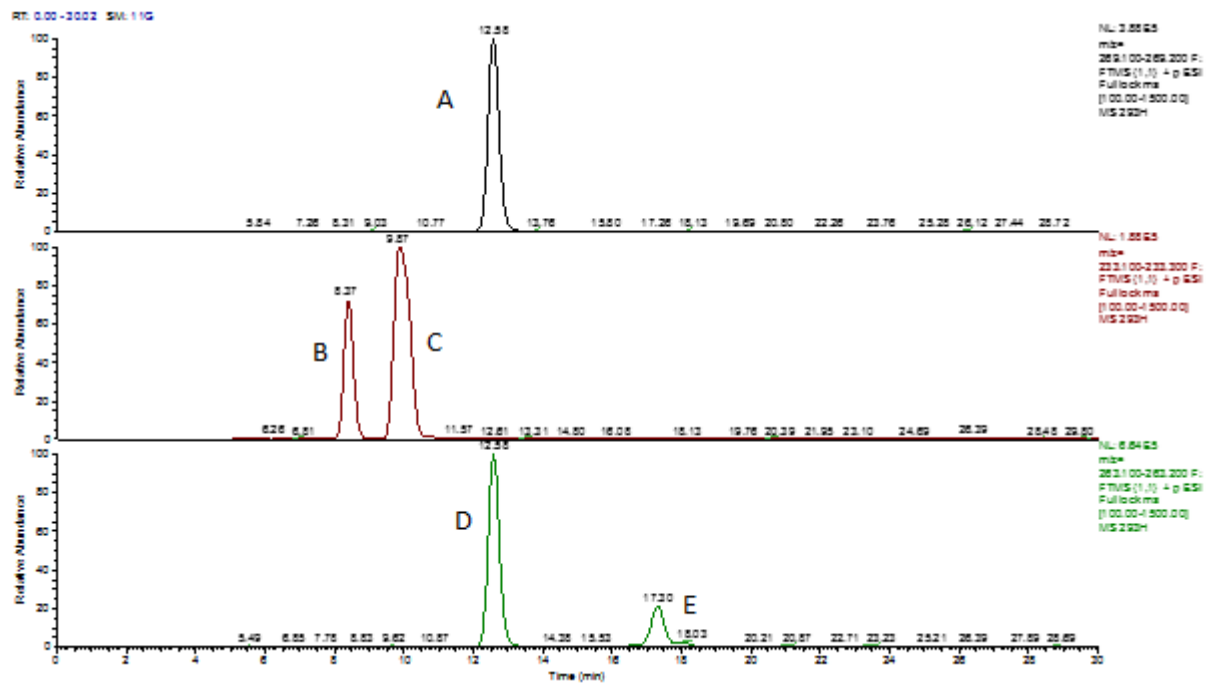


Figure 5-8 Extracted ion chromatographs of derivatised sugars found in samples from healthy participants with $^{13}\text{C}_6$ -glucose ($1\ \mu\text{g}$) as internal standard; A = $^{13}\text{C}_6$ -glucose, B = xylose, C = Arabinose, D = Glucose, E = Galactose

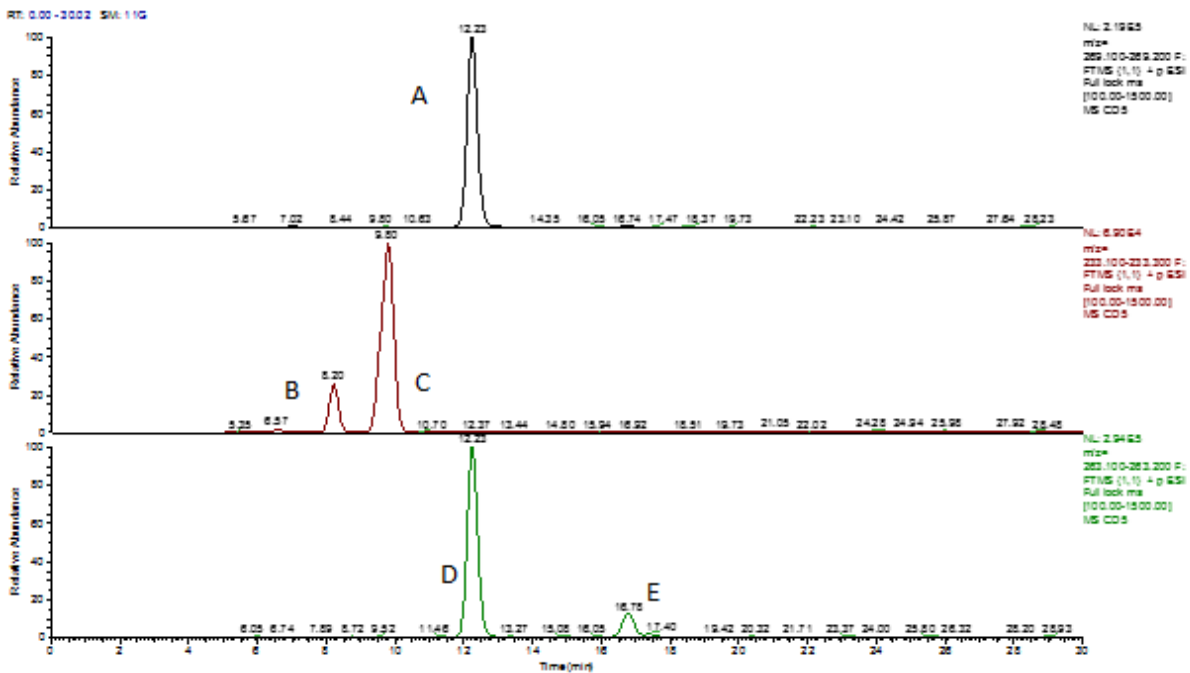


Figure 5-9 Extracted ion chromatographs of derivatised sugars found in samples from participants with CD with $^{13}\text{C}_6$ -glucose (1 μg) as internal standard; A = $^{13}\text{C}_6$ -glucose, B = xylose, C = Arabinose, D = Glucose, E = Galactose

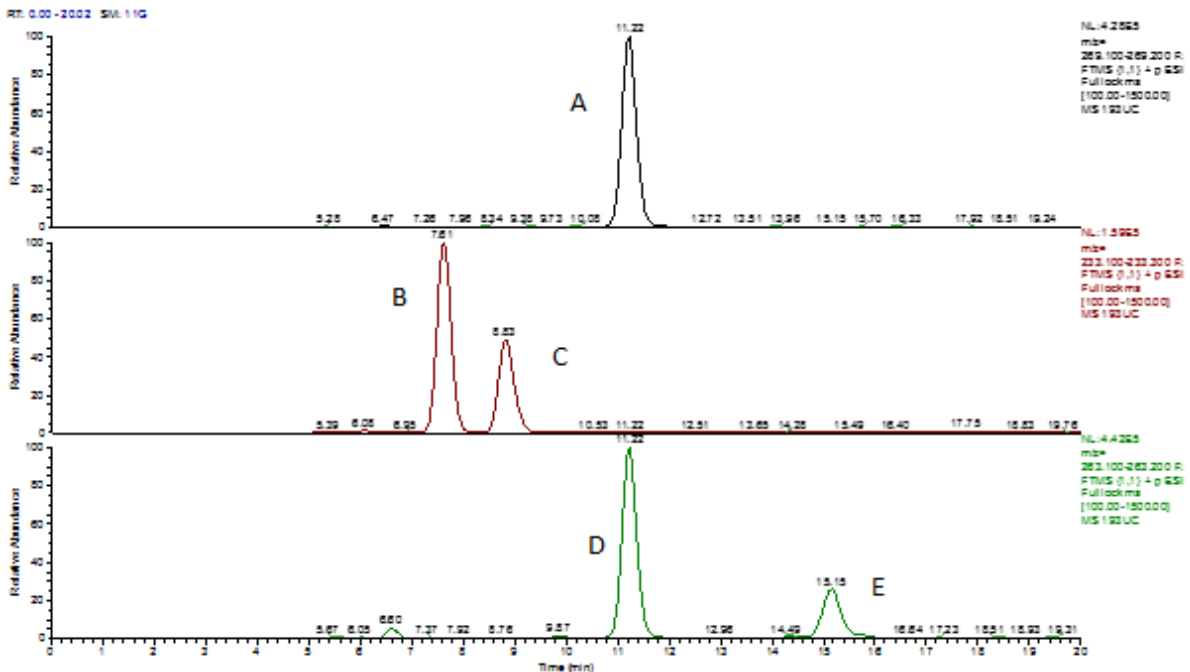


Figure 5-10 Extracted ion chromatographs of derivatised sugars found in samples from participants with UC with $^{13}\text{C}_6$ -glucose (1 μg) as internal standard; A = $^{13}\text{C}_6$ -glucose, B = xylose, C = Arabinose, D = Glucose, E = Galactose

The derivatisation of the faecal samples was deemed successful because all the sugars of interest in the study could be clearly identified in each case with the exception of ribose which

was not detected as expected. As the tagging of ribose in the reactions using the test mixtures was successful the failure to see any peaks for ribose in the faecal samples is probably related to the relative abundance of ribose in the test samples which might be too low to be detected.

5.3.3 Statistical comparisons of the sugars

The statistical analysis of the data derived from the LCMS analysis of the study samples was carried out using IBM® SPSS® Statistics version 20 and is presented below in the following table (Table 5.3).

Table 5-3 Mean values of Sugars from the participant groups from the study.

	Treatment Groups (Mean values)		
	<i>Healthy</i>	<i>Chrons disease</i>	<i>Ulcerative colitis</i>
	Mean	Mean	Mean
Level of Glucose	4.1365 _a	9.1643 _b	2.5744 _a
Level of Xylose	0.9408 _a	2.8939 _a	0.5257 _a
Level of Galactose	1.8230 _a	6.3460 _b	2.7232 _{a,b}
Level of Arabinose	3.4270 _{a,b}	5.3187 _a	1.8221 _b

Note: Values in the same row and sub-table not sharing the same subscript are significantly different at $p < .05$ in the two-sided test of equality for column means. Cells with no subscript are not included in the test. Tests assume equal variances. Tests are adjusted for all pairwise comparisons within a row of each innermost sub-table using the Bonferroni correction.

From the table above, the following observations can be made:

- a) The levels of the all of the sugars focused on in this study are generally higher for the participants with CD compared to both of the other groups, healthy controls group and participants with UC.
- b) The levels of glucose for the participants with CD are significantly higher than those in both of the other study groups, healthy controls or participants with UC.

- c) The levels of xylose although different at first glance between the three groups of participants is not a statistically significant difference.
- d) The levels of galactose in the group of participants with CD are significantly higher than the participants in the HC group, and although higher than those in the group of participants with UC, this change is not a statistically significant increase.
- e) The levels of arabinose in the group of participants with CD are significantly higher than those in the group of participants with UC, similarly, although higher than for those in the HC group this is not a statistically significant increase.

5.4 Discussion

5.4.1 Levels of monosaccharide sugars

Table 5-4 Means and SDs of the levels of sugars in the three groups of participants used in the study.

Sample	Levels of sugars in the samples (Mean and SD) in µg/mL							
	Glucose		Xylose		Galactose		Arabinose	
	Mean	SD	Mean	SD	Mean	SD	Mean	SD
Healthy	4.1365	4.28276	0.9408	.88091	1.8230	1.95335	3.4270	2.27224
Crohn's disease	9.1643	6.83508	2.8939	4.72635	6.3460	6.56916	5.3187	3.98010
Ulcerative colitis	2.5744	2.32797	0.5257	1.02067	2.7232	2.63427	1.8221	1.64484

Table 5-5 One-way ANOVA for the differences in levels of the four monosaccharide sugars between healthy, Crohn's disease and ulcerative colitis patients.

Monosaccharide	F	Sig.
Glucose	6.671	.003
Xylose	2.499	.096
Galactose	4.499	.017
Arabinose	4.975	.012

The results of the ANOVA multiple comparisons test using Tukey's method highlighted that the levels of glucose among the participants with Crohn's disease (CD) was significantly higher than was found among both the healthy controls group ($p = 0.023$) and the group with ulcerative colitis (UC) ($p = 0.004$). The difference in the levels of glucose between the healthy controls group and group of participants with UC was not statistically significant ($p = 0.700$). On the other hand, the levels of galactose found in the group with CD were found to be significantly higher than for the healthy controls group ($p = 0.018$), although it was not found to be significantly different from was found with the group of participants with UC ($p = 0.092$). However, the galactose levels in healthy controls did not differ significantly from those of the group with UC ($p = 0.854$). The xylose levels were however found not to vary significantly between the three groups ($p = 0.096$). The levels of arabinose in the group of participants with CD were found to be significantly higher than for the group of participants in in the UC group ($p = 0.009$) but not for those in the healthy controls group ($p = 0.184$). There was also no significant difference in the levels of arabinose between the UC group of participants and the healthy controls group ($p = 0.332$). The interpretation of this analysis clearly highlights that there is a significant difference in the levels of sugars found for each of the test groups. This is in agreement with other studies which have used metabolomics, LCMS, GC-MS and ^1H NMR platforms to analyze biological samples including faecal samples which all allude to the fact that differences in the concentrations of the metabolites observed in biological samples, including faecal samples, can be used to diagnose IBD as well as to distinguish between the various phenotypes which is essential for ensuring the best outcome in the management and treatment of these conditions [173, 188, 189]. The differences in the concentrations of glucose, galactose and arabinose between the disease groups and the healthy controls group in the study as determined by the LCMS quantification further demonstrates the potential for

LCMS to distinguish between sufferers of CD, for which group the levels of glucose and arabinose were found to be higher, than for sufferers with UC for which group these sugars were found to be reduced. A similar variation in sugar levels was also highlighted by another metabolomics study of fecal extracts which utilized ^1H NMR as the analytical platform to study the differences in the concentrations of metabolites between the healthy and diseased state as well as the different phenotypes although there is some disagreement between both studies regarding the magnitudes of these differences which can be attributed to the differences of sensitivities between the analytical platforms used in both studies [190]. The concentrations of xylose were found to be higher in the group with Crohn's disease than the UC group although this change was not found to be statistically significant. A similar conclusion was arrived at in a previous report which utilized ^1H NMR as the analytical platform for a metabolomic profiling study of serum, plasma and urine samples [178]. The increased levels of glucose in the CD samples is of some interest since this might be a marker of increased levels of *Bacteroides* bacteria in these samples since they are the bacterial population with the greatest capability of carrying out carbohydrate digestion. Glucose could be derived from digestion of celluloses or beta glycans which are glucose polymers which can be digested by bacterial fermentation but not by human enzymes. The increases in the galactose in the CD samples could be similarly due to higher levels of *Bacteroides* in the CD samples. The less marked differences between UC and HC may be in line with the less extensive inflammation which is present in UC in comparison with CD.

5.5 Conclusions

A reductive amination tagging strategy which used $^2\text{H}_5$ -aniline as the tagging agent and with $^{13}\text{C}_6$ -glucose as internal standard was successfully applied to the analysis of 42 faecal samples

from 3 groups of participants, 15 patients with Crohn's disease, 12 patients with ulcerative colitis (UC) and 15 normal controls. The $^2\text{H}_5$ -aniline derivatisation was successful because appropriately derivatized sugars were detected and quantified by using a ZICHILIC column in combination with ESI LCMS. The statistical analysis of the samples appears to clearly indicate that there is difference in the levels of sugars found for each of the test groups. It also highlights the potential of this protocol to be used as a diagnostic tool for identifying sufferers of IBD due to the respective differences in the levels of glucose, galactose and arabinose in these test groups over the healthy controls group in general as well as the potential for LCMS to be used to distinguish between sufferers of CD, from which group the levels of glucose and arabinose were found to be significantly higher than for the group of sufferers with UC. This is significant because the faecal samples used in these experiments are noninvasive and relatively easily obtained than plasma samples. In addition, if glucose were selected as a diagnostic marker it would be possible to monitor it by using a sample kit rather than by using mass spectrometry. Higher levels of glucose in faeces might suggest a higher level of *Bacteroides* bacteria with their wider array of enzymes which are capable of digesting resistant starches.

Chapter Six:

**Synthesis of 2-hydrazino-1- methylpyridine (HMP) as
Tagging Agents for the Analysis of Ketosteroids by
LCMS**

6 SYNTHESIS OF 2-HYDRAZINO-1-METHYL-1-METHYLPYRIDINE (HMP) AS TAGGING AGENTS IN THE ANALYSIS OF KETOSTEROIDS BY LCMS

6.1 General introduction to steroids

Steroids are naturally occurring biologically active organic compounds found in plants, animals and fungi which are essential for the normal functions of the organism such as the normal development of the body, glucose regulation as well as ion absorption. In popular culture steroids are frequently associated with performance enhancing drugs taken by some athletes. Steroids are hydrophobic and insoluble in water therefore they are classed as lipids however, due to their unique molecular structure they do not resemble other lipids. All steroids are made up of four rings fused in a specific configuration to form the steroid molecular structure which consists of three six membered cyclohexane rings and one five membered ring.

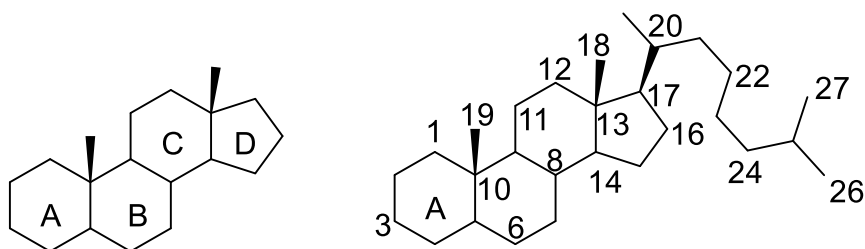


Figure 6-1 General structure of and numbering of steroids

The general steroid molecular structure is made up of seventeen carbon atoms which are arranged into four fused rings. These are the three 6 membered cyclohexane rings A, B and C and a five-membered cyclopentane D ring. Hundreds of different steroids exist and they vary from each other by either the types or numbers of carbon atoms and functional groups that are attached to the general steroid molecular structure as well as by the oxidation state of the rings or both. This difference in functional groups is responsible for the different functions/biological activities of the individual steroid. The variation in functional groups allows the grouping of steroids which share similar structural similarities into groups such as the Cholestanes of which Cholesterol is a good example which all have 27 carbon atoms their molecular structure.

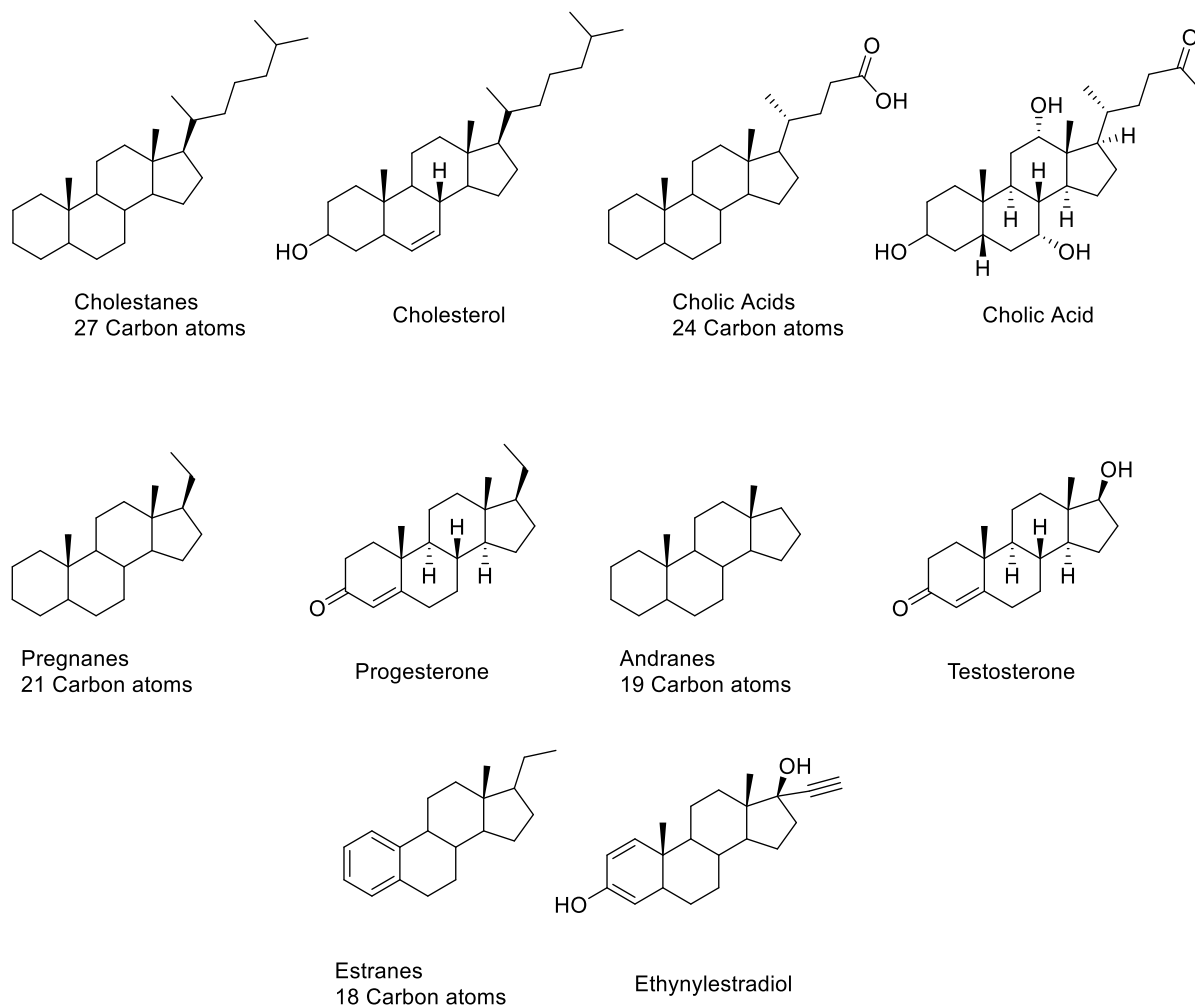


Figure 6-2 Some Classes of Steroids.

6.1.1 Nomenclature of steroids

There are hundreds of different types of steroids which vary by the types of functional groups attached to the general steroid molecular structure and also by the oxidation state of the rings. All steroids are manufactured in cells from sterols either cycloartenol in plants and lanosterol in animals and fungi.

6.1.2 Uses of Steroids

Many biological processes which are essential for normal functioning are influenced by steroid hormones therefore steroids are vital for normal life. An extensive review on the biological functions and significance of steroids can be found in the review by Zubeldia-Brenner et al [191]. An imbalance in the levels of steroids can also lead to several medical conditions a few of which are highlighted here such as primary hyperaldosteronism, which occurs in about 2% of hypertensive patients, adrenal insufficiency, which is caused by a lack of cortisol, "Cushing's syndrome, which is caused by a persistent and inappropriate excess of cortisol, congenital adrenal hyperplasia (CAH), which is a clinical condition/disease which affects the levels of the steroid hormones produced by the adrenal cortex, disorders of the gonadal function such as hypogonadism, which is one of the causes of male sexual dysfunction and in women is responsible for menstrual disorders, hirsutism, and virilisation [192]. Anabolic steroids are synthetic substances that are designed to mimic the effects of the male sex hormones. They act by stimulating the production of proteins, which are used to build muscles and can also lead to an increase in testosterone levels which accounts for their use in popular culture and sports [193, 194]. Anabolic steroids have other therapeutic uses such as the treatment of muscle degeneration associated with disease, late onset of puberty and other conditions resulting from imbalances of male hormones [194-197]. The abuse of anabolic steroids is associated with several negative health consequences such as hair loss, infertility, mood swings and depression, liver tumours, heat attacks and the development of breasts in males [198, 199].

6.1.3 Determination of Steroids by LCMS

The analysis of steroids was originally routinely performed by gas chromatography with coupled mass spectrometry (GC-MS). Liquid chromatography with coupled mass spectrometry

(LCMS) has however become more important in recent years for this purpose [200]. A comprehensive review of the progress in use of mass spectrometry for the routine analysis and detection of steroids from biological samples is covered in the review by Gouveia, et al [201]. The quantities of steroids in these samples is often very small and as a result extremely sensitive techniques are required for their successful detection. The chemical derivatisation of samples have been reported as a useful technique to improve the sensitivity of detection of analytes by mass spectrometry. Derivatisation with charged derivatising or tagging agents have also been reported to provide additional improvements to the detection sensitivity achieved by ESI-MS. Extensive reviews of these developments are presented in reviews by Santa *et al* [202, 203]. Some derivatisation studies reported the detection of sub picomolar quantities of steroids by LCMS [204, 205].

Promising reagents for the derivatisation of compounds which contain carbonyl functional groups are 2-hydrazino-1-methylpyridine (HMP) and 2-hydrazinopyridine (HP). HMP contains a quaternary ammonium group which enhances its ionisation in addition to the hydrophobic aromatic structure which they both share. HMP was reported to have been used by Shibayama *et al.* in a study of oxo-steroids like testosterone (T) and dehydroepiandrosterone (DHEA) from saliva samples [206]. It has also been reported to have been successfully applied to the analysis of brain neurosteroid levels amongst others [207, 208].

6.1.4 Aim

The aim of this study was to chemically synthesise and investigate the suitability of the tagging agent, 2-hydrazino-1- methylpyridine (HMP), for the analysis of steroids to evaluate its suitability.

bility for application to the analysis of ketosteroids in biological samples. In addition, an attempt was made to synthesise a deuterated analogue of HMP for use in situations where a standard sample e.g. pooled control samples might be used as an internal standard against affected samples. The HMP tagging agent as well as a 3 methyl analogue of HMP, 2-hydrazinyl-1,3-dimethylpyridin-1-ium (3MHMP) and its deuterated analogue, 2-hydrazinyl-3-methyl-1-(methyl-d₃)pyridin-1-ium, (3MHMP-d₃), were also synthesised and isolated prior to initial studies into their application for the analysis of standard solutions of steroids and plasma samples by ESI-LCMS on an Orbitrap mass spectrometer (Figure 6-4).

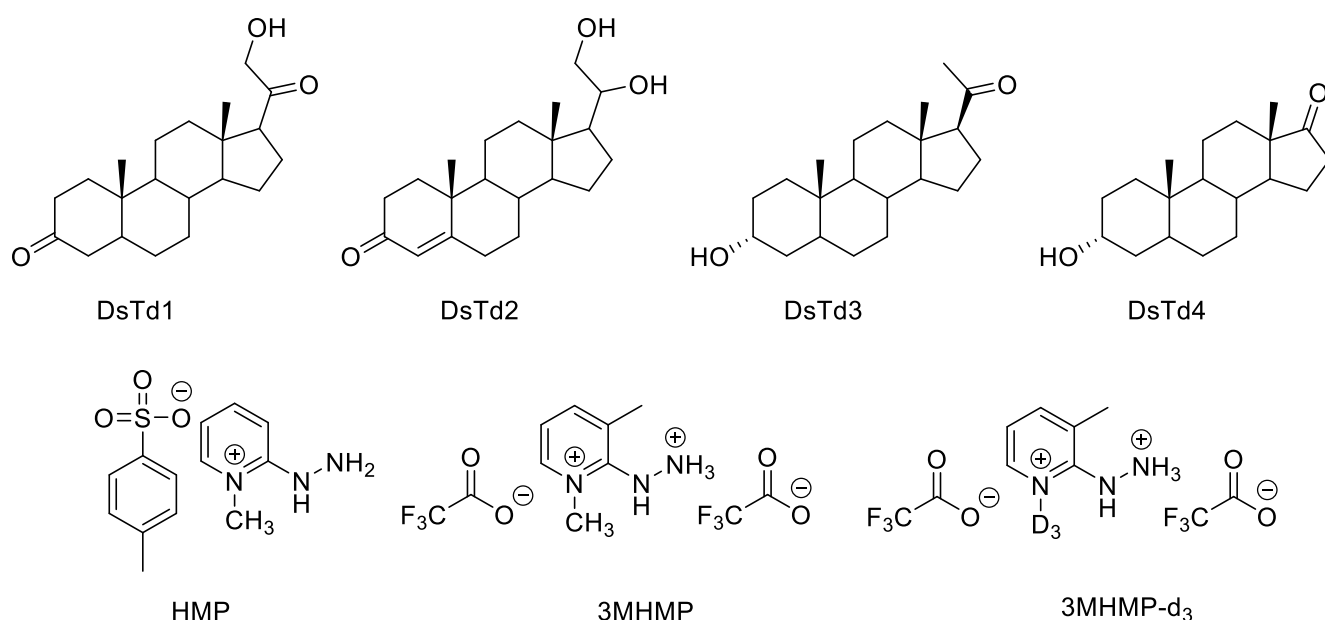


Figure 6-3 The structures of HMP, 3MHMP and 3MHMP-d₃ and the steroid standards 5 α -Pregnane-21-ol-3,20,-dione, (DsTd1), 4-Pregnene-20 β ,21-diol-3-one, (DsTd2), 5 α -Pregnane-3 β -ol-20-one, (DsTd3), 3 β -Hydroxy-5 α -androstan-17-one, (DsTd4), used in the study.

The general scheme for the derivatisation reaction between HMP and a steroid is represented in the schematic diagram below which shows the reaction for DsTd2 with HMP (Figure 6-4).

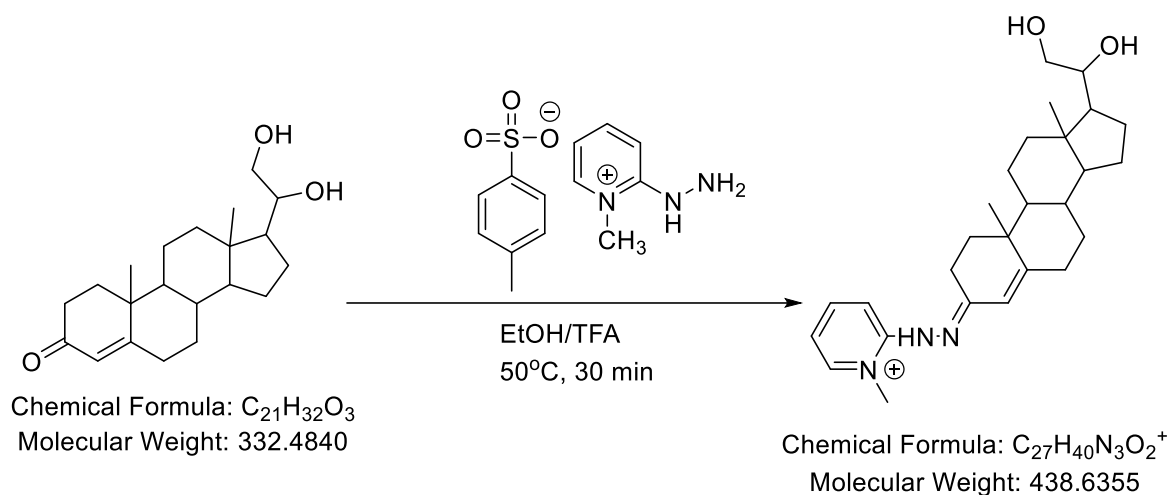


Figure 6-4 The reaction of DsT2 with HMP, to produce the target stable derivative.

The tagging reaction is catalysed by acid and involves the reaction of a carbonyl group on the steroid with the hydrazine moiety of HMP resulting in a stable hydrazone with a 106 Dalton increase in the molecular weight of the starting steroid as a result of the loss of one molecule of H_2O during the process. It is envisaged that this will result in a Steroid-HMP derivative which will ionise better than the original steroid because the tag carries a permanent positive charge which will aid the ionisation of the tagged derivative in positive mode ESI mass spectroscopy.

6.2 Materials and methods

1H spectra were measured on a Bruker DPX-400 MHz spectrometer with chemical shifts given in ppm (δ values), relative to proton and carbon traces in solvent. Coupling constants are reported in Hz. Mass spectra were obtained on an Exactive Orbitrap mass spectrometer. Anhydrous solvents were obtained from a Puresolv purification system, from Innovative Technologies, or purchased as such from Aldrich. Rotary evaporators were used to produce dry samples in preparation for analysis by removing water or organic solvents. Melting points were

recorded on a Reichert hot stage microscope, and are uncorrected. Chromatography was carried out using 200Å, 400 mesh silica gel.

6.2.1 Chemicals and reagents

All commercially available solvents and reagents were obtained from Sigma-Aldrich, UK. All Steroid standards, 5 α -Pregnane-21-ol-3, 20,-dione, (DsTd1), 4-Pregnene-20 β ,21-diol-3-one, (DsTd2), and 5 α -Pregnane-3 β -ol-20-one, (DsTd3) were obtained from Ikapharm Ramat-gan P.O.B. 31, Israel, while 3 β -Hydroxy-5 α -androstan-17-one, (DsTd4) was obtained from The British Drug House LTD (BDH) Poole England, and were used as supplied without further purification. All other intermediates were synthesized in the laboratory as described in the experimental section.

6.2.2 Synthesis of Tagging Agents

HMP was synthesised as its para toluene sulfonate salt in one step from 2-fluoro-1-methylpyridin-1-ium 4-methylbenzenesulfonate utilizing a slight modification of the method reported by Higashi *et al* [209]. The general scheme for the reaction is depicted below (Figure 6-5).

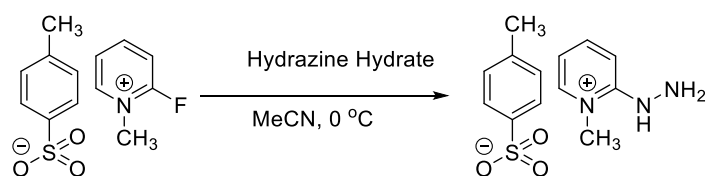


Figure 6-5: Schematic depicting the reaction for the synthesis of HMP.

The HMP analogue, 3MHMP, and its deuterated analogue 3MHMP-d₃ were synthesised in three synthetic steps from 2-fluoro-3-methylpyridine utilizing the method reported by *Higashi et al.* with some modifications [209]. In order to synthesize the deuterated analogue of HMP, 3MHMP was initially synthesized to validate the synthetic route to 3MHMP-d₃ as the deuterated sulfonate required for the synthesis, 2-fluoro-3-methyl-1-(methyl d₃)pyridin-1-ium-4-methyl benzenesulfonate, is not commercially available and needed to be synthesized from 2-fluoro-3-methyl pyridine using a modification of the method reported by *Fujimoto et al* [210]. Methyl-d₃ 4-methyl benzenesulfonate was synthesized utilizing the method reported by *Shields et al* [211]. This was then reacted with tert-butylhydrazinecarboxylate in a modification of the method reported by *Corr et al* to give N-Boc protected 3MHMP-d₃ [212]. Deprotection with TFA gave the desired product 3MHMP-d₃. The general scheme for the overall reaction is depicted below (Figure 6-6).

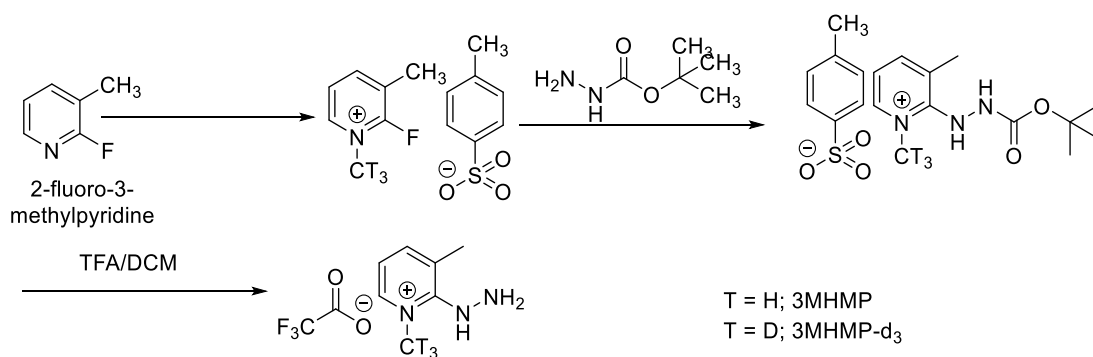
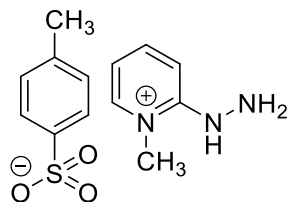


Figure 6-6 Schematic depicting the overall reaction scheme for the synthesis of HMP analogues 3MHMP and 3MHMP-d₃.

A detailed description of the synthetic procedures utilized to afford the tagging compounds is reported below.

6.2.2.1 2-hydrazinyl-1-methylpyridin-1-ium-methylbenzenesulfonate [209, 213].



Hydrazine hydrate solution (80%, 132 mL) in MeCN (30 mL) was added to 2-fluoro-1methyl pyridinium p-toluenesulfonate (FMP-TS) (300 mg) in MeCN (6 mL) at 0 °C after stirring for 10 min at 0 °C and then maintained for 20 min at room temperature under N₂.

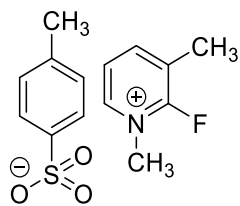
The residue was dissolved for a second time in MeCN (2 mL) after this resulting mixture was concentrated. Following this, it was filtered, and the crude product was recrystallized (twice) from MeCN–ethyl acetate (5:1, v/v) to give colorless needles of HMP (98 mg) as a toluenesulfonate salt which could be stored at 4 °C for up to 6 months.

mp: 133–134 °C

ESI-MS: m/z 124.3 [M+H⁺]

¹H NMR (500 MHz, DMSO-*d*₆) δ 8.05 (d, *J* = 6.6 Hz, 1H), 7.92 (t, *J* = 8.0 Hz, 1H), 7.52 (d, *J* = 9.0 Hz, 1H), 7.48 (d, *J* = 7.8 Hz, 2H), 7.11 (d, *J* = 7.7 Hz, 2H), 6.82 (t, *J* = 6.6 Hz, 1H), 4.70 s, 3H), 2.29 (s, 3H).

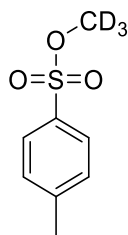
6.2.2.2 2-fluoro-1,3-dimethylpyridin-1-ium 4-methylbenzenesulfonate [210].



Methyl-*p*-toluenesulfonate 0.335 g (1.79 mmol.) was added to 2-fluoro-3-methylpyridine 0.200 mg (1.79 mmol.), heating the resultant mixture for 30 minutes at 100° C by microwave irradiation and then cooling the heated mixture to yield 0.393 g of crystalline 2-fluoro-1,3-dimethylpyridinium tosylate (73%). This crystalline starting material is subsequently washed with ether then dried and used without further purification.

¹H NMR (500 MHz, DMSO-*d*₆) δ 8.73 (t, *J* = 5.2 Hz, 1H), 8.60 (t, *J* = 7.6 Hz, 1H), 7.87 (dd, *J* = 7.8, 6.2 Hz, 1H), 7.47 (d, *J* = 7.8 Hz, 2H), 7.11 (d, *J* = 7.8 Hz, 2H), 4.19 (d, *J* = 4.1 Hz, 3H), 2.42 (d, *J* = 1.6 Hz, 3H), 2.29 (s, 3H).

6.2.2.3 Methyl-*d*₃ 4-methylbenzenesulfonate [211].



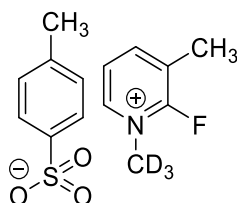
A mixture of methanol-*d*₃, 2 mL, 49.2 mmol, and Triethylamine, 7.6 mL, 54.49 mmol was added dropwise to a cooled, 0 °C, solution of *p*-toluenesulfonyl chloride, 10.32 g, 54.49 mmol, in toluene, 10 mL, over a period of 10 minutes. The resulting reaction mixture was then stirred at 0 °C for a further 1 hour before being filtered through a pad of celite. The filter pad was washed with a further 20 mL of ice cold toluene. The filtrate was concentrated under reduced

pressure and purified by flash column chromatography eluting with ethyl acetate in Hexane (25%) to give the desired product, 2.403 g, 12.71 mmol, 23%.

ESI-MS: m/z 190.1 $[M+H^+]$

1H NMR (500 MHz, $DMSO-d_6$) δ 7.79 (d, $J = 8.4$ Hz, 2H), 7.50 (d, $J = 8.1$ Hz, 2H), 2.44 (s, 3H).

6.2.2.4 2-fluoro-3-methyl-1-(methyl- d_3)pyridin-1-ium 4-methylbenzenesulfonate [210].



Methyl- d_3 *p*-toluenesulfonate 0.221 g (1.169 mmol.) was added to 2-fluoro-3-methylpyridine 0.130 mg (1.169 mmol.), heating the resultant mixture for 30 minutes at 100° C by microwave irradiation and then cooling the heated mixture to yield 0.221 g of crystalline 2-fluoro-3-methyl-1-methyl- d_3 pyridinium tosylate (64%). This crystalline starting material was subsequently washed with ether then dried and used without further purification.

mp: 119-120 °C

ESI-MS: m/z 129.2 $[M+H^+]$

1H NMR (500 MHz, $DMSO-d_6$) δ 8.72 (ddd, $J = 6.1, 4.1, 1.7$ Hz, 1H), 8.61 (dd, $J = 8.5, 6.8$ Hz, 1H), 7.88 (dd, $J = 7.8, 6.2$ Hz, 1H), 7.50 – 7.44 (m, 2H), 7.11 (d, $J = 7.8$ Hz, 2H), 2.43 (d, $J = 1.6$ Hz, 3H), 2.29 (s, 3H).

6.2.2.5 2-[2-(tert-butoxycarbonyl)hydrazinyl]-1,3-dimethylpyridinium] (trifluoroacetate) [212].



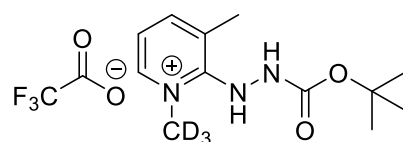
tert-butyl hydrazinecarboxylate, 0.089 g, 0.67 mmol, was added to a solution of 2-fluoro-1,3-dimethylpyridin-1-ium 4-methylbenzenesulfonate, 0.01 g, 0.336 mmol, in acetonitrile, 5 mL, and stirred at room temperature for 1 hour and then filtered through a pad of potassium carbonate. The filter pad was then washed further with acetonitrile, 20 mL. The filtrate was concentrated under reduced pressure and purified by HPLC to give the desired product 0.038 g, 27%.

mp: 160 °C

ESI-MS: m/z 238.2 [M+H⁺]

¹H NMR (500 MHz, DMSO-*d*₆) δ 9.81 (s, 1H), 9.27 (s, 1H), 8.30 (d, J = 6.5 Hz, 1H), 8.04 (d, J = 7.5 Hz, 1H), 7.25 (t, J = 6.9 Hz, 1H), 4.00 (s, 3H), 2.39 (s, 3H), 1.43 (s, 9H).

6.2.2.6 2-[2-(tert-butoxycarbonyl)hydrazinyl]-3-methyl-1-(methyl-*d*₃)pyridinium] (trifluoroacetate) [212].



tert-butyl hydrazinecarboxylate, 0.198 g, 1.5 mmol, was added to a solution of 2-fluoro-3-methyl-1-(methyl-d₃)pyridin-1-ium 4-methylbenzenesulfonate, 0.225 g, 0.75 mmol, in acetonitrile, 5 mL, and stirred at room temperature for 1 hour and then filtered through a pad of potassium carbonate. The filter pad was then washed further with acetonitrile, 20 mL. The filtrate was concentrated under reduced pressure and purified by HPLC to give the desired product 0.095 g, 30%.

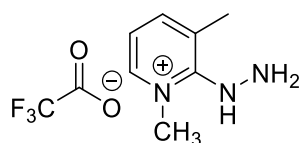
mp: 153 °C

ESI-MS: m/z 241.2 [M+H⁺]

¹H NMR (500 MHz, DMSO-*d*₆) δ 9.80 (s, 1H), 9.27 (s, 1H), 8.29 (d, *J* = 6.4 Hz, 1H), 8.04 (d, *J* = 7.6 Hz, 1H), 7.25 (t, *J* = 7.0 Hz, 1H), 2.39 (s, 3H), 1.43 (s, 9H).

*contains ~ 25% of the *p*-toluenesulfonate salt. ¹H NMR (500 MHz, DMSO-*d*₆) δ 7.50 – 7.46 (m, 2H), 7.11 (d, *J* = 7.9 Hz, 2H), 2.29 (s, 3H).

6.2.2.7 2-hydrazinyl-1,3-dimethylpyridinium (trifluoroacetate).



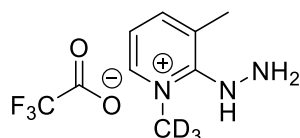
To a solution of 2-[2-(tert-butoxycarbonyl)hydrazinyl]-1,3-dimethylpyridinium] (trifluoroacetate), 0.038g, 0.082 mmol, in DCM, 3 mL, TFA 300 μL was added and the reaction stirred at 100 °C for 2 hours then concentrated and purified by HPLC to give the desired product, 0.015g, 50 % as a white solid.

¹H NMR (500 MHz, DMSO-*d*₆) δ 12.33 (s, 1H), 9.48 (s, 1H), 8.34 (s, 1H), 8.07 (s, 1H), 7.30 (s, 1H), 4.09 (s, 3H), 2.39 (s, 3H).

ESI-MS: m/z 138 [M+H⁺]

mp: 132 °C

6.2.2.8 2-hydrazinyl-3-methyl-1-(methyl-d3)pyridinium (trifluoroacetate).



To a solution of 2-[2-(tert-butoxycarbonyl)hydrazinyl]-3-methyl-1-(methyl-d3)pyridinium] (trifluoroacetate), 0.095 g, 0.20 mmol, in DCM, 3 mL, TFA 300 μ L was added and the reaction stirred at 100 °C for 2 hours then concentrated and purified by HPLC to give the desired product, 0.050 g, 66 % as a white solid.

mp: 110 °C

¹H NMR (400 MHz, DMSO-*d*₆) δ 12.33 (s, 1H), 9.47 (s, 1H), 8.39 (s, 1H), 8.13 (s, 1H), 7.37 (s, 1H), 2.39 (s, 3H).

*contains ~ 25% of the *p*-toluenesulfonate salt. ¹H NMR (400 MHz, DMSO-*d*₆) δ 7.50 – 7.46 (m, 2H), 7.11 (d, *J* = 7.8 Hz, 2H), 2.29 (s, 3H).

6.3 Derivatisation of the steroids

A solution of HMP, (1 mg/mL), in ethanol was first prepared by dissolving 1 mg of the synthesised HMP in ethanol (1mL). Standard solutions of the 4 steroid standards were also prepared with a final concentration of 0.1 μ g/mL each by dissolving 1 mg of standard steroid in 1 mL of ethanol and then transferring 0.1 mL of this solution into a separate vial containing 0.9 mL of

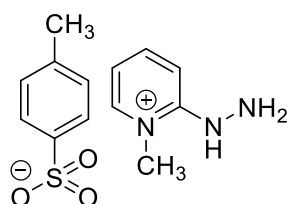
ethanol to give a concentration of 10 µg/ mL. This dilution was repeated two more times to achieve a final concentration of 0.1µg/mL To a vial containing 50 µL of each of the standard steroid solutions, (0.1 µg/mL), 50 µL of the HMP solution, (1 mg/mL), was added followed by 16.7 µL of TFA and the resulting mixtures vortexed and heated at 50 °C for 30 minutes. The reactions were then blown to dryness under a stream of nitrogen and re-dissolved in 1 mL of mobile phase, (MeCN:H₂O, 1:3 buffered with 0.01% FA), and then analyzed by LCMS.

6.4 Results

6.4.1 Characterization of synthesised compounds.

Synthesised compounds were isolated and analyzed by various methods to confirm that the target compounds were successfully synthesised. A summary of the characterization for each of the synthesised compounds is presented below.

6.4.1.1 2-hydrazinyl-1-methylpyridin-1-ium 4-methylbenzenesulfonate.



The proton NMR of the salt showed a combination of the AA'BB' and ABC systems as expected for the salt. The ABC system for the N-methyl-2-substituted pyridinium compound at δ_{H} (ppm) 8.05 (d, $J = 6.6$ Hz, 1H), 7.92 (t, $J = 8.0$ Hz, 1H), 7.52 (d, $J = 9.0$ Hz, 1H) the proton at 6.82 (t, $J = 6.6$ Hz, 1H) being from the proton at position-5, meta to the pyridinium "N" and appears as a triplet because it is split by the protons at positions 6 and 4.

The exchangeable protons on the hydrazine moiety were not seen in the spectrum. The AA' BB' system from the sulphonamide moiety appear at δ_{H} (ppm) 7.48 (d, $J = 7.8$ Hz, 2H), 7.11 (d, $J = 7.7$ Hz, 2H). The methyl group attached to the pyridinium ion was observed at δ_{H} (ppm) 3.70 (s, 3H), while the methyl on the sulphonamide was observed at 2.29 (s, 3H). This taken with the mass spectrum positively identifies the compound.

mp: 133–134 °C

^1H NMR (500 MHz, $\text{DMSO-}d_6$) δ 8.05 (d, $J = 6.6$ Hz, 1H), 7.92 (t, $J = 8.0$ Hz, 1H), 7.52 (d, $J = 9.0$ Hz, 1H), 7.48 (d, $J = 7.8$ Hz, 2H), 7.11 (d, $J = 7.7$ Hz, 2H), 6.82 (t, $J = 6.6$ Hz, 1H), 3.70 (s, 3H), 2.29 (s, 3H).

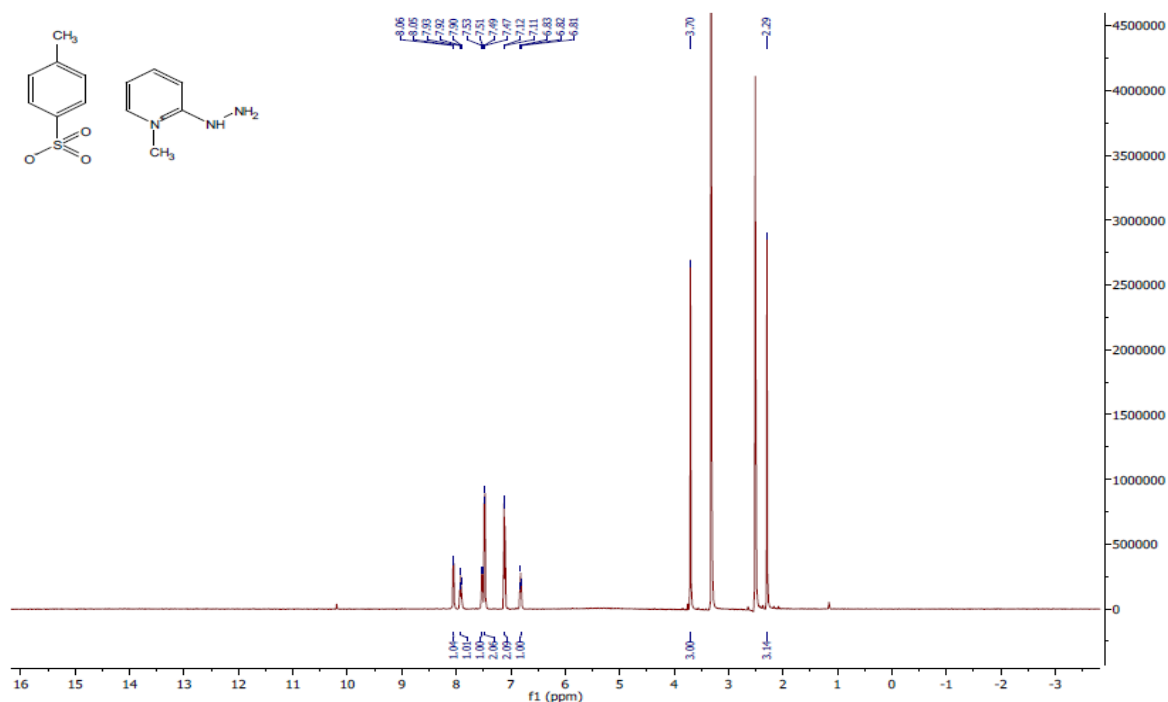


Figure 6-7 ^1H NMR Spectrum for 2-hydrazinyl-1-methylpyridin-1-ium 4-methylbenzenesulfonate

ESI-MS: m/z 124.3 [M+H⁺], 418.9 [2M+toluenesulfonate⁺]

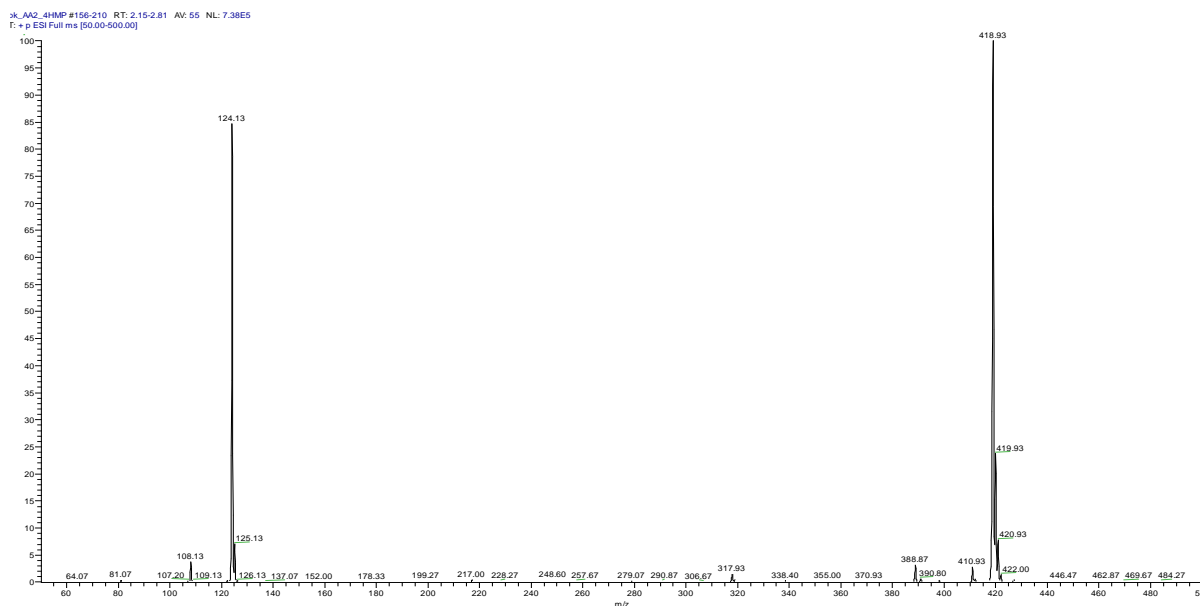
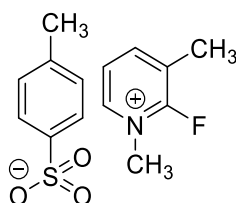


Figure 6-8 MS Spectrum for 2-hydrazinyl-1-methylpyridin-1-ium 4-methylbenzenesulfonate

6.4.1.2 2-fluoro-1, 3-dimethylpyridin-1-ium 4-methylbenzenesulfonate.



The proton NMR in DMSO of the salt showed 5 sets of aromatic protons expected. The protons at δ_H 8.73 (t, $J = 5.2$ Hz, 1H), 8.60 (t, $J = 7.6$ Hz, 1H), 7.87 (dd, $J = 7.8, 6.2$ Hz, 1H) (ppm) are for the N-methyl-2, 3-substituted pyridinium compound and the AA' BB' system from the toluene sulphonate appear at δ_H 7.47 (d, $J = 7.8$ Hz, 2H), 7.11 (d, $J = 7.8$ Hz, 2H) (ppm). The methyl groups attached to the pyridinium ion was observed at δ_H 4.19 (d, $J = 4.1$ Hz, 3H) (ppm), for the N-CH₃ group and δ_H 2.42 (d, $J = 1.6$ Hz, 3H) (ppm), for the 3-CH₃ group while the methyl on the toluene sulphonate appear at δ_H 2.29 (s, 3H). Taken together with the mass spectrum this confirms that the target compound was successfully synthesised.

^1H NMR (500 MHz, $\text{DMSO-}d_6$) δ 8.73 (t, $J = 5.2$ Hz, 1H), 8.60 (t, $J = 7.6$ Hz, 1H), 7.87 (dd, $J = 7.8, 6.2$ Hz, 1H), 7.47 (d, $J = 7.8$ Hz, 2H), 7.11 (d, $J = 7.8$ Hz, 2H), 4.19 (d, $J = 4.1$ Hz, 3H), 2.42 (d, $J = 1.6$ Hz, 3H), 2.29 (s, 3H).

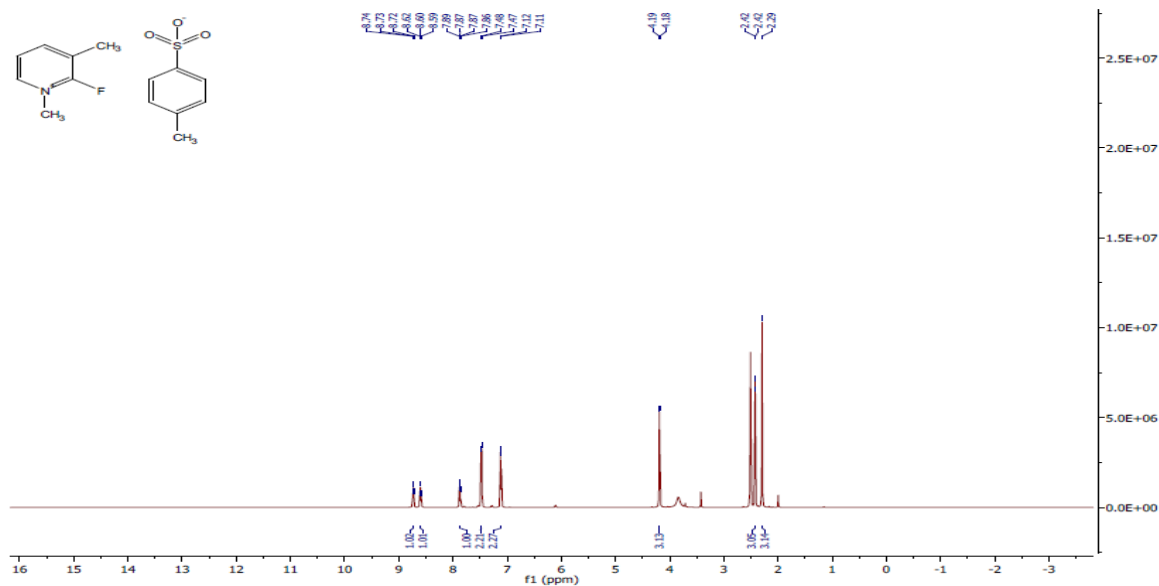


Figure 6-9 ^1H NMR Spectrum for 2-fluoro-1,3-dimethylpyridin-1-ium 4-methylbenzenesulfonate.

ESI-MS: m/z 126.1 $[\text{M}+\text{H}^+]$

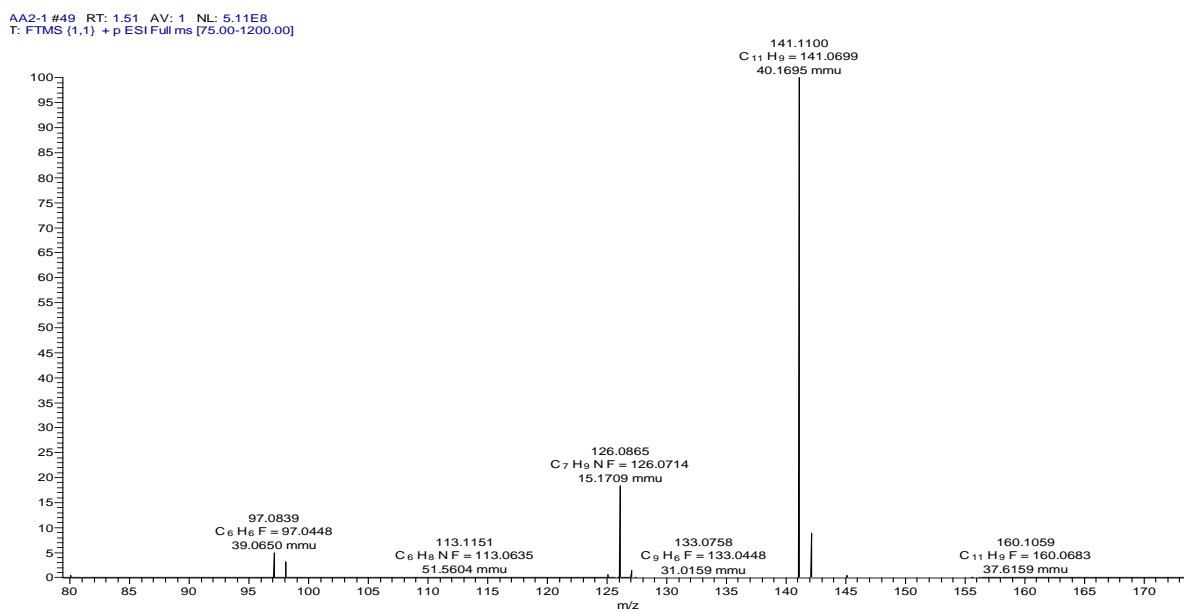
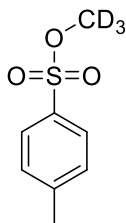


Figure 6-10 MS Spectrum for 2-fluoro-1,3-dimethylpyridin-1-ium 4-methylbenzenesulfonate.

6.4.1.3 Methyl-d3 4-methylbenzenesulfonate [211].



The proton NMR in DMSO showed 3 sets of protons, 2 aromatic and a CH₃ as expected. The protons at δ_{H}

7.79 (d, $J = 8.4$ Hz, 2H), 7.50 (d, $J = 8.1$ Hz, 2H) (ppm) are from the AA'BB' system while the protons at 2.44 (s, 3H) (ppm) are from the toluene sulphonate CH₃ group. The deuterium atoms expectedly do not show up on the NMR spectrum. This taken together with the mass spectrum positively confirms that the target compound was successfully synthesised.

¹H NMR (500 MHz, DMSO-*d*₆) δ 7.79 (d, $J = 8.4$ Hz, 2H), 7.50 (d, $J = 8.1$ Hz, 2H), 2.44 (s, 3H).

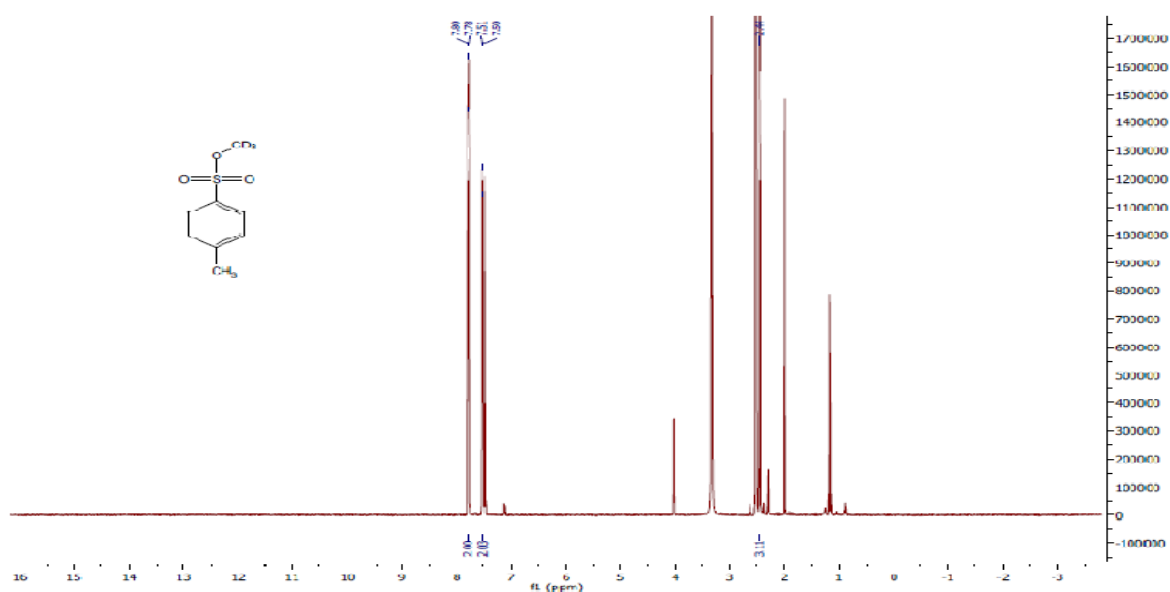


Figure 6-11 ¹H NMR Spectrum for Methyl-d3 4-methylbenzenesulfonate

ESI-MS: m/z 190.1 [M+H⁺]

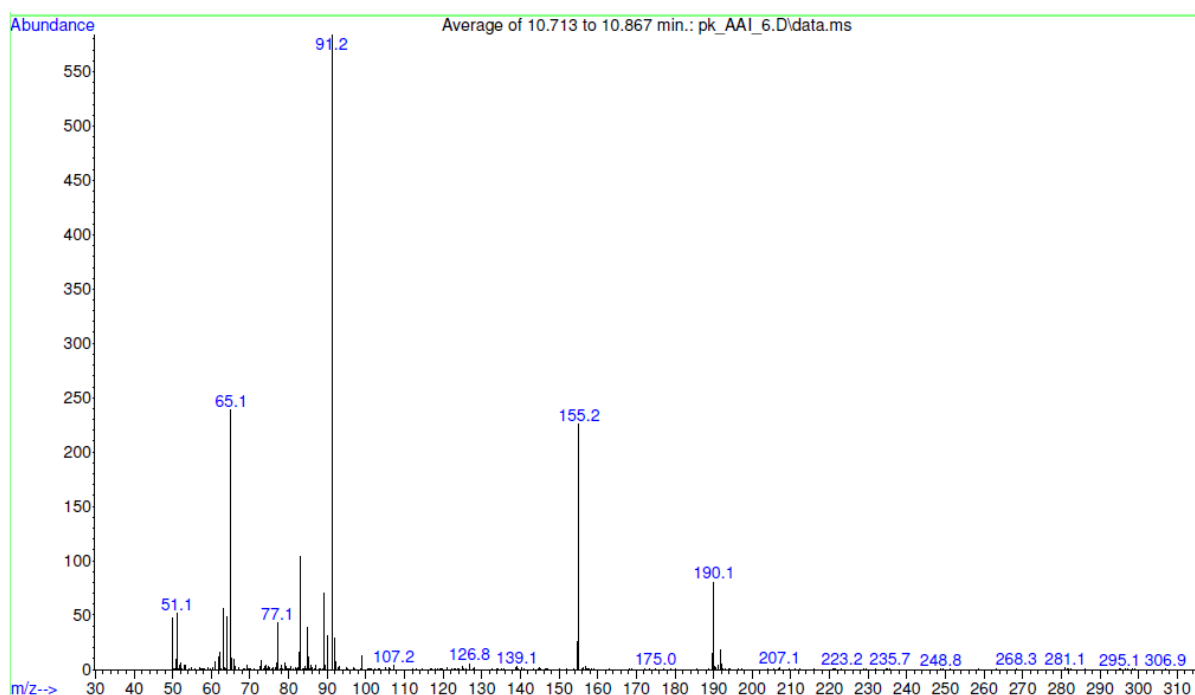
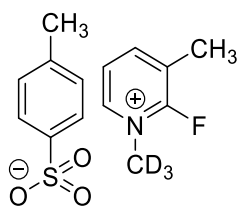


Figure 6-12 MS Spectrum for Methyl-d₃ 4-methylbenzenesulfonate

6.4.1.4 2-fluoro-3-methyl-1-(methyl-d₃)pyridin-1-ium 4-methylbenzenesulfonate.



The proton NMR in DMSO of the salt showed 5 sets of aromatic protons expected. The protons at δ_H 8.72 (ddd, $J = 6.1, 4.1, 1.7$ Hz, 1H), 8.61 (dd, $J = 8.5, 6.8$ Hz, 1H), 7.88 (dd, $J = 7.8, 6.2$ Hz, 1H) (ppm) are for the N-methyl-d₃ 1-2, 3-substituted pyridinium compound and the AA' BB' System from the toluene sulfonate appear at δ_H 7.50 – 7.44 (m, 2H), 7.11

(d, $J = 7.8$ Hz, 2H), (ppm) as a multiplet due to long range coupling from the toluene CH_3 protons and a doublet. Two methyl groups were observed at δ_{H} 2.42 – 2.40 (m, 3H), (ppm) ascribed to the 3- CH_3 group while the methyl on the toluene sulfonate appears at δ_{H} 2.29 (s, 3H), (ppm). Taken together with the mass spectrum this confirms that the target compound was successfully synthesised.

mp: 119-120 °C

^1H NMR (500 MHz, $\text{DMSO-}d_6$) δ 8.72 (ddd, $J = 6.1, 4.1, 1.7$ Hz, 1H), 8.61 (dd, $J = 8.5, 6.8$ Hz, 1H), 7.88 (dd, $J = 7.8, 6.2$ Hz, 1H), 7.50 – 7.44 (m, 2H), 7.11 (d, $J = 7.8$ Hz, 2H), 2.43 (d, $J = 1.6$ Hz, 3H), 2.29 (s, 3H).

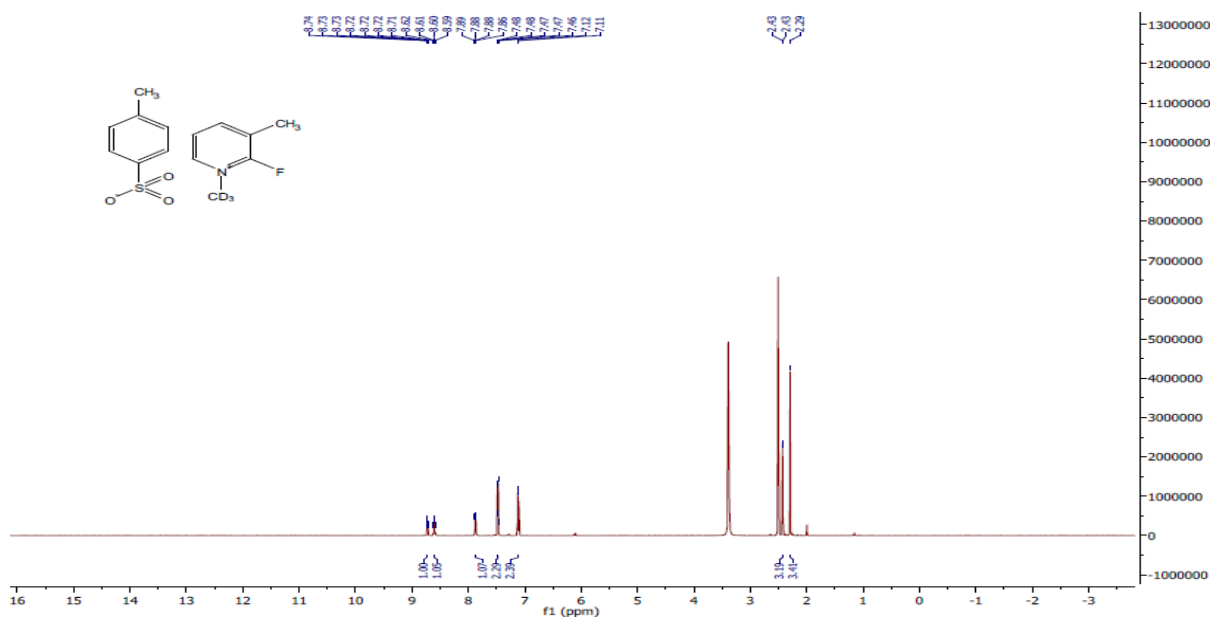


Figure 6-13 ^1H NMR Spectrum for 2-fluoro-3-methyl-1-(methyl-d3)pyridin-1-ium 4-methylbenzenesulfonate.

ESI-MS: m/z 129.2 [$\text{M}+\text{H}^+$]

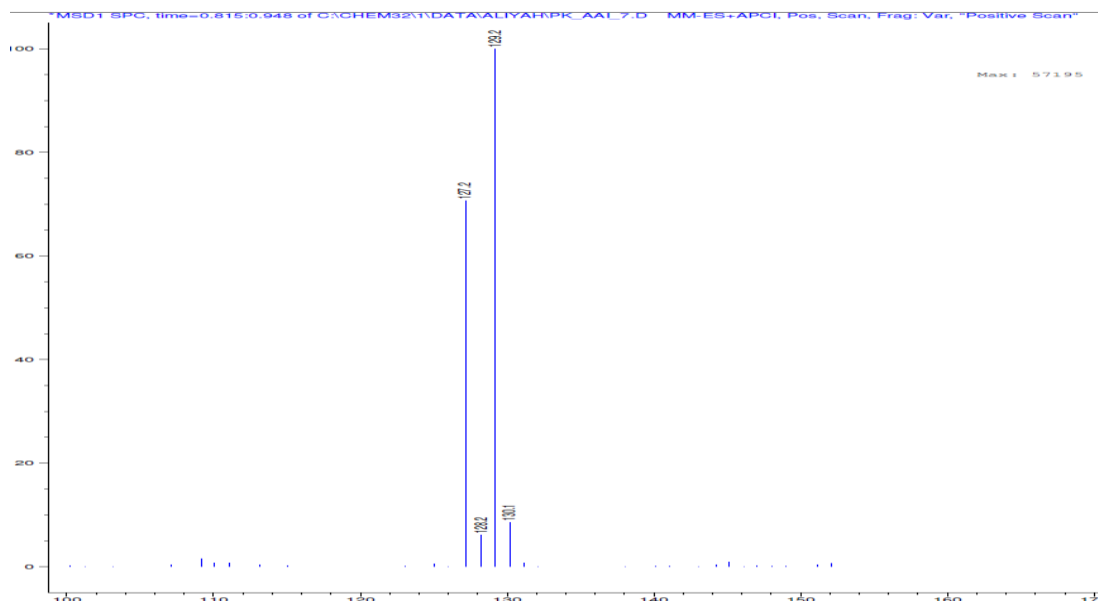
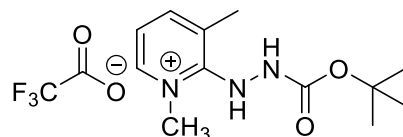


Figure 6-14 MS Spectrum for 2-fluoro-3-methyl-1-(methyl-d3)pyridin-1-ium 4-methylbenzenesulfonate.

6.4.1.5 2-[2-(tert-butoxycarbonyl)hydrazinyl]-1,3-dimethylpyridinium] (trifluoroacetate).



The proton NMR of the synthesised compound in DMSO showed five sets of aromatic peaks in total. Three aromatic protons at δ_{H} 8.30 (d, $J = 6.5$ Hz, 1H), 8.04 (d, $J = 7.5$ Hz, 1H), 7.25 (t, $J = 6.9$ Hz, 1H), (ppm), belong to the pyridinium moiety. Two methyl signals were observed at δ_{H} 4.00 (s, 3H), N-CH₃, and 2.39 (s, 3H), 3-CH₃, (ppm) for methyl groups on the pyridinium moiety. The signal at δ_{H} 1.43 (s, 9H), (ppm), is the carbamate (C(CH₃)₃).

mp: 160 °C

¹H NMR (500 MHz, DMSO-*d*₆) δ 9.81 (s, 1H), 9.27 (s, 1H), 8.30 (d, $J = 6.5$ Hz, 1H), 8.04 (d, $J = 7.5$ Hz, 1H), 7.25 (t, $J = 6.9$ Hz, 1H), 4.00 (s, 3H), 2.39 (s, 3H), 1.43 (s, 9H).

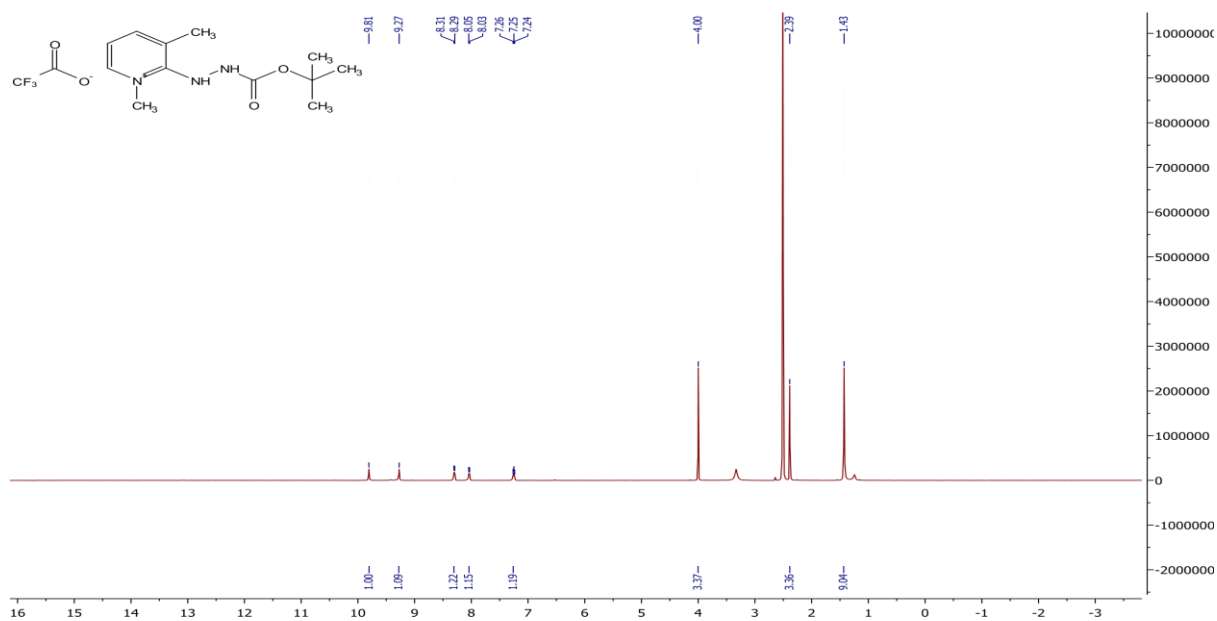


Figure 6-15 ^1H NMR Spectra for 2-[2-(tert-butoxycarbonyl)hydrazinyl]-1,3-dimethylpyridinium] (trifluoroacetate)
ESI-MS: m/z 238.2 $[\text{M}+\text{H}^+]$

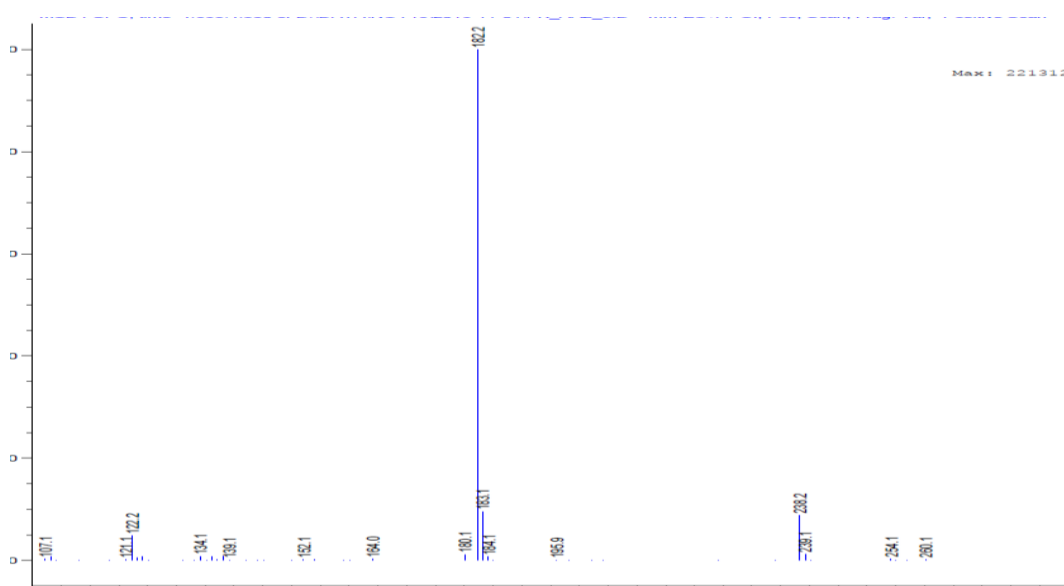
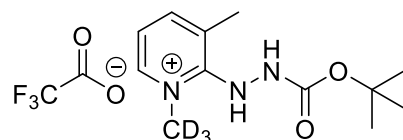


Figure 6-16 MS Spectra for 2-[2-(tert-butoxycarbonyl)hydrazinyl]-1,3-dimethylpyridinium] (trifluoroacetate)

6.4.1.6 2-[2-(tert-butoxycarbonyl)hydrazinyl]-3-methyl-1-(methyl- d_3)pyridinium] (trifluoroacetate).



The Proton NMR in DMSO showed three sets of broad aromatic peaks at δ_H 8.29 (d, $J = 6.4$ Hz, 1H), 8.04 (d, $J = 7.6$ Hz, 1H), 7.25 (t, $J = 7.0$ Hz, 1H), (ppm) belonging to the pyridinium moiety. One methyl signal was also seen at δ_H 2.39 (s, 3H), (ppm), for the 3- CH_3 methyl group and another at δ_H 1.43 (s, 9H), (ppm) belonging to the *t*-butyl group from the carbamate. Exchangeable proton signals were also observed at δ_H 9.80 (s, 1H), 9.27 (s, 1H), (ppm), which are attributed to the NH protons on the hydrazine substituent. As expected no signals were observed for the N-CD_3 . Together with the mass spectrum this convincingly indicates that the target molecule was successfully synthesised.

mp: 153 °C

^1H NMR (500 MHz, $\text{DMSO-}d_6$) δ 9.80 (s, 1H), 9.27 (s, 1H), 8.29 (d, $J = 6.4$ Hz, 1H), 8.04 (d, $J = 7.6$ Hz, 1H), 7.25 (t, $J = 7.0$ Hz, 1H), 2.39 (s, 3H), 1.43 (s, 9H).

*contains ~ 25% of the *p*-toluenesulfonate salt. ^1H NMR (500 MHz, $\text{DMSO-}d_6$) δ 7.50 – 7.46 (m, 2H), 7.11 (d, $J = 7.9$ Hz, 2H), 2.29 (s, 3H).

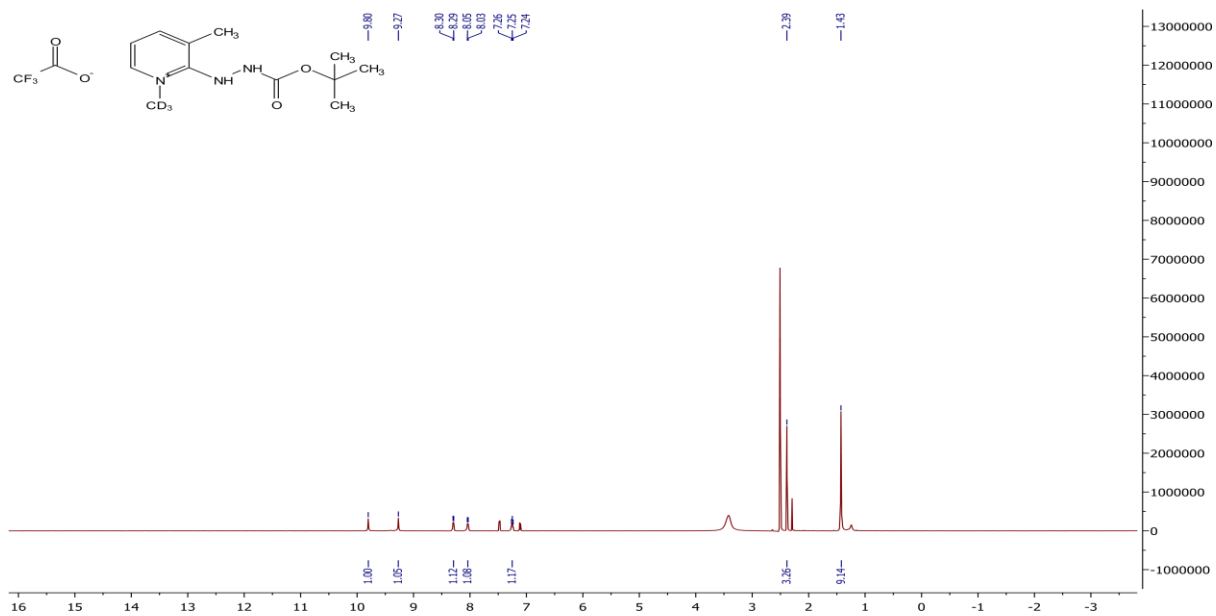


Figure 6-17 ¹H NMR Spectrum for 2-[2-(tert-butoxycarbonyl)hydrazinyl]-3-methyl-1-(methyl-d₃)pyridinium](trifluoroacetate)

ESI-MS: m/z 241.2 [M+H⁺]

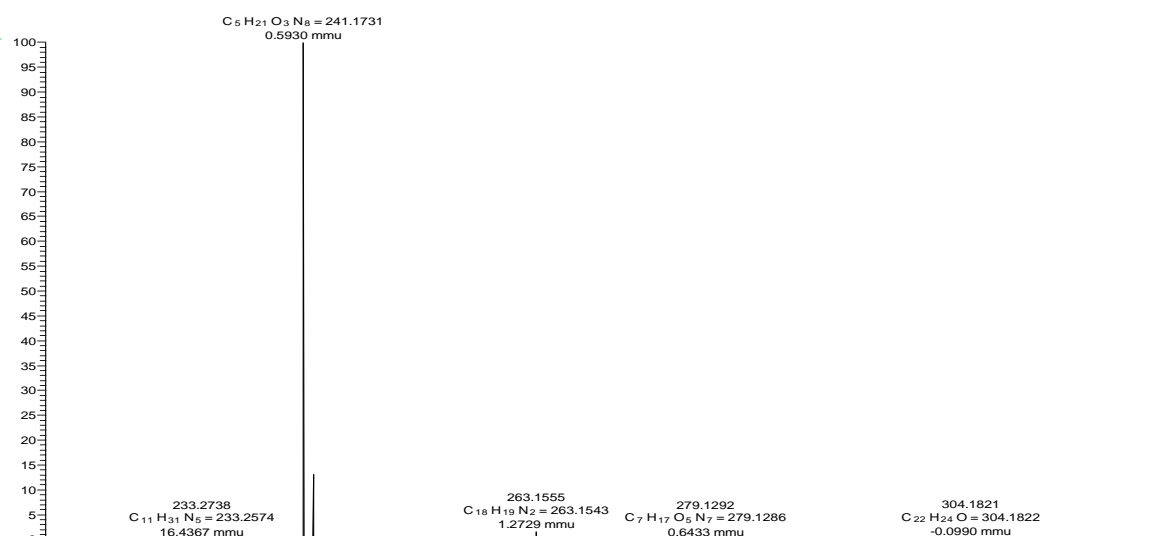
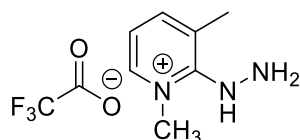


Figure 6-18 MS Spectrum for 2-[2-(tert-butoxycarbonyl)hydrazinyl]-3-methyl-1-(methyl-d₃)pyridinium] (trifluoroacetate)
6.4.1.7 2-hydrazinyl-1,3-dimethylpyridinium (trifluoroacetate).



The proton NMR for the final compound in DMSO also showed 3 sets of broad aromatic peaks at δ_{H} 8.34 (s, 1H), 8.07 (s, 1H), 7.30, (ppm) belonging to the pyridinium moiety. Two methyl signals were also seen at δ_{H} 4.09 (s, 3H), N-CH₃ and 2.39 (s, 3H) 3-CH₃ for the methyl groups. Exchangeable proton signals were also observed at δ_{H} 12.33 (s, 1H), 9.48 (s, 1H) which are attributed to the NH protons on the hydrazine substituent. Together with the mass spectrum this convincingly indicates that the target molecule was successfully synthesised.

mp: 132 °C

¹H NMR (500 MHz, DMSO-*d*₆) δ 12.33 (s, 1H), 9.48 (s, 1H), 8.34 (s, 1H), 8.07 (s, 1H), 7.30 (s, 1H), 4.09 (s, 3H), 2.39 (s, 3H).

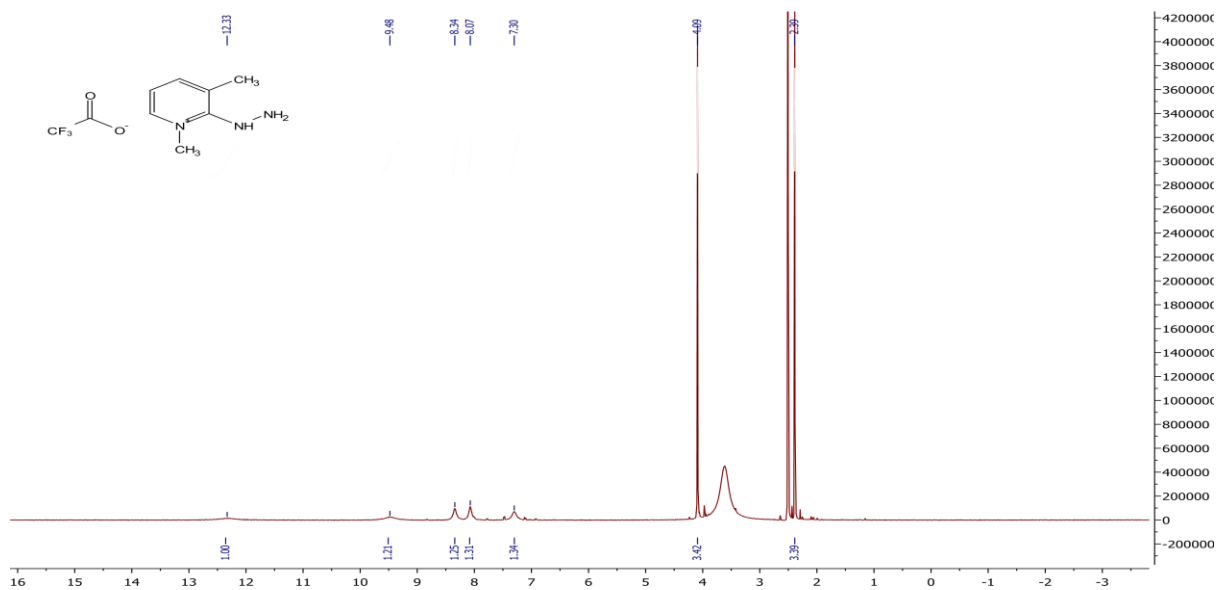


Figure 6-19 ¹H NMR Spectrum for 2-hydrazinyl-1,3-dimethylpyridinium (trifluoroacetate)

ESI-MS: m/z 138 [M+H⁺]

!T: 1.37 AV: 1 NL: 5.55E6
+ p ESI:Full lock ms [75.00-1200.00]

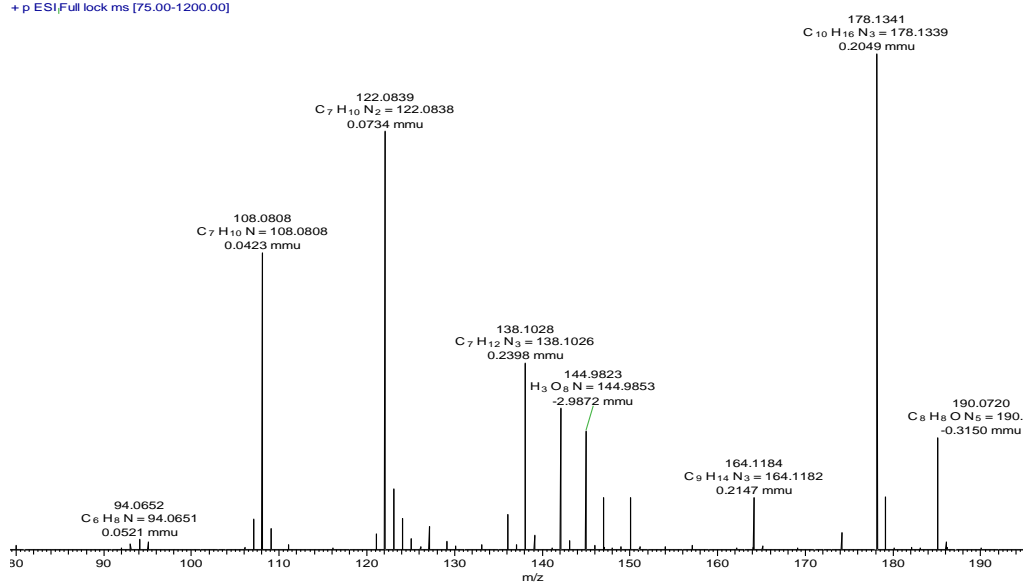
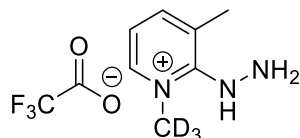


Figure 6-20 MS Spectrum for 2-hydrazinyl-1,3-dimethylpyridinium (trifluoroacetate)

6.4.1.8 2-hydrazinyl-3-methyl-1-(methyl-d3)pyridinium (trifluoroacetate).



The Proton NMR in DMSO showed three sets of broad aromatic peaks at δ_{H} 8.39 (s, 1H), 8.13 (s, 1H), 7.37 (s, 1H), (ppm) belonging to the pyridinium moiety. One methyl signal was also seen at δ_{H} 2.39 (s, 3H), (ppm), for the 3-CH₃ methyl. Exchangeable proton signals were also observed at δ_{H} 12.33 (s, 1H), 9.47 (s, 1H), (ppm), which are attributed the NH protons on the hydrazine substituent. As expected no signals were observed for the N-CD₃. Together with the mass spectrum this convincingly indicates that the target molecule was successfully synthesised.

mp: 110 °C

¹H NMR (400 MHz, DMSO-*d*₆) δ 12.33 (s, 1H), 9.47 (s, 1H), 8.39 (s, 1H), 8.13 (s, 1H), 7.37 (s, 1H), 2.39 (s, 3H).

*contains ~ 25% of the *p*-toluenesulfonate salt. ¹H NMR (400 MHz, DMSO-*d*₆) δ 7.50 – 7.46 (m, 2H), 7.11 (d, *J* = 7.8 Hz, 2H), 2.29 (s, 3H).

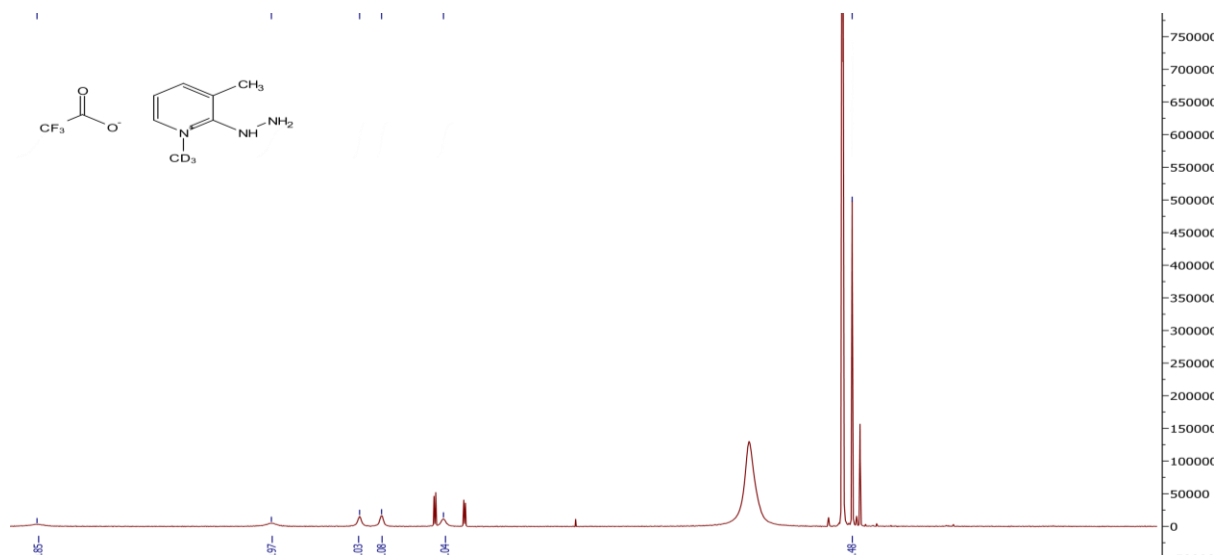


Figure 6-21 ^1H NMR Spectrum for 2-hydrazinyl-3-methyl-1-(methyl-d3)pyridinium (trifluoroacetate)

ESI-MS: m/z 141.1 $[\text{M}+\text{H}^+]$

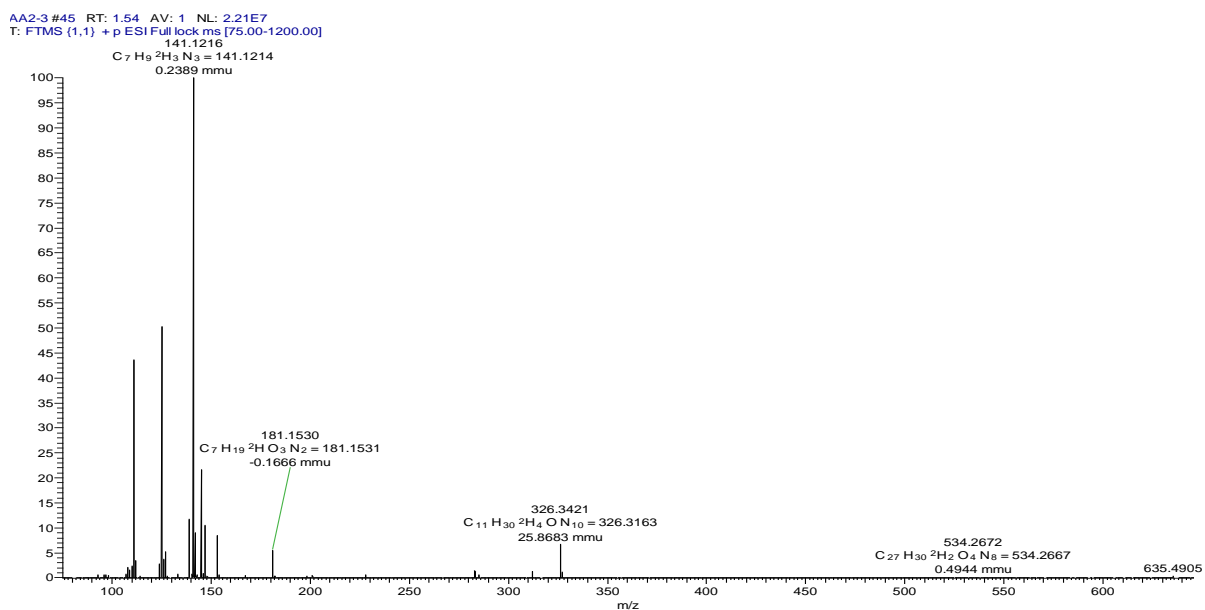
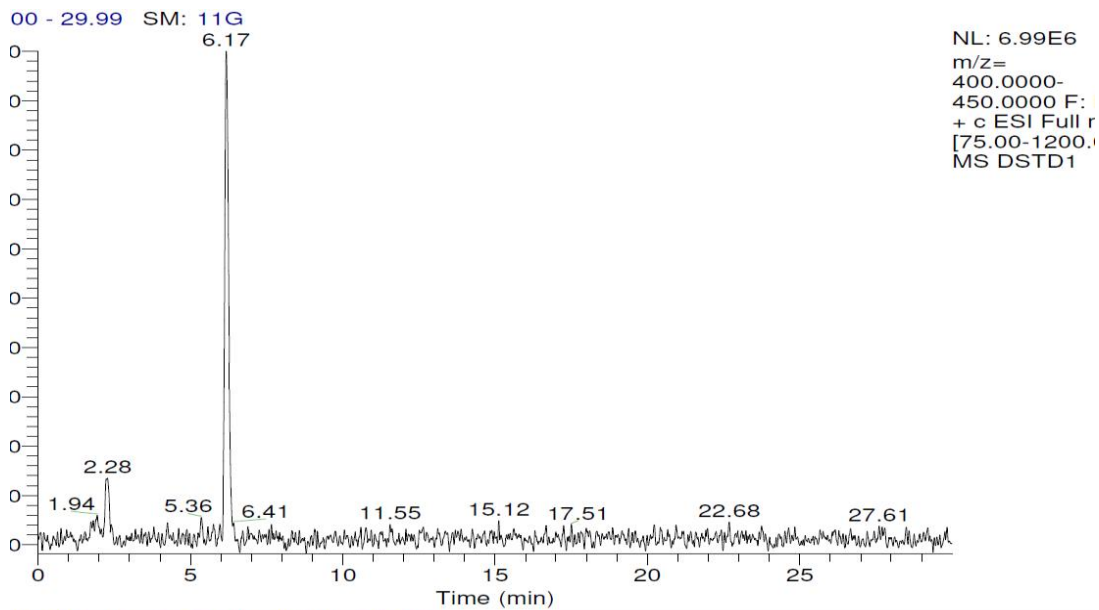


Figure 6-22 MS Spectrum for 2-hydrazinyl-3-methyl-1-(methyl-d3)pyridinium (trifluoroacetate)

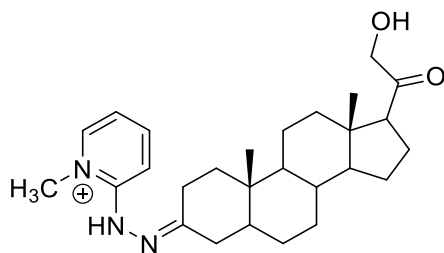
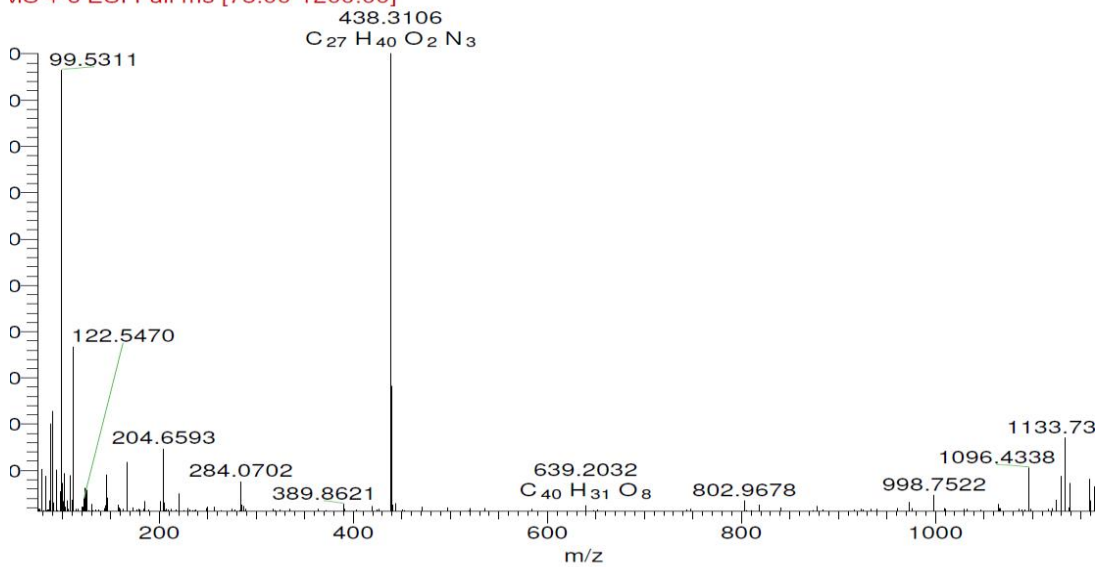
6.5 Formation of derivatives of the steroids

In order to check the success of the synthesis, the synthesised tagging agents were utilized in derivatisation reactions using the method outlined above (section 6.3). The reactions were

then blown to dryness under a stream of nitrogen and re-dissolved in 1 mL of mobile phase, (MeCN:H₂O, 1:3 buffered with 0.01% FA), and then analyzed by LCMS. In order to test the synthesis of the HMP derivatisation of some keto-steroids were prepared. Figures 6-23 to 6-26 show extracted ion traces and mass spectra for the HMP derivatives showing that the derivatisation agent had both been successfully prepared and efficiently performed the derivatisation. Unfortunately, it was not possible to observe any derivative formation from the deuterated MHMP-d₃ which could be attributed to the inability to fully separate the deuterated MHMP-d₃ target from other impurities arising from the reaction.

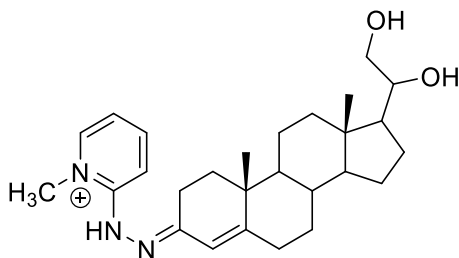
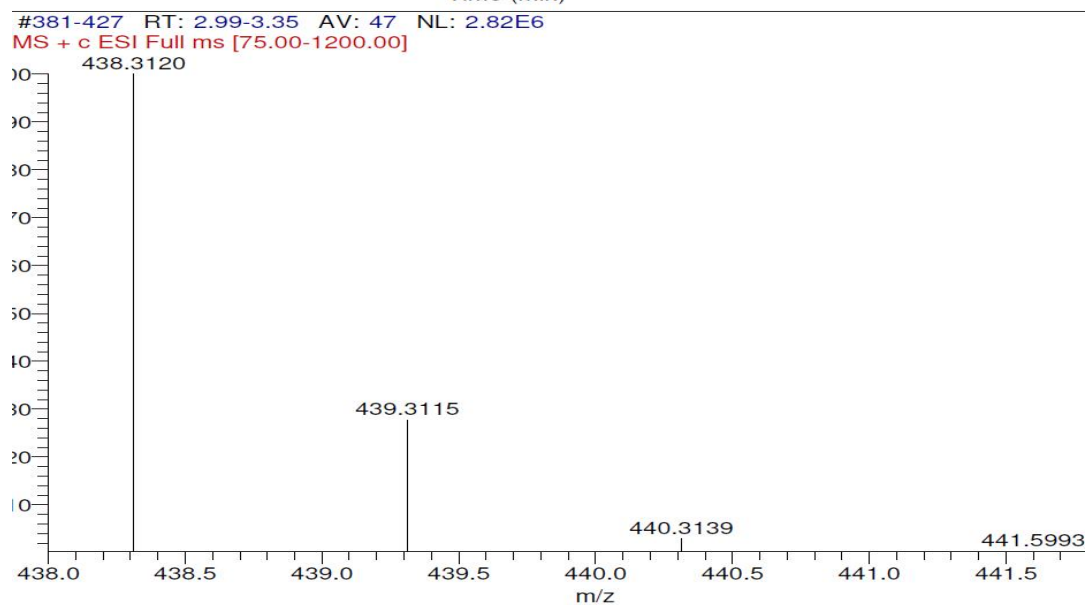
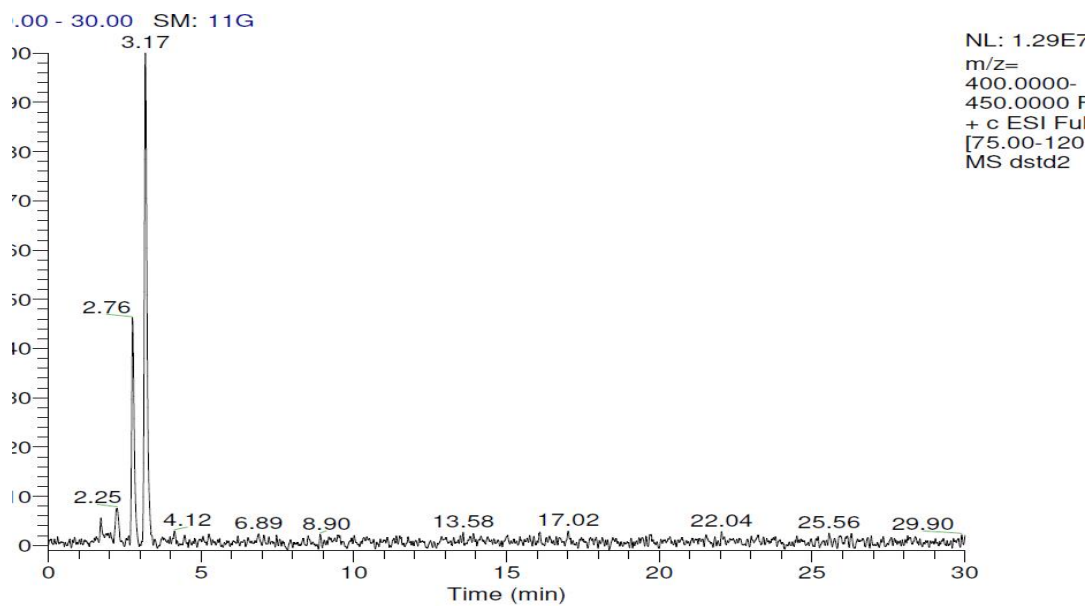


1 #786 RT: 6.17 AV: 1 NL: 5.57E6
MS + c ESI Full ms [75.00-1200.00]



Chemical Formula: C₂₇H₄₀N₃O₂⁺
Molecular Weight: 438.64
DsTd1-HMP Derivative

Figure 6-23 Extracted ion Chromatograph for DsTD1 derivatisation with HMP.

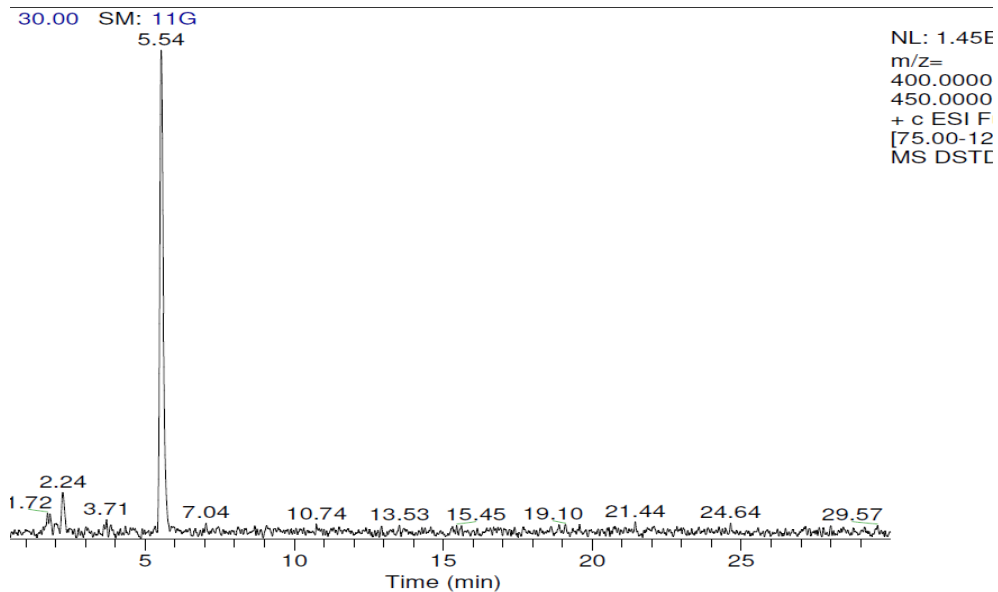


Chemical Formula: $C_{27}H_{40}N_3O_2^+$

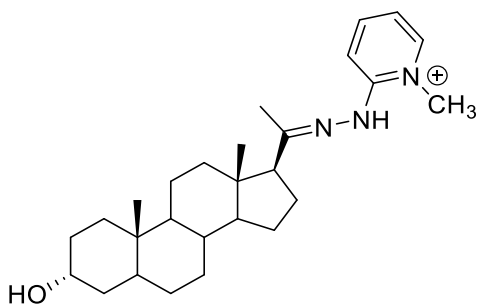
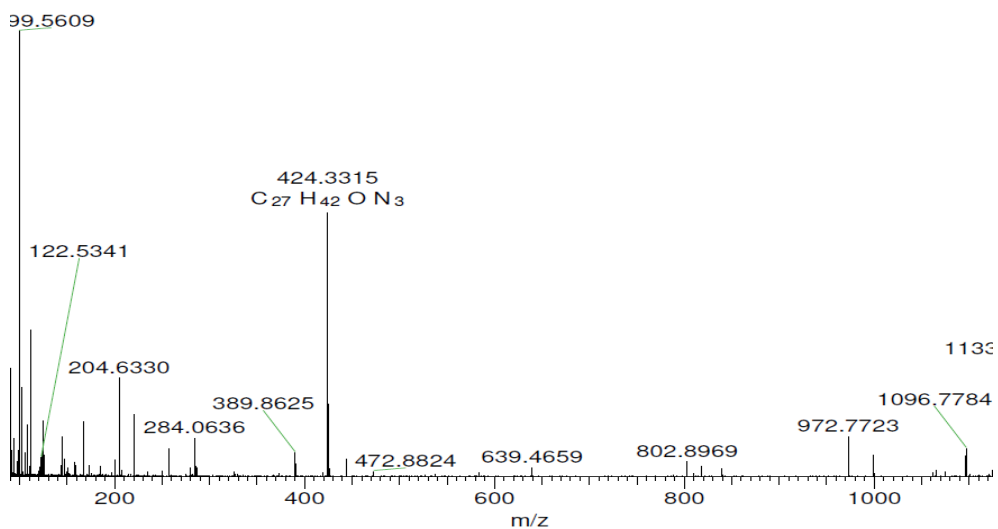
Molecular Weight: 438.64

DsTd2-HMP Derivative

Figure 6-24 Extracted ion Chromatograph for DsTD2 derivatisation with HMP.

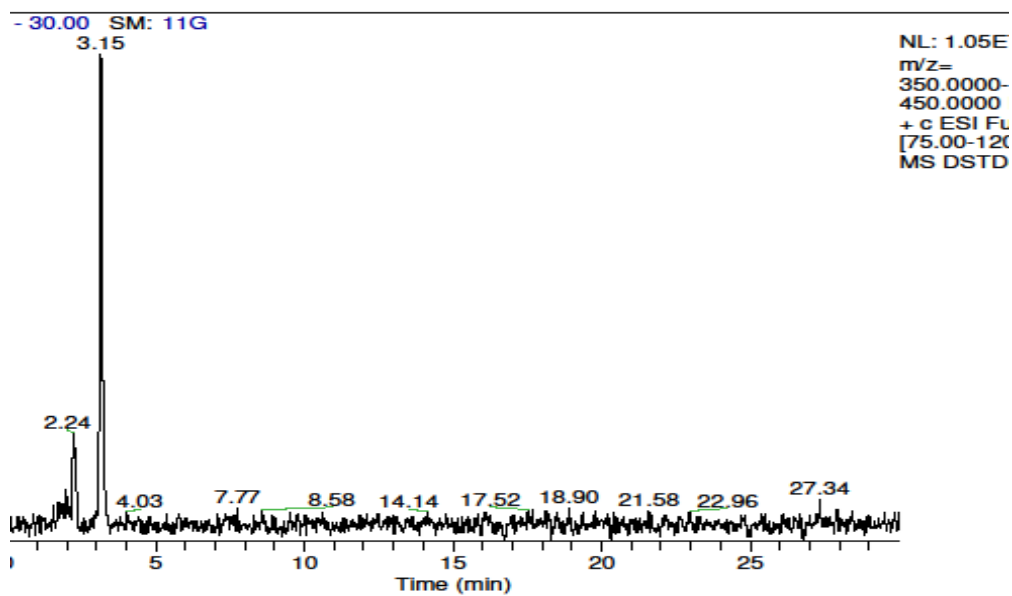


71-727 RT: 5.26-5.70 AV: 57 NL: 5.58E6
 + c ESI Full ms [75.00-1200.00]

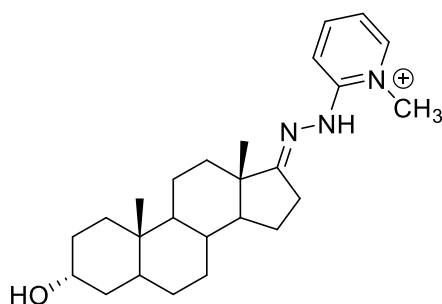
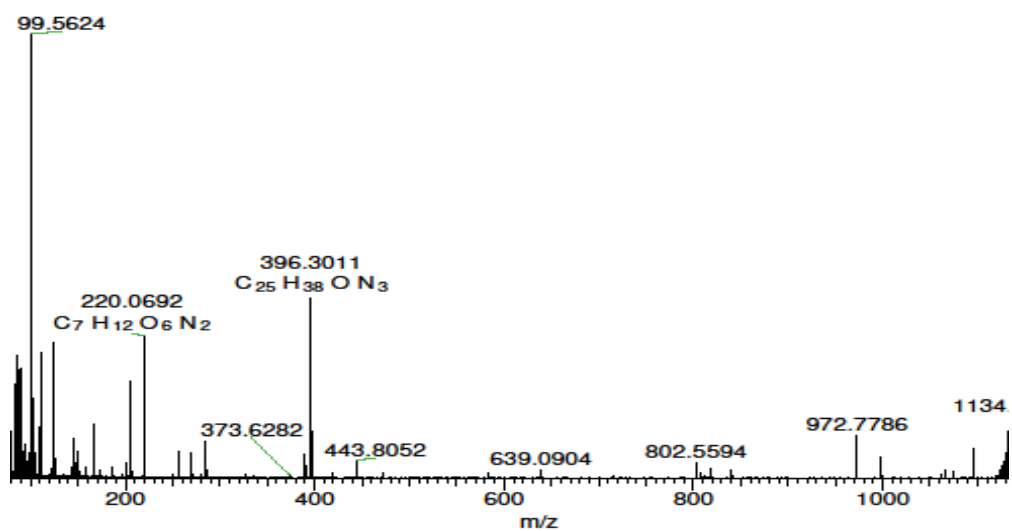


Chemical Formula: C₂₇H₄₂N₃O⁺
 Molecular Weight: 424.65
 DsTd3-HMP Derivative

Figure 6-25 Extracted ion Chromatograph for DsTD3 derivatisation with HMP.



376-421 RT: 2.95-3.30 AV: 46 NL: 5.90E6
+ c ESI Full ms [75.00-1200.00]



Chemical Formula: C₂₅H₃₈N₃O⁺

Molecular Weight: 396.60

DsTd4-HMP Derivative

Figure 6-26 Extracted ion Chromatograph for DsTD4 derivatisation with HMP.

The samples were run on an ACE 3 C18 column (150 × 3.0 mm id, 5µm) Hichrom Reading UK, and temperature of 30 °C. Isocratic elution using a mixture of water: acetonitrile (3:1), buffered with 0.01% (formic acid) FA and a flow rate of 0.4 mL/min. The injection volume and run time were 10 µL and 30 min, respectively

The synthesized HMP was passed on to a co-worker who utilized them in the derivatisation reactions. The results from this study is reported in a recently accepted publication [213].

Chapter Seven:

General Discussion and Future Work

7.0 General Discussion and Future work

7.1 Tagging Methods in the Analysis of Sugars

The PMTA derivatising agent was successful in tagging the sugars and enabling their detection in positive mode ESI LCMS. Their retention times were also greatly improved but the resolution of the peaks for the different sugars was very poor as they eluted very closely to each other. $^2\text{H}_5$ -aniline on the other hand gave better separation between the peaks for each sugar. It would therefore be interesting to synthesise deuterated analogues of PMTA such as those depicted below, (Figure 7-1), in an attempt to mimic the effect on the resolution of the different sugars observed with $^2\text{H}_5$ -aniline.

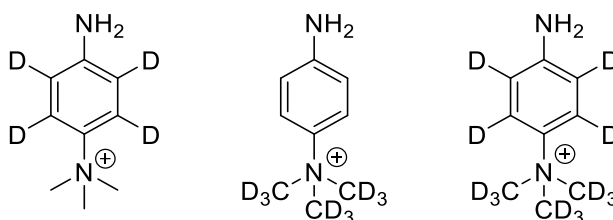


Figure 7-1 Proposed alternative deuterated analogues of PMTA.

Some preliminary work was carried out to determine whether or not the PMTA derivatising agent might be applied to the analysis of glycan chains on glycoproteins. Alpha-1 acid glycoprotein was used as a model protein. However, the initial results were inconclusive. The analysis of glycan chains on therapeutic proteins is an important area and it could be very productive to develop a sensitive and selective method for this application.

7.2 The Analysis of SCFAs in Urine in Relation to Diet

A tagging method was successfully applied to the analysis of SCFAs in urine. The method was highly selective and sensitive for acetic acid, propionic acid and butyric acid. Application of this method to subjects fed two different diets found no difference between the levels of SCFAs in urine between the two diets. There is room for improvement in the method *via* reducing background contamination with SCFAs. This could be done by carrying the work out in a clean area with dedicated pipettes in order to avoid background contamination. The method is currently very sensitive but is limited by the background contamination. It would be very valuable to be able to improve this method since there is not highly sensitive method for the analysis of SCFAs and these are important metabolic intermediates.

7.3 Analysis of oxidised fatty acids in marathon runners using Choline as a tagging agent.

The results from the marathon study were interesting because they showed some changes in the levels of oxidised fatty acids during the course of the run. These are however inconsistent with the results from existing studies. It would therefore be interesting to repeat the experiment but this time include more time points to cover the 0 to 2 hr time period over which the other studies were run to determine if the differences observed between this study and the other existing studies is due to consumption of the oxidised fatty acids being measured by further metabolism due to the longer duration of the marathon run compared with the other

study times. Also it would be necessary to include controls to see if the derivatisation procedure was actually generating some of the oxidised fatty acids by running for instance linoleic acid and determining whether or not trace amounts of oxidised acids formed during the tagging process. The use of deuterated choline to tag before and an unlabelled choline to tag after exercise samples could enable direct comparison of samples by mixing the labelled and unlabelled tagged samples.

7.4 Analysis of Sugars in IBD

The IBD study successfully identified differences in the levels of glucose between the test groups. This is important because glucose can now be further investigated as a potential diagnostic biomarker to diagnose IBD as well as to differentiate between CD and UC. The study was limited 4 sugars and could now be expanded to include more sugars. In addition, it is necessary to validate the observations by applying the method to samples from another independent cohort of patients.

7.5 Synthesis of HMP for the Derivatisation of Keto Steroids

In the keto-steroid study, both HMP and the analogue 3MHMP were successfully synthesised however the synthesis of the deuterated HMP analogue 3HMP-d3 was more challenging. The failure of the derivatisation reaction with the synthesised material failed and therefore a repeat of the synthesis of 3HMP-d3 analogue is required as well as another derivatisation experiment to investigate the failure to see

any of the derivatised product in the experiment run. The HMP was successfully applied by another PhD student for the analysis of testosterone and dihydro epiandrostene dione in saliva. It would be interesting to see if the derivatisation method could be extended to the analysis of other ketosteroids in biological fluids.

8.0 Appendix

Appendix Chapter 3

Appendix 1 Table for Peak Areas of fatty acids labelled and unlabelled.

Labelled			Unlabelled					
Acetate (1µg)	Propionate (1µg)	Butyrate (1µg)	Acetate		Propionate		Butyrate	
			Conc	Area	Conc	Area	Conc	Area
79256092	51860582	33013233	0	4850291	0	334249	0	3523041
89679649	52565698	35063075	0	5130989	0	338221	0	3730488
90948756	55410023	30725435	0	5323045	0	301046	0	3507920
51828595	38470589	18516652	0.1	6711117	0.04	3988912	0.04	12834715
55057413	36766944	19559130	0.1	7747739	0.04	4011285	0.04	13163383
53062023	37629189	19762007	0.1	7408886	0.04	3945215	0.04	13224796
51577485	28287224	20296638	0.2	11648753	0.08	7364398	0.08	19784270
51918456	28078591	19977776	0.2	11532998	0.08	6980737	0.08	21656805
52785365	28602832	17748061	0.2	11841676	0.08	6711163	0.08	19960103
27971725	16358881	9403908	0.4	12163162	0.16	8573422	0.16	21403992
27325020	16690085	9617160	0.4	12214448	0.16	8430071	0.16	21434207
30628886	17102327	10415064	0.4	13465382	0.16	8883705	0.16	22874755
14072334	9681109	5425572	0.8	12498738	0.32	9873878	0.32	23876963
14543106	8949965	5183504	0.8	12191871	0.32	9660210	0.32	23153638
14966409	9541931	5355742	0.8	13182047	0.32	9927584	0.32	25887869
3875897	2138686	1988504	1.6	6964013	0.64	4536810	0.64	12004504
3525425	1836096	2418419	1.6	6553730	0.64	4480376	0.64	11008324
4032553	2212668	1935442	1.6	7017839	0.64	4990380	0.64	11690796

APPENDIX Chapter 5

Analysis of Glucose

Descriptives

Glucose

	N	Mean	Std. Deviation	Std. Error	Minimum	Maximum
Healthy	15	4.1365	4.28276	1.10580	.37	15.45
Chrons Disease	15	9.1643	6.83508	1.76481	.17	24.54
Ulcerative Colitis	12	2.5744	2.32797	.67203	.48	9.26
Total	42	5.4858	5.63624	.86969	.17	24.54

ANOVA

Glucose

	Sum of Squares	Mean Square	F	Sig.
Between Groups	331.995	165.998	6.671	.003
Within Groups	970.458	24.884		
Total	1302.454			

Multiple Comparisons

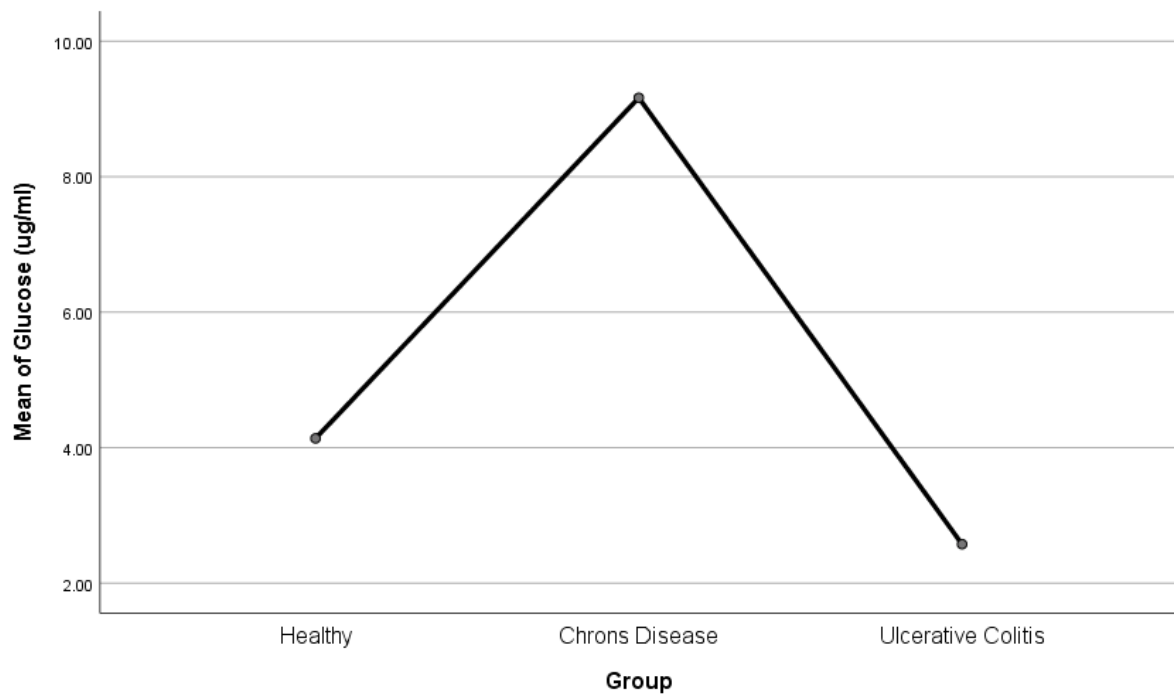
Dependent Variable: Glucose

Tukey HSD

(I) Group	(J) Group	Mean Difference (I-J)	Std. Error	Sig.
Healthy	Chrons Disease	-5.02781*	1.82148	.023
	Ulcerative Colitis	1.56209	1.93198	.700
Chrons Disease	Healthy	5.02781*	1.82148	.023
	Ulcerative Colitis	6.58990*	1.93198	.004
Ulcerative Colitis	Healthy	-1.56209	1.93198	.700
	Chrons Disease	-6.58990*	1.93198	.004

*. The mean difference is significant at the 0.05 level.

Means Plots



Analysis of Xylose

Descriptives

Xylose

	N	Mean	Std. Deviation	Std. Error	Minimum	Maximum
Healthy	15	0.9408	.88091	.22745	.05	2.99
Chrons Disease	15	2.8939	4.72635	1.22034	.04	18.32
Ulcerative Colitis	12	0.5257	1.02067	.29464	.01	3.62
Total	42	1.5197	3.04546	.46993	.01	18.32

ANOVA

Xylose

	Sum of Squares	Mean Square	F	Sig.
Between Groups	45.208	22.604	2.631	.085
Within Groups	335.060	8.591		
Total	380.269			

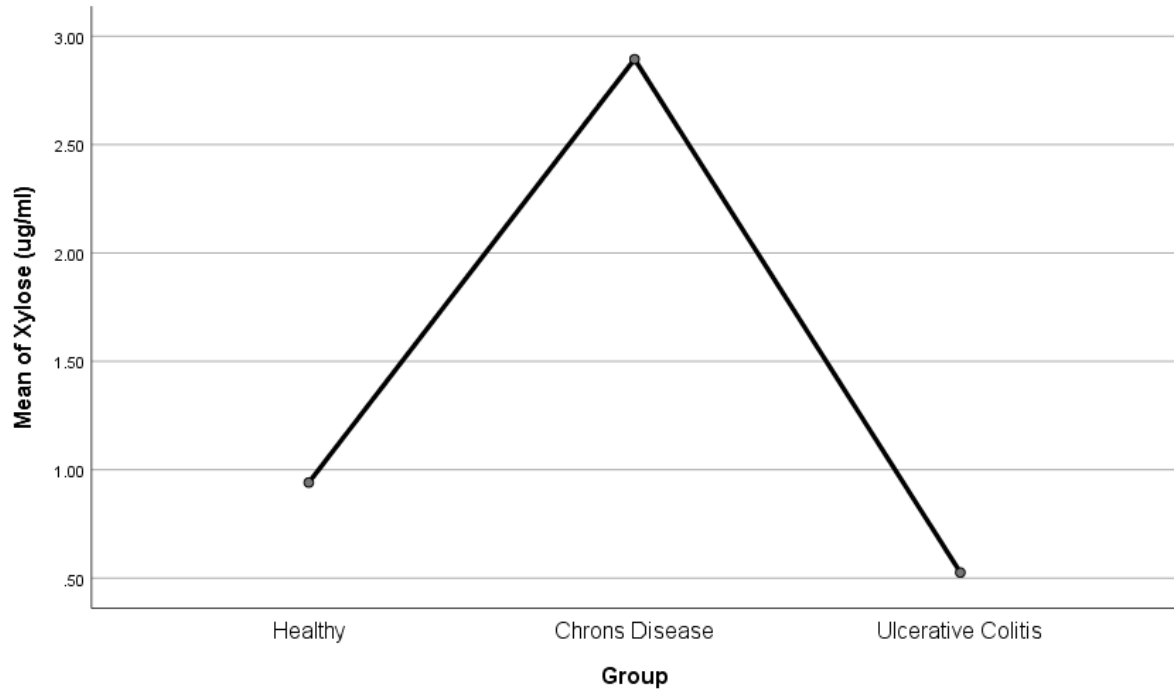
Multiple Comparisons

Dependent Variable: Xylose

Tukey HSD

(I) Group	(J) Group	Mean Difference (I-J)	Std. Error	Sig.
Healthy	Chrons Disease	-1.95303	1.07028	.175
	Ulcerative Colitis	.41517	1.13521	.929
Chrons Disease	Healthy	1.95303	1.07028	.175
	Ulcerative Colitis	2.36820	1.13521	.106
Ulcerative Colitis	Healthy	-.41517	1.13521	.929
	Chrons Disease	-2.36820	1.13521	.106

Means Plots



Analysis of Galactose

Descriptives

Galactose

	N	Mean	Std. Deviation	Std. Error	Minimum	Maximum
Healthy	15	1.8230	1.95335	.50435	.20	7.70
Chrons Disease	15	6.3460	6.56916	1.69615	.22	22.16
Ulcerative Colitis	12	2.7232	2.63427	.76045	.18	8.71
Total	42	3.6956	4.69358	.72423	.18	22.16

ANOVA

Glactose

	Sum of Squares	Mean Square	F	Sig.
Between Groups	169.311	84.656	4.499	.017
Within Groups	733.905	18.818		
Total	903.216			

Multiple Comparisons

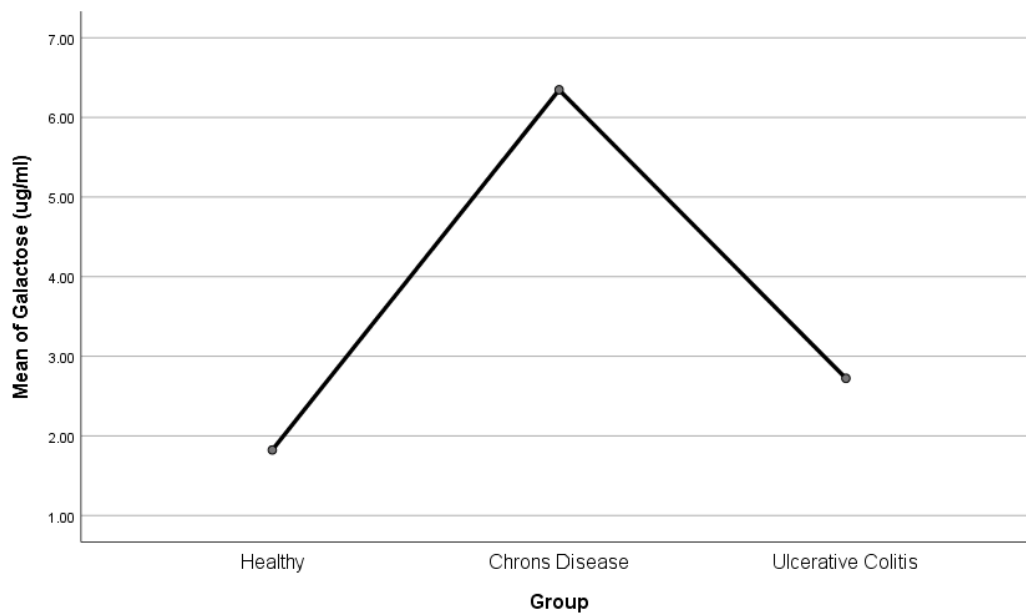
Dependent Variable: Galactose

Tukey HSD

(I) Group	(J) Group	Mean Difference (I-J)	Std. Error	Sig.
Healthy	Chrons Disease	-4.52294*	1.58401	.018
	Ulcerative Colitis	-.90017	1.68009	.854
Chrons Disease	Healthy	4.52294*	1.58401	.018
	Ulcerative Colitis	3.62276	1.68009	.092
Ulcerative Colitis	Healthy	.90017	1.68009	.854
	Chrons Disease	-3.62276	1.68009	.092

*. The mean difference is significant at the 0.05 level.

Means Plots



Analysis Arabinose

Descriptives

Arabinose

	N	Mean	Std. Deviation	Std. Error	Minimum	Maximum
Healthy	15	3.4270	2.27224	.58669	.91	8.30
Chrons Disease	15	5.3187	3.98010	1.02766	.89	12.33
Ulcerative Colitis	12	1.8221	1.64484	.47483	.26	5.21
Total	42	3.6441	3.14848	.48582	.26	12.33

ANOVA

Arabinose

	Sum of Squares	Mean Square	F	Sig.
Between Groups	82.608	41.304	4.975	.012
Within Groups	323.821	8.303		
Total	406.429			

Multiple Comparisons

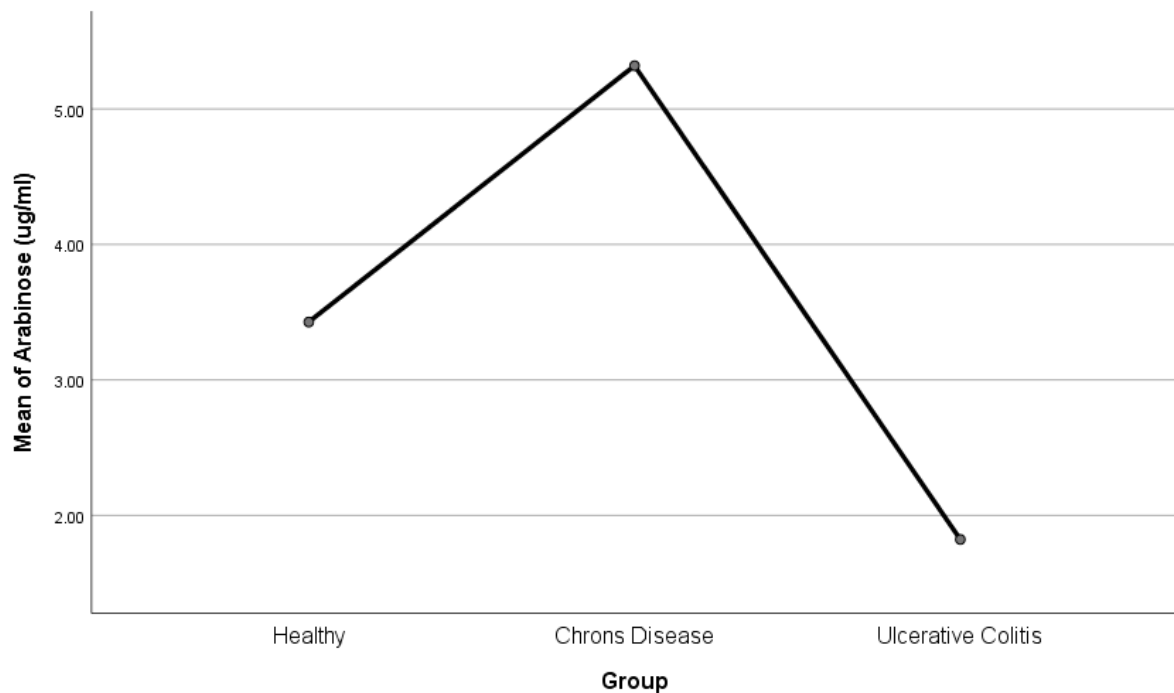
Dependent Variable: Arabinose

Tukey HSD

(I) Group	(J) Group	Mean Difference (I-J)	Std. Error	Sig.
Healthy	Chrons Disease	-1.89166	1.05218	.184
	Ulcerative Colitis	1.60496	1.11600	.332
Chrons Disease	Healthy	1.89166	1.05218	.184
	Ulcerative Colitis	3.49662*	1.11600	.009
Ulcerative Colitis	Healthy	-1.60496	1.11600	.332
	Chrons Disease	-3.49662*	1.11600	.009

*. The mean difference is significant at the 0.05 level.

Means Plots



9.0 References

1. Clish, C.B., *Metabolomics: an emerging but powerful tool for precision medicine*. Cold Spring Harbor molecular case studies, 2015. **1**(1): p. a000588-a000588.
2. Dunn, W.B., *Current trends and future requirements for the mass spectrometric investigation of microbial, mammalian and plant metabolomes*. Phys Biol, 2008. **5**(1): p. 011001.
3. Dunn, W.B., N.J. Bailey, and H.E. Johnson, *Measuring the metabolome: current analytical technologies*. Analyst, 2005. **130**(5): p. 606-25.
4. Watson, D.G., *The potential of mass spectrometry for the global profiling of parasite metabolomes*. Parasitology, 2009. **137**(9): p. 1409-1423.
5. Sawada, Y., et al., *Widely targeted metabolomics based on large-scale MS/MS data for elucidating metabolite accumulation patterns in plants*. Plant Cell Physiol, 2009. **50**(1): p. 37-47.
6. Fiehn, O., *Metabolomics – the link between genotypes and phenotypes*. Plant Molecular Biology, 2002. **48**(1): p. 155-171.
7. Schwarz, D., et al., *Recent applications of metabolomics toward cyanobacteria*. Metabolites, 2013. **3**(1): p. 72-100.
8. Fiehn, O., et al., *Metabolite profiling for plant functional genomics*. Nat Biotechnol, 2000. **18**(11): p. 1157-61.
9. Fiehn, O., *Combining genomics, metabolome analysis, and biochemical modelling to understand metabolic networks*. Comp Funct Genomics, 2001. **2**(3): p. 155-68.
10. Allen, J., et al., *High-throughput classification of yeast mutants for functional genomics using metabolic footprinting*. Nature Biotechnology, 2003. **21**: p. 692.
11. Wiechert, W., et al., *Fluxomics: mass spectrometry versus quantitative imaging*. Current opinion in plant biology, 2007. **10**(3): p. 323-330.
12. Kell, D.B., *Systems biology, metabolic modelling and metabolomics in drug discovery and development*. Drug Discov Today, 2006. **11**(23-24): p. 1085-92.
13. Dettmer, K., P.A. Aronov, and B.D. Hammock, *Mass spectrometry-based metabolomics*. Mass Spectrom Rev, 2007. **26**(1): p. 51-78.
14. Peironcelly, J.E., et al., *Automated Pipeline for De Novo Metabolite Identification Using Mass-Spectrometry-Based Metabolomics*. Analytical Chemistry, 2013. **85**(7): p. 3576-3583.
15. Albratty, M.M., *Metabonomic analysis of Drosophila mutants using high resolution mass spectrometry*, in *Strathclyde Institute of Pharmacy and Biomedical Sciences*. 2013, University of Strathclyde.
16. Beale, D.J., et al., *Review of recent developments in GC–MS approaches to metabolomics-based research*. Metabolomics, 2018. **14**(11): p. 152.
17. Boizard, F., et al., *A capillary electrophoresis coupled to mass spectrometry pipeline for long term comparable assessment of the urinary metabolome*. Scientific reports, 2016. **6**: p. 34453-34453.
18. Pontes, J.G.M., et al., *NMR-based metabolomics strategies: plants, animals and humans*. Analytical Methods, 2017. **9**(7): p. 1078-1096.

19. Kamleh, M.A., J.A. Dow, and D.G. Watson, *Applications of mass spectrometry in metabolomic studies of animal model and invertebrate systems*. Brief Funct Genomic Proteomic, 2009. **8**(1): p. 28-48.
20. Bingol, K., *Recent Advances in Targeted and Untargeted Metabolomics by NMR and MS/NMR Methods*. High-throughput, 2018. **7**(2): p. 9.
21. Bingol, K. and R. Bruschiweiler, *Multidimensional approaches to NMR-based metabolomics*. Anal Chem, 2014. **86**(1): p. 47-57.
22. Nagana Gowda, G.A. and D. Raftery, *Recent Advances in NMR-Based Metabolomics*. Anal Chem, 2017. **89**(1): p. 490-510.
23. Ho, C.S., et al., *Electrospray ionisation mass spectrometry: principles and clinical applications*. The Clinical biochemist. Reviews, 2003. **24**(1): p. 3-12.
24. Kamleh, A., et al., *Metabolomic profiling using Orbitrap Fourier transform mass spectrometry with hydrophilic interaction chromatography: a method with wide applicability to analysis of biomolecules*. Rapid Communications in Mass Spectrometry, 2008. **22**(12): p. 1912-1918.
25. Ekman, R., Silberring, J., Westman-Brinkmaln, A., and Kraj, A. , *Mass Spectrometry: Instrumentation and Application*. 2009: John Wiley and Sons, USA
26. Watson, D.G., *The potential of mass spectrometry for the global profiling of parasite metabolomes*. Parasitology, 2010. **137**(9): p. 1409-1423.
27. Griffiths, J., *A Brief History of Mass Spectrometry*. Analytical Chemistry, 2008. **80**(15): p. 5678-5683.
28. Märk T.D., D.G.H., *Electron Impact Ionization*. 2013: Springer Science & Business Media. 375.
29. Kaufman, H.R., et al., *Performance Correlation for Electron-bombardment Ion Sources*. 1965: National Aeronautics and Space Administration.
30. Cappiello, A., et al., *New trends in the application of electron ionization to liquid chromatography—mass spectrometry interfacing*. Mass Spectrometry Reviews, 2001. **20**(2): p. 88-104.
31. Hunt, D.F., C.N. McEwen, and T.M. Harvey, *Positive and negative chemical ionization mass spectrometry using a Townsend discharge ion source*. Analytical Chemistry, 1975. **47**(11): p. 1730-1734.
32. Adamowicz, P. and M. Kała, *Simultaneous screening for and determination of 128 date-rape drugs in urine by gas chromatography–electron ionization-mass spectrometry*. Forensic Science International, 2010. **198**(1): p. 39-45.
33. Calder, A.G., et al., *The determination of low d5-phenylalanine enrichment (0.002–0.09 atom percent excess), after conversion to phenylethylamine, in relation to protein turnover studies by gass chromatography/electron ionization mass spectrometry*. Rapid Communications in Mass Spectrometry, 1992. **6**(7): p. 421-424.
34. Arrebola, F.J., et al., *Determination of 81 multiclass pesticides in fresh foodstuffs by a single injection analysis using gas chromatography–chemical ionization and electron ionization tandem mass spectrometry*. Analytica Chimica Acta, 2003. **484**(2): p. 167-180.
35. Colombini, M.P., F. Modugno, and E. Ribechini, *Direct exposure electron ionization mass spectrometry and gas chromatography/mass spectrometry techniques to study organic coatings on archaeological amphorae*. Journal of Mass Spectrometry, 2005. **40**(5): p. 675-687.

36. Fales, H.M., et al., *Biological applications of electron ionization and chemical ionization mass spectrometry*. Recent Prog Horm Res, 1972. **28**: p. 591-626.
37. Field, F.H., *Chemical ionization mass spectrometry*. Accounts of Chemical Research, 1968. **1**(2): p. 42-49.
38. G., H.A., *Chemical Ionization Mass Spectrometry*. 1992.
39. Dass, C., *Fundamentals of contemporary mass spectrometry*. 2007, Wiley-Interscience: Hoboken, N.J. .:
40. Dougherty, R.C., *Negative chemical ionization mass spectrometry: Applications in environmental analytical chemistry*. Biomedical Mass Spectrometry, 1981. **8**(7): p. 283-292.
41. Byrdwell, W.C., *Atmospheric pressure chemical ionization mass spectrometry for analysis of lipids*. Lipids, 2001. **36**(4): p. 327-346.
42. Hillenkamp, F., et al., *Matrix-Assisted Laser Desorption/Ionization Mass Spectrometry of Biopolymers*. Analytical Chemistry, 1991. **63**(24): p. 1193A-1203A.
43. Karas, M., D. Bachmann, and F. Hillenkamp, *Influence of the wavelength in high-irradiance ultraviolet laser desorption mass spectrometry of organic molecules*. Analytical Chemistry, 1985. **57**(14): p. 2935-2939.
44. Karas, M., et al., *Matrix-assisted ultraviolet laser desorption of non-volatile compounds*. International Journal of Mass Spectrometry and Ion Processes, 1987. **78**: p. 53-68.
45. Tanaka, K., et al., *Protein and polymer analyses up to m/z 100 000 by laser ionization time-of-flight mass spectrometry*. Rapid Communications in Mass Spectrometry, 1988. **2**(8): p. 151-153.
46. Avila, C.C., F.G. Almeida, and G. Palmisano, *Direct identification of trypanosomatids by matrix-assisted laser desorption ionization–time of flight mass spectrometry (DIT MALDI-TOF MS)*. Journal of Mass Spectrometry, 2016. **51**(8): p. 549-557.
47. Lachaud, L., et al., *Identification of *Leishmania* by Matrix-Assisted Laser Desorption Ionization–Time of Flight (MALDI-TOF) Mass Spectrometry Using a Free Web-Based Application and a Dedicated Mass-Spectral Library*. Journal of Clinical Microbiology, 2017. **55**(10): p. 2924.
48. Abouseada, N., et al., *Matrix-assisted laser desorption ionisation time-of-flight mass spectrometry rapid detection of carbapenamase activity in Acinetobacter baumannii isolates*. Indian J Med Microbiol, 2017. **35**(1): p. 85-89.
49. Huguenin, A., et al., *MALDI-TOF mass spectrometry: a new tool for rapid identification of cercariae (Trematoda, Digenea)*. Parasite, 2019. **26**: p. 11.
50. Dhillon, A.S., et al., *MAP kinase signalling pathways in cancer*. Oncogene, 2007. **26**: p. 3279.
51. Nielen, M.W.F. and S. Malucha, *Characterization of polydisperse synthetic polymers by size-exclusion chromatography/matrix-assisted laser desorption/ionization time-of-flight mass spectrometry*. Rapid Communications in Mass Spectrometry, 1997. **11**(11): p. 1194-1204.
52. Fukuyama, Y., et al., *Ionic Liquid Matrixes Optimized for MALDI-MS of Sulfated/Sialylated/Neutral Oligosaccharides and Glycopeptides*. Analytical Chemistry, 2008. **80**(6): p. 2171-2179.
53. Thingholm, T.E., et al., *Highly selective enrichment of phosphorylated peptides using titanium dioxide*. Nature Protocols, 2006. **1**(4): p. 1929-1935.

54. Zou, X., et al., *Highly specific capture and direct MALDI-MS analysis of phosphorylated peptides using novel multifunctional chitosan-GMA-IDA-Fe (III) nanosphere*. Analytical and Bioanalytical Chemistry, 2011. **401**(4): p. 1251-1261.
55. Clarke, W., *Chapter 1 - Mass spectrometry in the clinical laboratory: determining the need and avoiding pitfalls*, in *Mass Spectrometry for the Clinical Laboratory*, H. Nair and W. Clarke, Editors. 2017, Academic Press: San Diego. p. 1-15.
56. Dunn, W.B., *Chapter two - Mass Spectrometry in Systems Biology: An Introduction*, in *Methods in Enzymology*, D. Jameson, M. Verma, and H.V. Westerhoff, Editors. 2011, Academic Press. p. 15-35.
57. Wiley, W.C. and I.H. McLaren, *Time-of-Flight Mass Spectrometer with Improved Resolution*. Review of Scientific Instruments, 1955. **26**(12): p. 1150-1157.
58. Carlsohn, E. and C.L. Nilsson, *Chapter 12 - Proteomic Techniques for Functional Identification of Bacterial Adhesins*, in *Lectins*, C.L. Nilsson, Editor. 2007, Elsevier Science B.V.: Amsterdam. p. 299-325.
59. Webster, J. and D. Oxley, *Protein identification by MALDI-TOF mass spectrometry*. Methods Mol Biol, 2012. **800**: p. 227-40.
60. Clark, C.M., et al., *Coupling MALDI-TOF mass spectrometry protein and specialized metabolite analyses to rapidly discriminate bacterial function*. Proceedings of the National Academy of Sciences, 2018. **115**(19): p. 4981.
61. Dave, K.A., et al., *Preparation and Analysis of Proteins and Peptides Using MALDI TOF/TOF Mass Spectrometry*. Current Protocols in Protein Science, 2011. **63**(1): p. 16.13.1-16.13.21.
62. Loo, J.A., *The Tools of Proteomics*, in *Advances in Protein Chemistry*, R.D. Smith and T.D. Veenstra, Editors. 2003, Academic Press. p. 25-56.
63. Adamson, J.T. and K. Hakansson, *Chapter 14 - Electrospray Ionization Fourier Transform Ion Cyclotron Resonance Mass Spectrometry for Lectin Analysis*, in *Lectins*, C.L. Nilsson, Editor. 2007, Elsevier Science B.V.: Amsterdam. p. 343-371.
64. *Talking About a Revolution: FT-ICR Mass Spectrometry Offers High Resolution and Mass Accuracy for Pr.* [cited 2019 19/05/2019]; Available from: <https://www.biocompare.com/Editorial-Articles/41589-Talking-About-a-Revolution-FT-ICR-Mass-Spectrometry-Offers-High-Resolution-and-Mass-Accuracy-for-Pr/>.
65. Makarov, A., *Electrostatic axially harmonic orbital trapping: a high-performance technique of mass analysis*. Anal Chem, 2000. **72**(6): p. 1156-62.
66. Makarov, A., et al., *Performance evaluation of a hybrid linear ion trap/orbitrap mass spectrometer*. Anal Chem, 2006. **78**(7): p. 2113-20.
67. Makarov, A., et al., *Dynamic range of mass accuracy in LTQ Orbitrap hybrid mass spectrometer*. J Am Soc Mass Spectrom, 2006. **17**(7): p. 977-982.
68. Makarov, A., et al., *Performance Evaluation of a Hybrid Linear Ion Trap/Orbitrap Mass Spectrometer*. Vol. 78. 2006. 2113-20.
69. Makarov, A. and M. Scigelova, *Coupling liquid chromatography to Orbitrap mass spectrometry*. J Chromatogr A, 2010. **1217**(25): p. 3938-45.
70. Liu, P., et al., *Profiling of Thiol-Containing Compounds by Stable Isotope Labeling Double Precursor Ion Scan Mass Spectrometry*. Analytical Chemistry, 2014. **86**(19): p. 9765-9773.
71. Bruheim, P., H.F.N. Kvitvang, and S.G. Villas-Boas, *Stable isotope coded derivatizing reagents as internal standards in metabolite profiling*. Journal of Chromatography A, 2013. **1296**: p. 196-203.

72. Guo, K., F. Bamforth, and L. Li, *Qualitative Metabolome Analysis of Human Cerebrospinal Fluid by ¹³C/¹²C-Isotope Dansylation Labeling Combined with Liquid Chromatography Fourier Transform Ion Cyclotron Resonance Mass Spectrometry*. *Journal of The American Society for Mass Spectrometry*, 2011. **22**(2): p. 339-347.
73. Guo, K. and L. Li, *Differential ¹²C/¹³C-Isotope Dansylation Labeling and Fast Liquid Chromatography/Mass Spectrometry for Absolute and Relative Quantification of the Metabolome*. *Analytical Chemistry*, 2009. **81**(10): p. 3919-3932.
74. Zhou, R., K. Guo, and L. Li, *5-Diethylamino-naphthalene-1-sulfonyl Chloride (DensCl): A Novel Triplex Isotope Labeling Reagent for Quantitative Metabolome Analysis by Liquid Chromatography Mass Spectrometry*. *Analytical Chemistry*, 2013. **85**(23): p. 11532-11539.
75. Yang, C., Q. Hua, and K. Shimizu, *Metabolic flux analysis in Synechocystis using isotope distribution from ¹³C-labeled glucose*. *Metab Eng*, 2002. **4**(3): p. 202-16.
76. Young, J.D., et al., *Mapping photoautotrophic metabolism with isotopically nonstationary (¹³C) flux analysis*. *Metab Eng*, 2011. **13**(6): p. 656-65.
77. Huege, J., et al., *Modulation of the major paths of carbon in photorespiratory mutants of synechocystis*. *PLoS One*, 2011. **6**(1): p. e16278.
78. Knoop, H., et al., *Flux Balance Analysis of Cyanobacterial Metabolism: The Metabolic Network of Synechocystis sp. PCC 6803*. *PLOS Computational Biology*, 2013. **9**(6): p. e1003081.
79. Knoop, H. and R. Steuer, *A computational analysis of stoichiometric constraints and trade-offs in cyanobacterial biofuel production*. *Frontiers in bioengineering and biotechnology*, 2015. **3**: p. 47-47.
80. Zhou, R., et al., *IsoMS: Automated Processing of LC-MS Data Generated by a Chemical Isotope Labeling Metabolomics Platform*. *Analytical Chemistry*, 2014. **86**(10): p. 4675-4679.
81. Ren, J.-L., et al., *Advances in mass spectrometry-based metabolomics for investigation of metabolites*. *RSC Advances*, 2018. **8**(40): p. 22335-22350.
82. Gori, S.S., et al., *Profiling thiol metabolites and quantification of cellular glutathione using FT-ICR-MS spectrometry*. *Anal Bioanal Chem*, 2014. **406**(18): p. 4371-9.
83. Guo, K. and L. Li, *Differential ¹²C/¹³C-isotope dansylation labeling and fast liquid chromatography/mass spectrometry for absolute and relative quantification of the metabolome*. *Anal Chem*, 2009. **81**(10): p. 3919-32.
84. Mattingly, S.J., et al., *A Carbonyl Capture Approach for Profiling Oxidized Metabolites in Cell Extracts*. *Metabolomics*, 2012. **8**(6): p. 989-996.
85. Fu, X.-A., et al., *A novel microreactor approach for analysis of ketones and aldehydes in breath*. *Analyst*, 2011. **136**(22): p. 4662-4666.
86. Ye, T., et al., *Chemoselective ¹⁵N tag for sensitive and high-resolution nuclear magnetic resonance profiling of the carboxyl-containing metabolome*. *Anal Chem*, 2009. **81**(12): p. 4882-8.
87. MAIER, T.B., Thomas; BÄR, Thomas; VENNEMANN, Matthias; GEKELER, Volker; ZIMMERMANN, Astrid; GIMMICH, Petra; PADIYA, Kamlesh, J.; JOSHI, Hemant; JOSHI, Uday; MAKHIJA, Mahindra; HAREL, Dipak; , *NOVEL TETRAHYDROFUSEDPYRIDINES AS HISTONE DEACETYLASE INHIBITORS*. 2009.
88. Shields, S.W. and J.M. Manthorpe, *Efficient, scalable and economical preparation of tris(deuterium)- and ¹³C-labelled N-methyl-N-nitroso-p-toluenesulfonamide*

- (Diazald(R)) and their conversion to labelled diazomethane. *J Labelled Comp Radiopharm*, 2014. **57**(12): p. 674-9.
89. Traylor, P.S. and S.J. Singer, *The Preparation and Properties of Some Tritiated Diazonium Salts and Related Compounds**. *Biochemistry*, 1967. **6**(3): p. 881-887.
 90. Fischer, K., M. Wacht, and A. Meyer, *Simultaneous and Sensitive HPLC Determination of Mono- and Disaccharides, Uronic Acids, and Amino Sugars after Derivatization by Reductive Amination*. *Acta hydrochimica et hydrobiologica*, 2003. **31**(2): p. 134-144.
 91. Andersen, K.E., C. Bjerregaard, and H. Sørensen, *Analysis of Reducing Carbohydrates by Reductive Tryptamine Derivatization Prior to Micellar Electrokinetic Capillary Chromatography*. *Journal of Agricultural and Food Chemistry*, 2003. **51**(25): p. 7234-7239.
 92. Sato, S., et al., *One-pot reductive amination of aldehydes and ketones with α -picolineborane in methanol, in water, and in neat conditions*. *Tetrahedron*, 2004. **60**(36): p. 7899-7906.
 93. Andreas, N.J., et al., *Multiplatform characterization of dynamic changes in breast milk during lactation*. *ELECTROPHORESIS*, 2015. **36**(18): p. 2269-2285.
 94. Bawazeer, S., et al., *A method for the analysis of sugars in biological systems using reductive amination in combination with hydrophilic interaction chromatography and high resolution mass spectrometry*. *Talanta*, 2017. **166**: p. 75-80.
 95. Watson, D.G., *Pharmaceutical Analysis: A Textbook for Pharmacy Students and Pharmaceutical Chemists*. 2012, Oxford: Churchill Livingstone.
 96. Diercks, D.B., et al., *Urinary Metabolomic Analysis for the Identification of Renal Injury in Patients With Acute Heart Failure*. *Academic Emergency Medicine*, 2012. **19**(1): p. 18-23.
 97. Guo, K. and L. Li, *High-Performance Isotope Labeling for Profiling Carboxylic Acid-Containing Metabolites in Biofluids by Mass Spectrometry*. *Analytical Chemistry*, 2010. **82**(21): p. 8789-8793.
 98. Hu, J., et al., *Short-chain fatty acids in control of energy metabolism*. *Crit Rev Food Sci Nutr*, 2018. **58**(8): p. 1243-1249.
 99. Ibrahim, A., R.G. Daniel, and G.W. David, *Development of a Sensitive Liquid Chromatography Mass Spectrometry Method for the Analysis of Short Chain Fatty Acids in Urine from Patients with Ulcerative Colitis*. *Current Metabolomics*, 2018. **6**(2): p. 124-130.
 100. Callahan, D.L., et al., *Profiling of polar metabolites in biological extracts using diamond hydride-based aqueous normal phase chromatography*. *J Sep Sci*, 2009. **32**(13): p. 2273-80.
 101. Cubbon, S., et al., *Hydrophilic Interaction Chromatography for Mass Spectrometric Metabonomic Studies of Urine*. *Analytical Chemistry*, 2007. **79**(23): p. 8911-8918.
 102. Yang, W.-C., J. Adamec, and F.E. Regnier, *Enhancement of the LC/MS Analysis of Fatty Acids through Derivatization and Stable Isotope Coding*. *Analytical Chemistry*, 2007. **79**(14): p. 5150-5157.
 103. Pouteau, E., et al., *Acetate, propionate and butyrate in plasma: determination of the concentration and isotopic enrichment by gas chromatography/mass spectrometry with positive chemical ionization*. *Journal of Mass Spectrometry*, 2001. **36**(7): p. 798-805.

104. Buchanan, E., et al., *The use of exclusive enteral nutrition for induction of remission in children with Crohn's disease demonstrates that disease phenotype does not influence clinical remission*. *Aliment Pharmacol Ther*, 2009. **30**(5): p. 501-7.
105. Eggink, M., et al., *Targeted LC-MS derivatization for aldehydes and carboxylic acids with a new derivatization agent 4-APEBA*. *Analytical and Bioanalytical Chemistry*, 2010. **397**(2): p. 665-675.
106. Eggink, M., et al., *Development of a Selective ESI-MS Derivatization Reagent: Synthesis and Optimization for the Analysis of Aldehydes in Biological Mixtures*. *Analytical Chemistry*, 2008. **80**(23): p. 9042-9051.
107. Svolos, V., et al., *Treatment of Active Crohn's Disease With an Ordinary Food-based Diet That Replicates Exclusive Enteral Nutrition*. *Gastroenterology*, 2018.
108. Alghamdi, A., et al., *Untargeted Metabolomics of Extracts from Faecal Samples Demonstrates Distinct Differences between Paediatric Crohn's Disease Patients and Healthy Controls but No Significant Changes Resulting from Exclusive Enteral Nutrition Treatment*. *Metabolites*, 2018. **8**(4).
109. Murase, M., Y. Kimura, and Y. Nagata, *Determination of portal short-chain fatty acids in rats fed various dietary fibers by capillary gas chromatography*. *Journal of Chromatography B: Biomedical Sciences and Applications*, 1995. **664**(2): p. 415-420.
110. Moreau, N.M., et al., *Simultaneous measurement of plasma concentrations and ¹³C-enrichment of short-chain fatty acids, lactic acid and ketone bodies by gas chromatography coupled to mass spectrometry*. *J Chromatogr B Analyt Technol Biomed Life Sci*, 2003. **784**(2): p. 395-403.
111. Tedelind, S., et al., *Anti-inflammatory properties of the short-chain fatty acids acetate and propionate: a study with relevance to inflammatory bowel disease*. *World J Gastroenterol*, 2007. **13**(20): p. 2826-32.
112. Lewis, K., et al., *Enhanced translocation of bacteria across metabolically stressed epithelia is reduced by butyrate*. *Inflamm Bowel Dis*, 2010. **16**(7): p. 1138-48.
113. Manichanh, C., et al., *Reduced diversity of faecal microbiota in Crohn's disease revealed by a metagenomic approach*. *Gut*, 2006. **55**(2): p. 205-211.
114. Topping, D.L., et al., *Dietary fat and fiber alter large bowel and portal venous volatile fatty acids and plasma cholesterol but not biliary steroids in pigs*. *J Nutr*, 1993. **123**(1): p. 133-43.
115. Machiels, K., et al., *A decrease of the butyrate-producing species *Roseburia hominis* and *Faecalibacterium prausnitzii* defines dysbiosis in patients with ulcerative colitis*. *Gut*, 2014. **63**(8): p. 1275-83.
116. Harper, S. and K. Howse, *An Upper Limit to Human Longevity?* *Journal of Population Ageing*, 2008. **1**(2): p. 99-106.
117. Williams, P.T., *Relationship of distance run per week to coronary heart disease risk factors in 8283 male runners. The National Runners' Health Study*. *Arch Intern Med*, 1997. **157**(2): p. 191-8.
118. Trappe, S., *Marathon runners: how do they age?* *Sports Med*, 2007. **37**(4-5): p. 302-5.
119. Faulkner, J.A., et al., *The aging of elite male athletes: age-related changes in performance and skeletal muscle structure and function*. *Clin J Sport Med*, 2008. **18**(6): p. 501-7.
120. Sarris, J., et al., *Lifestyle medicine for depression*. *BMC Psychiatry*, 2014. **14**(1): p. 107.

121. O'Hagan, C., G. De Vito, and C.A. Boreham, *Exercise prescription in the treatment of type 2 diabetes mellitus : current practices, existing guidelines and future directions*. Sports Med, 2013. **43**(1): p. 39-49.
122. Colberg, S.R., et al., *Exercise and type 2 diabetes: the American College of Sports Medicine and the American Diabetes Association: joint position statement*. Diabetes care, 2010. **33**(12): p. e147-e167.
123. van Dijk, J.-W., et al., *Exercise therapy in type 2 diabetes: is daily exercise required to optimize glycemic control?* Diabetes care, 2012. **35**(5): p. 948-954.
124. Ehrsam, R., et al., *Exercise prescription for the overweight and the obese: how to quantify and yet keep it simple*. Br J Sports Med, 2009. **43**(12): p. 951-3.
125. Williams, P.T., *Lower prevalence of hypertension, hypercholesterolemia, and diabetes in marathoners*. Med Sci Sports Exerc, 2009. **41**(3): p. 523-9.
126. Scarborough, P., et al., *The economic burden of ill health due to diet, physical inactivity, smoking, alcohol and obesity in the UK: an update to 2006-07 NHS costs*. J Public Health (Oxf), 2011. **33**(4): p. 527-35.
127. England, P.H. *Guidance Physical activity: applying All Our Health*. 2018 [cited 2019 27/05/2019]; Available from: <https://www.gov.uk/government/publications/physical-activity-applying-all-our-health/physical-activity-applying-all-our-health>.
128. Muhsen Ali, A., et al., *Metabolomic Profiling of Submaximal Exercise at a Standardised Relative Intensity in Healthy Adults*. Metabolites, 2016. **6**(1).
129. HELLSTEN-WESTING, Y., et al., *The effect of high-intensity training on purine metabolism in man*. Acta Physiologica Scandinavica, 1993. **149**(4): p. 405-412.
130. Tanaka, H. and D.R. Seals, *Endurance exercise performance in Masters athletes: age-associated changes and underlying physiological mechanisms*. J Physiol, 2008. **586**(1): p. 55-63.
131. Sparling, P.B., E.M. O'Donnell, and T.K. Snow, *The gender difference in distance running performance has plateaued: an analysis of world rankings from 1980 to 1996*. Med Sci Sports Exerc, 1998. **30**(12): p. 1725-9.
132. Baker, A.B. and Y.Q. Tang, *Aging performance for masters records in athletics, swimming, rowing, cycling, triathlon, and weightlifting*. Exp Aging Res, 2010. **36**(4): p. 453-77.
133. Hunter, S.K., et al., *Is there a sex difference in the age of elite marathon runners?* Med Sci Sports Exerc, 2011. **43**(4): p. 656-64.
134. Ransdell, L.B., J. Vener, and J. Huberty, *Masters Athletes: An Analysis of Running, Swimming and Cycling Performance by Age and Gender*. Journal of Exercise Science & Fitness, 2009. **7**(2, Supplement): p. S61-S73.
135. Knechtle, B., et al., *Personal best marathon performance is associated with performance in a 24-h run and not anthropometry or training volume*. Br J Sports Med, 2009. **43**(11): p. 836-9.
136. El Helou, N., et al., *Impact of Environmental Parameters on Marathon Running Performance*. PLOS ONE, 2012. **7**(5): p. e37407.
137. Lepers, R. and T. Cattagni, *Do older athletes reach limits in their performance during marathon running?* Age (Dordrecht, Netherlands), 2012. **34**(3): p. 773-781.
138. Evangelia, D., E. Chris, and G.W. David, *The Application of Metabolomic Profiling to the Effects of Physical Activity*. Current Metabolomics, 2014. **2**(4): p. 233-263.

139. Carnethon, M.R., M. Gulati, and P. Greenland, *Prevalence and cardiovascular disease correlates of low cardiorespiratory fitness in adolescents and adults*. JAMA, 2005. **294**(23): p. 2981-2988.
140. Morgan, A., K. Mooney, and M. Mc Auley, *Obesity and the dysregulation of fatty acid metabolism: implications for healthy aging*. Expert Rev Endocrinol Metab, 2016. **11**(6): p. 501-510.
141. Soardo, G., et al., *Oxidative stress is activated by free fatty acids in cultured human hepatocytes*. Metab Syndr Relat Disord, 2011. **9**(5): p. 397-401.
142. Joffe, Y.T., M. Collins, and J.H. Goedecke, *The relationship between dietary fatty acids and inflammatory genes on the obese phenotype and serum lipids*. Nutrients, 2013. **5**(5): p. 1672-705.
143. Yang, J., et al., *Quantitative profiling method for oxylipin metabolome by liquid chromatography electrospray ionization tandem mass spectrometry*. Anal Chem, 2009. **81**(19): p. 8085-93.
144. Zaikin, V.G. and J.M. Halket, *Derivatization in mass spectrometry--8. Soft ionization mass spectrometry of small molecules*. Eur J Mass Spectrom (Chichester), 2006. **12**(2): p. 79-115.
145. Qi, B.-L., et al., *Derivatization for liquid chromatography-mass spectrometry*. TrAC Trends in Analytical Chemistry, 2014. **59**: p. 121-132.
146. Brooks, C.J.W., et al., *Derivatives suitable for GC-MS*. Chemistry and Physics of Lipids, 1978. **21**(4): p. 403-416.
147. Halket, J.M., et al., *Chemical derivatization and mass spectral libraries in metabolic profiling by GC/MS and LC/MS/MS*. J Exp Bot, 2005. **56**(410): p. 219-43.
148. Ko, B.J. and J.S. Brodbelt, *Enhanced electron transfer dissociation of peptides modified at C-terminus with fixed charges*. J Am Soc Mass Spectrom, 2012. **23**(11): p. 1991-2000.
149. Frey, B.L., et al., *Ion-Ion Reactions with Fixed-Charge Modified Proteins to Produce Ions in a Single, Very High Charge State*. International journal of mass spectrometry, 2008. **276**(2-3): p. 136-143.
150. Patil, P. and A. Pratap, *Choline Chloride Catalyzed Amidation of Fatty Acid Ester to Monoethanolamide: A Green Approach*. J Oleo Sci, 2016. **65**(1): p. 75-9.
151. Murad, A. and G.W. David, *Tagging Fatty Acids Via Choline Coupling for the Detection of Carboxylic Acid Metabolites in Biological Samples*. Current Analytical Chemistry, 2018. **14**: p. 1-6.
152. Nieman, D.C., et al., *Metabolomics approach to assessing plasma 13- and 9-hydroxy-octadecadienoic acid and linoleic acid metabolite responses to 75-km cycling*. American Journal of Physiology-Regulatory, Integrative and Comparative Physiology, 2014. **307**(1): p. R68-R74.
153. Dandona, P., et al., *The Suppressive Effect of Dietary Restriction and Weight Loss in the Obese on the Generation of Reactive Oxygen Species by Leukocytes, Lipid Peroxidation, and Protein Carbonylation1*. The Journal of Clinical Endocrinology & Metabolism, 2001. **86**(1): p. 355-362.
154. Lehmann, W.D., M. Stephan, and G. Furstenberger, *Profiling assay for lipoxygenase products of linoleic and arachidonic acid by gas chromatography-mass spectrometry*. Anal Biochem, 1992. **204**(1): p. 158-70.
155. Vangaveti, V., B.T. Baune, and R.L. Kennedy, *Hydroxyoctadecadienoic acids: novel regulators of macrophage differentiation and atherogenesis*. Therapeutic advances in endocrinology and metabolism, 2010. **1**(2): p. 51-60.

156. Nieman, D.C., et al., *9- and 13-Hydroxy-octadecadienoic acids (9+13 HODE) are inversely related to granulocyte colony stimulating factor and IL-6 in runners after 2h running*. Brain, Behavior, and Immunity, 2016. **56**: p. 246-252.
157. De Preter, V. and K. Verbeke, *Metabolomics as a diagnostic tool in gastroenterology*. World journal of gastrointestinal pharmacology and therapeutics, 2013. **4**(4): p. 97.
158. Evenepoel, P., et al., *Uremic toxins originating from colonic microbial metabolism*. Kidney International, 2009. **76**: p. S12-S19.
159. Bajor, A., P.-G. Gillberg, and H. Abrahamsson, *Bile acids: short and long term effects in the intestine*. Scandinavian journal of gastroenterology, 2010. **45**(6): p. 645-664.
160. Nieman, D.C., et al., *9- and 13-Hydroxy-octadecadienoic acids (9+13 HODE) are inversely related to granulocyte colony stimulating factor and IL-6 in runners after 2h running*. Brain Behav Immun, 2016. **56**: p. 246-52.
161. Grabitske, H.A. and J.L. Slavin, *Low-digestible carbohydrates in practice*. J Am Diet Assoc, 2008. **108**(10): p. 1677-81.
162. Cantarel, B.L., V. Lombard, and B. Henrissat, *Complex carbohydrate utilization by the healthy human microbiome*. PLoS One, 2012. **7**(6): p. e28742.
163. Mahowald, M.A., et al., *Characterizing a model human gut microbiota composed of members of its two dominant bacterial phyla*. Proceedings of the National Academy of Sciences, 2009. **106**(14): p. 5859-5864.
164. Joossens, M., et al., *Dysbiosis of the faecal microbiota in patients with Crohn's disease and their unaffected relatives*. Gut, 2011: p. gut. 2010.223263.
165. Krogius-Kurikka, L., et al., *Microbial community analysis reveals high level phylogenetic alterations in the overall gastrointestinal microbiota of diarrhoea-predominant irritable bowel syndrome sufferers*. BMC gastroenterology, 2009. **9**(1): p. 95.
166. McNiven, E.M., J.B. German, and C.M. Slupsky, *Analytical metabolomics: nutritional opportunities for personalized health*. The Journal of nutritional biochemistry, 2011. **22**(11): p. 995-1002.
167. Olivares, M., J.M. Laparra, and Y. Sanz, *Host genotype, intestinal microbiota and inflammatory disorders*. British Journal of Nutrition, 2013. **109**(S2): p. S76-S80.
168. Jacobs, J.P., et al., *A Disease-Associated Microbial and Metabolomics State in Relatives of Pediatric Inflammatory Bowel Disease Patients*. Cellular and Molecular Gastroenterology and Hepatology, 2016. **2**(6): p. 750-766.
169. De Preter, V., *Metabolomics in the Clinical Diagnosis of Inflammatory Bowel Disease*. Digestive Diseases, 2015. **33**(suppl 1)(Suppl. 1): p. 2-10.
170. Dotan, I., *New serologic markers for inflammatory bowel disease diagnosis*. Digestive diseases, 2010. **28**(3): p. 418-423.
171. Johnston, C., et al., *PTU-033 Serum metabolite profiles differentiate Crohn's disease from ulcerative colitis and from healthy controls*. Gut, 2010. **59**(Suppl 1): p. A61-A61.
172. Jaakkola, T., et al., *Faecal and Serum Metabolomics in Paediatric Inflammatory Bowel Disease*. Journal of Crohn's and Colitis, 2016. **11**(3): p. 321-334.
173. Jansson, J., et al., *Metabolomics Reveals Metabolic Biomarkers of Crohn's Disease*. PLOS ONE, 2009. **4**(7): p. e6386.
174. Hisamatsu, T., et al., *Novel, objective, multivariate biomarkers composed of plasma amino acid profiles for the diagnosis and assessment of inflammatory bowel disease*. PLoS One, 2012. **7**(1): p. e31131.
175. Marchesi, J.R., et al., *Rapid and noninvasive metabolomic characterization of inflammatory bowel disease*. Journal of proteome research, 2007. **6**(2): p. 546-551.

176. Le Gall, G., et al., *Metabolomics of fecal extracts detects altered metabolic activity of gut microbiota in ulcerative colitis and irritable bowel syndrome*. J Proteome Res, 2011. **10**(9): p. 4208-18.
177. Williams, H.R., et al., *Characterization of inflammatory bowel disease with urinary metabolic profiling*. Am J Gastroenterol, 2009. **104**(6): p. 1435-44.
178. Schicho, R., et al., *Quantitative metabolomic profiling of serum, plasma, and urine by (1)H NMR spectroscopy discriminates between patients with inflammatory bowel disease and healthy individuals*. J Proteome Res, 2012. **11**(6): p. 3344-57.
179. Stephens, N.S., et al., *Urinary NMR metabolomic profiles discriminate inflammatory bowel disease from healthy*. J Crohns Colitis, 2013. **7**(2): p. e42-8.
180. Bjerrum, J.T., et al., *Metabonomics in ulcerative colitis: diagnostics, biomarker identification, and insight into the pathophysiology*. J Proteome Res, 2010. **9**(2): p. 954-62.
181. Balasubramanian, K., et al., *Metabolism of the colonic mucosa in patients with inflammatory bowel diseases: an in vitro proton magnetic resonance spectroscopy study*. Magn Reson Imaging, 2009. **27**(1): p. 79-86.
182. Sharma, U., et al., *Similarity in the metabolic profile in macroscopically involved and un-involved colonic mucosa in patients with inflammatory bowel disease: an in vitro proton ((1)H) MR spectroscopy study*. Magn Reson Imaging, 2010. **28**(7): p. 1022-9.
183. Zhang, Y., et al., *1H NMR-based spectroscopy detects metabolic alterations in serum of patients with early-stage ulcerative colitis*. Biochemical and Biophysical Research Communications, 2013. **433**(4): p. 547-551.
184. Walton, C., et al., *Analysis of volatile organic compounds of bacterial origin in chronic gastrointestinal diseases*. Inflamm Bowel Dis, 2013. **19**(10): p. 2069-78.
185. Ooi, M., et al., *GC/MS-based profiling of amino acids and TCA cycle-related molecules in ulcerative colitis*. Inflamm Res, 2011. **60**(9): p. 831-40.
186. Ohman, L. and M. Simren, *Intestinal microbiota and its role in irritable bowel syndrome (IBS)*. Curr Gastroenterol Rep, 2013. **15**(5): p. 323.
187. Ahmed, I., et al., *An investigation of fecal volatile organic metabolites in irritable bowel syndrome*. PLoS One, 2013. **8**(3): p. e58204.
188. Lin, H.-M., et al., *Metabolomic Analysis Identifies Inflammatory and Noninflammatory Metabolic Effects of Genetic Modification in a Mouse Model of Crohn's Disease*. Journal of Proteome Research, 2010. **9**(4): p. 1965-1975.
189. Lin, H.-M., et al., *Nontargeted Urinary Metabolite Profiling of a Mouse Model of Crohn's Disease*. Journal of Proteome Research, 2009. **8**(4): p. 2045-2057.
190. Le Gall, G., et al., *Metabolomics of Fecal Extracts Detects Altered Metabolic Activity of Gut Microbiota in Ulcerative Colitis and Irritable Bowel Syndrome*. Journal of Proteome Research, 2011. **10**(9): p. 4208-4218.
191. Zubeldia-Brenner, L., et al., *Developmental and Functional Effects of Steroid Hormones on the Neuroendocrine Axis and Spinal Cord*. Journal of neuroendocrinology, 2016. **28**(7): p. 10.1111/jne.12401.
192. Holst, J.P., et al., *Steroid hormones: relevance and measurement in the clinical laboratory*. Clinics in laboratory medicine, 2004. **24**(1): p. 105-118.
193. Yu, J.-G., et al., *Effects of long term supplementation of anabolic androgen steroids on human skeletal muscle*. PloS one, 2014. **9**(9): p. e105330-e105330.
194. Hoffman, J.R. and N.A. Ratamess, *Medical issues associated with anabolic steroid use: are they exaggerated?* Journal of sports science & medicine, 2006. **5**(2): p. 182-193.

195. Supasyndh, O., et al., *Effect of oral anabolic steroid on muscle strength and muscle growth in hemodialysis patients*. Clinical journal of the American Society of Nephrology : CJASN, 2013. **8**(2): p. 271-279.
196. Woerdeman, J. and W. de Ronde, *Therapeutic effects of anabolic androgenic steroids on chronic diseases associated with muscle wasting*. Expert Opin Investig Drugs, 2011. **20**(1): p. 87-97.
197. Verdonck, A., et al., *Effect of low-dose testosterone treatment on craniofacial growth in boys with delayed puberty*. Eur J Orthod, 1999. **21**(2): p. 137-43.
198. Niedfeldt, M.W., *Anabolic Steroid Effect on the Liver*. Curr Sports Med Rep, 2018. **17**(3): p. 97-102.
199. de Souza, G.L. and J. Hallak, *Anabolic steroids and male infertility: a comprehensive review*. BJU Int, 2011. **108**(11): p. 1860-5.
200. Pozo, O.J., et al., *Detection and characterization of anabolic steroids in doping analysis by LC-MS*. TrAC Trends in Analytical Chemistry, 2008. **27**(8): p. 657-671.
201. Gouveia, M.J., et al., *Mass spectrometry techniques in the survey of steroid metabolites as potential disease biomarkers: a review*. Metabolism: clinical and experimental, 2013. **62**(9): p. 1206-1217.
202. Santa, T., *Derivatization in liquid chromatography for mass spectrometric detection*. Drug Discov Ther, 2013. **7**(1): p. 9-17.
203. Santa, T., *Derivatization reagents in liquid chromatography/electrospray ionization tandem mass spectrometry*. Biomedical Chromatography, 2011. **25**(1-2): p. 1-10.
204. Star-Weinstock, M., et al., *LC-ESI-MS/MS Analysis of Testosterone at Sub-Picogram Levels Using a Novel Derivatization Reagent*. Analytical Chemistry, 2012. **84**(21): p. 9310-9317.
205. Methlie, P., et al., *Multisteroid LC-MS/MS assay for glucocorticoids and androgens, and its application in Addison's disease*. Endocrine connections, 2013. **2**(3): p. 125-136.
206. Shibayama, Y., et al., *Simultaneous determination of salivary testosterone and dehydroepiandrosterone using LC-MS/MS: Method development and evaluation of applicability for diagnosis and medication for late-onset hypogonadism*. J Chromatogr B Analyt Technol Biomed Life Sci, 2009. **877**(25): p. 2615-23.
207. Nadarajah, N., et al., *Multiplexed analysis of steroid hormones in saliva by LC-MS/MS with 2-hydrazinopyridine derivatization*. Clinical Mass Spectrometry, 2017. **4-5**: p. 1-10.
208. Higashi, T., et al., *Methods for differential and quantitative analyses of brain neurosteroid levels by LC/MS/MS with ESI-enhancing and isotope-coded derivatization*. J Pharm Biomed Anal, 2016. **117**: p. 155-62.
209. Higashi, T., A. Yamauchi, and K. Shimada, *2-hydrazino-1-methylpyridine: a highly sensitive derivatization reagent for oxosteroids in liquid chromatography-electrospray ionization-mass spectrometry*. J Chromatogr B Analyt Technol Biomed Life Sci, 2005. **825**(2): p. 214-22.
210. Michitaro Fujimoto, T.F., Toshimitsu Mozai, Yoshikazu Funazo *Method for preparing pharmacologically active cyanoguanidine derivative*. 1981: USA.
211. Shields, S.W.J. and J.M. Manthorpe, *Efficient, scalable and economical preparation of tris(deuterium)- and ¹³C-labelled N-methyl-N-nitroso-p-toluenesulfonamide (Diazald®) and their conversion to labelled diazomethane*. Journal of Labelled Compounds and Radiopharmaceuticals, 2014. **57**(12): p. 674-679.

212. Corr, M.J., et al., *Amidine Dications as Superelectrophiles*. Journal of the American Chemical Society, 2009. **131**(49): p. 17980-17985.
213. Alzahrani, M.A., et al., *Development of a Derivatization Method for Investigating Testosterone and Dehydroepiandrosterone Using Tandem Mass Spectrometry in Saliva Samples from Young Professional Soccer Players Pre- and Post-Training*. Scientia Pharmaceutica, 2019. **87**(2): p. 11.